

---

# Analysis of the Neural Circuit Underlying the Detection of Visual Motion in *Drosophila melanogaster*

Étienne Serbe

---



München, April 5<sup>th</sup> 2016

---

**Analysis of the Neural Circuit  
Underlying the Detection of Visual  
Motion in *Drosophila melanogaster***

Étienne Serbe

---

Dissertation der Graduate School of Systemic Neuroscience  
der Ludwig-Maximilians-Universität  
by  
Étienne Serbe

München, April 5<sup>th</sup> 2016

First Reviewer / Supervisor: Prof. Dr. Alexander Borst

Second Reviewer: PD Dr. Lars Kunz

Date of Submission: 2016, April 5<sup>th</sup>

Date of Defense: 2016, September 16<sup>th</sup>

# Contents

<b>Summary</b>	<b>vii</b>
<b>Acknowledgements</b>	<b>ix</b>
<b>Introduction</b>	<b>1</b>
From Sensory Perception to Specific Neural Responses . . . . .	1
Detection of Visual Motion and the Hassenstein-Reichardt Correlator (HRC) . .	2
Neuroanatomy of the Optic Lobe . . . . .	3
Retina . . . . .	3
Lamina . . . . .	5
Medulla . . . . .	5
Lobula Complex . . . . .	6
Neurogenetics . . . . .	6
The GAL4/UAS System . . . . .	6
Cell Visualization . . . . .	8
Activity Recording . . . . .	8
Cell Activation and Inactivation . . . . .	9
State-of-the-art Circuit Neuroscience Techniques . . . . .	10
Whole-Cell Patch-Clamp Electrophysiology . . . . .	10
Two-Photon Calcium Imaging . . . . .	10
Behavioral Readouts . . . . .	12
Connectomics . . . . .	12
Finding the Neural Implementation of the Motion Detector . . . . .	12
ON/OFF Split and Input Elements . . . . .	13
T4/T5-Output . . . . .	14
<b>Manuscript Nr. 1:</b>	
<b>Comprehensive Characterization of the Major Presynaptic Elements to the</b>	
<b><i>Drosophila</i> OFF Motion Detector</b>	<b>15</b>
Author Contributions . . . . .	15
Summary . . . . .	16
Main Text . . . . .	16
Supplementary Information . . . . .	30

---

CONTENTS

---

<b>Manuscript Nr. 2</b>	
<b>Neural Circuit Components of the <i>Drosophila</i> OFF Motion Vision Pathway</b>	<b>42</b>
Author Contributions . . . . .	42
Summary . . . . .	43
Main Text . . . . .	43
Supplemental Information . . . . .	51
<b>Manuscript Nr. 3:</b>	
<b>A Directional Tuning Map of <i>Drosophila</i> Elementary Motion Detectors</b>	<b>55</b>
Author Contributions . . . . .	55
Summary . . . . .	56
Main Text . . . . .	56
Supplementary Information . . . . .	63
<b>Manuscript Nr. 4:</b>	
<b>Optogenetic and Pharmacologic Dissection of Feedforward Inhibition in     <i>Drosophila</i> Motion Vision</b>	<b>65</b>
Author Contributions . . . . .	65
Summary . . . . .	66
Main Text . . . . .	66
<b>Manuscript Nr. 5:</b>	
<b>Neural Mechanisms for <i>Drosophila</i> Contrast Vision</b>	<b>76</b>
Author Contributions . . . . .	76
Summary . . . . .	77
Main Text . . . . .	77
Supplementary Information . . . . .	91
<b>Manuscript Nr. 6:</b>	
<b>Asymmetry of <i>Drosophila</i> ON and OFF motion detectors enhances real-     world velocity estimation</b>	<b>110</b>
Author Contributions . . . . .	110
Summary . . . . .	111
Main Text . . . . .	111
Supplementary Information . . . . .	124
<b>Discussion</b>	<b>137</b>
ON/OFF Split and ON/OFF Differences . . . . .	138
T4/T5 as Elementary Motion Detectors . . . . .	141
T5 and its Four Inputs . . . . .	141
The Role of Lobula Plate Intrinsic Cells . . . . .	143
Vertebrate/Invertebrate Parallels . . . . .	144
LPTC Response/Behavior Relationship . . . . .	145

## Contents

---

Combination of Techniques and Technique Optimization . . . . .	147
Conclusion and Outlook . . . . .	149
<b>Bibliography</b>	<b>162</b>
<b>List of Figures</b>	<b>163</b>
<b>Curriculum Vitae</b>	<b>164</b>
<b>Affidavit</b>	<b>166</b>
<b>List of Publications and Author Contributions</b>	<b>167</b>

# Summary

It is crucial for every sighted animal to detect the direction of motion. Computing its own motion as well as the motion of objects, conspecifics, predators and preys is necessary to successfully navigate, feed, and mate. The aerobic fruit fly *Drosophila melanogaster* can be seen as a true expert in motion vision with astonishing maneuverability due to its ability of processing visual information in the millisecond scale. Their photoreceptor cells convert light into electrical signals, and only a few synapses downstream, wide-field integrating lobula plate tangential cells respond in a fully direction-selective manner to visual motion. To unravel the underlying mechanisms, *Drosophila* represents a well suited model organism due to its genetic armory.

In the publications of this cumulative thesis, I analyzed various neurons of the motion vision circuitry in order to identify its location within the circuit and its function for the computation of direction selectivity. In the following, I will summarize the key findings of the six publications [MS1-6] that compose the main part of this thesis.

First, to find out whether lobula plate tangential cells already receive direction-selective input, we characterized their presynaptic partners T4 and T5. Via two-photon calcium imaging we demonstrated that the dendrites of these neurons respond in a direction-selective manner and come in four subtypes which are individually responsible for the detection of motion in one of the four cardinal directions. Furthermore, we showed that T4 and T5 responses are polarity specific, that is, T4 neurons only respond to moving brightness increments and T5 neurons only respond to moving brightness decrements. Silencing experiments revealed that the two neuron classes represent the output stage of the ON (T4) and OFF (T5) pathway. Postsynaptic lobula plate tangential cells responses to ON and OFF stimuli were selectively impaired when blocking the synaptic output of either T4 or T5 cells, respectively. These results were also confirmed by behavioral experiments [MS3].

Immunohistochemistry and optogenetic activation of T4/T5 cells combined with electrophysiology and pharmacology revealed that they provide excitatory cholinergic input to lobula plate tangential cells. After optogenetic T4/T5 activation, tangential cells responded with a fast excitation and a delayed inhibition. These results demonstrated that T4 and T5 cells directly activate lobula plate tangential cells and suggested that the null direction hyperpolarization is mediated by feedforward inhibition via another cell type [MS4].

Next, we compared the response properties and features of the ON and the OFF path-

way. Blocking one pathway left flies unaffected when following motion of naturalistic stimuli. Their temporal tuning, however, differed substantially. In lobula plate tangential cells, maximum responses are shifted toward higher velocities for OFF stimuli compared to ON stimuli. The ON/OFF asymmetries could be reproduced by optimizing the performance of an *in silico* motion estimation model using natural scenes. Consequently, ON/OFF asymmetries in the fly visual system reflect an adaptation to ON/OFF asymmetries present in naturalistic environments [MS6].

To find out whether T4 and T5 cells are the first direction-selective neurons in the motion vision pathway we characterized individual candidate neurons of the OFF pathway upstream of T5. Here, we demonstrated that L4 cells, reciprocally connected to L2, respond in a non-direction-selective, tonic fashion and are crucial for OFF motion detection [MS2]. Together with L2 they give input to Tm2 cells which lie presynaptic to T5. Based on anatomical studies the network arrangement of L2/L4/Tm2 was proposed as a possible mechanism for the generation of direction-selective signals. However, Tm2 as well as the other three major inputs of T5 cells (Tm1, Tm4, and Tm9) showed an increase of activity upon OFF stimulation irrespective of the direction of motion [MS1, MS2]. Hence, we could demonstrate that the computation of direction selectivity in the OFF pathway is located on the dendrites of T5 cells. Additionally, we were able to reveal that all of them are subject to lateral inhibition and have a receptive field size corresponding to the acceptance angle of an ommatidium. They exhibited substantially different temporal dynamics, suggesting that they make up a set of differentially tuned temporal filters within the OFF pathway. Silencing experiments showed that all of them are involved in the computation of OFF motion, but to various degrees, correlating with the number of synapses they form with postsynaptic T5 cells. Combinatorial blocking of Tm cell pairs led to a further reduction in tangential cell OFF responses compared to single cell blocks, ruling out redundancy. Furthermore, we compared effects from electrophysiological and behavioral experiments and found a non-linear relationship which confirmed that lobula plate tangential cell responses play an important role in the generation of visually driven behavior [MS1].

Finally, I analyzed the neural mechanism underlying the computation of changes in contrast. I found that flies react to certain contrast illusions like humans and that key elements of the ON pathway, Mi1 and Tm3, play an important role in their computation. Even in motion blind flies this behavior is still present, indicating that contrast and motion vision circuits share first components and then diverge downstream of Mi1 and Tm3 [MS5].



# Acknowledgements

The first and most important person i would like to deeply thank is Axel. During my PhD i realized why your supervisor is also called 'Doktorvater'. Besides excellent stientific guidance and motivation, Axel also takes care of your personal complacency. He does not only send you to important conferences, but also gives you all liberties a scientist needs, has always an open ear for your problems and provides you with delicious food and cold refreshments at his parties. Thank you for being a great boss.

Next, i would like to thank the rest of the department for a comfortable, scientifically fruitful and happy environment. Here, i have to highlight a couple of people who became really close friends: Meeting Jones and Maxito during a lab rotation, I knew that this group is not only leading research on its field but also has a friendly atmosphere. Starting the PhD with MM, it early became clear that the most efficient and enjoyable way of spending your time in and outside the lab is teamwork (e.g. as ETMM, Mattienne, 'Team Spirit', Hells Bandidos, MPI Gangstaz). This led to uncountable fun hours culminating in the festivities of the publication matrix hosted by ETMMALI, Schorsch, Armin, and Axel. Here, Fendlerin, Micky D and Flo played important roles. Special thanks also to Alexander, Snoop Mau55 and Jesús for many inspiring and successful scientific discussions, but definitely also to my double partner Bulle for priceless technical help and pleasant table tennis hours.

Finally, I want to appreciate the help and support of all the people that facilitated organizing my dual life as a PhD student and nearly semi-professional football player: Bruno's and my family, Albi, Geo, Änder, and the whole SG Kleinweiler-Wengen.

# Introduction

## From Sensory Perception to Specific Neural Responses

Every second, when we walk or look around, we are exposed to an enormous set of sensory information. Nevertheless, we manage to successfully extract important features necessary for survival. Especially rather simple tasks are often performed sub-consciously and in parallel revealing the huge computational capacity and complexity of our nervous system. The underlying neural mechanisms for the processing of many sensory perceptions, however, remain elusive. An interesting example is the extraction of motion, irrespective of the sensory modality. How can we distinguish something that is moving from right to left or the other way around? Is the processing implemented in the same fashion for visual, acoustic and tactile stimuli?

First, the stimuli are detected by neuroepithelia (e.g. photoreceptors). These respond in a non-direction-selective manner indicating the presence or absence of an adequate stimulus. Consequently, downstream neural circuits need to compare locally separated signals to extract the direction of motion.

In order to unravel the exact underlying mechanisms it seems appropriate to work with a neural network that consists of as few cells as possible and that is hard wired. The fly visual system fulfills these criteria and has been studied for many decades. Mathematical models are used to simulate mechanisms how direction selectivity is generated. The current challenge is to find a possible implementation in the fly brain. With the genetically modifiable organism *Drosophila melanogaster* it is possible to characterize single elements of the underlying circuitry and how they could represent elements of algorithmic models. In the following I will introduce the Hassenstein-Reichardt correlator (a mathematical model) that suggests a possible mechanism of the computation of direction selectivity, the anatomy of the *Drosophila* optic lobe and the latest neurogenetic tools, techniques and insights in fly motion vision that will aid the dissection of the neural implementation.

## Detection of Visual Motion and the Hassenstein-Reichardt Correlator (HRC)

Every sighted animal has the ability to detect the direction of motion in order to successfully fulfill survival critical tasks such as finding potential mating partners or prey, escaping from predators or generally navigating through the environment. Algorithmic models describe possible mechanisms for the computation of direction selectivity by comparing two spatially separated signals after one of them is temporally delayed [1, 2]. The most famous example is the Hassenstein-Reichardt correlator [1] that could quantitatively reproduce the turning tendency of the beetle *Chlorophanus viridis* walking on a spherical Y-maze. An array of elementary motion detectors spanning the beetle's visual field was proposed to collectively extract the direction of image motion. A single elementary motion detector consists of two mirror symmetric subunits (Figure 1; [3, 4]). Both subunits spot luminance levels of two neighboring points in space via photoreceptor like elements (semicircles in Figure 1). The signals are multiplied after one of them is temporally delayed by a low-pass filter. Finally, the output values of both subunits are subtracted leading to a fully opponent direction-selective signal.

The observed behavior of *Chlorophanus* is called optomotor response, a phenomenon present all around the animal kingdom. The innate behavior serves the course stabilization, i.e. when displaced involuntarily, and is extensively studied in insects (for a list: [5]), particularly in different fly species: the blowfly *Calliphora* [6], the house fly *Musca* [7], and the fruit fly *Drosophila* [8]. These species, exhibiting astonishing maneuverability based on visual guidance despite poor spatial vision [8, 9], appear to be well suited for the analysis of the neural mechanisms underlying the computation of visual motion. Additionally, their relatively small brains are wired in a stereotyped fashion, largely ruling out effects caused by plasticity. The algorithmic model describes not only the turning behavior, but also the electrophysiological response properties of large output neurons of the optic lobes, called lobula plate tangential cells (Figure 2B). Also the fact that their mutation [10] turns *Drosophila* optomotor-blind and that microsurgical lesions affect the optomotor response makes them promising candidates of controlling visually driven behavior [11, 12]. These cells respond in a fully opponent direction-selective manner, which means, they respond positively toward preferred direction (PD) and negatively toward null direction (ND) stimulation [13]. They, thus, represent the output stage of a Hassenstein-Reichardt correlator. Consequently, the interaction of their presynaptic elements have to be analyzed to unravel the mechanism for the computation of direction selectivity.

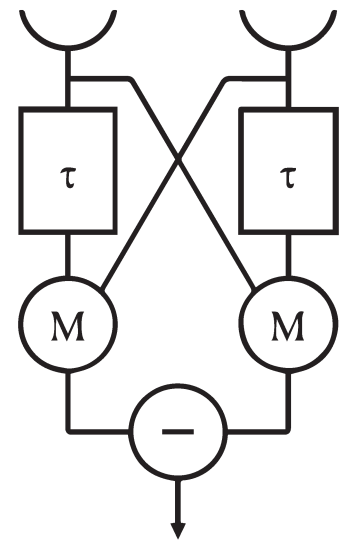


**Figure 1: The Hassenstein-Reichardt Correlator.**

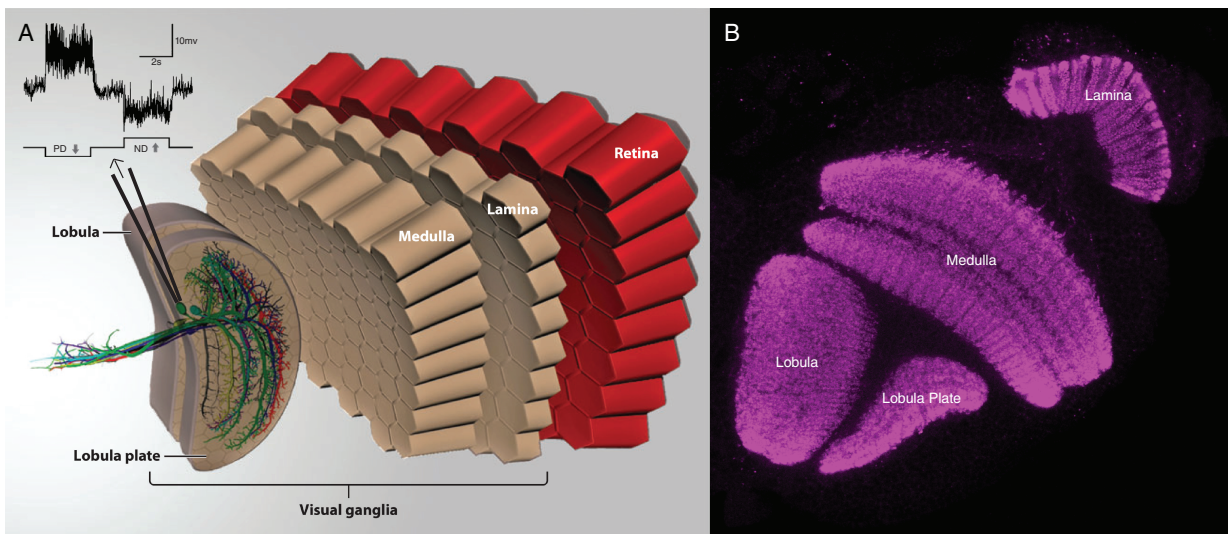


**Figure 2: The Fly Optic Lobe.** (A) Schematic of the fly optic lobe and vertical system lobula plate tangential cells and their responses toward PD and ND stimulation (traces in the upper left corner; modified from [14]). (B) Maximum intensity z-projection of the fly optic lobe, shown in a horizontal cross section. A and B show the division of the optic lobe into the different neuropils: lamina, medulla, lobula, and lobula plate.

## Neuroanatomy of the Fly Optic Lobe

*Drosophila melanogaster* detects its visual environment with its two compound eyes consisting of  $\sim 750$  facets [15], also called ommatidia. The majority of the  $\sim 300000$  neurons of the fly brain are located in the optic lobes ( $\sim 60000$  per hemisphere) and devoted to the processing of visual information (Figure 2; [16]). Photoreceptor cells in the retina convert photons into electrical signals, processed in repetitive, retinotopically arranged columns that pass through four neuropiles called lamina, medulla, lobula, and lobula plate (Figure 2A). The lobula and the lobula plate together are also referred to as the 'lobula complex'. The gross anatomy and the different cell types were described using Camillo Golgi's staining techniques [17, 18, 19]. In the following I will introduce the different brain regions and its cellular substrate.

### Retina

The hexagonally shaped ommatidia are distributed across  $\sim 340^\circ$  of the fly's visual field with an interommatidial angle of  $\sim 5^\circ$  [20]. Each ommatidium contains photoreceptors, pigment cells for optical isolation and lens-secreting cone cells (Figure 3A; [21]). Photoreceptors R1-R6 surround R7 and R8, which lie on top of another, forming seven rhabdomeres (Figure 3A). They are optically isolated (open rhabdom) and can, thus, function as independent light guides [22]. Depending on the expression of different light-sensitive Rhodopsins (Rh) in the central photoreceptors, ommatidia come in two subtypes that are stochastically distributed across the retina: pale ( $\sim 35\%$ ) and yellow

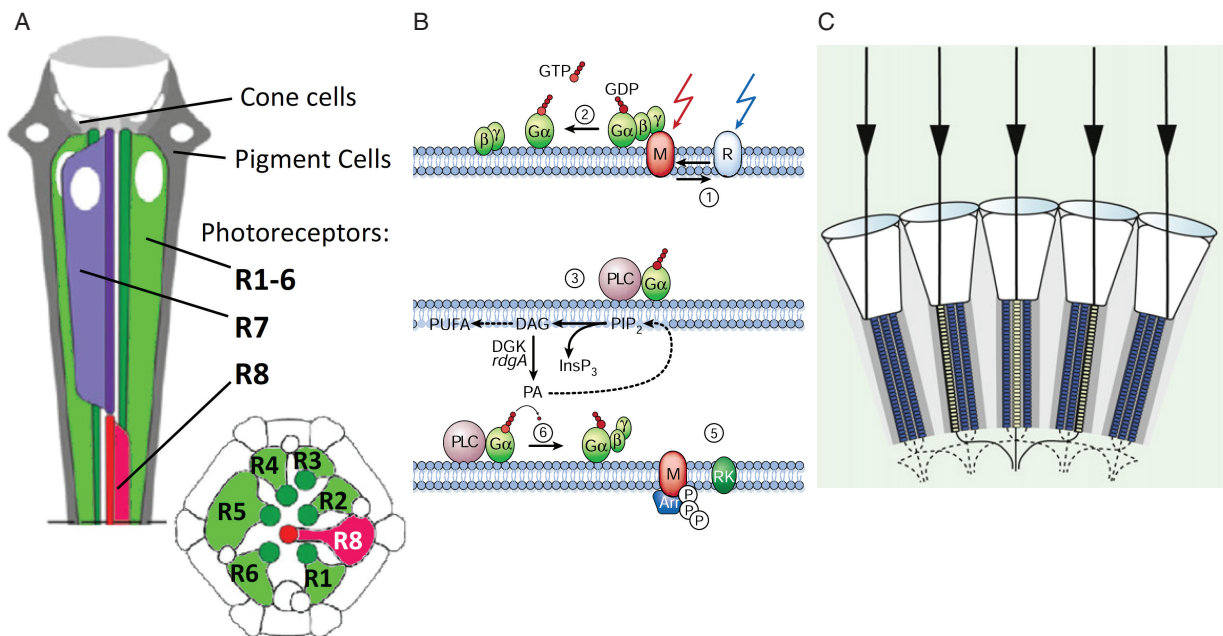


**Figure 3: *Drosophila's* Retina.** (A) Schematic overview of an ommatidium (modified from [28]). (B) Illustration of the phototransduction cascade (modified from [24]). (C) Schematic of the organization of a neural superposition eye (modified from [29]).

(~65%). In both subtypes R1-R6 contain Rh1. Pale ommatidia express UV-sensitive Rh3 in R7 and blue-sensitive Rh5 in R8, yellow ommatidia express another UV-sensitive Rh4 in R7 and green-sensitive Rh6 in R8 [23]. Light with the wavelength matching the sensitivity of the rhodopsin type induces a conformational change to meta-rhodopsin. This process is called photoisomerization (for review, see [24]). This leads to the dissociation of the alpha-subunit of a heterotrimeric G-protein. Then, phospholipase C (PLC) hydrolyses PIP<sub>2</sub> to produce soluble InsP<sub>3</sub> and DAG resulting in an activation of cation-permeable channels and membrane depolarization (Figure 3B). Histamine transmission leads to a hyperpolarization in the postsynaptic targets via a ligand-gated chloride channel [25]. Noteworthy, all photoreceptors from different ommatidia that receive visual input from the same point in space converge upon the same cartridge in the lamina. Consequently, not the ommatidia themselves but the cartridges in the lamina (neuro-ommatidia), receiving input from photoreceptors of different facets, form the functional units of processing visual information. This wiring principle is called neural superposition and allows the fly to possess an increased sensitivity without any loss of spatial resolution (Figure 3C; [26, 27]).

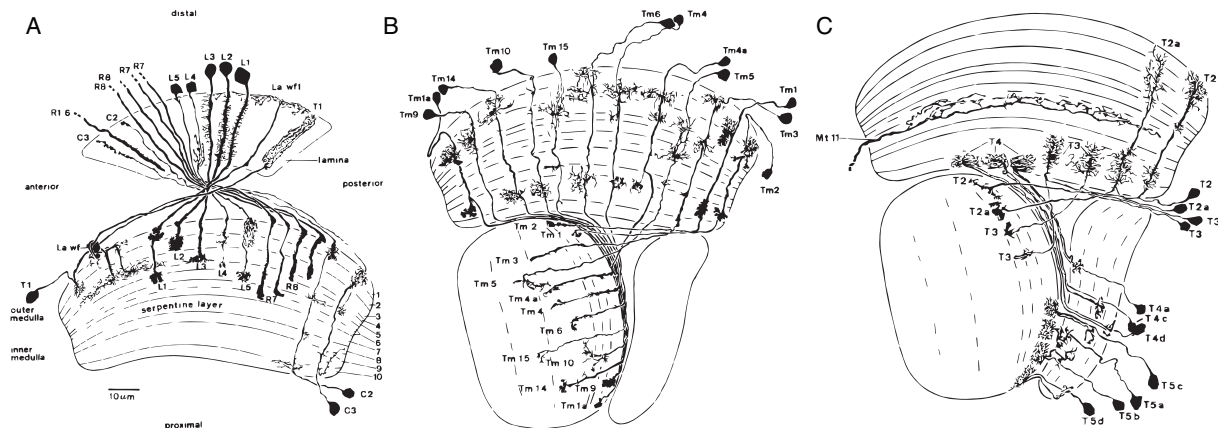


**Figure 4: Cell Types of *Drosophila*'s Optic Lobe (modified from [19]).** (A) The 12 cell types of the lamina. (B) Diversity of transmedullary cells projecting from the medulla to the lobula. (C) Bushy T-cell types. T4 and T5 come in four subtypes: a-d.

## Lamina

The photoreceptors R1-R6 feed their signals into the first neuropil, the lamina, containing ~6000 cells (Figure 4A; [16]). There, they synapse onto the five lamina monopolar cells L1 to L5 in every column [30]. Their cell bodies lie in the cell body rind located distal to the lamina. Additionally, the lamina houses centrifugal, wide-field, and tangential neurons: C2, C3, T1, Lai, Lat, Lawf1, Lawf2 [19]. L1-L5 provide feed-forward signals to different layers of the medulla: L1 to layer M1 and M5, L2 to layer M2, L3 to layer M3, L4 to layer M2 and M4, and L5 to layer M1, M2, and M5. The other cell types, however, have their axons in the lamina with their dendrites residing either in the medulla or the lamina itself. In contrast to the photoreceptors R1-R6, R7 and R8 do not form synapses in the lamina but project directly to the medulla. R7 has its endings in medulla layer M6 and R8 in layer M4 [19].

## Medulla

After the first optic chiasm lies the second and largest [31] optic lobe neuropil, the medulla, containing ~40000 cells [16]. It is arranged in a columnar and stratified fashion (M1-10) [19]. Anterior medullary columns receive input from posterior lamina cartridges and vice versa. This results in a X shaped structure formed by the crossing neurons, the first optic chiasm. Strata represent concentrations of synaptic specializations that are arranged tangentially along the lateral extent of the medulla. The lamina monopolar cells, described above, innervate the outer five strata M1-M5. Except for a few laterally extended cells like Mt cells that innervate whole strata, the medulla contains largely repetitive elements that reside in every column. These cells are called Mi for medulla intrinsic, Tm for transmedullary (Figure 4B), TmY and bushy T cells (Figure 4C), de-

pending on their projection pattern. All of them have their dendrites in the medulla but project to different neuropils: Mi, Tm, and TmY have their dendrites in the first six strata of the medulla and send their projections to the medulla, to the lobula, and to both the lobula and lobula plate, respectively [19]. Depending on the strata they are occupying, every cell class is subdivided into individual cell types, numbered from 1 up to 26 (e.g. Tm1-Tm26). Further downstream bushy T cells project from the proximal medulla to the lobula and lobula plate (Figure 4C). For example, T4 cells connect the tenth layer of the medulla and with the lobula plate. Taken together, the medulla contains ~30 different cell types in each column and at least 70 other cell types [18, 19].

## Lobula Complex

The second optic chiasm is located between the proximal ending of the medulla and connects the medulla with the lobula complex. Here, the lobula is located anterior and the lobula plate posterior (Figure 2B). The lobula receives most of its input via Tm and TmY cells. Only few lobula intrinsic neurons, such as Li1 and Li2, have been described. Most cell types that reside in the lobula are either lobula tangential neurons or lobula columnar neurons, which both project to the central brain. Most prominent, however, is another bushy T cell type, T5 cells. They have their dendrites in the first layer of the lobula and connect it with the four layers of the lobula plate. Interestingly, both, T4 and T5 cells come in four different subtypes in each visual column (a to d) depending on the layer which they are innervating in the lobula plate, where the lobula plate tangential cells reside (Figure 4C). The dendritic fields of the latter span over large extents of the layers and project to central brain regions. Interestingly, the lobula plate also houses lobula plate intrinsic cells (Lpi) which connect neighboring layers [19].

## Neurogenetics of *Drosophila melanogaster*

### The GAL4/UAS System

Thomas Hunt Morgan decided to use *Drosophila* as a model organism to investigate the chromosomal theory of inheritance [32]. This led to many generations of drosophilists working on the analysis of genetic processes. Later, with the generation of mutant flies using x-rays or chemicals, the fruit fly became a powerful subject for analyzing the effects of mutagenesis [33, 34]. The surviving offspring of these mutants were classified by changes in their behavior or anatomy. To study cell-specific effects, Brand and Perrimon (1993) [35] expressed the yeast transcriptional activator GAL4 in subsets of cells using randomly inserted transposable P-elements (driver line) [36]. Next, they generated another transgenic fly line, carrying an upstream activation sequence (UAS) linked to a gene of interest (reporter or effector line). When crossing the two fly lines, the UAS binds specifically to GAL4 leading to the expression of the gene of interest in the

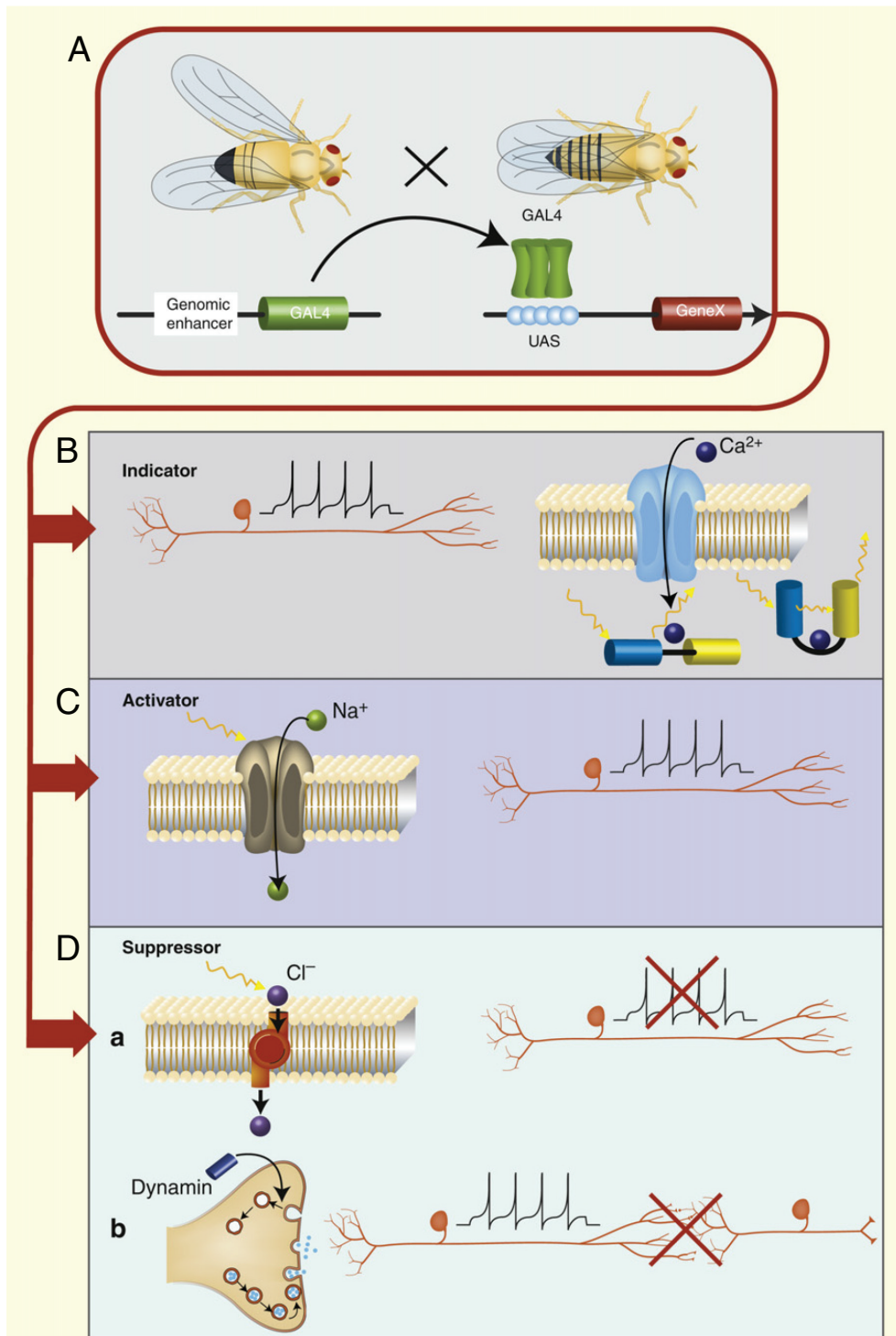


**Figure 5: Neurogenetic Toolbox of *Drosophila* (modified from [29]).** (A) The Gal4/UAS system. (B) Visualization of the cells' activity via calcium imaging. (C) Activation of cells via activators. (D) Inactivating cells by either constant hyperpolarizing them (a; KIR) or by suppressing their vesicle reuptake (b; *shibire<sup>ts</sup>*).



subset of cells containing the GAL4 (Figure 5A). Consequently, any gene of interest can be expressed specifically in individual neurons, given there exists a specific driver line. Random p-element insertion (enhancer trap), however, results in non-directional and mostly wide spread GAL4 expression. Flanking the GAL4 with a short fragment of genomic DNA (enhancer fragment) and a site-specific integration system leads to reproducible recombination at a precise position producing a defined expression of GAL4 in, on average, <100 cells [37]. The enhancer fragments control the expression pattern and the landing sites of the integration system the expression strength. To further decrease the number of cells of the expression pattern of the driver line it is possible to suppress GAL4 activity in a subset of cells via the usage of GAL80 [38] or to apply an intersectional approach (Split Gal4)[39]. For the latter, two different driver lines carry either the DNA-binding (DBD) or the transcription-activation (AD) domain of GAL4. Crossing the two fly lines results in GAL4 expression in the subset of cells where both domains are present. This approach enables the generation of single cell GAL4 expressing fly lines. Nowadays exist stock collections that contain thousands of different fly lines, which make it possible for every drosophilist to search for a driver line with the desired expression pattern [40].

### **Cell Visualization**

These can then be crossed to effector lines to investigate the function of neural circuit elements. In order to examine the expression pattern of individual GAL4 lines it is common to use fluorescent proteins like GFP (for review, see [41]). They exhibit particular excitation and emission spectra and can thus also be used in combination. An additional expression of the markers DenMark or synaptotagmin makes it possible to visualize synaptic input or output sites, respectively [42, 43, 44].

### **Activity Recording**

Once identified and characterized the cells, one can monitor their activity with constantly improving genetically encoded calcium sensors like ratiometric FRET-based calcium biosensors (Figure 5B; [45, 46, 47]) or non-ratiometric indicators with calmodulin directly inserted into a single protein [48, 49, 50, 51]. The difference between the two classes is the mechanistic principle. FRET-based calcium biosensors consist of two different fluorescent protein variants that interact via fluorescence resonance energy transfer (FRET; Figure 5B). The molecule linking the two fluorophores undergoes a conformational change upon calcium binding which results in differences in the fluorescence resonance energy transfer. Consequently, the ratio of the emission intensities of the two fluorophores changes and can be used as a readout for the cell's calcium level. More recently, however, the non-ratiometric calcium sensor family called GCaMP is mostly used. These GFP variants detect the cells' internal calcium changes by fluorescence variation that is coupled to the calcium concentration. High calcium concentrations lead

to an increased fluorescence and vice versa. The downsides of calcium sensors are that they cannot detect hyperpolarizations, either exhibit high calcium affinity or fast kinetics, often display a nonlinear relationship between fluorescence and calcium changes, and influence the physiological calcium signals via buffering. These points make it difficult to transfer the calcium signals to the cells' actual voltage responses.

## Cell Activation and Inactivation

In order to describe the role of circuit elements it is necessary to analyze the effects whilst activating or blocking their synaptic output (Figure 5D). It is possible to activate cells expressing either temperature-sensitive cation channels, such as TrpA1, or light-gated ion channels like Channelrhodopsin and its variants (Figure 5C). The transient receptor potential (TRP) channel TrpA1 opens reversibly at a temperature beyond 26°, activating its target via cation influx. Alternatively, optogenetics are used to manipulate neurons upon visual stimulation in a temporally precise manner (for review, see [52]). For example, Channelrhodopsin-2, a light-gated proton channel [53], can be used to activate neurons in a millisecond-timescale when stimulated with blue light (Figure 5C; [54]). Nowadays, its genetically tailored variants show useful features. ReaChR and Chrimson [55, 56] exhibit a red-shifted absorption spectrum making it possible to activate deeper areas and not to interfere with the visual system. The channelrhodopsin variant with a modification at the C128 position converts a brief pulse of light into a stable step in membrane potential [57]. The induced photocurrents can precisely be terminated by stimulation with a light pulse of a different wavelength. Especially for experiments in the visual system such a bistable response behavior can be very useful. Effects upon visual stimulation can be investigated over longer time scales without the need of continuous optogenetic silencing, possibly interfering with the sensitivity spectra of photoreceptors.

Another variant called SwiChR behaves in a similar way but is chloride-conducting and, thus, leads to an inactivation of the targeted cell [58]. Other ways to inactivate neurons in *Drosophila* is the expression of the Tetanus Toxin Light Chain (TNT), the inward rectifying potassium channel KIR (Figure 5D(a)), or the temperature-sensitive dynamin orthologue shibire<sup>ts</sup> (Figure 5D(b)). TNT cleaves the exocytosis necessary protein synaptobrevin and eliminates evoked synaptic transmission [59]. Shibire<sup>ts</sup>, when activated above a temperature of 29° (restrictive temperature), prevents neurons from vesicle re-uptake in a reversible fashion (Figure 5D; [60]). The advantage of this property is that it does not influence the response properties of the cell until the temperature is raised. Consequently, when raised under normal conditions, developmental defects can be ruled out. Introducing the inward rectifying potassium channel KIR leads to a constant hyperpolarization of the target cell, potentially also functioning across-gap junctions [61]. Furthermore, it is possible to genetically ablate cells using death-inducing genes like *hid* [62, 63] or *reaper* [64], which lead to cell apoptosis of the GAL4 targets.

## State-of-the-art Circuit Neuroscience Techniques

Before the emergence of the Gal4/UAS system together with the generation of a vast number of fly lines it was not possible to follow a directed approach to unravel the neural mechanisms of motion detection in the fly visual system. The following techniques were mostly used:

- Analyses of projection patterns of different cell types described via Golgi stainings,

which only offer hypotheses of connections [65].

- Response properties of individual cell types using intracellular recordings combined with anatomical analysis [66]. The limiting factor of this approach, however, is the size of the cells.

- Deoxyglucose activity labeling of optic lobe regions upon visual stimulation, which does not deliver any insights in temporal response properties of the cells located in the region of interest [67].

Consequently, many hypotheses about cell types and pathways involved in motion processing were proposed, but their confirmations remained unclear due to the lack of tools making it possible to manipulate specific cell types. In the next section I will describe the latest techniques used in neuroscience making it possible to resolve the function of individual circuits and circuit elements.

## Whole-Cell Patch-Clamp Electrophysiology

Intracellular recordings with sharp electrodes of lobula plate tangential cells in blowflies led to a detailed characterization of their response properties and their connectivity [68, 69, 70]. Due to their fully-opponent direction-selective response properties they are often referred to the output stage of the Hassenstein-Reichardt correlator. However, response properties of upstream elements were only sporadically described because of their difficult accessibility and size [71]. The emergence of the patch-clamp technique [72] made it possible to electrically record from large neurons in the genetically modifiable model organism *Drosophila melanogaster*. With this technique, recordings can be performed reliably over several hours without damaging the neuron (Figure 6A; [73, 13]). Hence, it is possible to use the lobula plate tangential cell responses as a readout while manipulating upstream neural elements of the circuits involved in motion detection.

## Two-Photon Calcium Imaging

Due to the small size of the neurons, patch-clamping of the cells upstream of the lobula plate was only once conducted successfully [75]. Nevertheless, describing the response properties of the cells that are located between photoreceptors and lobula plate tangential cells reflects a necessary experiment to localize the emergence of direction selectiv-

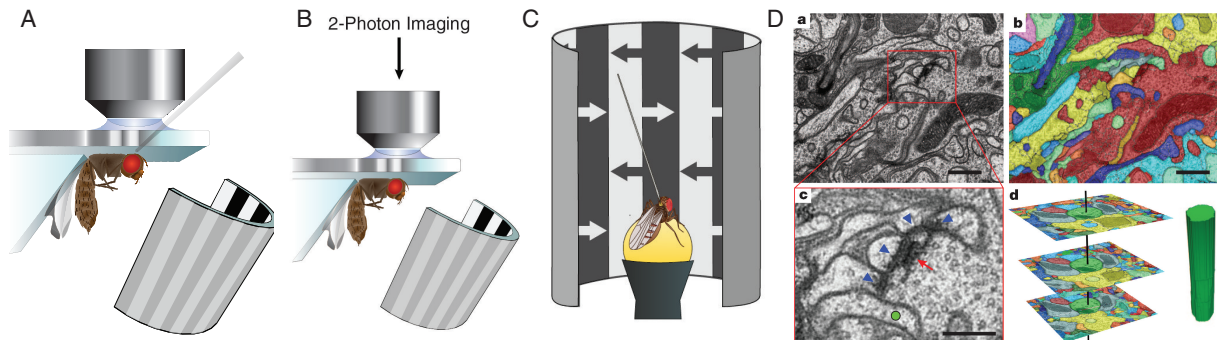


**Figure 6: State-of-the-art Circuit Neuroscience Techniques.** (A) Illustration of a whole-cell patch-clamp electrophysiology preparation. (B) Illustration of a two-photon calcium imaging preparation. (C) Illustration of a walking *Drosophila* on a styrofoam ball used as a behavioral readout. (D) Connectome reconstruction using serial-section electron microscopy (modified from [74]). (a) Representative micrograph. (b) Segmentation of (a) into neurite profiles (single colors). (c) Analysis and evaluation of connections between neurites (blue arrows: postsynaptic densities; red arrow: T-bar ribbon; green circle: non-synaptic process). (d) 3-D reconstruction processing of the single sections

ity in the fly visual system. For this, calcium sensors (Figure 5B) can be expressed in the circuit elements to record their activity upon visual stimulation (Figure 6B). Advantages of using the calcium level of neurons as a readout are at least fourfold:

- Expressing the calcium indicator genetically decreases the experimental effort, that is, the calcium sensor expressing cells only have to be accessible optically.
- Calcium changes can be detected in every part of the cell, making it possible to see differences at the level of the input and output sites of the neuron.
- Calcium responses in axon terminals reflect outgoing signals to the postsynaptic cell.
- Calcium imaging can be performed over several hours of multiple cells in one recording, allowing to record the activity of neural populations and their spatio-temporal relationships.

The fluorescence changes are ideally detected using two-photon imaging [76]. This method allows to precisely stimulate only a specific plane, reducing phototoxicity, avoiding artifactual illumination of fly photoreceptors, increasing the penetration depth compared to one-photon microscopy, and circumvents bleaching outside of the focal plane. A femtosecond-pulsed laser is focused to a region of interest where two photons, which individually could not excite the fluorophore, coincide, leading to fluorescence of the calcium sensor, expressed in the neuron. The laser wavelength usually is in the infrared range. The exact wavelength depends on the excitation spectrum of the fluorophore. For example, when using GCaMP5 with an excitation peak around 485nm, the ideal laser wavelength would be between 900 and 950nm [50]. The usage of an infrared laser also leads to an increased penetration depth compared to one-photon microscopy.

## Behavioral Readouts

Lobula plate tangential cells project to the central brain and there are several studies which indicate that they drive optomotor driven behaviors, such as head movements and turning responses [77, 12, 10]. In order to precisely detect changes in the fly's behavior, different approaches can be used:

- Surrounded by a visual stimulation device flies can be attached to a hook that allows

stationary flight. Changes in their flight behavior can either be measured by the torque [8] or, optically, as the differences of the wing beat amplitude of the fly [78].

- Using a fly walking on a patterned styrofoam ball allows tracking of its turning responses upon visual stimulation (Figure 6C; [79]).

- More recently, it is possible to track flies with high-speed cameras while they are freely walking [80] or flying [81].

Some of these approaches can then be combined with genetic activation or inactivation

[80], calcium imaging [82] or even electrophysiology [83].

## Connectomics

Based on overlapping projection patterns observed in Golgi stainings first connectivity motifs arised. Nevertheless, to confirm synaptic contacts the resolution of light microscopy based approaches is insufficient. In the early 1930s first electron microscopes were built [84]. Electron wavelengths, compared to photon wavelengths, can be up to 100,000 times shorter, making it possible to achieve resolutions up to 50 pm (Figure 6D(a); [85]). This enables the detection of synaptic contacts of reconstructed cells (Figure 6D(b and c)). After staining the brain region of interest in a particular manner, for example with osmium, the brain is cut serially and scanned section by section [86](Figure 6D(d)). This technique is called serial sectioning Transmission Electron Microscopy (ssTEM) and was used in several studies to reconstruct the wiring of *Drosophila's* optic lobe [74, 87, 88, 89, 90, 91]. Recently, variants of this approach were described that scan the top of a resin-embedded tissue subsequently after milling the surface using either a microtome [92] or a focused ion beam [93]. Consequently, large brain areas can be reconstructed in a highly automated fashion, skipping most manual steps and automatically generating aligned serial images.

## Finding the Neural Implementation of the Motion Detector

The possibility to compare the results of modeling with visually driven behaviors and physiology made fly motion vision an attractive subject over the last decades. Never-

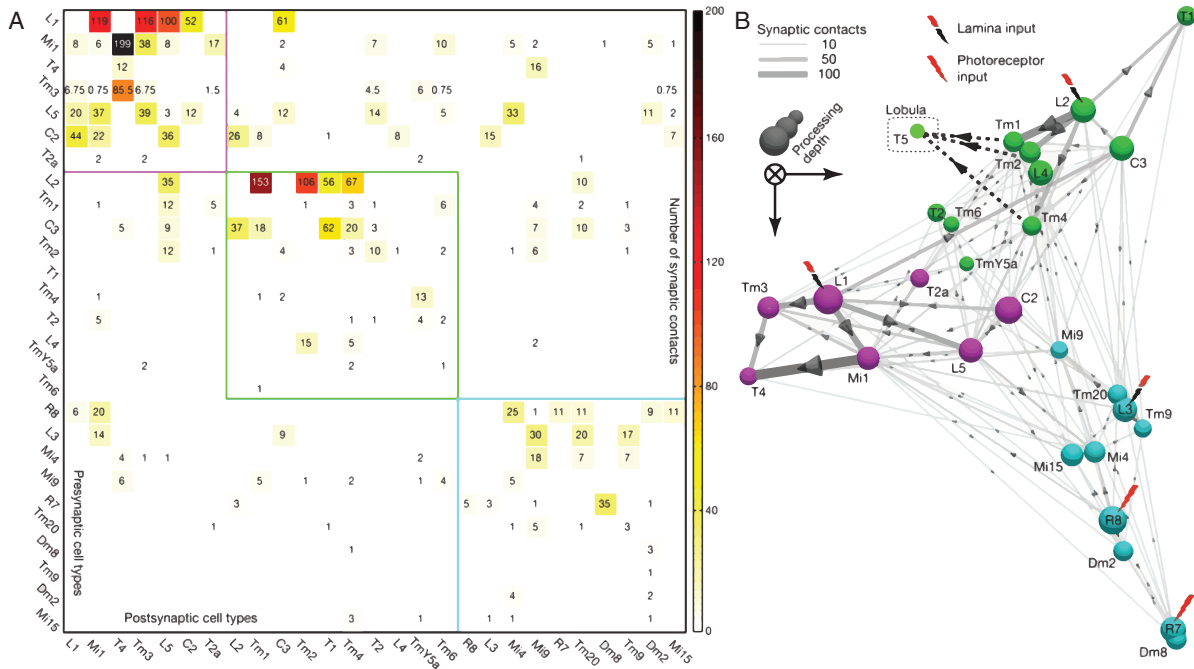


**Figure 7: Medulla Connectome Module (modified from [74]).** (A) Synaptic connectivity matrix with three identified pathways, named after their input neurons: L1 (magenta), L2 (green) and L3 (cyan). (B) Medulla connectome module as a 3D graph. Distance resembles the strength of the connection between the neurons. Colors of the spheres show to which pathway they belong.

theless, the rise of the genetic modifiability and the constantly growing genetic toolbox provided detailed insights into a possible neural representation of the motion detector in the fly optic lobe. In the following I want to give an overview of the key findings of the last years that described the function and necessity of individual elements in the fly visual system. The publications in the main section are based on this knowledge and on each other.

## ON/OFF Split and Input Elements

The first relay station of the optic lobe, the lamina, contains 12 cartridge neurons throughout the lamina's depth [87]. Most prominent are the large monopolar cells L1-L5. L1-L4 receive direct histaminergic input from photoreceptors [94, 90]. They are activated upon stimulation with luminance decreases and their activity is suppressed when stimulated with illumination [95, 96, 97, 98, 99]. L1 and L2 together have been shown to be necessary and largely sufficient for motion-dependent behavior [100]. When blocking the synaptic output of L1 and L2 separately, flies are unable to detect either moving bright edges (ON) or moving dark edges (OFF), respectively [101, 98]. Notably, L1 is inhibitory (glutamatergic) and L2 excitatory (cholinergic) [89], resulting in a postsynaptic sign inversion of the similarly responding cells, which explains how they can be seen as the input elements for the ON and the OFF pathway [102]. Interestingly, L1/L5 and cholin-

ergic L2/L4 are strongly interconnected [89, 103]. L3 on the other hand projects without further contacts within the lamina to the medulla [103]. The other seven cell types rather serve modulatory functions via feedback and wide-field signals [104, 105]. Taken together, this shows that a split in different functional pathways is already present at the level of the lamina and further conveyed to the medulla. The presence of different retinotopic pathways in the medulla was already proposed by the analysis of the cells' projection patterns using Golgi stainings [65]. Later, electron microscopy studies confirmed the pathway splitting by dense reconstruction, revealing the contacts of the medullary elements by chemical synapses (for detailed information see Figure 7; [89, 74, 103]). ON pathway elements of the medulla are Mi1, Mi4, Mi9, and Tm3, giving input to T4 cells [103]. In the OFF pathway on the other hand Tm1, Tm2, and Tm4 receive input from L2. Additionally, Tm2 and Tm4 are innervated by L4 [89]. L3 synapses solely onto Tm9 [74]. All four Tm cell types are thought to be cholinergic [89, 91] and synapse onto T5 cells showing a convergence of two initially split pathways. Together they make up nearly 90% of T5's input with Tm2 being numerically the strongest, followed by Tm9, Tm1, and Tm4 [91]. Douglass and Strausfeld (1995) were able to electrically record from the cell type Tm1 in the blowfly [106]. Noteworthy, Tm1 in *Calliphora* corresponds to Tm2 in *Drosophila*. They depolarize upon stimulation with brightness decrements and respond in a non-direction-selective manner upon stimulation with moving gratings [106].

In the first two publications of the main section we investigated the involvement of the four Tm cells in the motion detection circuitry. Therefore, we characterized their spatial and temporal response properties via calcium imaging and analyzed the necessity of the elements by blocking their synaptic outputs while recording from downstream lobula plate tangential cells or monitoring the flies' optomotor response upon visual stimulation.

## T4/T5-Output

As described above, in the ON as well as in the OFF pathway, four cells give input to T4 and T5 cells, respectively. Both send their axons to the four layers of the lobula plate. Deoxyglucose autoradiographs revealed that each layer is active for motion in one of the four cardinal directions [67]. The first for front-to-back, the second for back-to-front, the third for upward and the fourth for downward motion. Silencing their synaptic output turns lobula plate tangential cells motion insensitive [107] and walking flies motion blind [108]. Interestingly, walking flies with silenced T4 and T5 cells are still able to track objects [108].

In the publications three to six of the main part, we analyzed their response properties and their function in the motion detection pathway as well as in the contrast vision circuitry. Furthermore, we looked at differences between the two cell types, their neurotransmitters and a possible connectivity motif within the lobula plate.

# Manuscript Nr. 1: Comprehensive Characterization of the Major Presynaptic Elements to the *Drosophila* OFF Motion Detector

Etienne Serbe<sup>\*</sup>, Matthias Meier<sup>\*</sup>, Aljoscha Leonhardt, and Alexander Borst

<sup>\*</sup>equal contribution

Author Contributions:

**E.S.** and M.M. jointly performed and evaluated all calcium imaging and electrophysiology experiments. A.L. performed and evaluated the behavioral experiments. A.L. and A.B. performed computer simulations. A.B., **E.S.**, and M.M. designed the study. **E.S.** and M.M. wrote the manuscript with the help of the other authors.



## Neuron

### Comprehensive Characterization of the Major Presynaptic Elements to the *Drosophila* OFF Motion Detector

#### Highlights

- All *Drosophila* OFF motion pathway Tm cells are activated by brightness decrements
- None of the four cell types are direction selective
- Tm1, Tm2, Tm4, and Tm9 display a variety of temporal filter properties
- The four Tm cells are involved in OFF motion processing to different degrees

#### Authors

Etienne Serbe, Matthias Meier, Aljoscha Leonhardt, Alexander Borst

#### Correspondence

serbe@neuro.mpg.de (E.S.),  
mmeier@neuro.mpg.de (M.M.)

#### In Brief

Serbe et al. use calcium imaging, electrophysiology, and behavior to assess the roles of columnar elements in the OFF motion vision pathway of *Drosophila*. Here, the complex interaction of four cell types shapes the flies' responses to motion stimuli.

Please cite this article in press as: Serbe et al., Comprehensive Characterization of the Major Presynaptic Elements to the *Drosophila* OFF Motion Detector, *Neuron* (2016), <http://dx.doi.org/10.1016/j.neuron.2016.01.006>

Neuron  
Article

CellPress

## Comprehensive Characterization of the Major Presynaptic Elements to the *Drosophila* OFF Motion Detector

Etienne Serbe,<sup>1,2,\*</sup> Matthias Meier,<sup>1,2,\*</sup> Aljoscha Leonhardt,<sup>1</sup> and Alexander Borst<sup>1</sup>

<sup>1</sup>Max-Planck-Institute of Neurobiology, Am Klopferspitz 18, 82152 Martinsried, Germany

<sup>2</sup>Co-first author

\*Correspondence: [serbe@neuro.mpg.de](mailto:serbe@neuro.mpg.de) (E.S.), [mmeier@neuro.mpg.de](mailto:mmeier@neuro.mpg.de) (M.M.)

<http://dx.doi.org/10.1016/j.neuron.2016.01.006>

### SUMMARY

Estimating motion is a fundamental task for the visual system of sighted animals. In *Drosophila*, direction-selective T4 and T5 cells respond to moving brightness increments (ON) and decrements (OFF), respectively. Current algorithmic models of the circuit are based on the interaction of two differentially filtered signals. However, electron microscopy studies have shown that T5 cells receive their major input from four classes of neurons: Tm1, Tm2, Tm4, and Tm9. Using two-photon calcium imaging, we demonstrate that T5 is the first direction-selective stage within the OFF pathway. The four cells provide an array of spatiotemporal filters to T5. Silencing their synaptic output in various combinations, we find that all input elements are involved in OFF motion detection to varying degrees. Our comprehensive survey challenges the simplified view of how neural systems compute the direction of motion and suggests that an intricate interplay of many signals results in direction selectivity.

### INTRODUCTION

Extracting the direction of visual motion is an essential operation for most animals to successfully perform tasks like navigation, prey capture, predator avoidance, and mating. Correlation-type motion detectors represent a class of algorithmic models that achieve direction selectivity by multiplying signals from two adjacent photoreceptors after asymmetric temporal filtering (Figure 1A; Hassenstein and Reichardt, 1956). In various vertebrate and invertebrate species, this is realized separately for brightness increments (ON) and decrements (OFF; Werblin and Dowling, 1969; Joesch et al., 2010; Borst and Euler, 2011). In the mouse retina, for example, direction selectivity in OFF-type starburst amacrine cells is proposed to arise from spatially offset bipolar cell input (Kim et al., 2014). These cells exhibit temporally diverse calcium (Baden et al., 2013) and glutamate release signals (Borghuis et al., 2013). In *Drosophila melanogaster*, photoreceptor signals are processed in a retinotopic way within

the four neuropils of the optic lobe, called lamina, medulla, lobula, and lobula plate (Figure 1B). In the lobula plate, wide-field tangential cells respond to motion stimuli in a fully opponent, direction-selective manner: they depolarize to motion along their preferred direction (PD) and hyperpolarize to motion along the opposite or null direction (ND; Joesch et al., 2008; Schnell et al., 2010). Tangential cells receive excitatory cholinergic input from two types of neurons, called T4 and T5 cells (Mauss et al., 2014). They were first described via Golgi stainings (Cajal and Sánchez, 1915) and exist in four subtypes, depending on their projection layer in the lobula plate (Figure 1B; Fischbach and Dittrich, 1989). Genetically silencing both cell types turns tangential cells motion insensitive and walking flies motion blind (Schnell et al., 2012; Bahl et al., 2013). Each of the four subtypes responds only to either brightness increments (ON for T4) or decrements (OFF for T5), moving in one of the four cardinal directions (front to back, back to front, upward, and downward). Blocking either T4 or T5 results in selectively diminished responses of lobula plate tangential cells to ON and OFF stimuli, respectively (Maisak et al., 2013). The splitting of ON and OFF signals starts at the level of lamina monopolar cells, which receive direct input from photoreceptors. L1 signals feed into the ON pathway; L2–L4 signals feed into the OFF pathway (Joesch et al., 2010, 2013; Clark et al., 2011; Eichner et al., 2011; Takemura et al., 2011; Silies et al., 2013; Meier et al., 2014). Electron microscopy reconstructions identified the primary interneurons that connect lamina monopolar cells to the dendrites of T4 and T5 cells. L1 synapses mainly onto the medulla intrinsic neuron Mi1 and onto the transmedulla neuron Tm3, which both contact T4 cells (Takemura et al., 2013). In the OFF pathway, reciprocally connected L2 and L4 cells (Riviera-Alba et al., 2011) connect to Tm1, Tm2, and Tm4 cells while L3 cells synapse onto Tm9 cells (Figure 1B; Takemura et al., 2013). These four Tm cells have been described as cholinergic and collectively account for nearly 90% of T5 input synapses, with Tm2 being the numerically dominant input (~33%), followed by Tm9 (~22%), Tm1 (~20%), and Tm4 (~13%; Takemura et al., 2011; Shinomiya et al., 2014). Calcium imaging and electrophysiological recordings revealed that Tm1 and Tm2 respond to OFF stimuli with transient activation, independent of the direction of motion (Meier et al., 2014; Strother et al., 2014; Behnia et al., 2014). Their dynamic properties, estimated using a white-noise stimulus, revealed an offset in peak response times of 13 ms. This led to the suggestion that Tm1 and Tm2 cells form the

# Comprehensive Characterization of the Major Presynaptic Elements to the *Drosophila* OFF Motion Detector

Please cite this article in press as: Serbe et al., Comprehensive Characterization of the Major Presynaptic Elements to the *Drosophila* OFF Motion Detector, *Neuron* (2016), <http://dx.doi.org/10.1016/j.neuron.2016.01.006>

CellPress

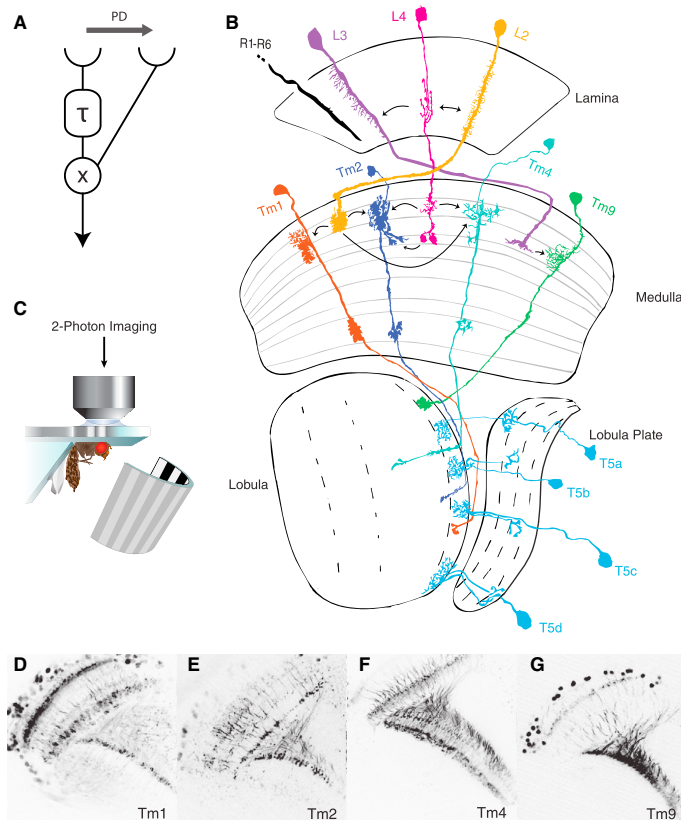


**Figure 1. The OFF Pathway of *Drosophila* Motion Vision**

(A) Schematic representation of a subunit of a Hassenstein-Reichardt correlator tuned to rightward motion (preferred direction, PD). Signals from two spatially offset inputs are multiplied (X) after one of them has been temporally delayed by a low-pass filter with the time constant  $\tau$ .

(B) Wiring diagram of the proposed OFF pathway neurons. Photoreceptors R1–R6 project onto interconnected lamina monopolar cells L2 (yellow), L3 (purple), and L4 (magenta). The L2–L4 sub-pathway consists of transmedullary neurons Tm2 (dark blue) and Tm4 (cyan). L3 contacts Tm9 cells (green). Tm1 (orange) only receives input via L2 (yellow). All four Tm cells project into the lobula, giving input to the four subtypes of T5 (light blue). Arrows indicate synaptic contacts between cell types. (Modified from Fischbach and Dittrich, 1989.)

(C) Experimental setup for two-photon calcium imaging.

(D–G) Contrast-inverted maximum intensity z projections of two-photon image stacks through the optic lobe of flies expressing GCaMP6f in Tm1 (D), Tm2 (E), Tm4 (F), and Tm9 (G) cells.

two input lines of an OFF elementary motion detector (Behnia et al., 2014). Indeed, blocking Tm2 cells strongly reduces the responses of tangential cells to moving dark edges (Meier et al., 2014). Whether Tm1 is equally critical has not been clarified; neither have the roles of the other two input neurons, Tm4 and Tm9. We therefore set out to explore the response properties and necessity of all four major inputs to T5 cells, which constitutes a crucial step toward a mechanistic understanding of how direction selectivity is computed in the OFF pathway of *Drosophila*.

First, we performed two-photon calcium imaging (Figure 1C) to assess the visual response properties of all major T5 inputs, including direction selectivity, response dynamics, and receptive fields. Second, we blocked the synaptic output of single-cell types, as well as combinations of two-cell types, using *shibire<sup>ts</sup>* (Kitamoto, 2001) and analyzed responses of tangential cells and walking flies to visual motion stimuli. Our results demonstrate that all four Tm cell types are activated by brightness decrements, irrespective of the direction of motion, confirming the notion that T5 cells are the first direction-selective cells within the OFF pathway (Maisak et al., 2013;

Fisher et al., 2015). Their responses revealed substantially different temporal dynamics. Blocking their synaptic output individually and in combination exclusively impaired OFF motion vision, though by different magnitudes. Combinatorial blocking of two Tm cell types resulted in an increased reduction of the OFF motion response. These data do not map easily onto classical models of motion detection involving two input

## RESULTS

### Response Properties of Tm1, Tm2, Tm4, and Tm9 Cells

To directly examine the response properties of Tm cells, we expressed calcium indicator GCaMP5 (Akerboom et al., 2012) under the control of cell-type-specific Gal4 lines (Brand and Perrimon, 1993). We manually chose regions of interest that corresponded to single axonal terminals in the lobula where T5 dendrites are located (Figures 1D–1G) and determined the fluorescence change during visual stimulation. First, we characterized the calcium responses of T5's presynaptic elements by presenting edges of both polarities (ON and OFF edges) moving in the four cardinal directions. With these visual stimuli, we addressed two questions: First, are neurons upstream of T5 cells direction selective? Second, do they exhibit rectified responses with respect to the contrast polarity of the stimulus? In agreement with previous studies (Meier et al., 2014; Strother et al., 2014; Behnia et al., 2014), we found that Tm1 and Tm2 cells

# Comprehensive Characterization of the Major Presynaptic Elements to the *Drosophila* OFF Motion Detector

Please cite this article in press as: Serbe et al., Comprehensive Characterization of the Major Presynaptic Elements to the *Drosophila* OFF Motion Detector, *Neuron* (2016), <http://dx.doi.org/10.1016/j.neuron.2016.01.006>

CellPress

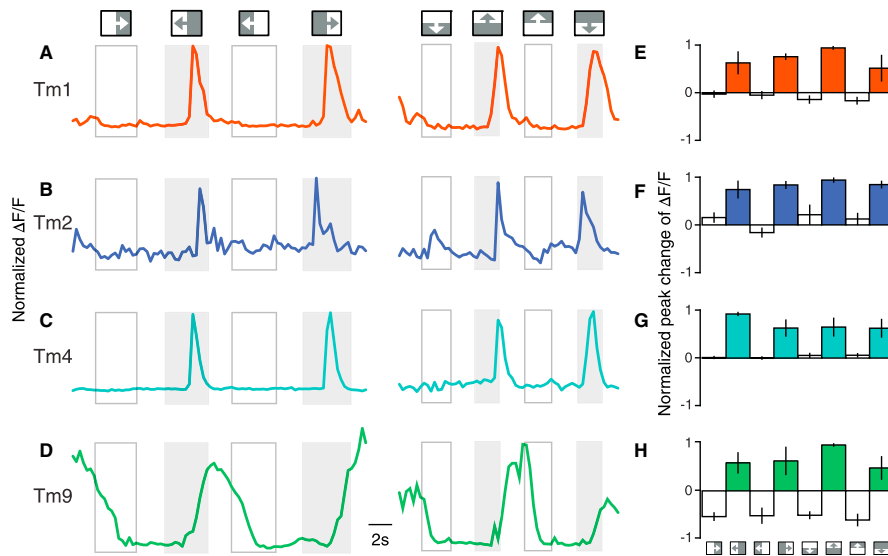


**Figure 2. OFF Edges Activate Tm Cells Irrespective of the Direction of Motion**

(A–D) Normalized  $\Delta F/F$  calcium responses of single Tm1 (A), Tm2 (B), Tm4 (C), and Tm9 (D) cells. Flies were visually stimulated with ON and OFF edges moving horizontally (left panel) and vertically (right panel). Empty boxes indicate stimulation periods of ON edge motion; gray boxes indicate stimulation periods of OFF edge motion. Directions and polarity of edge motion are illustrated by little boxes on top. Between stimulations, luminance levels remain constant; i.e., after presentation of OFF edges, the stimulation device remains dark until the subsequent ON stimulus. After presentation of ON edges, the arena remains bright. (E–H) Average normalized peak changes in calcium signals during edge presentation. Stimuli are represented at the bottom of (H). Tm1 (E;  $n = 11$  cells in  $N = 11$  flies), Tm2 (F;  $n = 8$ ,  $N = 8$ ), Tm4 (G;  $n = 9$ ,  $N = 9$ ), and Tm9 (H;  $n = 8$ ,  $N = 8$ ). Error bars indicate  $\pm$  SEM.

See also Figure S7.

respond to moving brightness decrements (OFF edges) with a transient increase in calcium, independent of the direction of motion. In this experiment, neither Tm1 nor Tm2 cells showed any response when stimulated with moving brightness increments (ON edges; Figures 2A and 2B). Tm4 cells exhibited similar characteristics with short increases of activity when stimulated with OFF edges moving along all four cardinal directions (Figure 2C). The calcium levels of Tm9, however, changed more tonically, inversely following the local luminance level: when presented with a moving ON edge, the cell's initial calcium level dropped, and it only increased when a dark edge was moved through the fly's visual field (Figure 2D). Again, this was true for all four directions. To quantify the calcium responses to moving edges—and to detect increases, as well as decreases—we calculated the extremum (maximum or minimum) of the derivative of the fluorescence change for each stimulus (Figures 2E–2H). This demonstrated that all transmedullary neurons, anatomically identified to be presynaptic to T5, are not themselves direction selective and respond with increased activity to visual stimulation with dark edges. The response kinetics of the different Tm cells, however, looked qualitatively different. To more precisely characterize the temporal properties of Tm cells and to investigate whether the four cell types exhibit rectified responses with respect to contrast polarity, we increased the temporal resolution of the scanning microscope from 1.8 to 480 Hz by

acquiring data from a single line through one axonal arbor in the lobula. Moreover, we expressed a faster calcium indicator, GCaMP6f (Chen et al., 2013), in the Tm cells. We used a  $4.5^\circ$ -wide, dark, vertical bar appearing and disappearing on a bright background for seven durations (50, 75, 125, 225, 425, 825, and 1,625 ms). All four Tm cells responded with an increase in calcium levels to local brightness decrements (Figures 3A–3D). Consistent with the edge stimulation results, this set of experiments revealed a broad range of response kinetics for the four Tm cell types. Furthermore, we observed a drop in calcium signaling upon stimulus offset. Based on these observations, we simulated their responses by fitting a three-stage filter model to the mean calcium traces (Figure 3E). Within this model, inputs were first linearly high-pass filtered ( $\tau_{HP}$ ), then rectified by setting negative values to zero, and finally low-pass filtered ( $\tau_{LP}$ ). Using this simple model, we were able to reproduce the measured calcium dynamics and estimate filter time constants for each cell type from the observed responses (Figures 3F–3I). In agreement with the data from the stimulation with moving edges, the four cell types could be classified in three groups: fast, transient Tm2 ( $\tau_{HP} = 0.36$  s and  $\tau_{LP} = 0.1$  s; Figures 3B and 3G) and Tm4 ( $\tau_{HP} = 0.25$  s and  $\tau_{LP} = 0.2$  s; Figures 3C and 3H), intermediate Tm1 ( $\tau_{HP} = 1.23$  s and  $\tau_{LP} = 0.23$  s; Figures 3A and 3F), and tonic Tm9 ( $\tau_{LP} = 0.63$  s; Figures 3D and 3I). In contrast to the other cell types, the slow dynamics of Tm9 responses were best predicted

# Comprehensive Characterization of the Major Presynaptic Elements to the *Drosophila* OFF Motion Detector

Please cite this article in press as: Serbe et al., Comprehensive Characterization of the Major Presynaptic Elements to the *Drosophila* OFF Motion Detector, *Neuron* (2016), <http://dx.doi.org/10.1016/j.neuron.2016.01.006>

CellPress

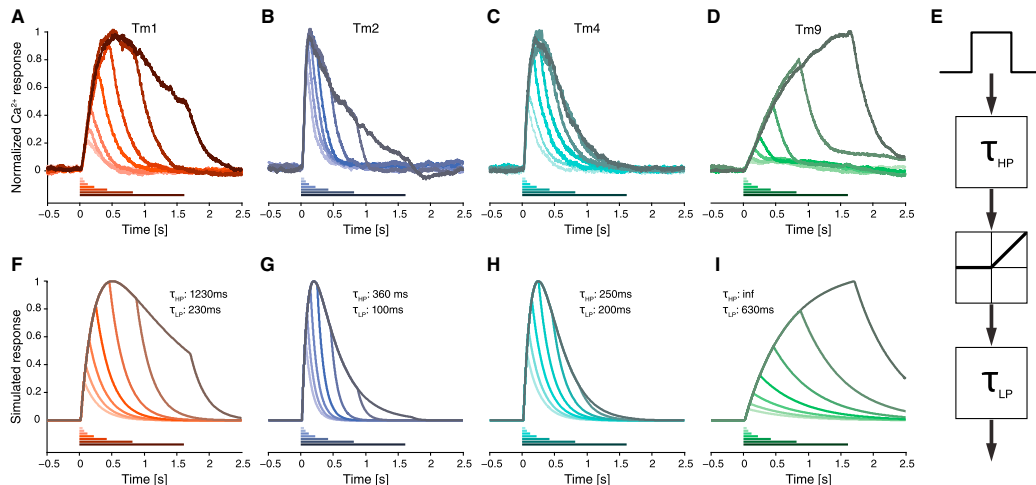


**Figure 3. Temporal Tm Cell Response Properties**

(A–D) Normalized  $\Delta F/F$  calcium responses of Tm1 (A;  $n = 32$ ,  $N = 5$ ), Tm2 (B;  $n = 38$ ,  $N = 5$ ), Tm4 (C;  $n = 26$ ,  $N = 3$ ), and Tm9 (D;  $n = 44$ ,  $N = 4$ ), obtained by line scans through individual axonal arbors. Flies were presented with a  $4.5^\circ$ -wide, dark, vertical bar appearing on a bright background for seven periods: 50, 75, 125, 225, 425, 825, and 1,625 ms. Color-coded bars at the bottom of the graphs indicate the duration of stimulus presentation.

(E) Simulation procedure. The input signals were high-pass filtered ( $\tau_{HP}$ ), rectified, and low-pass filtered ( $\tau_{LP}$ ). Filter time constants are indicated in each panel. (F–I) Simulated responses of Tm1 (F), Tm2 (G), Tm4 (H), and Tm9 (I) obtained by using the indicated time constants for the low-pass and high-pass filtering. For Tm9, no high-pass filtering was applied.

See also Figures S1 and S7.

by a pure low-pass filter. Also, prolonging the period of stimulus presentation to 2 and 4 s supported the finding that Tm9 cells respond tonically to visual stimulation with dark bars (Figure S1). To exclude that calcium buffering caused the slow dynamics of the Tm9 responses, we repeated the experiments using flies heterozygous for Gal4 and upstream activating sequence (UAS)-GCaMP6f to reduce expression levels of GCaMP. Here, we obtained the same results. In summary, the preceding results demonstrate that Tm1, Tm2, Tm4, and Tm9 are directionally unselective and thus confine the computation of direction selectivity in the OFF pathway to the dendrites of T5 cells. Furthermore, our data indicate that Tm cells provide a variety of temporal filters, ranging from fast, transient Tm2 and Tm4 over intermediate Tm1 to slow and sustained Tm9 cells.

## Receptive Field Characteristics of Tm1, Tm2, Tm4, and Tm9

Current models for motion detection are based on the spatio-temporal correlation of input signals. It is thus crucial to characterize receptive field sizes and spatial integration properties of columnar neurons. To probe the receptive fields of the four Tm cells, we recorded changes in fluorescence at a lower temporal resolution of 1.8 Hz. Because our previous experiments (Figures 2 and 3) had revealed that all four cell types respond to changes in local luminance, we stimulated flies with  $4.5^\circ$ -wide, dark, vertical bars flickering on a bright background with 0.5 Hz at different azimuthal positions, each shifted by  $1.5^\circ$ . All

four Tm cells tested with this stimulus exhibited similar receptive field sizes, ranging from  $4.2^\circ$  to  $5.5^\circ$  of half-width (Figures 4A–4E). We next used horizontal bars and presented them at different elevations. Again, we found comparable receptive field sizes with half-widths between  $3.9^\circ$  and  $4.2^\circ$  (Figure 4E). From this, we conclude that Tm1, Tm2, Tm4, and Tm9 cells have small isotropic receptive fields. The size of the measured receptive fields approximately corresponded to the visual acceptance angle of one neuro-ommatidium (Götz, 1964; Land, 1997), which indicates that the main activation of Tm cells is restricted to visual information detected by only one ommatidium. Stimulating the fly's eye in consecutive steps along the azimuth with terminals of several adjacent Tm9 cells in focus nicely revealed the retinotopic organization of columnar elements projecting from the medulla to the lobula (Movie S1). Next, we investigated spatial integration properties by centering a flickering dark, vertical bar at the position of maximal excitability of individual Tm cells. After each period of stimulation, we increased the width of the bar. All four cell types showed maximum responses when stimulated with bars of a  $4.5^\circ$  to  $7.5^\circ$  width but decreased activity when presented with stimuli spanning larger areas in visual space (Figures 4F–4I). Hence, all cells seem to be subject to lateral inhibition, preventing them from responding to wide-field flicker. The responses of Tm9 cells diverged from the other cell types for full-field stimulation ( $180^\circ$  azimuth): while the calcium response levels elicited by flicker between a  $13.5^\circ$  and a  $67.5^\circ$  width were small, the response to full-field darkening amounted

# Comprehensive Characterization of the Major Presynaptic Elements to the *Drosophila* OFF Motion Detector

Please cite this article in press as: Serbe et al., Comprehensive Characterization of the Major Presynaptic Elements to the *Drosophila* OFF Motion Detector, *Neuron* (2016), <http://dx.doi.org/10.1016/j.neuron.2016.01.006>

CellPress

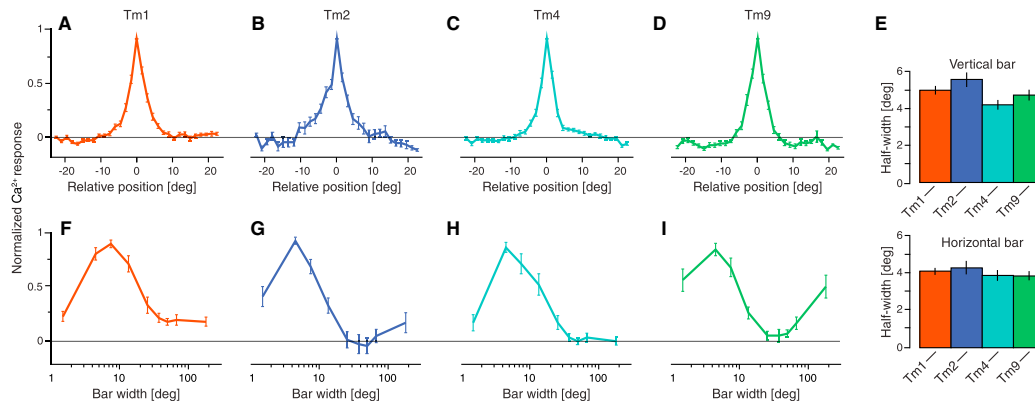


**Figure 4. Receptive Field Properties of Tm Cells**

(A–D) Spatial receptive fields measured by normalized calcium responses of Tm1 (A; n = 45, N = 10), Tm2 (B; n = 29, N = 8), Tm4 (C; n = 30, N = 5), and Tm9 (D; n = 31, N = 8) to 4.5°-wide, dark, vertical bars appearing and disappearing at various positions (shifted by 1.5°) on a bright background at a frequency of 0.5 Hz. (E) Quantification of receptive field half-width for vertical bars (top panel) and horizontal bars (bottom panel). Tm1 (n = 37, N = 8), Tm2 (n = 26, N = 6), Tm4 (n = 20, N = 3), and Tm9 (n = 24, N = 3).

(F–I) Spatial integration properties measured by normalized calcium responses of Tm1 (F; n = 15, N = 9), Tm2 (G; n = 16, N = 7), Tm4 (H; n = 9, N = 4), and Tm9 (I; n = 9, N = 4) to dark, vertical bars of increasing size (bar widths: 1.5°, 4.5°, 7.5°, 13.5°, 25.5°, 37.5°, 49.5°, 67.5°, and 180°). Error bars indicate  $\pm$  SEM. See also [Figure S7](#).

to approximately 50% of the maximum response. Tm9 has been shown to receive its main synaptic inputs through a different set of neurons from those for Tm1, Tm2, and Tm4 (L3 for Tm9, compared to L2 for Tm1, Tm2, and Tm4; [Takemura et al., 2013](#)). Together with the particular spatial integration property, the anatomical distinctness of Tm9 suggests that lateral inhibition could be implemented by two different mechanisms in the OFF pathway. Taken together, using calcium levels as a proxy for neuronal activity, we established that Tm1, Tm2, Tm4, and Tm9 are small-field columnar neurons that receive isotropic lateral inhibition.

## Blocking OFF Pathway Tm Cells Reduces Responses of Lobula Plate Tangential Cells Specifically to OFF Edges

The response properties of *Drosophila* lobula plate tangential cells have been well characterized using various visual stimuli ([Joesch et al., 2008, 2010; Schnell et al., 2010; Mauss et al., 2015](#)). Furthermore, these large-field interneurons have been demonstrated to receive excitatory input from T4 and T5 cells ([Schnell et al., 2012; Mauss et al., 2014](#)). Hence, responses of lobula plate tangential cells can be used as a readout to assess the contribution of presynaptic elements within the motion detection circuit ([Joesch et al., 2010; Schnell et al., 2012; Maisak et al., 2013; Meier et al., 2014](#)). We performed somatic whole-cell patch clamp recordings from tangential cells of the vertical system (VS) and horizontal system (HS) while blocking the output of different Tm cells. We stimulated flies with either multiple ON or OFF edges ([Figure S7](#)). Synaptic transmission was silenced by expressing temperature-sensitive *shibire<sup>ts</sup>* ([Pfeiffer et al., 2012](#)) under the control of specific Gal4 driver lines. We confirmed the identities of cell types in the Gal4 lines by expressing GFP

in a small subset of neurons using a flip-out approach ([Figures 5A–5D; Nern et al., 2015](#)). To increase block strength without a loss of expression specificity, we used flies with two copies of UAS-*shibire<sup>ts</sup>* (*shi<sup>ts</sup>/shi<sup>ts</sup>*) and one copy of the Gal4 driver. Tangential cells of control flies responded with approximately equal strength to motion of bright or dark edges ([Figures 5E–5H](#)). We could thus use these stimuli to probe contrast-polarity-specific effects of Tm cell blocks. Based on the diversity of temporal response properties observed in our calcium imaging experiments reported earlier, we hypothesized that different Tm cell types may play distinct roles depending on motion velocity, as was recently shown for input elements to the ON direction-selective T4 cells ([Ammer et al., 2015](#)). We therefore tested flies using edges moving at nine velocities across two orders of magnitude (3.125°/s–800°/s; [Figure S2](#)). When Tm1 was removed from the circuit, lobula plate tangential cells responded only with about half of the magnitude of control flies to moving dark edges ([Figures 5E and 5I](#)). In agreement with a previous study, responses were strongly reduced when Tm2 was blocked ([Meier et al., 2014](#)). Both effects were present over all velocities tested ([Figures 5F and 5J](#)). Blocking Tm4 produced the weakest phenotype ([Figures 5G and 5K](#)). Interrupting Tm9 signaling resulted in the strongest effect of all cells tested and, as with the other cells, did so consistently across all stimulus velocities ([Figures 5H and 5L](#)). To our surprise, here, we did not find differential effects of blocking any of the four Tm cell types when using different edge velocities. To compare the overall effects of silencing single Tm cells, we calculated the average response relative to control flies over the whole range of stimulus velocities ([Figures 5M–5P](#)). Critically, in all silencing experiments, responses to ON edges were not significantly altered. Blocking

# Comprehensive Characterization of the Major Presynaptic Elements to the *Drosophila* OFF Motion Detector

Please cite this article in press as: Serbe et al., Comprehensive Characterization of the Major Presynaptic Elements to the *Drosophila* OFF Motion Detector, *Neuron* (2016), <http://dx.doi.org/10.1016/j.neuron.2016.01.006>

CellPress

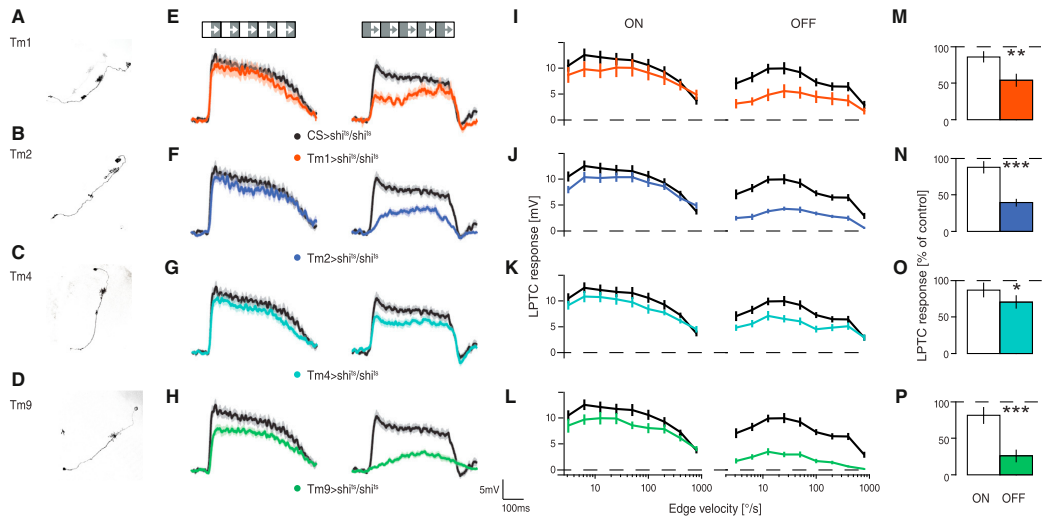


## Figure 5. Blocking Tm Cells Impairs OFF Motion Vision

(A–D) Stochastic labeling of single Tm1 (A), Tm2 (B), Tm4 (C), and Tm9 (D) cells, showing the specificity of the Gal4 driver lines.

(E–H) Example traces of mean responses to motion along the PD minus the response to motion along the ND of lobula plate tangential cell (LPTC) responses upon stimulation with multiple ON (left) and OFF (right) edges (50°/s) in control CS > shi<sup>19</sup>/shi<sup>19</sup> (black), Tm1 > shi<sup>19</sup>/shi<sup>19</sup> (E), Tm2 > shi<sup>19</sup>/shi<sup>19</sup> (F), Tm4 > shi<sup>19</sup>/shi<sup>19</sup> (G), and Tm9 > shi<sup>19</sup>/shi<sup>19</sup> (H) flies. Stimulus presentation is indicated by the panels on top.

(I–L) Mean PD-ND LPTC responses of control (black), Tm1 (J), Tm2 (K), Tm4 (L), and Tm9 (L) block flies upon ON (left panel) and OFF edge (right panel) stimulation for nine velocities (3.125°/s, 6.25°/s, 12.5°/s, 25°/s, 50°/s, 100°/s, 200°/s, 400°/s, and 800°/s).

(M–P) Responses averaged over all nine velocities of Tm1 (M), Tm2 (N), Tm4 (O), and Tm9 (P) block flies plotted as percentages of the controls. Responses were obtained from HS and VS cells. Because no difference was detected, data from both cell types were pooled. CS > shi<sup>19</sup>/shi<sup>19</sup> data are from 13 cells (5 HS, 8 VS) in 5 flies, Tm1 block data are from 10 cells (3 HS, 7 VS) in 7 flies, Tm2 block data are from 14 cells (7 HS, 7 VS) in 7 flies, Tm4 block data are from 16 cells (5 HS, 11 VS) in 9 flies, and Tm9 block data are from 15 cells (3 HS, 12 VS) in 8 flies. In all four Tm cell blocks, ON responses are not significantly reduced in comparison to control flies. OFF responses, however, are reduced at different significance levels. \*p < 0.05, \*\*p < 0.01, \*\*\*p < 0.001, tested using two-tailed t tests against the controls. Error shades and error bars indicate ± SEM. See also Figures S2–S4 and S7.

any of the four Tm cell types specifically impaired the responses of lobula plate tangential cells to moving dark edges, irrespective of stimulus velocity. The magnitude of effects, however, covered a wide range, with strong phenotypes for Tm9 (25.69% ± 6.37% of control, mean ± SEM, n = 15 recordings, p < 0.001) and Tm2 (39.22% ± 4.50%, n = 14, p < 0.001), intermediate effects for Tm1 (53.98% ± 8.33%, n = 10, p < 0.01), and a weak phenotype for silencing Tm4 (70.59% ± 8.41%, n = 16, p < 0.05).

## Combinatorial Blocking of Tm Cells Increases OFF Edge Phenotypes

Tm cells could contribute in parallel or modularly to direction selectivity in T5. Combining two cell-specific Gal4 lines, thereby driving the expression of *shibire<sup>ts</sup>* in two cell populations simultaneously, allowed us to investigate how different Tm cells interact. To detect potential synergistic effects, we decreased individual blocking strength by using flies with only one copy of *shibire<sup>ts</sup>* (shi<sup>19</sup>/+). When we repeated the same experiment as described earlier, the tangential cell responses of Tm1 block flies to dark-edge stimulation were only reduced to 76.29% ± 7.88% (percent of control, n = 11, p = 0.18; Figures 6A and 6B) as opposed to 54% for two copies of *shibire<sup>ts</sup>*. Blocking Tm2 with one copy of

*shibire<sup>ts</sup>* resulted in a response reduction to 69.13% ± 4.25% (n = 11, p = 0.07; Figures 6G and 6H), while blocking Tm4 cells did not result in a detectable reduction of tangential cell responses (89.17% ± 7.95%, n = 12, p = 0.50; Figures 6M and 6N). Only responses of Tm9 block flies to dark edges remained significantly different from those of control flies (51.39% ± 6.02%, n = 10, p < 0.01; Figures 6S and 6T), even with only one copy of *shibire<sup>ts</sup>*. Overall, we found that the effect size was reduced while relative effects remained the same, with blocking Tm9 resulting in the strongest reduction of the OFF response, followed by Tm2, Tm1, and finally Tm4. This offered an opportunity to compare partial single-cell blocks with the combinations of two incompletely blocked classes of neurons. The images in Figure S3 provide an overview of the expression patterns of the six binary combinations of the four Tm cell types. Combining Tm9 with one of the other three cell types resulted in the strongest reductions of tangential cell responses to OFF edges (Figures 6E, 6J, and 6O–6R). All three Tm9 combinations decreased responses beyond what we had determined for the single Tm9 block. Furthermore, Tm1/Tm2 and Tm2/Tm4 blocks reduced the responses of lobula plate tangential cells to moving dark stimuli (Figures 6C, 6F, 6I, and 6L) compared to the isolated

# Comprehensive Characterization of the Major Presynaptic Elements to the *Drosophila* OFF Motion Detector

Please cite this article as: Serbe et al., Comprehensive Characterization of the Major Presynaptic Elements to the *Drosophila* OFF Motion Detector, *Neuron* (2016), <http://dx.doi.org/10.1016/j.neuron.2016.01.006>

CellPress

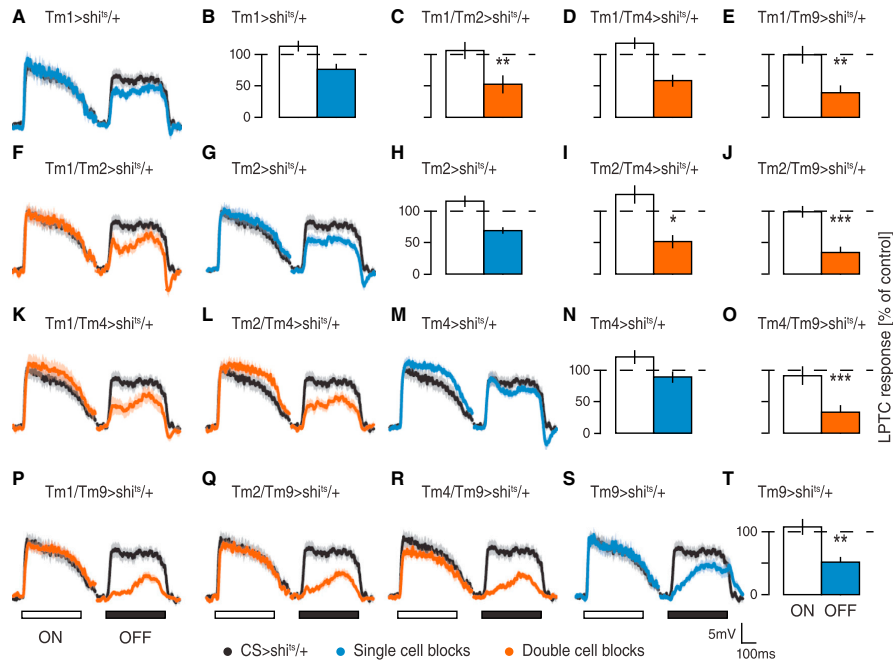


**Figure 6. Combinatorial Blocking of Tm Cells**

(A, F, G, K–M, and P–S) Mean traces of control (black), single-block (blue), and double-block (orange) flies for ON (left) and OFF (right) edge stimulation at a representative velocity of 50°/s.

(B–E, H–J, N, O, and T) Mean ON and OFF lobula plate tangential cell (LPTC) responses of single (blue) and double (orange) Tm cell block flies compared to control flies over nine velocities. Control CS > shi<sup>ts</sup>/+ data are from 13 cells (5 HS, 8 VS) in 5 flies, Tm1 > shi<sup>ts</sup>/+ data are from 11 cells (4 HS, 7 VS) in 6 flies, Tm2 > shi<sup>ts</sup>/+ data are from 13 cells (6 HS, 7 VS) in 9 flies, Tm4 > shi<sup>ts</sup>/+ data are from 12 cells (4 HS, 8 VS) in 6 flies, Tm9 > shi<sup>ts</sup>/+ data are from 10 cells (3 HS, 7 VS) in 7 flies, Tm1/Tm2 > shi<sup>ts</sup>/+ data are from 11 cells (3 HS, 8 VS) in 7 flies, Tm1/Tm4 > shi<sup>ts</sup>/+ data are from 11 cells (4 HS, 7 VS) in 7 flies, Tm1/Tm9 > shi<sup>ts</sup>/+ data are from 10 cells (3 HS, 7 VS) in 7 flies, Tm2/Tm4 > shi<sup>ts</sup>/+ data are from 13 cells (3 HS, 10 VS) in 7 flies, Tm2/Tm9 > shi<sup>ts</sup>/+ data are from 12 cells (4 HS, 8 VS) in 8 flies, and Tm4/Tm9 > shi<sup>ts</sup>/+ data are from 10 cells (3 HS, 7 VS) in 7 flies. In all block flies, ON responses are not significantly reduced in comparison to control flies. OFF responses, however, are reduced at different levels. \*p < 0.05, \*\*p < 0.01, \*\*\*p < 0.001, tested using two-tailed t tests against the controls. Error shades and error bars indicate ± SEM. See also Figures S3–S5 and S7.

Tm2 block. When the output of Tm1 and Tm4 was blocked simultaneously, we observed an intermediate reduction of tangential cell responses to OFF edges (Figures 6D and 6K). For all single- and double-block experiments with one copy of *shibire<sup>ts</sup>*, responses to ON edges remained unaltered. Effects were consistent across all velocities tested for PD and ND stimulation (Figure S4). These results corroborate the conclusion drawn from single blocks, namely, that all four Tm cell types are involved in the detection of moving brightness decrements. Moreover, all combinatorial restrictions of two Tm cell outputs decreased OFF responses beyond the level of the respective single-cell blocks. To further investigate the effects of blocking T5 input elements on motion responses in tangential cells, we used square wave gratings (Figure S7) moving at eight temporal frequencies (from 0.07 to 8.89 Hz; Figure S5). In contrast to ON or OFF edges, square wave gratings did not allow for a specific stimulation of ON or OFF pathways. However, in contrast to a

moving edge, they led to ongoing, permanent stimulation of local T5 motion-detecting cells, as well as their input neurons. The responses to square wave gratings were only mildly reduced. The reduction pattern, however, was similar to that for OFF edges (Figures S5A–S5N). Compared to controls (Figures S5O–S5X), it is apparent that responses to gratings in almost all blocking conditions decreased as temporal frequency increased. This effect can be explained through differentially tuned responses of lobula plate tangential cells to ON and OFF edges: tangential cells respond maximally to bright edges moving ~100 deg/s, whereas their responses to dark edges peak ~300 deg/s (Ammer et al., 2015). Hence, the ON channel appears to contribute more strongly to responses at lower frequencies. High frequencies seem to be mostly mediated through the OFF system. This asymmetry could thus account for the increased reductions in high-frequency regimes for the strongest OFF blocks (Figures S5R, S5S, S5U, S5W, and S5X).



# Comprehensive Characterization of the Major Presynaptic Elements to the *Drosophila* OFF Motion Detector

Please cite this article in press as: Serbe et al., Comprehensive Characterization of the Major Presynaptic Elements to the *Drosophila* OFF Motion Detector, *Neuron* (2016), <http://dx.doi.org/10.1016/j.neuron.2016.01.006>

CellPress

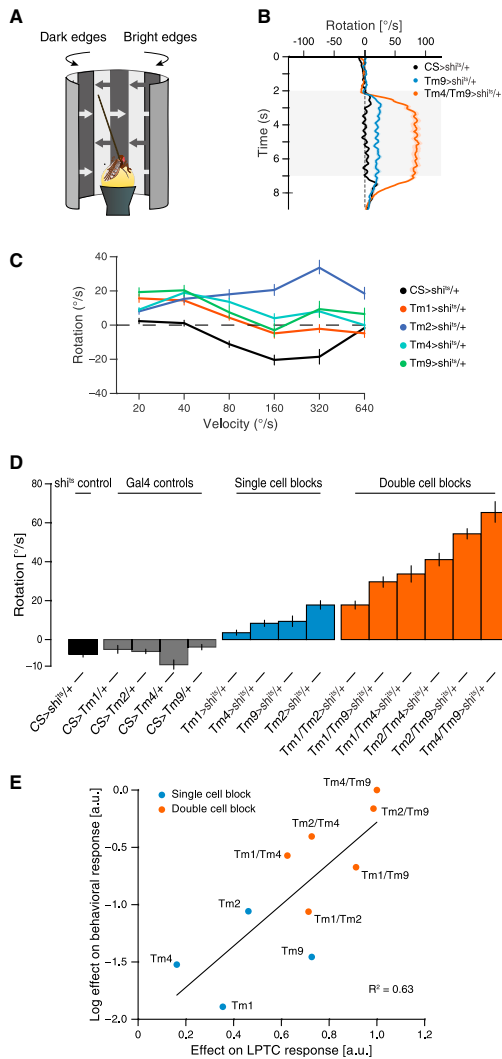


**Figure 7. Blocking Tm Cells Affects Turning Behavior in Walking Flies**

(A) Schematic illustration of the behavioral setup used in this study. A tethered fruit fly is walking on an air-suspended ball, facing a visual stimulation device. The fly is presented with a balanced motion stimulus (see [Experimental Procedures](#)).

(B) Exemplary optomotor responses of three genotypes to visual stimulation moving at 40°/s. Positive (rightward) rotation follows ON edges; negative (leftward) rotation follows OFF edges. Control flies do not exhibit any turning response for this velocity (black line), Tm9 block flies follow the bright edges with a low turning speed (blue line), and Tm4/Tm9 block flies turn with the direction of ON motion with a high angular velocity (orange line).

## Blocking Tm Cells Affects Optomotor Responses in Walking Flies

The detection of visual motion is ultimately used to control behavior. The model proposed by [Hassenstein and Reichardt \(1956\)](#) was derived from quantitative observations of tethered walking beetles. To examine the effects of Tm cell blocks on the flies' turning responses during visual stimulation ([Figure 7A](#)), we monitored tethered *Drosophilae* walking on an air-suspended ball and repeated the blocking experiments as described earlier. We used multiple dark and bright edges, simultaneously moving in opposing directions ([Clark et al., 2011](#)). Compared to the direct measurement of optomotor responses to edge motion of a single polarity, this stimulus allows for a differential measurement of the flies' sensitivity to moving ON and OFF edges. Turning responses in walking and flying *Drosophilae* are not a direct readout of the membrane potential of lobula plate tangential cells ([Schnell et al., 2014](#)). Instead, signals are subject to leaky integration over a time window of multiple seconds. When examining responses, this may lead to robust behavioral responses despite strongly reduced lobula plate tangential cell signals. The opposing edge assay circumvents this issue by having edges of opposite polarities compete before the integration stage, such that small differences are amplified and become detectable at the level of turning responses. Critically, our electrophysiological experiments demonstrate that ON responses are generally not affected by blocking either of the four cells, suggesting that any imbalance we detect in behavior results from a defect specific to OFF motion processing.

At a stimulus velocity of 40°/s, control flies showed no turning response during presentation of opposing edges ([Figure 7B](#)), indicating that ON and OFF responses are intact and in balance. When we disrupted the output of either Tm9 or Tm4 and Tm9 in combination, block flies constantly followed the direction of moving ON edges (positive turning responses) with different amplitudes. This suggests an impairment of OFF motion detection at the behavioral level. When we used opposing edges moving at multiple velocities, control flies exhibited no turning response for slowly moving stimuli (20°/s and 40°/s) and started following dark edges (negative turning) when stimulated with patterns moving at higher speeds (80°/s–320°/s; [Figures 7C and S6](#)).

(C) Mean turning responses of control (black), Tm1 block (orange), Tm2 block (blue), Tm4 block (cyan), and Tm9 block (green) flies for stimulation with six velocities (20°/s, 40°/s, 80°/s, 160°/s, 320°/s, and 640°/s).

(D) Mean turning response of control (black and gray), single-block (blue), and double-block (orange) flies to stimulation with the balanced motion stimulus over all velocities tested. All blocking experiments were performed using one copy of *shibire<sup>ts</sup>*. shi-control (N = 14), Tm1-control (N = 13), Tm2-control (N = 17), Tm4-control (N = 15), Tm9-control (N = 13), Tm1 (N = 12), Tm2-block (N = 13), Tm4-block (N = 13), Tm9-block (N = 12), Tm1/Tm2-block (N = 16), Tm1/Tm4-block (N = 12), Tm1/Tm9-block (n = 12), Tm2/Tm4-block (n = 16), Tm2/Tm9-block (n = 17), Tm4/Tm9-block (n = 14).

(E) Comparison of block effect strengths in the turning response of walking flies (y axis, log-transformed data) versus the effect of Tm cell blocks on the responses of lobula plate tangential cell (LPTCs; x axis, data not transformed). Single-cell blocks are colored in blue; double-cell blocks are in orange. The black line indicates a linear fit with  $R^2 = 0.63$ , indicating an exponential relationship between the behavioral effect and the reduction of the motion response as observed in the tangential cells. For details, see [Experimental Procedures](#). Error shades and error bars indicate  $\pm$  SEM. See also [Figures S3, S6, and S7](#).

# Comprehensive Characterization of the Major Presynaptic Elements to the *Drosophila* OFF Motion Detector

Please cite this article in press as: Serbe et al., Comprehensive Characterization of the Major Presynaptic Elements to the *Drosophila* OFF Motion Detector, *Neuron* (2016), <http://dx.doi.org/10.1016/j.neuron.2016.01.006>

CellPress

Turning behavior of Tm1, Tm4, and Tm9 block flies differed from control flies in a roughly constant way across all velocities, showing positive responses (following bright edges) for low velocities and no turning response for higher velocities. To our surprise, and in contrast to our electrophysiological data (Figure 5), we could see a velocity-dependent effect in Tm2 block flies, which followed the motion of bright edges more strongly at high velocities (Figure 7C). These data suggest that removing Tm2 from the circuit has comparatively little effect at low velocities but a pronounced effect at high velocities, suggesting a specialized role of Tm2 for processing of fast input signals.

To compare effects from electrophysiological recordings with the behavioral data, we averaged the turning response over all velocities tested (Figure 7D). On average, all control flies exhibit a small negative turning tendency that can be explained by the high-velocity stimuli where OFF signals dominate (Ammer et al., 2015; Figures 7C and S6). Blocking Tm2 with one copy of *shibire<sup>ts</sup>* resulted in the strongest turning response, whereas flies with blocked Tm1 cells showed only weak turning responses syndirectional with bright edges. Tm4 and Tm9 block flies exhibited intermediate phenotypes. Hence, suppressing synaptic transmission in single Tm cell types resulted in phenotypes that resembled those of T5 block flies (Maisak et al., 2013) and were qualitatively comparable to the results obtained in electrophysiological experiments. Next, we looked at the turning responses of flies with combinations of two Tm cell types silenced. When we combined Tm9 with Tm4- or Tm2-specific driver lines, we observed the strongest effects, in accordance with our electrophysiological data (Figure 7D). For combinatorial blocks of Tm1/Tm9, Tm1/Tm4, and Tm2/Tm4, the behavioral response was increased compared to single blocks (Figure 7D). Only the combined block of Tm1 and Tm2 cells did not elicit a turning response stronger than that for the Tm2 block alone. To investigate the relation between behavioral and tangential cell responses, we plotted effects of single- and double-cell silencing observed in the tangential cell responses versus those observed in walking flies (Figure 7E). To compare positive measures of effect strength in behavior and electrophysiology, we subtracted the electrophysiological phenotypes (in percent of control) from 100 and normalized them via division by the strongest phenotype. We then normalized the behavioral effect in the same way. We found an interesting relationship between the response reduction at the level of lobula plate tangential cells and the behaviorally measured ON-OFF imbalance. This relation is well explained by an exponential fit (black line in Figure 7E), suggesting that the transformation of tangential cell responses into behavioral output is highly nonlinear. A saturating transfer function, for instance, would explain how small and intermediate block effects at the level of the lobula plate produce comparatively weak effects at the level of walking behavior. Only when lobula plate tangential cell activity is heavily suppressed do walking flies show strong deficiencies for dark-edge motion, as indicated by the opposing edge results. Given that lobula plate networks feed into complex post-synaptic cascades before controlling motor output, this is not surprising. Generally, our electrophysiological findings predicted the behavioral phenotypes well, lending further credence to our results and indicating that the reductions we see at the level of lobula plate tangential cells

have direct impact on course control of behaving flies. Considering the combined dataset of tangential cell responses and behavior of walking flies, we conclude that all four Tm cells investigated here contribute to the computation of motion in the OFF pathway.

## Reichardt Detector Simulations Using Tm Cells' Temporal Filters

A classical elementary motion detector (Hassenstein and Reichardt, 1956) consists of two spatially offset input lines that are multiplied after temporal filtering (Figure 1A). This is done in a mirror-symmetric fashion, and the outputs of the multiplication stages are subtracted from each other (insets in Figures 8A–8F). We used the calculated temporal filters of the Tm cells from Figures 3F–3I to simulate the responses of elementary motion detectors that are built from the six binary combinations of two Tm cells to grating stimulation (Figures 8A–8F). To obtain velocity tuning curves, we modeled responses to temporal frequencies ranging from 0.1 to 10 Hz (Figure 8). Except for the combination of Tm2 and Tm4, which have almost identical response dynamics, all Tm cell combinations led to direction-selective responses that varied in relative amplitude and tuning (Figures 8A–8F). Tuning curves of the four pairs Tm1/Tm2, Tm1/Tm4, Tm9/Tm2, and Tm9/Tm4 showed similar shapes and response amplitudes, peaking ~0.5 Hz. The Tm1/Tm9 model produced the strongest responses, peaking ~0.2 Hz. We calculated the mean of all detector outputs and normalized the tuning curve to compare the results with the physiological data (from Figure S5). The frequency tuning curves were largely similar, and both peaked ~0.5 Hz (Figure 8G). The shape of the tangential cell tuning curve, however, was wider than that of the simulation curve, which can be explained by saturation effects in tangential cells. From this, we conclude that the measured temporal response properties of all Tm cells are suitable for correlation-type elementary motion detectors.

## DISCUSSION

In this study, we characterized the response properties of the four Tm cell types Tm1, Tm2, Tm4, and Tm9 and analyzed their involvement in *Drosophila* OFF motion detection. We demonstrated that none of these cells are direction selective and thus conclude that the computation of direction selectivity in the OFF pathway takes place on the dendrites of T5 cells.

At multiple levels, this circuit arrangement bears a striking resemblance to a network motif found in the mammalian retina (Kim et al., 2014). First, comparable to T5 cells, direction-selective starburst amacrine cells receive synaptic input from several anatomically similar cell types, i.e., the OFF bipolar cells 1, 2, 3a, 3b, and 4 (Masland, 2012). Second, like the Tm cells presynaptic to T5, these OFF bipolar cells have been shown to respond in a directionally unselective manner (Yonehara et al., 2013; Park et al., 2014). Third, the five OFF bipolar cell types show dynamics similar to those of the four Tm cells described here, ranging from sustained over slow decaying to fast transient (Baden et al., 2013; Borghuis et al., 2013). Depending on their temporal response properties, Tm cells receive input from particular groups of lamina monopolar cells. The two fast and transient

# Comprehensive Characterization of the Major Presynaptic Elements to the *Drosophila* OFF Motion Detector

Please cite this article as: Serbe et al., Comprehensive Characterization of the Major Presynaptic Elements to the *Drosophila* OFF Motion Detector, *Neuron* (2016), <http://dx.doi.org/10.1016/j.neuron.2016.01.006>

CellPress

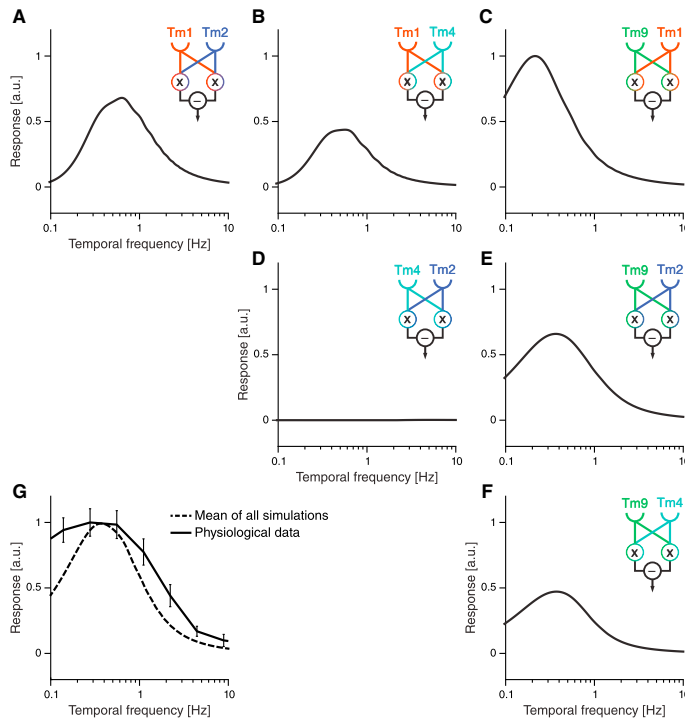


**Figure 8. Simulated Frequency Tunings for the Six Combinations of Tm Cells**

(A–F) Reichardt detector responses to grating stimulation using the simulated temporal filters (Figure 3) of Tm1/Tm2 (A), Tm1/Tm4 (B), Tm1/Tm9 (C), Tm2/Tm4 (D), Tm2/Tm9 (E), and Tm4/Tm9 (F). The responses were normalized to the maximal response of the Tm1/Tm9 detector (C).

(G) Comparison of the normalized mean response of all six simulations with the normalized physiological data of control flies (from Figure S5). Error bars indicate  $\pm$  SEM. See also Figure S5.

wave gratings moving at a temporal frequency of about 0.5 Hz (Figures 8G and S5). Except for Tm2/Tm4, whose filter time constants are almost identical, all combinations resulted in frequency optima in a range compatible with tangential cell responses. Furthermore, the mean signal of all simulations matches the tuning curve of electrophysiologically measured responses well. These simulations only represent a simplified view. They do not take into account several important aspects, such as the temporal frequency tuning of the ON channel, the different synaptic weights, or any spatial offsets of Tm cells on the T5 dendrites. Nevertheless, this simple model confirms the functional plausibility of the time constants of the four Tm cells tested.

cells, Tm2 and Tm4, receive their major input from L2 and L4; intermediate Tm1 cells primarily receive input from L2; and tonic Tm9 cells receive input from similarly slow and sustained L3 (Clark et al., 2011; Freifeld et al., 2013; Silies et al., 2013; Takemura et al., 2013; Meier et al., 2014). Finally, the mechanism for the computation of direction selectivity on the dendrites of starburst amacrine cells has been proposed to rely on dendritically offset input from bipolar cells with different temporal filter properties (Kim et al., 2014). For T5, comparable spatial shifts among dendritic target sites of Tm1, Tm2, and Tm9 have been reported (Shinomiya et al., 2014). The aforementioned study, however, was not able to identify the preferred direction of corresponding T5 cells and thus could not correlate it with the particular arrangement of Tm cell input on the dendrite. Nevertheless, the remarkable resemblance of neural circuits between invertebrates and mammals suggests a universality of underlying computational principles (Borst and Helmstaedter, 2015).

Are the measured temporal response properties functionally relevant for the computation of direction-selective signals? We addressed this question by modeling six elementary motion detectors through filtering of the signals in the two neighboring arms with the time constants of all six possible binary combinations of Tm cells (Figure 8). Lobula plate tangential cells exhibit a maximal steady-state response when presented with square

We also demonstrated that the functional importance of each of the four Tm cell types correlates with the number of synaptic contacts to T5 (Shinomiya et al., 2014). Silencing Tm4 cells, which out of the four provide the smallest number of synapses onto T5 cells, resulted in the weakest phenotype, followed by Tm1. Blocking Tm2 and Tm9, numerically the strongest inputs to T5, produced the strongest impairment of the OFF response (Figures 5 and 7). However, silencing L3, which is thought to be the main input to Tm9, does not result in similar, purely OFF-specific effects (Silies et al., 2013; Tuthill et al., 2013). This can be due to two facts. First, L3 also strongly connects to crucial ON pathway element Mi1 (Takemura et al., 2013; Ammer et al., 2015). Second, additional inputs to Tm9 cells may influence their response properties.

Given the increased effects of impairment when blocking pairs of Tm cells, we are able to rule out complete redundancy of individual elements (Figures 6 and 7). How do these four cell types then map onto the elements of correlation-type models? First, the interaction of several Tm cell types may give rise to a nonlinear stage more complex than the simple multiplication in the Hassenstein-Reichardt correlator. It is conceivable that the biophysical implementation of a suitable nonlinearity requires more than two appropriately tuned input lines. Our behavioral data lend some support to this hypothesis, because the

# Comprehensive Characterization of the Major Presynaptic Elements to the *Drosophila* OFF Motion Detector

Please cite this article in press as: Serbe et al., Comprehensive Characterization of the Major Presynaptic Elements to the *Drosophila* OFF Motion Detector, *Neuron* (2016), <http://dx.doi.org/10.1016/j.neuron.2016.01.006>

CellPress

strongest combinatorial blocks display a supra-linear increase in effect strength compared to the sum of the single-cell effects (Figure 7E). Second, standard algorithms generally model the asymmetric processing of direct and delayed lines as single-stage linear filters. For biophysical realizations, this filtering may be more complex. Multiple cells with varying intrinsic membrane properties and different synaptic transmission characteristics could provide many degrees of freedom when implementing filters that are appropriate for motion detection. Thus, temporal processing within one input line of the algorithmic model (Figure 1A) may involve the combination of two or more cells; Tm9 and Tm4, for instance, could both correspond to a module implementing what is the delay line in the Hassenstein-Reichardt model. Third, the four cells may in principle play different roles in different stimulus regimes defined by, for instance, velocity, contrast, luminance, or color. Our results provide some evidence for such a division of labor. In walking flies, the velocity-dependent phenotype of Tm2 block flies, together with the cells' fast response characteristics (Figure 3B), suggests a specific role for Tm2 at high velocities (Figure 7C). Such a design principle may be realized in at least two ways. Functional specialization could be a static property of the system, derived from cell-intrinsic spatiotemporal or chromatic filter properties, or a dynamic property that is subject to regulation depending on stimulus conditions. A recent study showed that changes in the behavior of hawkmoths under dim light conditions can be reproduced by adapting the filter time constants of a Hassenstein-Reichardt correlator (Sponberg et al., 2015). Tm9 could represent a candidate to detect changes in global luminance due to its slow filter properties, which make it sensitive to both brightness increments and decrements at all timescales (Figures 3D and 3I), as well as due to its responsiveness to full-field flicker (Figure 4I). Moreover, inputs from the color vision pathway have been demonstrated to improve motion discrimination (Wardill et al., 2012). Histaminergic photoreceptors R7 and R8, known to be involved in color perception (for review, see Behnia and Desplan, 2015), project to the medulla layers where Tm cell dendrites reside. Both Tm2 and Tm9 express a histamine-gated chloride channel (Gao et al., 2008), potentially linking the color and motion detection pathways. Finally, different Tm cells could be of different importance depending on the behavioral state of the animal, e.g., whether it is at rest, walking, or flying. Such behavioral-state dependency has been described at the level of the lobula plate tangential cells (Maimon et al., 2010; Chiappe et al., 2010; Haag et al., 2010; Jung et al., 2011; Schnell et al., 2014) and could be well explained by changes in contribution of synaptic input to T4 and T5 cells. Such a scenario could explain why blocking Tm2, Tm4, and their combinations resulted in stronger phenotypes in walking flies compared to tangential cell responses in a quiescent preparation (Figure 7E).

Taken together, our study sheds light on the circuitry underlying the computation of motion and uncovers striking parallels between vertebrate and invertebrate systems. Unraveling the exact mechanisms awaits further investigation. More naturalistic stimuli and modified algorithmic or biophysically realistic models that reflect the complexity of the neural correlate will play critical roles in this endeavor.

## EXPERIMENTAL PROCEDURES

For calcium imaging, we used the genetically encoded indicators GCaMP5 (Akerboom et al., 2012) and GCaMP6f (Chen et al., 2013). Blocking experiments were accomplished using Tm cell-specific Gal4 lines crossed with pUAS-FRC100-20XUAS-TTS-Shibire-ts1 (Pfeiffer et al., 2012) flies. Fly line specificity was tested using stochastic flip-out labeling (Nem et al., 2015) and expression of mCD8-GFP. All genotypes used in this study can be found in Table S1. Flies were prepared as described before: imaging experiments (Reiff et al., 2010), electrophysiology (Joesch et al., 2008), and behavior (Bahl et al., 2013). Two-photon microscopy and visual stimulus presentation was as described in Maisak et al. (2013). The recording protocol for electrophysiological experiments was adapted from Joesch et al. (2008). Under polarized light contrast, the glial sheet was digested locally by applying a stream of 0.5 mg/ml collagenase IV (Gibco) through a cleaning micropipette (~5  $\mu$ m opening). Recordings for the blocking electrophysiology experiments were obtained within 2 hr after a 60 min heat-shock application at 37°C. For statistical analysis, we used a two-tailed t test to compare *shibire*<sup>ts1</sup> controls and block flies (\* $p < 0.05$ , \*\* $p < 0.01$ , \*\*\* $p < 0.001$ ). Behavioral experiments were conducted as previously described (Ammer et al., 2015). For immunostaining procedures, see Schnell et al. (2010). Data were evaluated offline using custom written software (Matlab and Python) and Origin (OriginLab). For modeling the time constants in Figure 3, we fit a three-stage filter model to the mean calcium traces. Within this model, inputs were first high-pass filtered, then rectified by setting negative values to zero, and finally low-pass filtered (Figure 3E). For the modeling results in Figure 8, we simulated grating responses of hypothetical Reichardt detectors whose inputs were band-pass filters as determined in Figure 3E. See Supplemental Experimental Procedures for detailed methods.

## SUPPLEMENTAL INFORMATION

Supplemental Information includes Supplemental Experimental Procedures, seven figures, one table, and one movie and can be found with this article online at <http://dx.doi.org/10.1016/j.neuron.2016.01.006>.

## AUTHOR CONTRIBUTIONS

E.S. and M.M. jointly performed and evaluated all calcium imaging and electrophysiology experiments. A.L. performed and evaluated the behavioral experiments. A.L. and A.B. performed computer simulations. A.B., E.S., and M.M. designed the study. E.S. and M.M. wrote the manuscript with the help of the other authors.

## ACKNOWLEDGMENTS

We thank J. Haag for technical support and help with the two-photon microscope; R. Kutlesa and C. Theile for excellent help with behavior experiments; W. Essbauer, R. Kutlesa, C. Theile, and M. Sauter for fly work and immunostainings; T. Schilling for artwork; and D. Soll for the Dlg antibody. We thank G. Ammer, A. Arenz, J. Pujol-Marti, and A. Mauss for carefully reading the manuscript. All authors are members of the Graduate School for Systemic Neurosciences, Munich. We thank B. Dickson, G. Rubin, and A. Nem for providing us with unpublished fly lines.

Received: June 25, 2015

Revised: November 18, 2015

Accepted: December 18, 2015

Published: February 4, 2016

## REFERENCES

Akerboom, J., Chen, T.-W., Wardill, T.J., Tian, L., Marvin, J.S., Mutlu, S., Calderón, N.C., Esposti, F., Borghuis, B.G., Sun, X.R., et al. (2012). Optimization of a GCaMP calcium indicator for neural activity imaging. *J. Neurosci.* 32, 13819–13840.

# Comprehensive Characterization of the Major Presynaptic Elements to the *Drosophila* OFF Motion Detector

Please cite this article in press as: Serbe et al., Comprehensive Characterization of the Major Presynaptic Elements to the *Drosophila* OFF Motion Detector, *Neuron* (2016), <http://dx.doi.org/10.1016/j.neuron.2016.01.006>

CellPress

- Ammer, G., Leonhardt, A., Bahl, A., Dickson, B.J., and Borst, A. (2015). Functional specialization of neural input elements to the *Drosophila* ON motion detector. *Curr. Biol.* 25, 2247–2253.
- Baden, T., Berens, P., Bethge, M., and Euler, T. (2013). Spikes in mammalian bipolar cells support temporal layering of the inner retina. *Curr. Biol.* 23, 48–52.
- Bahl, A., Ammer, G., Schilling, T., and Borst, A. (2013). Object tracking in motion-blind flies. *Nat. Neurosci.* 16, 730–738.
- Behnia, R., and Desplan, C. (2015). Visual circuits in flies: beginning to see the whole picture. *Curr. Opin. Neurobiol.* 34, 125–132.
- Behnia, R., Clark, D.A., Carter, A.G., Clandinin, T.R., and Desplan, C. (2014). Processing properties of ON and OFF pathways for *Drosophila* motion detection. *Nature* 512, 427–430.
- Borghuis, B.G., Marvin, J.S., Looger, L.L., and Demb, J.B. (2013). Two-photon imaging of nonlinear glutamate release dynamics at bipolar cell synapses in the mouse retina. *J. Neurosci.* 33, 10972–10985.
- Borst, A., and Euler, T. (2011). Seeing things in motion: models, circuits, and mechanisms. *Neuron* 71, 974–994.
- Borst, A., and Helmstaedter, M. (2015). Common circuit design in fly and mammalian motion vision. *Nat. Neurosci.* 18, 1067–1076.
- Brand, A.H., and Perrimon, N. (1993). Targeted gene expression as a means of altering cell fates and generating dominant phenotypes. *Development* 118, 401–415.
- Cajal, S.R., and Sánchez, D. (1915). Contribución al conocimiento de los centros nerviosos de los insectos. *Trab. Lab. Inv. Biol.* 13, 1–168.
- Chen, T.W., Wardill, T.J., Sun, Y., Pulver, S.R., Renninger, S.L., Baohan, A., Schreiner, E.R., Kerr, R.A., Orger, M.B., Jayaraman, V., et al. (2013). Ultrasensitive fluorescent proteins for imaging neuronal activity. *Nature* 499, 295–300.
- Chiappe, M.E., Seelig, J.D., Reiser, M.B., and Jayaraman, V. (2010). Walking modulates speed sensitivity in *Drosophila* motion vision. *Curr. Biol.* 20, 1470–1475.
- Clark, D.A., Bursztyn, L., Horowitz, M.A., Schnitzer, M.J., and Clandinin, T.R. (2011). Defining the computational structure of the motion detector in *Drosophila*. *Neuron* 70, 1165–1177.
- Eichner, H., Joesch, M., Schnell, B., Reiff, D.F., and Borst, A. (2011). Internal structure of the fly elementary motion detector. *Neuron* 70, 1155–1164.
- Fischbach, K.-F., and Dittrich, A.P.M. (1989). The optic lobe of *Drosophila melanogaster*. I. A Golgi analysis of wild-type structure. *Cell Tissue Res.* 258, 441–475.
- Fisher, Y.E., Silies, M., and Clandinin, T.R. (2015). Orientation selectivity sharpens motion detection in *Drosophila*. *Neuron* 88, 390–402.
- Freifeld, L., Clark, D.A., Schnitzer, M.J., Horowitz, M.A., and Clandinin, T.R. (2013). GABAergic lateral interactions tune the early stages of visual processing in *Drosophila*. *Neuron* 78, 1075–1089.
- Gao, S., Takemura, S.-Y., Ting, C.-Y., Huang, S., Lu, Z., Luan, H., Rister, J., Thum, A.S., Yang, M., Hong, S.-T., et al. (2008). The neural substrate of spectral preference in *Drosophila*. *Neuron* 60, 328–342.
- Götz, K.G. (1964). Optomotorische Untersuchung des visuellen Systems einiger Augenmutanten der Fruchtfliege *Drosophila*. *Kybernetik* 2, 77–92.
- Haag, J., Wertz, A., and Borst, A. (2010). Central gating of fly optomotor response. *Proc. Natl. Acad. Sci. USA* 107, 20104–20109.
- Hassenstein, B., and Reichardt, W. (1956). Systemtheoretische Analyse der Zeit-, Reihenfolgen- und Vorzeichenauswertung bei der Bewegungsperzeption des Rüsselkäfers *Chlorophanus*. *Z. Naturforsch.* B 11, 513–524.
- Joesch, M., Plett, J., Borst, A., and Reiff, D.F. (2008). Response properties of motion-sensitive visual interneurons in the lobula plate of *Drosophila melanogaster*. *Curr. Biol.* 18, 368–374.
- Joesch, M., Schnell, B., Raghu, S.V., Reiff, D.F., and Borst, A. (2010). ON and OFF pathways in *Drosophila* motion vision. *Nature* 468, 300–304.
- Joesch, M., Weber, F., Eichner, H., and Borst, A. (2013). Functional specialization of parallel motion detection circuits in the fly. *J. Neurosci.* 33, 902–905.
- Jung, S.N., Borst, A., and Haag, J. (2011). Flight activity alters velocity tuning of fly motion-sensitive neurons. *J. Neurosci.* 31, 9231–9237.
- Kim, J.S., Greene, M.J., Zlateski, A., Lee, K., Richardson, M., Turaga, S.C., Purcaro, M., Balkam, M., Robinson, A., Behabadi, B.F., et al.; EyeWires (2014). Space-time wiring specificity supports direction selectivity in the retina. *Nature* 509, 331–336.
- Kitamoto, T. (2001). Conditional modification of behavior in *Drosophila* by targeted expression of a temperature-sensitive *shibire* allele in defined neurons. *J. Neurobiol.* 47, 81–92.
- Land, M.F. (1997). Visual acuity in insects. *Annu. Rev. Entomol.* 42, 147–177.
- Maimon, G., Straw, A.D., and Dickinson, M.H. (2010). Active flight increases the gain of visual motion processing in *Drosophila*. *Nat. Neurosci.* 13, 393–399.
- Maisak, M.S., Haag, J., Ammer, G., Serbe, E., Meier, M., Leonhardt, A., Schilling, T., Bahl, A., Rubin, G.M., Nern, A., et al. (2013). A directional tuning map of *Drosophila* elementary motion detectors. *Nature* 500, 212–216.
- Masland, R.H. (2012). The neuronal organization of the retina. *Neuron* 76, 266–280.
- Mauss, A.S., Meier, M., Serbe, E., and Borst, A. (2014). Optogenetic and pharmacologic dissection of feedforward inhibition in *Drosophila* motion vision. *J. Neurosci.* 34, 2254–2263.
- Mauss, A.S., Pankova, K., Arenz, A., Nern, A., Rubin, G.M., and Borst, A. (2015). Neural circuit to integrate opposing motions in the visual field. *Cell* 162, 351–362.
- Meier, M., Serbe, E., Maisak, M.S., Haag, J., Dickson, B.J., and Borst, A. (2014). Neural circuit components of the *Drosophila* OFF motion vision pathway. *Curr. Biol.* 24, 385–392.
- Nern, A., Pfeiffer, B.D., and Rubin, G.M. (2015). Optimized tools for multicolor stochastic labeling reveal diverse stereotyped cell arrangements in the fly visual system. *Proc. Natl. Acad. Sci. USA* 112, E2967–E2976.
- Park, S.J.H., Kim, I.-J., Looger, L.L., Demb, J.B., and Borghuis, B.G. (2014). Excitatory synaptic inputs to mouse on-off direction-selective retinal ganglion cells lack direction tuning. *J. Neurosci.* 34, 3976–3981.
- Pfeiffer, B.D., Truman, J.W., and Rubin, G.M. (2012). Using translational enhancers to increase transgene expression in *Drosophila*. *Proc. Natl. Acad. Sci. USA* 109, 6626–6631.
- Reiff, D.F., Plett, J., Mank, M., Griesbeck, O., and Borst, A. (2010). Visualizing retinotopic half-wave rectified input to the motion detection circuitry of *Drosophila*. *Nat. Neurosci.* 13, 973–978.
- Rivera-Alba, M., Vitaladevuni, S.N., Mishchenko, Y., Lu, Z., Takemura, S.Y., Scheffer, L., Meinertzhagen, I.A., Chklovskii, D.B., and de Polavieja, G.G. (2011). Wiring economy and volume exclusion determine neuronal placement in the *Drosophila* brain. *Curr. Biol.* 21, 2000–2005.
- Schnell, B., Joesch, M., Forstner, F., Raghu, S.V., Otsuna, H., Ito, K., Borst, A., and Reiff, D.F. (2010). Processing of horizontal optic flow in three visual interneurons of the *Drosophila* brain. *J. Neurophysiol.* 103, 1646–1657.
- Schnell, B., Raghu, S.V., Nern, A., and Borst, A. (2012). Columnar cells necessary for motion responses of wide-field visual interneurons in *Drosophila*. *J. Comp. Physiol. A Neuroethol. Sens. Neural Behav. Physiol.* 198, 389–395.
- Schnell, B., Weir, P.T., Roth, E., Fairhall, A.L., and Dickinson, M.H. (2014). Cellular mechanisms for integral feedback in visually guided behavior. *Proc. Natl. Acad. Sci. USA* 111, 5700–5705.
- Shinomiya, K., Karupudurai, T., Lin, T.Y., Lu, Z., Lee, C.H., and Meinertzhagen, I.A. (2014). Candidate neural substrates for off-edge motion detection in *Drosophila*. *Curr. Biol.* 24, 1062–1070.
- Silies, M., Gohl, D.M., Fisher, Y.E., Freifeld, L., Clark, D.A., and Clandinin, T.R. (2013). Modular use of peripheral input channels tunes motion-detecting circuitry. *Neuron* 79, 111–127.
- Sponberg, S., Dyhr, J.P., Hall, R.W., and Daniel, T.L. (2015). Insect Flight: luminance-dependent visual processing enables moth flight in low light. *Science* 348, 1245–1248.
- Strother, J.A., Nern, A., and Reiser, M.B. (2014). Direct observation of ON and OFF pathways in the *Drosophila* visual system. *Curr. Biol.* 24, 976–983.

# Comprehensive Characterization of the Major Presynaptic Elements to the *Drosophila* OFF Motion Detector

Please cite this article in press as: Serbe et al., Comprehensive Characterization of the Major Presynaptic Elements to the *Drosophila* OFF Motion Detector, *Neuron* (2016), <http://dx.doi.org/10.1016/j.neuron.2016.01.006>

CellPress

- Takemura, S.Y., Karuppudurai, T., Ting, C.-Y., Lu, Z., Lee, C.-H., and Meinertzhagen, I.A. (2011). Cholinergic circuits integrate neighboring visual signals in a *Drosophila* motion detection pathway. *Curr. Biol.* 21, 2077–2084.
- Takemura, S.Y., Bharioke, A., Lu, Z., Nern, A., Vitaladevuni, S., Rivlin, P.K., Katz, W.T., Olbris, D.J., Plaza, S.M., Winston, P., et al. (2013). A visual motion detection circuit suggested by *Drosophila* connectomics. *Nature* 500, 175–181.
- Tuthill, J.C., Nern, A., Holtz, S.L., Rubin, G.M., and Reiser, M.B. (2013). Contributions of the 12 neuron classes in the fly lamina to motion vision. *Neuron* 79, 128–140.
- Wardill, T.J., List, O., Li, X., Dongre, S., McCulloch, M., Ting, C.-Y., O’Kane, C.J., Tang, S., Lee, C.-H., Hardie, R.C., and Jussola, M. (2012). Multiple spectral inputs improve motion discrimination in the *Drosophila* visual system. *Science* 336, 925–931.
- Werblin, F.S., and Dowling, J.E. (1969). Organization of the retina of the mudpuppy, *Necturus maculosus*. II. Intracellular recording. *J. Neurophysiol.* 32, 339–355.
- Yonehara, K., Farrow, K., Ghanem, A., Hillier, D., Balint, K., Teixeira, M., Jüttner, J., Noda, M., Neve, R.L., Conzelmann, K.-K., and Roska, B. (2013). The first stage of cardinal direction selectivity is localized to the dendrites of retinal ganglion cells. *Neuron* 79, 1078–1085.

Comprehensive Characterization of the Major Presynaptic Elements to the *Drosophila*  
OFF Motion Detector

---

Neuron, Volume 89

**Supplemental Information**

**Comprehensive Characterization  
of the Major Presynaptic Elements  
to the *Drosophila* OFF Motion Detector**

**Etienne Serbe, Matthias Meier, Aljoscha Leonhardt, and Alexander Borst**

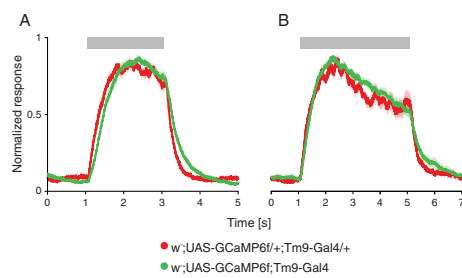


**Figure S1. Related to Figure 3. Different expression levels of GCaMP do not affect the response kinetics of Tm9**

(A and B) Normalized line scan calcium responses in Tm9 axonal arbors upon stimulation with a 4.5° wide, dark bar appearing for 2s (A) and 4s (B) to investigate long term temporal dynamics of Tm9 responses. To exclude effects of GCaMP6f expression level on the dynamics of the response, two traces were obtained using flies with homozygous (green) and heterozygous (red) expression of the Gal4 and the UAS construct. Error shades indicate ±SEM.



# Comprehensive Characterization of the Major Presynaptic Elements to the *Drosophila* OFF Motion Detector

---

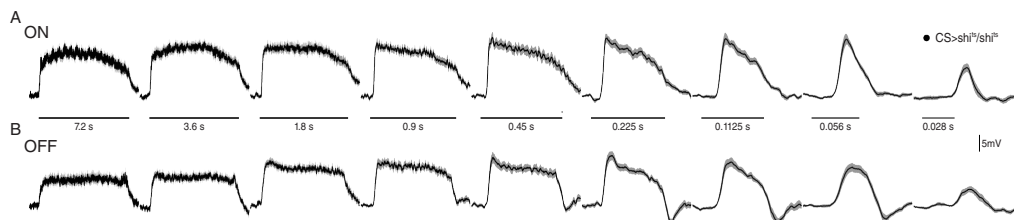


**Figure S2. Related to Figure 5. LPTC responses to multiple edges moving at different velocities**

Average voltage traces of lobula plate tangential cells in control flies (N=5, n=13), stimulated with multiple moving ON (A) and OFF (B) edges at 9 different velocities (3.125°/s, 6.25°/s, 12.5°/s, 25°/s, 50°/s, 100°/s, 200°/s, 400°/s, and 800°/s). Black bars indicate duration of stimulus presentation. Error shades indicate  $\pm$  SEM.

# Comprehensive Characterization of the Major Presynaptic Elements to the *Drosophila* OFF Motion Detector

---

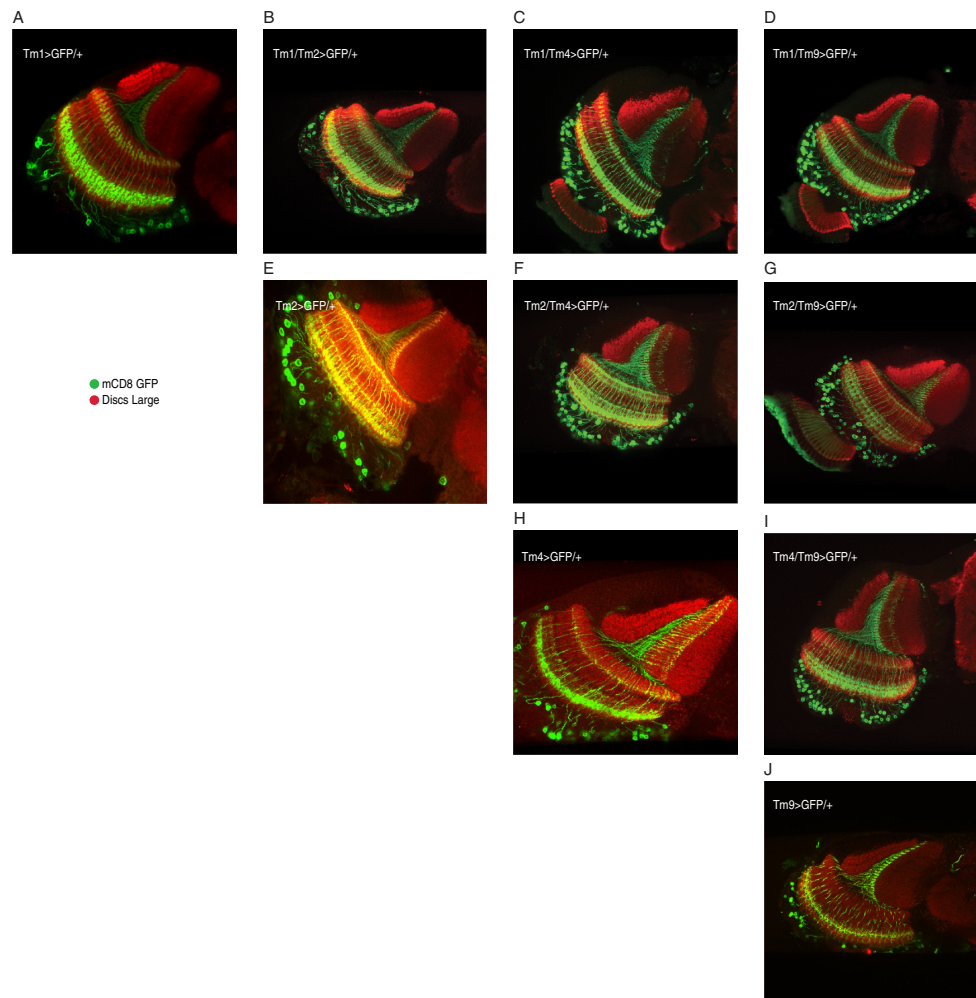


**Figure S3. Related to Figures 5-7. Tm cell expression patterns**

(A-J) Confocal images of the Gal4 driver cell lines used in the silencing experiments, shown in horizontal cross sections. Tm1 (A), Tm2 (E), Tm4 (H), and Tm9 (J) neurons are labeled in green (mCD8-GFP expression) and neuropils in red (antibody against Discs Large). The six possible binary combinations (B-D, F, G, I) of the Gal4 driver lines exhibit clear expression of two neuron types.

# Comprehensive Characterization of the Major Presynaptic Elements to the *Drosophila* OFF Motion Detector

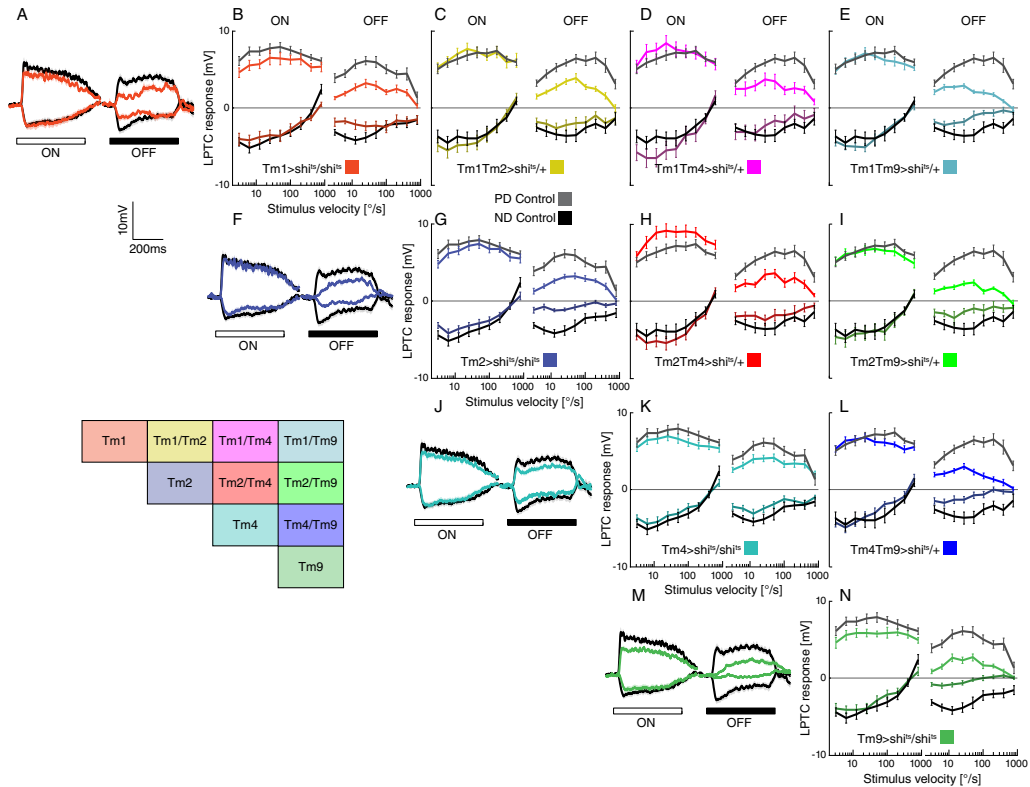
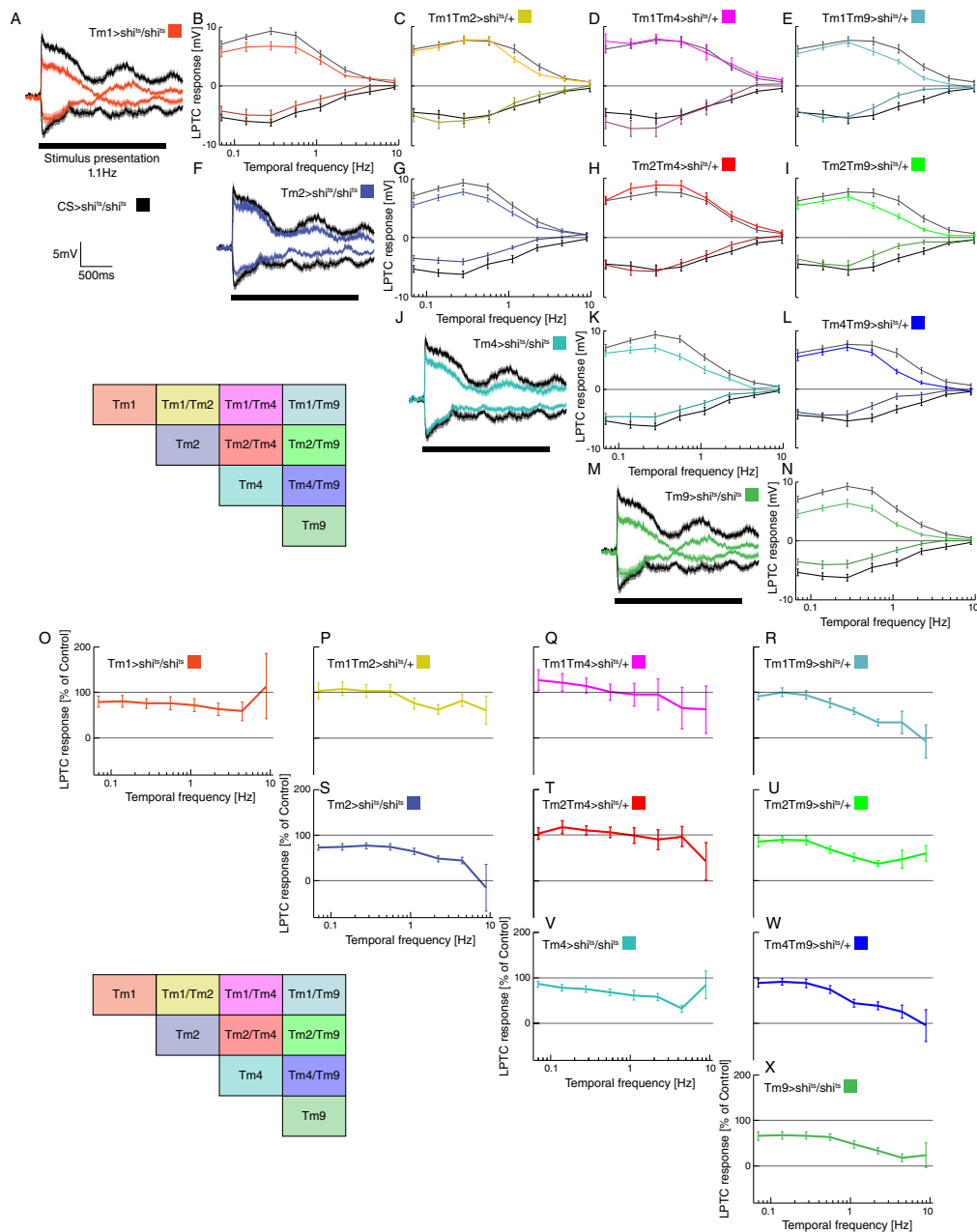


**Figure S4. Related to Figures 5 and 6. Preferred and null direction responses of LPTCs to multiple ON and OFF edges** (A, F, J, M) Mean voltage traces of lobula plate tangential cells stimulated with multiple ON and OFF edges moving at 50°/s in preferred (PD) and null direction (ND). Black traces depict recordings from control flies. Red traces in (A) represent LPTC responses in Tm1 block flies, blue traces in (F) Tm2 block flies, cyan traces in (J) Tm4 block flies, and green traces in (M) Tm9 block flies. Error shades indicate  $\pm$  SEM. (B-E, G-I, K, L, and N) Average responses (errorbars indicate  $\pm$  SEM) of all four single block (with two copies of shibire<sup>ts</sup>) and six possible combinations with corresponding controls (black) to multiple ON and OFF edges moving with nine different velocities (3.125°/s, 6.25°/s, 12.5°/s, 25°/s, 50°/s, 100°/s, 200°/s, 400°/s, 800°/s) in PD (light colors) and ND (dark colors). Colored boxes on the bottom left indicate locations of corresponding panels in the matrix.

# Comprehensive Characterization of the Major Presynaptic Elements to the *Drosophila* OFF Motion Detector



# Comprehensive Characterization of the Major Presynaptic Elements to the *Drosophila* OFF Motion Detector

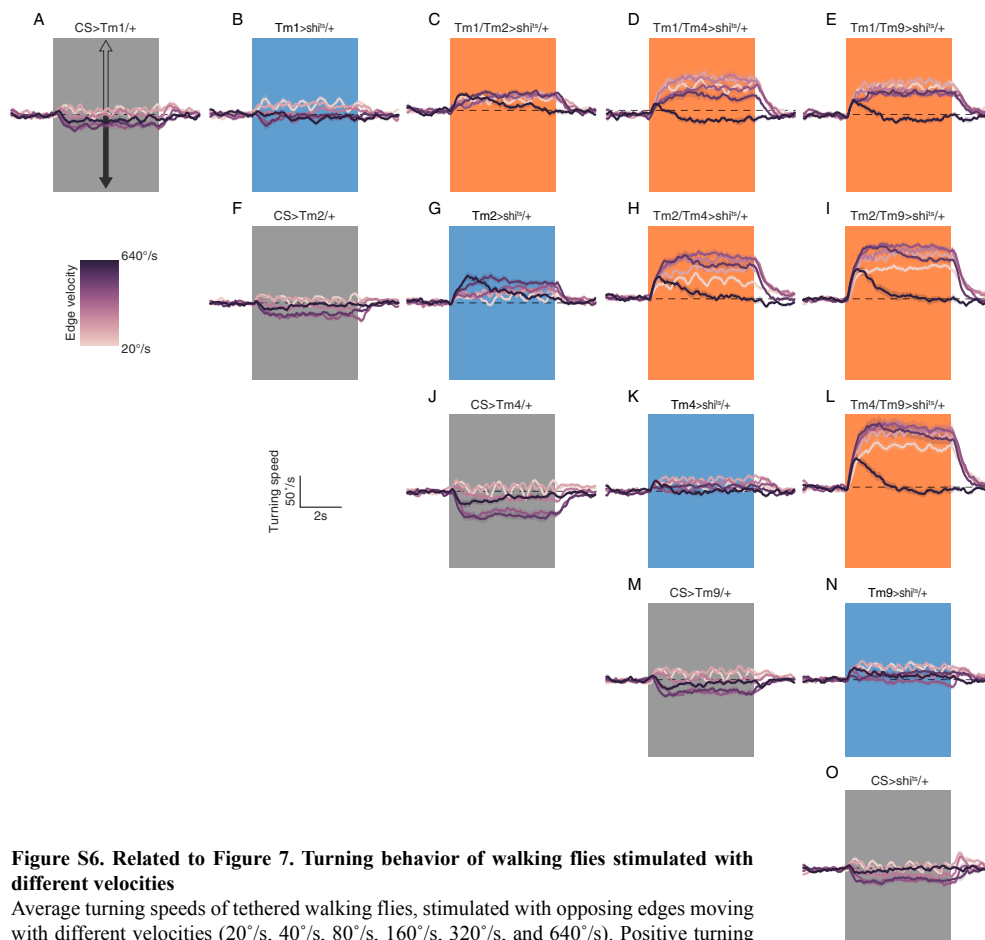


**Figure S6. Related to Figure 7. Turning behavior of walking flies stimulated with different velocities**

Average turning speeds of tethered walking flies, stimulated with opposing edges moving with different velocities (20°/s, 40°/s, 80°/s, 160°/s, 320°/s, and 640°/s). Positive turning responses correspond to flies turning with ON-edges, negative turning responses indicate turning with OFF-edges (see arrows in A). Stimulus presentation is indicated by shaded boxes. Errorshades indicate  $\pm$  SEM. (A, F, J, M, and O) Four Gal4 controls and the *shibire*<sup>ts</sup> control. (B, G, K, and N) Single cell blocks with one copy of *shibire*<sup>ts</sup>. (C-E, H, I and L) Double cell blocks with one copy of *shibire*<sup>ts</sup>.

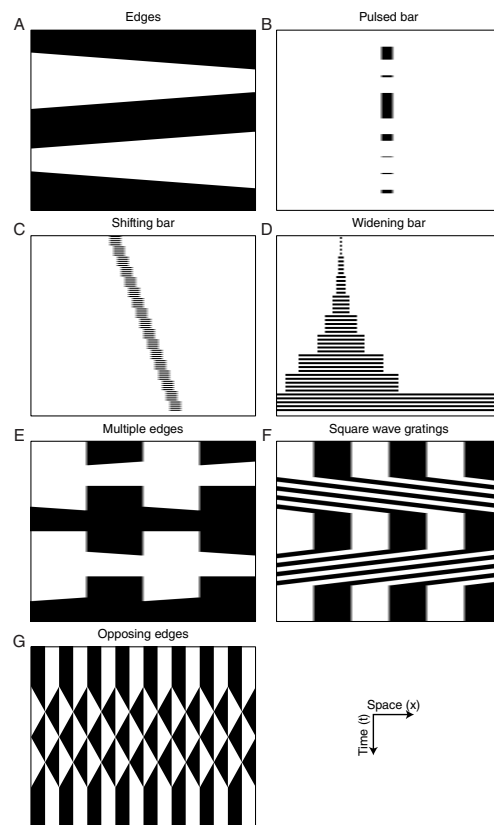


**Figure S7. Related to Figures 2-7. Space-time (xt) plots of all visual stimuli used in the study**  
(A) Single ON and OFF Edges were used for stimulation in Figure 2. (B) Flickering bars with randomly ordered durations were used to test temporal properties in Figure 3. (C and D) Shifting and widening bars were used to test spatial properties in Figure 4. (E) Multiple edges were used in electrophysiological experiments in Figures 5 and 6. (F) Square wave gratings were used in electrophysiological experiments in Figure S5. (G) Opposing edges were used for behavioral experiments in Figure 7.

**Movie S1. Related to Figure 4. Retinotopic organization of Tm9 cells**

Representative raw two-photon microscope time course of Tm9 cells expressing GCaMP5 (smoothed in ImageJ). The fly is stimulated with a 4.5° wide vertical dark bar that is flickering five times at one position and is subsequently shifted by 1.5° (see Figure 3, Supplemental Experimental Procedures). The movie has been accelerated 8 times (15fps compared to 1.87Hz acquisition). The insert at the top right indicates the stimulus. Tm9 cell activity follows the stimulus in a retinotopic fashion.

Comprehensive Characterization of the Major Presynaptic Elements to the *Drosophila*  
OFF Motion Detector

---

**Table S1. Related to Figures 1-7. Genotypes used throughout the study.**



# Comprehensive Characterization of the Major Presynaptic Elements to the *Drosophila* OFF Motion Detector

---

## Supplemental Experimental Procedures

### Flies

Flies were raised on standard cornmeal-agar medium with 12hr light/12hr dark cycles, 25°C, and 60% humidity. Female flies were used for all experiments. For calcium imaging, we used the genetically encoded indicators GCaMP5 (Akerboom et al., 2012) and GCaMP6f (Chen et al., 2013). Blocking experiments were accomplished using Tm cell-specific Gal4 lines crossed with pJFRC100-20XUAS-TTS-Shibire-ts1 (Pfeiffer et al., 2012) flies. Fly line specificity was tested using stochastic flip-out labeling (Nern et al., 2015) and expression of mCD8-GFP. We used different driver lines because of different expression strengths and specificities. All genotypes used in this study can be found in Table S1. Flies were prepared as described previously: imaging experiments, Reiff et al., 2010; electrophysiology, Joesch et al., 2008; and behavior, Bahl et al., 2013.

### Immunohistochemistry and confocal imaging

For immuno-staining procedures see Schnell et al., 2010. Primary antibodies used were mouse anti-Discs Large (DLG, RRID:MGI\_4354991, Developmental Studies Hybridoma Bank) and anti-GFP-Alexa488 conjugate (RRID:AB\_221477, Molecular Probes). For visualization we used (1:200 in PBT): goat anti-mouse Alexa 568 (RRID:AB\_10562737). Brains were mounted (Vectashield) and optically sectioned in the horizontal plane with a Leica SP5 confocal microscope. For documentation, single sections were processed in ImageJ 1.46r (NIH, Bethesda, Maryland, USA).

### Behavioral experiments

Flies were placed on an air-suspended polyurethane ball in a virtual environment projected onto three monitors spanning approximately 270° (horizontal) and 114° (vertical) of the fly's visual field. This stimulation system offered less than 0.1° of angular pixel size, a value well below *Drosophila*'s optical resolution capability. We used six such setups for recording fly locomotion as described previously (Bahl et al., 2013). On two setups, stimuli were presented at a screen refresh frequency of 120Hz; on four setups, the refresh frequency was 144Hz. We never observed qualitative or quantitative differences between these setups in any of the experiments. All monitors were equilibrated in brightness and contrast. Temperature within the immediate surround of the fly was controlled using a custom-built closed-loop thermoregulation system. We employed the following temperature protocol for all experiments and genotypes: Temperature was kept at 25°C for the first 5 minutes and then, within 10 minutes, raised to a restrictive 34°C.

### Two-photon microscopy and visual stimulation

Two-photon microscopy and visual stimulus presentation was as described in Maisak et al., 2013. Edges had a contrast of 88%, moving at 30°/s. Each edge motion was shown twice within a single sweep, resulting in a total of eight stimulation periods, each lasting 4s. Subsequent stimuli were preceded by a 3s pause. To map the receptive fields, we flickered 4.5° wide vertical and horizontal dark bars on a bright background with 0.5 Hz at 20 different positions shifted by 1.5°. The position with the maximum response was set to 0°. The responses of the surrounding locations were normalized and plotted dependent on their distance to the peak response. The spatial integration experiments were conducted using vertical dark bars, increasing in size. We measured the responses of flickering bars with 9 different widths (1.5°, 4.5°, 7.5°, 13.5°, 25.5°, 37.5°, 49.5°, 67.5°, 180°) at the peak response position. The responses were normalized to their peak response. For the line scan experiments, a 4.5° vertical dark bar was presented on a bright background for 7 different periods: 50ms, 75ms, 125ms, 225ms, 425ms, 825ms, and 1625ms. The duration of bar presentation was varied in a randomized fashion and each stimulus was presented three times. For the electrophysiology experiments, multiple edges were used as stimuli moving simultaneously at nine different velocities (3.125°/s, 6.25°/s, 12.5°/s, 25°/s, 50°/s, 100°/s, 200°/s, 400°/s, 800°/s). To stimulate HS cells, a vertical, stationary square wave grating with 45° spatial wavelength was presented. For ON edge motion, the right (PD) or the left edge (ND) of each light bar started moving until it merged with the neighboring bar. For OFF edge motion, the right or the left edge of each dark bar was moving. To stimulate VS cells, the pattern was rotated by 90°. Consequently, we used the 36 different stimuli for every recording in a randomized fashion for one to three trials. For behavioral experiments, the balanced motion stimulus resembled previous iterations (Clark et al., 2011). Briefly, we presented flies with a stationary square wave grating that had an initial spatial wavelength of 45° visual angle and a constant Michelson contrast of 50%. Each individual trial lasted 9s. Between 2s and 7s, bright edges moved in one

# Comprehensive Characterization of the Major Presynaptic Elements to the *Drosophila* OFF Motion Detector

---

direction at a fixed velocity while dark edges moved in the other direction at the same velocity. In contrast to previous versions, we reset the stimulus to the initial state after edges had traversed  $20^\circ$  of visual angle. This allowed us to keep the stimulus duration fixed for varying edge velocities. Additionally, we applied a random phase shift after each reset in order to rule out symmetry effects. This was done for 6 velocities ( $20^\circ/s$ ,  $40^\circ/s$ ,  $80^\circ/s$ ,  $160^\circ/s$ ,  $320^\circ/s$ , and  $640^\circ/s$ ) and 2 possible edge directions (dark edge leftwards/bright edge rightwards and vice versa), resulting in 12 conditions that were repeated 50 times per fly. The stimulus was rendered in real-time using Panda3D, an open source game engine, and Python 2.7. x-t plots of all stimuli used are illustrated in Figure S7.

## Data analysis and simulations

Data were evaluated off-line using custom written software (Matlab and Python) and Origin (OriginLab Corporation, Massachusetts, USA). To evaluate the calcium imaging data, the raw image series were first converted into a relative fluorescence change ( $\Delta F/F$ ) series by using the first five images as reference. Then, a region was defined within a raw image, and average  $\Delta F/F$  values were determined within that region for each image, resulting in a  $\Delta F/F$  signal over time. Example calcium signal traces to edge stimulation were obtained by calculating the average  $\Delta F/F$  signal over trials. For Figures 2E-2H we normalized the derivative of the mean response trace of every cell. Then, we calculated the mean of the extrema over cells. The evaluation time was the stimulation period with additional four frames.

We fit a three-stage filter model to the mean calcium traces. Within this model, inputs were first high-pass filtered, then rectified by setting negative values to zero, and finally low-pass filtered (Figure 3E). The filters were linear RC filters and of first order. We simulated the visual stimuli as one-dimensional time series whose baseline was zero; for the duration of bar presentation, the values were set to one. The fitting procedure minimized the mean squared error between model output and the calcium traces by exhaustively scanning the two-dimensional parameter space spanned by the time constants of the filters. Errors were summed across presentation lengths of the dark bar, yielding a single optimum per cell type across all seven stimuli. We mapped time constants up to 2000ms in steps of 10ms and additionally allowed filtering to be switched off, equivalent to the time constant being either zero (for a low-pass) or infinite (for a high-pass). The time step for the simulations was 1ms.

To obtain the graphs in Figures 4A-4D and 4F-4I we calculated the mean of the  $\Delta F/F$  signal of a single axonal arbor of a Tm cell during the time when dark vertical bars were flickering at a certain position for five times and divided that response by the mean of the  $\Delta F/F$  signal when no stimulation was present. For electrophysiological experiments we calculated the mean over the stimulation time shifted by 25ms. For behavioral experiments we analyzed the data as described previously (Maisak et al., 2013). Briefly, optical tracking sensors were equipped with lens and aperture systems to focus on the sphere behind the fly. The tracking data were processed at 4 kHz internally, read out via a USB interface and processed by a computer at  $<200$  Hz. This allowed real-time calculation of the instantaneous rotation axis of the sphere. We resampled the rotation traces to 20Hz for further processing and applied a first-order low pass filter with a time constant of 100ms to each trace. For all flies, we manually selected 20 consecutive trials out of the 50 available that fulfilled the following criteria: First, the temperature was at a stable  $34^\circ\text{C}$ . Second, the average turning tendency of the fly was approximately  $0^\circ/s$ . Third, the average forward velocity of the fly was at least 5mm/s, indicating a visually responsive state. Flies were selected without blinding. Application of the criteria excluded, on average, 20% of all flies. For further processing, we subtracted responses for the two symmetrical edge directions in order to reduce the impact of walking asymmetries. Trials were then averaged. For statistical purposes, we calculated the turning tendency of each fly for each velocity condition as the mean of the turning response between 3s (walking onset) and 7s (stimulus offset). Other evaluation time frames produced qualitatively equivalent results. The scatter plot in Figure 7E was generated by linearly normalizing values to the average of the respective genotype that showed the largest effect and plotting electrophysiology block effects against the natural logarithm of behavioral block effects. We then fit a linear regression model to the transformed data using the least-squares method. All data analysis was performed using Python 2.7 and the NumPy library.

For the modelling results in Figure 8, we simulated grating responses of hypothetical Reichardt detectors whose inputs were bandpass filters as determined in Figure 8. Sinusoidal grating stimuli moved for 3s, preceded and followed by 1s of stationary presentation. The gratings had a spatial wavelength of 10 degrees; no further spatial filtering was applied. An array of 10 detectors viewed the grating. For each possible combination of cells, we then applied the corresponding filters to the two input signals, multiplied the output, and summed over all detectors. This was done twice with spatially mirrored input lines, and results were subtracted and rectified in order to generate an approximation of lobula plate tangential cell signals. Finally, we averaged across the stimulation period. For each cell type combination, we chose the spatial order of input filters such that the mean grating responses were positive. This simulation was performed for 150 temporal frequencies located on a logarithmic scale. Each output was normalized to the maximum response across all cell type combinations.

# Manuscript Nr. 2

## Neural Circuit Components of the *Drosophila* OFF Motion Vision Pathway

Matthias Meier\*, **Etienne Serbe**\*, Matthew S. Maisak, Jürgen Haag, Barry J. Dickson,  
and Alexander Borst

\*equal contribution

### Author Contributions:

M.M., **E.S.** and A.B. designed the study. M.M. and **E.S.** performed electrophysiological recordings. M.M., **E.S.**, M.S.M., and J.H. performed calcium imaging experiments. B.J.D. provided unpublished Gal4-lines. M.M., **E.S.** and A.B. wrote the paper with help of the other authors.

## Neural Circuit Components of the *Drosophila* OFF Motion Vision Pathway

Matthias Meier,<sup>1,3</sup> Etienne Serbe,<sup>1,3</sup> Matthew S. Maisak,<sup>1</sup> Jürgen Haag,<sup>1</sup> Barry J. Dickson,<sup>2,4</sup> and Alexander Borst<sup>1,\*</sup>

<sup>1</sup>Department of Circuits-Computation-Models, Max Planck Institute of Neurobiology, Am Klopferspitz 18, 82152 Martinsried, Germany

<sup>2</sup>Research Institute of Molecular Pathology, Dr. Bohr-Gasse 7, 1030 Vienna, Austria

### Summary

**Background:** Detecting the direction of visual motion is an essential task of the early visual system. The Reichardt detector has been proven to be a faithful description of the underlying computation in insects. A series of recent studies addressed the neural implementation of the Reichardt detector in *Drosophila* revealing the overall layout in parallel ON and OFF channels, its input neurons from the lamina (L1 → ON, and L2 → OFF), and the respective output neurons to the lobula plate (ON → T4, and OFF → T5). While anatomical studies showed that T4 cells receive input from L1 via Mi1 and Tm3 cells, the neurons connecting L2 to T5 cells have not been identified so far. It is, however, known that L2 contacts, among others, two neurons, called Tm2 and L4, which show a pronounced directionality in their wiring.

**Results:** We characterized the visual response properties of both Tm2 and L4 neurons via Ca<sup>2+</sup> imaging. We found that Tm2 and L4 cells respond with an increase in activity to moving OFF edges in a direction-unselective manner. To investigate their participation in motion vision, we blocked their output while recording from downstream tangential cells in the lobula plate. Silencing of Tm2 and L4 completely abolishes the response to moving OFF edges.

**Conclusions:** Our results demonstrate that both cell types are essential components of the *Drosophila* OFF motion vision pathway, prior to the computation of directionality in the dendrites of T5 cells.

### Introduction

The computation of motion is imperative for fundamental behaviors such as mate or prey detection, predator avoidance, and visual navigation. In the fruit fly *Drosophila*, motion cues are processed in the optic lobe, a brain area comprised of the lamina, medulla, lobula, and lobula plate, each arranged in a columnar, retinotopic fashion. Whereas photoreceptors respond to motion in a nondirectional way, wide-field tangential cells of the lobula plate depolarize to motion in their preferred direction (PD) and hyperpolarize to motion in the opposite or null direction (ND) [1, 2]. These direction-selective responses are well characterized by a mathematical model, the so-called Reichardt detector. In this model, signals from neighboring photoreceptors are multiplied after asymmetric

temporal filtering [3–5]. Due to the anatomical complexity and miniscule size of the columnar neurons of the optic lobe, identification of the neural elements of the motion detection circuit has long proven difficult.

In agreement with previous suggestions based on costratification of Golgi-stained columnar cells [6, 7] and cell-unspecific activity labeling using the deoxyglucose method [8], recent studies identified two parallel motion processing streams, one leading from lamina neuron L1 via T4 cells and the other from lamina neuron L2 via T5 onto the dendrites of the tangential cells [9, 10]. Within each pathway, four subpopulations of T4 and T5 cells are tuned to one of the four cardinal directions (front to back, back to front, upward, or downward), providing direction-selective signals to four different sublayers of the lobula plate [11, 12]. Here, they become spatially integrated on the dendrites of tangential cells [12, 13]. The two pathways are functionally segregated with regard to their selectivity for contrast polarity: the L1 pathway is selectively responsive to the motion of brightness increments (ON pathway), while the L2 pathway responds selectively to the motion of brightness decrements (OFF pathway) [10, 12, 14–16]. These findings suggest that important processing steps of motion computation take place between the axon terminals of L1/L2 and the output regions of T4/T5.

For the ON pathway, a recent connectomic EM study of the fly medulla [17] not only identified two neurons, Mi1 and Tm3, as the most prominent postsynaptic targets of L1, but also showed that these cells make up for more than 90% of all input synapses on the dendrites of T4 cells. Most interestingly, the innervation of Tm3 and Mi1 on a single T4 cell is asymmetric, consistent with the preferred direction of the T4 cell, i.e., the lobula plate layer where it terminates. Because connectomic analysis has not yet reached the lobula, where the dendrites of T5 cells reside [6], the connectivity for the OFF pathway is known only within the lamina and the medulla [17–22]. Here, several cell types have been found to be postsynaptic to L2 [17, 18], i.e., L4, Tm1, and Tm2. Tm1 and Tm2 both receive synaptic input from L2 in the second layer of the medulla [17, 18] projecting to the first layer of the lobula. Within the lamina, L4 sends its processes into three neighboring columns, one into its “home” column and two into the two neighboring posterior columns [19, 20]. Within each of these columns, L4 forms reciprocal connections with L2 and with the processes of those L4s originating from other columns [19–22]. In its home column, L4 receives additional synaptic input from a lamina amacrine cell, as well as from photoreceptor R6 [21, 22], which might explain why blocking synaptic output from L2 leaves the visual responses of L4 intact [23]. Within the medulla, L4 synapses onto three Tm2 cells, one located in the home column and two in the adjacent columns located posterior in visual space [17, 18] (Figure 1A; for illustration purposes, only two neighboring columns are depicted). Based on their connectivity and anatomical layout, there are two plausible hypotheses for these cells’ role in the motion detection circuit. First, Tm2 could exhibit a directional tuning for OFF motion from the front to the back, as suggested by the asymmetrical wiring between L4 and Tm2 [18]. Alternatively, Tm2 could act as one of the two input arms of the elementary OFF motion detector. In this case, Tm2 would reveal a preference for moving

<sup>3</sup>These authors contributed equally to this work

<sup>4</sup>Present address: Janelia Farm Research Campus, 19700 Helix Drive, Ashburn, VA 20147, USA

\*Correspondence: [borst@neuro.mpg.de](mailto:borst@neuro.mpg.de)



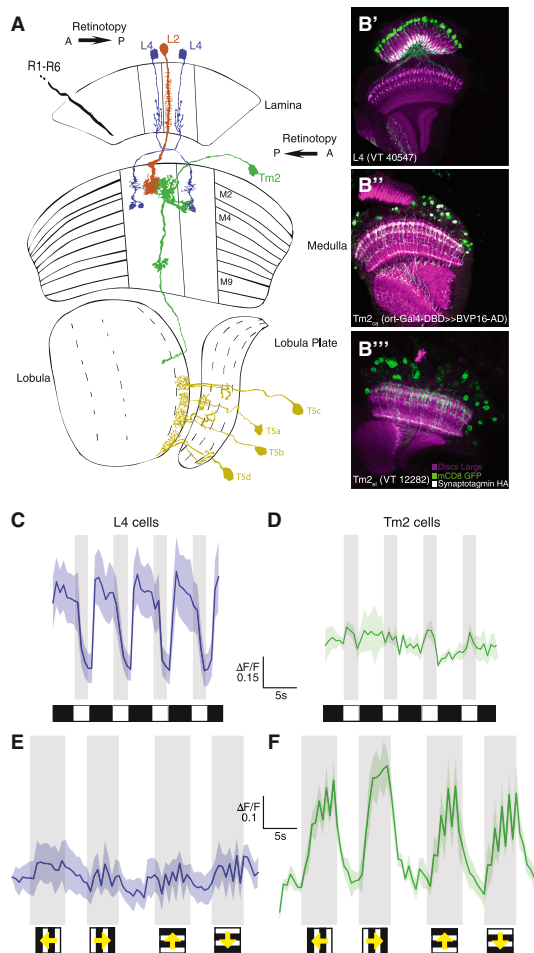


**Figure 1. Wiring Diagram and Basic Response Properties of L4 and Tm2**  
 (A) Photoreceptors (R1–R6) synapse onto the lamina monopolar cells L2 (red) and L4 (blue). These two cell types are connected in an intercolumnar and reciprocal manner in the lamina. Both give input to the transmedulla neuron Tm2 (green) in their home column. Additionally, two L4 cells from posterior columns are presynaptic to Tm2, with axonal output regions coinciding with T5 dendrites in the lobula. Adapted and modified from [6, 18].  
 (B) Confocal images of the Gal4-driver lines used in this study, shown in horizontal cross-sections. Neurons are marked in green (mCD8-GFP expression), neuropils in magenta (antibody against Dlg), and synaptic output regions in white (antibody against HA, bound to synaptotagmin). L4 (B') and Tm2<sub>Ca</sub> (B'') lines were used for Ca<sup>2+</sup> imaging. L4 (B') and Tm2<sub>el</sub> (B'') lines were used for blocking experiments.  
 (C and D) Average relative change of fluorescence in response to four-field flicker stimuli in L4 (C; n = 7) and Tm2 (D; n = 5) terminals (±SEM).  
 (E and F) Mean responses of L4 (E; n = 7) and Tm2 (F; n = 8) to square-wave gratings moving in all four cardinal directions at 30° s<sup>-1</sup>.  
 (C–F) Grey-shaded areas indicate the stimulation period. For Tm2, responses to vertical motion are slightly but significantly smaller than to horizontal motion (p < 0.015).

OFF edges, but its responses would be nondirectional; direction selectivity would only arise after a multiplicative interaction of the two input signals on the dendrites of T5 cells.

Functional analysis using behavioral readouts during selective blockade of L4 arrived at controversial conclusions: while one study found no impairment of motion-dependent behavior after silencing of L4 [23], another study observed a specific deficit in L4 block flies to detect motion from the front to the back, consistent with the first of the above hypotheses, as well as to detect moving OFF edges, consistent with the second hypothesis [24].

To probe these cells' specificity for OFF motion and their potential direction selectivity, we analyzed the visual response properties of Tm2 and L4 using Ca<sup>2+</sup> imaging. Both Tm2 and L4 are excited exclusively by moving OFF edges, albeit in a non-directional way. Both cells have a bell-shaped receptive field with a half width of approximately 5°. While L4 exhibits rather linear spatial integration properties and responds to changes in full-field luminance, Tm2 becomes inhibited by stimuli of increasing size. To investigate the participation of L4 and Tm2 in motion processing, we recorded the motion responses from wide-field tangential cells, instead of using a behavioral readout. When synaptic output from either Tm2 or L4 was blocked, responses of LPTCs to moving OFF edges are eliminated, demonstrating their crucial role in the OFF pathway of *Drosophila* motion vision.

## Results

To investigate the visual response properties of L4 and Tm2, we used cell-specific Gal4 driver lines. To verify these lines' specificity, we drove the expression of membrane-bound GFP and the hemagglutinin (HA)-tagged presynaptic marker protein synaptotagmin. We then antibody stained against GFP and HA, allowing us to compare the labeling with the branching as known from Golgi studies (GFP), as well as to determine the synaptic output layers (synaptotagmin). The L4 line shows specific expression of GFP within the optic lobe that is characteristic for this cell. Synaptotagmin staining of the line indicates synaptic output in the distal portion of the lamina and the second and fourth layer of the medulla, which is in agreement with previous Golgi and electron microscopy studies (Figure 1B') [6, 17, 18]. Both of our Tm2 driver lines showed a specific, Tm2-characteristic expression within the optic lobe and similar synaptotagmin staining, labeling the ninth layer of the medulla and the first layer of the lobula (Figures 1B'' and B'''). Additional synaptotagmin label occurs in the second and fourth layer of the medulla, where EM studies have shown that Tm2 is presynaptic to L5 [17, 18]. The strong synaptotagmin staining in the first layer of the lobula suggests that this is also an output region of Tm2 where it could provide input to T5.

### Visual Response Properties of L4 and Tm2

To optically record from these cells using two-photon microscopy [25], we used the Tm2<sub>Ca</sub> and L4 driver lines and crossed them with UAS-GCaMP5. To investigate how whole-field brightness changes are encoded in the terminals of both L4 and Tm2, we presented four spatially uniform bright pulses of light, each lasting for 2 s, interleaved by 4 s, and measured the change in fluorescence of individual L4 terminals in the second layer of the medulla and Tm2 terminals in the first layer of the lobula. In L4, the activity follows the full-field luminance in an almost tonic way, such that the lowest brightness level leads to the strongest response (Figure 1C). In contrast to L4, Tm2 does not respond to full-field luminance changes (Figure 1D). In order to test whether direction selectivity is already

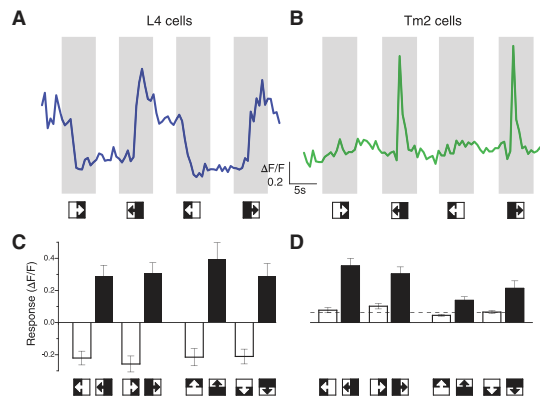
Neurons of the Fly OFF Motion Vision Pathway  
 387


Figure 2. L4 and Tm2 Responses to Moving Edges

(A and B) Single-cell response traces of L4 (A) and Tm2 (B) to horizontally moving edges of either polarity. Stimulation period is indicated by the shaded area.

(C and D) Mean responses of L4 (C;  $n = 10$ ) and Tm2 (D;  $n = 12$ ) to ON (white bars) and OFF (black bars) edges moving at  $30^\circ \text{ s}^{-1}$ . Chance response level is indicated by the dashed line (see the [Experimental Procedures](#)). Error bars indicate  $\pm$ SEM. For Tm2, responses to OFF edges moving in the vertical direction are significantly smaller than those for the horizontal direction ( $p < 0.01$ ).

See also [Figure S3](#).

present at the level of Tm2 or L4, we presented square-wave gratings moving in the four cardinal directions (back to front, front to back, upward, and downward). L4 responds with only small modulations in activity to square-wave motion ([Figure 1E](#)). In striking difference to L4, Tm2 responds strongly to gratings moving in all directions. Contradicting the hypothesis based on the asymmetric wiring in the medulla [18], Tm2 shows no directional preference, responding to gratings moving in all directions in a similar way, albeit with a somewhat smaller amplitude to vertical than to horizontal motion ([Figure 1F](#)).

Anatomical evidence has implicated both Tm2 and L4 as being postsynaptic to L2 and, thus, as potential elements in the OFF motion pathway [17, 18]. Therefore, we tested their sensitivity to the contrast polarity of moving edges. We presented either bright or dark edges, each moving in all four cardinal directions. Interestingly, L4 and Tm2 respond with quite different dynamics, as exemplified in single-cell traces in response to horizontal edge motion ([Figures 2A and 2B](#)). In L4, when an OFF edge passes the fly's visual field, the activity transiently increases settling at a plateau level that persists until the subsequent ON edge arrives. The ON edge strongly reduces L4's activity. Hence, L4 encodes moving edges with a persistent DC component, which is superimposed by a small transitory peak ([Figure 2A](#)). In contrast to L4, Tm2 responds solely with a fast, transient increase in activity to moving OFF edges ([Figure 2B](#)). When probed with moving ON and OFF edges in all directions, L4 responds to moving OFF edges equally in all four directions, primarily with a persistent change in activity. If L4's activity is at an elevated level, it becomes reduced by an ON edge ([Figures 2A and 2C](#)). As does L4, Tm2 responds to OFF edges moving in all four directions. However, in contrast to L4, Tm2 responds to moving OFF edges with a pronounced transient increase in activity. Tm2 does not respond at all to moving ON edges ([Figures 2B and 2D](#)).

To measure the receptive fields of Tm2 and L4, we periodically presented a dark vertical bar of  $4.5^\circ$  width on a bright background at different azimuthal positions and measured the response of both cells as defined by the difference between the relative fluorescence during bar presentation and the response level before ([Figures 3A and 3B](#)). L4 responded most strongly when the bar was within a window of about  $\pm 5^\circ$  around a position, leading to maximal response ([Figure 3A](#)). The average sensitivity profile, obtained after aligning the results from different cells with respect to their maximum, closely resembles a bell-shaped Gaussian with a half width of  $\sim 5^\circ$ . Tm2 responded to such stimuli in a similar way: again, maximum responses were elicited in a rather small window of about  $10^\circ$  widths, with no significant responses to stimulation outside this window ([Figure 3B](#)). In order to examine the spatial integration properties of L4 and Tm2, on a bright background, we presented a dark, vertical bar, increasing in size and centered at the position of a cell's maximum response. Based on L4's receptive field derived from the previous experiment and assuming linear spatial integration, we expected the responses to strongly increase with increasing bar width until approximately  $10^\circ$  and plateau thereafter. The response of L4 to small bar widths is consistent with this expectation; however, the response of L4 even increases when the bar width changes from  $25^\circ$  to  $50^\circ$  without any sign of saturation ([Figure 3C](#)). For Tm2, considering the data from the previous experiment ([Figure 3B](#)) and the fact that Tm2 doesn't respond to full-field flicker ([Figure 1D](#)), we expected a rather different spatial integration property. Indeed, Tm2 responses differ strongly from those of L4, displaying a maximum response to a bar of  $4.5^\circ$  and then decreasing rapidly as the bar becomes wider ([Figure 3D](#)). This implicates the existence of lateral inhibition, shaping the receptive field properties of Tm2.

In addition to the spatial response properties of these cells, their temporal dynamics are also of interest. Using the line-scan mode of the two-photon microscope, we measured single terminals of both cell types in response to flickering dark bars of  $4.5^\circ$  width at a temporal resolution of 480 Hz. As can be expected from their full-field flicker and edge responses, L4 and Tm2 responded with considerably different temporal dynamics. L4 reached its maximal response level approximately 100 ms after stimulus onset. At the end of the dark bar presentation, the fluorescence in L4 was still approximately 50% of the maximum response ([Figure 3E](#)). Tm2 responded with comparable rise times—reaching maximum response levels 100 ms after stimulus onset—but decayed much faster than L4. At the end of the bar presentation, Tm2 responses had decayed to 20% of their maximum value ([Figure 3F](#)). Note that all data obtained from  $\text{Ca}^{2+}$  imaging in layer 1 of the lobula are consistent with data from M9 (data not shown).

#### Motion Responses after Blocking L4 or Tm2

Our results from  $\text{Ca}^{2+}$  imaging of Tm2 and L4 cells revealed that none of these cells exhibit a preference for grating or edge motion in any direction. However, both cells become selectively excited by brightness decrease, as expected from being postsynaptic to L2. In order to assess their participation in motion processing, we blocked synaptic output of either Tm2 or L4 by expressing shibire [27] and recorded the responses of lobula plate tangential cells to moving ON and OFF edges (data from horizontal system [HS] and vertical system [VS] cells were pooled). Control flies of identical genotype but not subjected to a temperature shift showed strong and

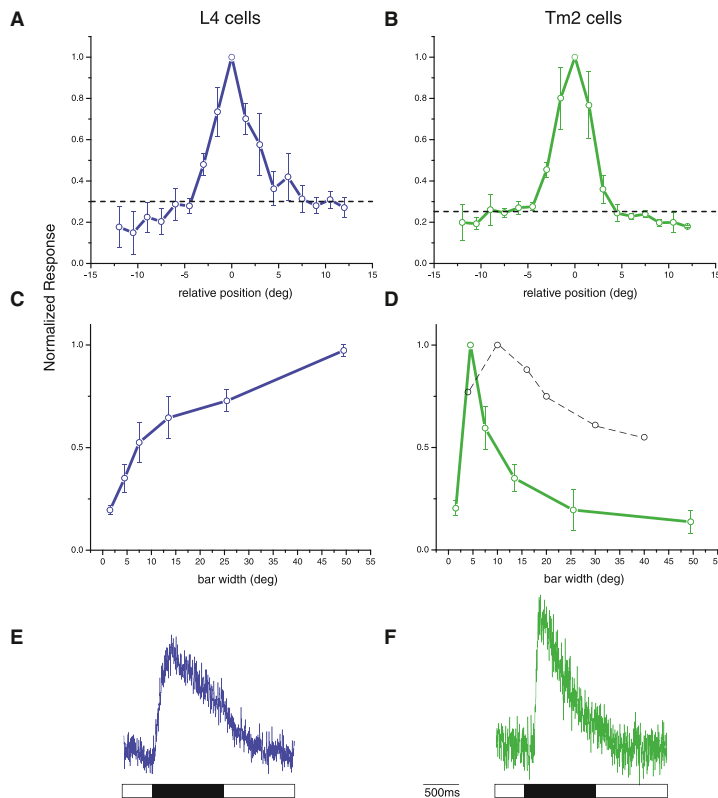


**Figure 3. Response Characteristics of L4 and Tm2 Cells upon Stimulation with Flickering Bars**

(A and B)  $\text{Ca}^{2+}$  response of L4 (A;  $n = 5$ ) and Tm2 (B;  $n = 5$ ) to 4.5°-wide, dark, vertical bars appearing and disappearing at various positions (shifted by 1.5°) on a bright background at a frequency of 0.5 Hz. Graphs were normalized to the position of the maximum response. Chance response level is indicated by the dashed line (see the [Experimental Procedures](#)). Error bars indicate  $\pm$ SEM.

(C and D) Normalized  $\text{Ca}^{2+}$  response of L4 (C;  $n = 7$ ) and Tm2 (D;  $n = 5$ ) cells to dark, vertical bars of increasing size (bar widths: 1.5°, 4.5°, 7.5°, 13.5°, 25.5°, and 49.5°). For comparison, L2 responses from [26] are indicated as a dashed line in (D).

(E and F)  $\text{Ca}^{2+}$  response of a single L4 (E; 50 sweeps) and Tm2 (F; ten sweeps) cell (in arbitrary units) stimulated by a 4.5°-wide dark bar for 1 s, recorded at 480 Hz. The duration of the stimulation is indicated by the black bar below.

See also [Figure S3](#).

responses between control and block flies is shown in [Figure S1](#) (available online). All of these findings are reminiscent on the results of previous studies in which either L2 or T5 cells were blocked, leading to a selective loss of tangential cell responses to OFF edges [10, 12].

We also tested the responses of L4 and Tm2 block flies to grating motion ([Figure S2](#)). As expected from the above results and the assumption that T4 and T5 cells contribute to the grating response with about equal weight, grating responses to horizontal and to vertical

reliable directional responses to both ON and OFF edges, depolarizing by about 8 mV during motion in the preferred direction and hyperpolarizing by about 5 mV during motion in the null direction of the tangential cells (black and gray traces in [Figures 4A–4D](#)). When L4 cells were blocked, the responses to ON edges moving along the preferred as well the null direction were almost indistinguishable from those in control flies (blue traces in [Figures 4A and 4C](#)). However, the responses to OFF edges were severely reduced, both for preferred-direction and for null-direction motion (blue traces in [Figures 4B and 4D](#)). When Tm2 was blocked, tangential cells responded strongly to ON edges moving along the preferred direction of the cells, but the response to null direction had less than half of the amplitude as compared to control flies (green traces in [Figures 4A and 4C](#)). For OFF edge motion, a similar result was obtained as for L4 block flies: Again, the response to motion along both the preferred and the null directions was almost completely abolished (green traces in [Figures 4B and 4D](#)). Using the time average of the difference between the preferred- and null-direction response as a measure, the results can be summarized as follows ([Figures 4E and 4F](#)): blocking synaptic output from L4 cells leaves the ON edge responses unaffected, but strongly and highly significantly reduces the OFF edge response (blue bars, compared to black bars); and blocking synaptic output from Tm2 cells reduces the ON edge responses somewhat, but abolishes the OFF edge response completely (green bars, compared to gray bars). A detailed comparison of preferred- and null-direction

motion in L4 and Tm2 block flies are found to be at roughly half of the amplitude as in control flies. However, consistently in HS and VS cells, the null-direction response is compromised more strongly than is the preferred-direction response. While this might indicate a direction-specific contribution of L4 and Tm2 at first sight, it can be readily explained by a slightly elevated threshold of the inhibitory input to the tangential cells. We therefore conclude that both L4 and Tm2 cells represent essential, nondirectional components of the OFF motion pathway in *Drosophila*.

## Discussion

Our results reveal that L4 and Tm2 cells are necessary components for the computation of OFF motion signals. In line with this notion, we find both L4 and Tm2 neurons being excited preferentially by moving OFF edges. Furthermore, we demonstrate that direction selectivity does not occur at the level of L4 or Tm2 cells, but is rather computed downstream of Tm2, presumably in the dendrites of T5 cells.

## Contrast Polarity and Direction Sensitivity

Using full-field flicker and moving edges of single contrast polarity, we measured the basic response characteristics of both L4 and Tm2 cells. L4 cells receive their main input from L2 in the lamina, where they form reciprocal, cholinergic connections [18, 21]. In agreement with previous studies [23, 28], we observed a decrease in  $\text{Ca}^{2+}$  when stimulating

# Neural Circuit Components of the *Drosophila* OFF Motion Vision Pathway

Neurons of the Fly OFF Motion Vision Pathway  
389

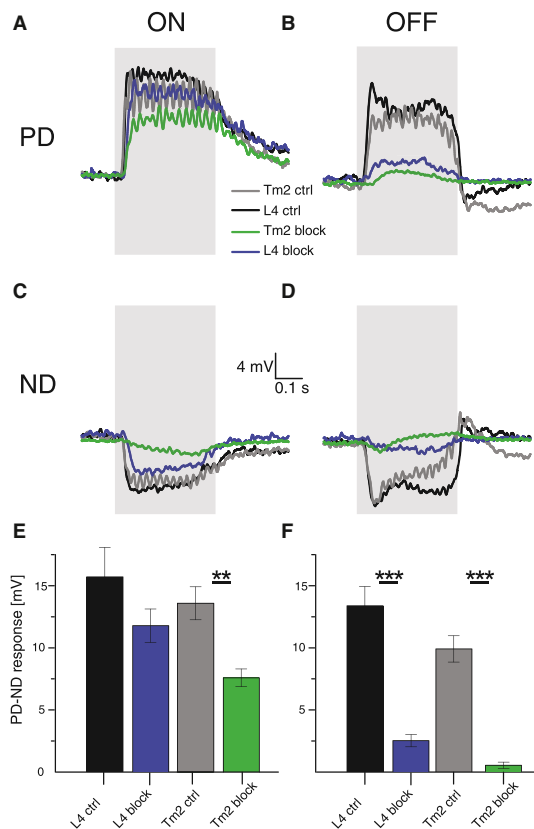


**Figure 4.** Voltage Responses of Lobula Plate Tangential Cells to Moving ON and OFF Edges

(A–D) Average time course of the membrane potential in response to ON (A and C) and OFF (B and D) edges moving along the preferred (PD; A and B) and null (ND; C and D) direction as recorded in two types of control flies (gray and black), as well as in flies in which synaptic output from L4 (blue) or Tm2 (green) cells was blocked. The stimulation period is indicated by the shaded area.

(E and F) Mean voltage responses (PD – ND) to ON (E) and OFF (F) edges of tangential cells in all four groups of flies. Recordings were done from HS [2] and VS [1] cells. HS cells have front to back as their PD and back to front as their ND; VS cells have downward as their PD and upward as their ND. Since no difference was detected between HS and VS cells, data from both cell types were pooled. L4 control data are from nine cells (four HS, five VS) in two flies, L4 block data are from ten cells (three HS, seven VS) in two flies, Tm2 control data are from 14 cells (six HS, eight VS) in eight flies, and Tm2 block data are from 11 cells (five HS, six VS) in five flies. In L4 block flies, ON responses are nonsignificantly different from control flies, whereas OFF responses are highly significantly reduced. In Tm2 block flies, ON responses are significantly different from control flies, and OFF responses are highly significantly reduced. \* $p < 0.05$ , \*\* $p < 0.001$ , \*\*\* $p < 0.0001$ , tested using two-tailed t tests against their controls. Error bars indicate  $\pm$ SEM. See also Figures S1–S3.

L4 with brightness increments and an increase of  $Ca^{2+}$  when presenting light decrements. Assuming an excitatory connection between L2 and L4, these results are consistent with data that have been described for L2 [23, 26, 29]. The temporal response characteristics of L4, however, differ substantially from those observed in L2 by the existence of a sustained

component in L4, which is not seen in L2. This discrepancy is in agreement with the finding that L4 receives input from photoreceptors, both directly from R6 and indirectly via the lamina amacrine cell, in addition to the input from L2 [22]. Tm2 receives its main input from L2. In agreement with this notion, we observed an increased  $Ca^{2+}$  signal in response to brightness decrements and no response to brightness increments. The transient nature of the signal and its selectivity for OFF edges parallels the reported findings for the  $Ca^{2+}$  signal in the terminal region of L2 [15, 29], suggesting that half-wave rectification in the L2 terminal represents the biophysical mechanism for OFF selectivity within the L2 pathway [29]. In contrast to L2, L4, and previous electrophysiological recordings in the calliphorid ortholog of Tm2 [28], Tm2 cells in *Drosophila* do not show any response to full-field luminance changes of either polarity. This finding indicates the existence of an inhibitory subregion of the receptive field. It also argues against the hypothesis that intercolumnar L4 connections onto Tm2 might implement a pooling of excitatory neighboring signals [18]. Furthermore, the observed nondirectional responses of both L4 and Tm2 allow us to rule out the hypothesis that the asymmetrical wiring between L4 and Tm2 could implement direction selectivity [18]. This passes the emergence of direction selectivity to the postsynaptic neurons—presumably T5—that have been shown to exhibit a precise directional tuning [12].

## Receptive Field Properties

Stimulation with dark bars at different positions and increasing widths revealed the receptive field properties of L4 and Tm2 cells. We could demonstrate that the spatial sensitivity distribution for excitatory input to both cells exhibits comparable characteristics in the azimuthal extent when probed by small bars. However, it differs significantly in response to larger objects. Here, the response of L4 cells increases with the size of the visual stimulus, and thus varies distinctly from the center-surround receptive field described in L2 [26]. This is a further indication for a contribution of additional inputs to L4, e.g., via wide-field amacrine cells. As is shown by a linear receptive field model—an isotropic Gaussian inhibitory center with a half width  $\sigma$  of  $2^\circ$  and a spatially constant excitatory surround—even a minute excitatory surround contribution, undetectable by local stimulation, is sufficient to account for the increase in response with increasing stimulus size (Figure 5E). Tm2, in contrast, seems to be inhibited by large objects, since their response decreases dramatically when stimulated with bars wider than  $4.5^\circ$ . With  $Ca^{2+}$  as a proxy for membrane voltage, this inhibitory surround has not been detected by the stimulation with small bars at such lateral positions, either because intracellular  $Ca^{2+}$  does not decrease with membrane hyperpolarization or because the  $Ca^{2+}$  indicator does not report these low concentrations. Compared to L2 [26], surround inhibition seems to be much more pronounced in Tm2 (L2 responses from [26] are indicated as dashed line in Figure 3D). Tm2 cells lack every response to objects larger than  $25^\circ$ , indicating the existence of further lateral inhibition at the level of Tm2 that leads to a sharpening of their receptive field, probably via wide-field amacrine cells. In order to quantitatively reproduce Tm2 responses to bars of increasing width and moving gratings, we modeled the receptive field of Tm2 as the difference of two Gaussians with a half width  $\sigma$  of  $2^\circ$  horizontally and  $4^\circ$  vertically for the inhibitory center and of  $10^\circ$  horizontally and  $20^\circ$  vertically for the excitatory surround. This combination resulted in a maximum local surround excitation that amounted



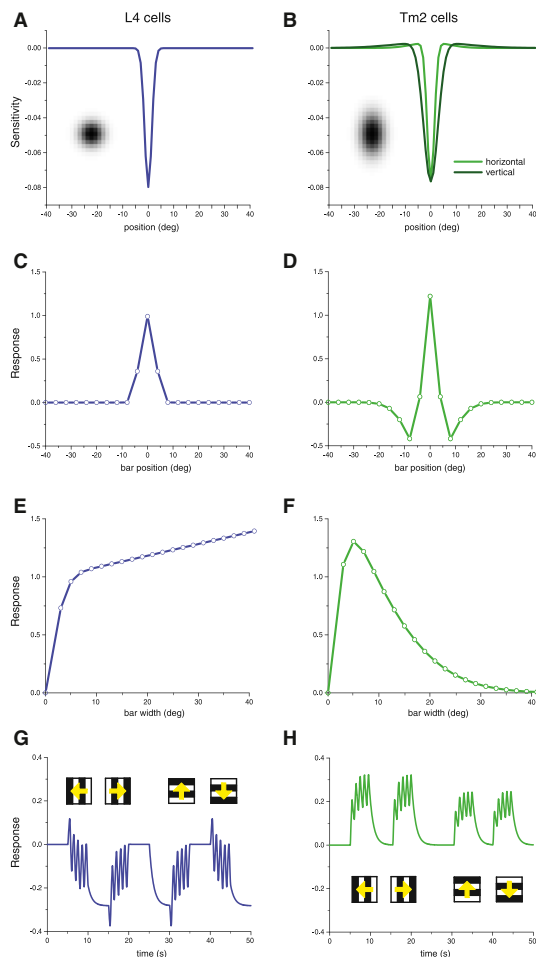


**Figure 5. Model Simulations of L4 and Tm2 Receptive Fields**  
 (A and B) Sensitivity profile across the receptive field of L4 (A) and Tm2 (B). The insets show a magnified view of the 2D receptive field, with each pixel corresponding to one  $1^\circ \times 2^\circ$  of visual space.  
 (C and D) Responses of L4 (C) and Tm2 (D) to a  $7^\circ$ -wide bar as a function of bar position.  
 (E and F) Responses of L4 (E) and Tm2 (F) to a bar, centered in the receptive field, as a function of bar width.  
 (G and H) Responses of L4 (G) and Tm2 (H) to a grating (spatial wavelength =  $20^\circ$ ) moving at a temporal frequency of 1 Hz along four orthogonal directions. Responses were obtained by low-pass filtering ( $\tau = 1$  s) of original signals from L4 and half-wave rectifying signals from Tm2.  
 See also Figure S3.

to only 3% of the peak center inhibition, but nevertheless was able to fully reproduce the strong decrease of the response of Tm2 with increasing bar width seen in the experiments (Figures 5B and 5F). A further interesting difference between L4 and Tm2 appears in their responses to moving square wave gratings: while L4 responses remain at rest, at best being slightly modulated at the temporal frequency of the local luminance changes (Figure 1E), Tm2 responses build up during grating motion with temporal modulations riding on

top (Figure 1F). As shown by model simulations, these differences are readily explained by the half-wave rectified response property of Tm2, but not in L4, assuming a temporal integration of the membrane potential either by intracellular  $\text{Ca}^{2+}$  and/or the buffering of the indicator (Figures 5G and 5H). Furthermore, assuming a slight anisotropy of the receptive field of Tm2 as explained above (Figure 5B), similar to what has been reported for L2 [26], the simulation results for grating motion are consistent with the somewhat smaller response amplitude of Tm2 to vertical than to horizontal motion (Figure 5H). Note, however, that the anisotropy of the Tm2 receptive field was not directly measured.

#### L4 and Tm2 Are Crucial OFF Pathway Elements

To test the role of L4 and Tm2 in motion detection in *Drosophila*, we blocked their synaptic output and recorded from tangential cells of the lobula plate. Unlike a behavioral study by Silies and colleagues that shows only mild reductions in responses to OFF motion stimuli when blocking L4 [23], we observed a strong impairment of tangential cell responses for OFF motion. This difference might be explained by differing expression levels of Gal4 in L4 fly lines: in the same study, silencing L4 in two different fly lines caused significantly different effects of responses toward opposing edges [23]. In another study, Tuthill and colleagues tested the effect of blocking all lamina neurons individually on turning behavior of flying *Drosophila* [24]. In agreement with our results, blocking L4 resulted in a selective impairment of the turning responses to OFF versus ON edges. In response to grating motion from the front to the back, these flies also exhibited a response reduction to about 50% of control level, as is expected from our data (Figures 4, S1, and S2). However, the same flies reacted with the same amplitude as control flies to grating motion from the back to the front. Since the behavioral response to back-to-front motion is much smaller than that to front-to-back motion, the residual tangential cell response might be sufficient to generate normal behavioral output under these conditions. Our results show that L4 is necessary for OFF motion signals in tangential cells (Figure 4). The same effect was observed when Tm2 was blocked. Blocking and  $\text{Ca}^{2+}$  imaging experiments match, because no direction-specific defect could be detected. This speaks in favor of the hypothesis that blocking Tm2 corresponds to the disruption of one input element to the Reichardt detector. L4, on the other hand, as one of the major input elements to Tm2 [18], seems to be needed either for a proper functioning of L2, or in conjunction with L2 to successfully evoke signals in Tm2. Our data also show a reduction in the responses of tangential cells in Tm2 block flies to ON stimuli, especially in the cells' null direction (Figure 4). This decrease of the ON response could be caused by disruption of a potential tonic input of Tm2 to the ON pathway via L5 [17, 18] or via its arborization in medulla layer 9. Together with the spatiotemporal response properties of Tm2 reported above, the following conclusions can be drawn regarding motion processing in the OFF pathway: (1) The narrow receptive field of Tm2 (Figure 3B) with a half width of about  $5^\circ$  indicates input from only a single optical cartridge. This is significantly smaller than the "anatomical receptive field," as reported in Takemura et al. [17] for Tm3, one of the inputs to the T4 cells, and thus might represent an interesting difference between the ON and the OFF motion pathway. (2) The strong surround inhibition we see in Tm2 (Figure 3D) readily explains the missing responses to field flicker stimuli that was observed in T5 cells

[12]. (3) The rather transient response of Tm2 (Figures 2B and 3F) makes it a candidate for the fast (i.e., high-pass filtered) input to the motion detection mechanism in the postsynaptic dendrite of T5 cells. This is all the more true since the calcium indicator is expected to slow down the signal significantly; thus, the membrane potential response in Tm2 will certainly be even faster. As a caveat, however, no data on Tm1 neurons exist so far to compare with. (4) The fact that blocking Tm2 abolishes the OFF response in the tangential cells for all stimulus directions (Figures 4B, 4D, and 4F) suggests that Tm2 serves as input element for all four types of T5 cells tuned to the four cardinal directions.

In summary, we thus conclude that L4 and Tm2 are essential OFF motion processing elements in the fly visual system that are not directionally selective. Consequently, direction selectivity in the OFF pathway is likely to arise at the level of the T5 dendrites.

## Experimental Procedures

### Flies

Flies were raised on standard cornmeal-agar medium with 12 hr light/12 hr dark cycles, 25°C, and 60% humidity. For Ca<sup>2+</sup> imaging, we used the genetically encoded indicator GCaMP5 [30] driven by two different Gal4 lines with the following genotypes: Tm2<sub>ca</sub> line (*w<sup>-</sup>;ort-Gal4-DBD,N9A >> BVP16-AD;UAS-GCaMP5*), provided by Chi-Hon Lee [31], and L4 line (*w<sup>-</sup>;UAS-GCaMP5;VT40547-Gal4*, VDRC stock number 200265). Cell-specific block effects in electrophysiological experiments were accomplished using UAS-shibire<sup>ts</sup> [27]. Fly lines with the following genotypes were used for electrophysiological recordings: L4 line (*shi<sup>ts</sup>/+;+;shi<sup>ts</sup>/VT40547-Gal4*, VDRC stock number 200265) and Tm2<sub>el</sub> line (*shi<sup>ts</sup>/+;+;shi<sup>ts</sup>/VT12282-Gal4*, VDRC stock number 203097). Expression and specificity of driver lines were investigated using a combination of membrane tethered GFP and synaptotagmin-hemagglutinin (courtesy of Andreas Prokop) [32, 33]. Fly lines had the following genotypes: Tm2<sub>ca</sub> line (*w<sup>-</sup>;UAS-SYT-HA,UAS-mCD8-GFP/ort-Gal4-DBD,N9A >> BVP16-AD;+*), Tm2<sub>el</sub> line (*w<sup>-</sup>;UAS-SYT-HA,UAS-mCD8-GFP/+;VT12282-Gal4/+*), and L4 line (*w<sup>-</sup>;UAS-SYT-HA,UAS-mCD8-GFP/+;VT40547-Gal4/+*). The Tm2<sub>ca</sub> line had a higher Gal4 expression level than did the Tm2<sub>el</sub> line. The Tm2<sub>el</sub> line, however, showed a more specific expression pattern. Detailed descriptions of preparation and experiments are found in [29] for Ca<sup>2+</sup> imaging and in [1] for electrophysiology.

### Immunohistochemistry and Confocal Imaging

Immunostainings were performed as described in [2]. As primary antibodies (1:200) we used mouse anti-discs large (DLG, Developmental Studies Hybridoma Bank), rabbit anti-GFP-Alexa488 conjugate (Molecular Probes), and rat anti-hemagglutinin (Roche). For visualization, we used the following secondary antibodies (1:200 in PBT): goat anti-mouse Alexa 568, goat anti-rat Alexa 568 (Molecular Probes), and goat anti-mouse Alexa 647 (Rockland Immunochemicals). Brains were mounted (IMM, Ibiid) and optically sectioned in the horizontal plane with a Leica SP5 confocal microscope. For documentation, single sections were processed in ImageJ 1.46r (NIH).

### Electrophysiology

The recording protocol was adapted from [1]. In addition, the glial sheet was digested locally by application of a stream of 0.5 mg/ml collagenase IV (GIBCO) through a cleaning micropipette (~5 μm opening) under polarized light contrast.

### Two-Photon Microscopy and Visual Stimulation

Two-photon microscopy and visual stimulus presentation were performed as described in [12]. Square-wave gratings had a spatial wavelength of 30° of visual angle and a contrast of 88%, moving at either 30° s<sup>-1</sup> or 60° s<sup>-1</sup>. Edges had the same contrast and were moving at 30° s<sup>-1</sup>. For the experiments shown in Figures 1 and 2, each grating or edge motion was shown twice within a single sweep, each lasting 4 s. Subsequent stimuli were preceded by a 3 s pause. For the experiments shown in Figures 3A and 3B, we flickered 4.5°-wide vertical dark bars on a bright background at 0.5 Hz at 10 different positions. The position yielding maximum response was set to 0°. The responses were normalized and plotted depending on their distance to the peak response. For Figures 3C and 3D, vertical dark

bars, increasing in size, were flickered at the peak response position. The responses were normalized to the peak response. For Figures 3E and 3F, a 4.5° vertical dark bar was flickered for 1 s on a bright background (line scan, averaged trace, ten repetitions). For the experiments shown in Figure 4, multiple edges were used as stimuli moving simultaneously at 60° s<sup>-1</sup>. For stimulation of HS cells, a vertical, stationary square-wave grating with 45° spatial wavelength was presented. For ON edge motion, the right (PD) or the left (ND) edge of each light bar started moving until it merged with the neighboring bar. For OFF edge motion, the right or the left edge of each dark bar was moving. For stimulation of VS cells, the pattern was rotated by 90°. A collection of all stimuli is presented as space-time plots in Figure S3.

### Data Evaluation

Data were evaluated offline using custom written software (MATLAB) and Origin (OriginLab). For evaluation of the Ca<sup>2+</sup> imaging data, the raw image series was first converted into a relative fluorescence change (ΔF/F) series using the first five images as reference. Then a region was defined within a raw image and average ΔF/F values were determined within that region for each image, resulting in a ΔF/F signal over time. The Ca<sup>2+</sup> signal traces in Figures 1C–1F were obtained by calculation of the average ΔF/F signal over trials and flies, with shading indicating the SEM. For the bar graphs in Figure 2C, the average signals of three frames before stimulus onset were subtracted from the mean response within the three last images of edge motion. For Figure 2D, the average Ca<sup>2+</sup> signal of three images prior to visual stimulation (reference value) was subtracted from the maximum response during each stimulus presentation. The dashed line was calculated by subtraction of the reference value from a maximum, obtained without visual stimulation (chance response level). The graphs in Figures 3A and 3B show the average signal (maximum – minimum of peaks, five presentations) to flickering bars normalized to the maximum response. Again, the dashed line represents chance level. The voltage traces in Figures 4A–4D were obtained by averaging of the responses of all cells upon visual stimulation with multiple edges of either polarity in the four cardinal directions. For the bar graphs in Figures 4E and 4F, the responses during edge motion (0.375 s) along the preferred and null direction were subtracted (PD – ND). The mean PD – ND responses were subsequently averaged across all cells, with error bars representing the SEM.

### Supplemental Information

Supplemental Information includes three figures and can be found with this article online at <http://dx.doi.org/10.1016/j.cub.2014.01.006>.

### Acknowledgments

We thank Chi-Hon Lee and Andreas Prokop for providing us with fly lines; David Soll for the DLG-antibody; Johannes Plett for designing and engineering the LED arena and for technical support; Christian Theile, Wolfgang Essbauer, and Michael Sauter for fly work; Romina Kutlesa for stainings; and Aljoscha Leonhardt, Elisabeth Hopp, and Georg Ammer for constructive discussions and help with programming.

Received: October 22, 2013

Revised: November 29, 2013

Accepted: January 3, 2014

Published: February 6, 2014

### References

- Joesch, M., Plett, J., Borst, A., and Reiff, D.F. (2008). Response properties of motion-sensitive visual interneurons in the lobula plate of *Drosophila melanogaster*. *Curr. Biol.* 18, 368–374.
- Schnell, B., Joesch, M., Forstner, F., Raghun, S.V., Otsuna, H., Ito, K., Borst, A., and Reiff, D.F. (2010). Processing of horizontal optic flow in three visual interneurons of the *Drosophila* brain. *J. Neurophysiol.* 103, 1646–1657.
- Hassenstein, B., and Reichardt, W. (1956). Systemtheoretische Analyse der Zeit-, Reihenfolgen- und Vorzeichenbewertung bei der Bewegungsperzeption des Rüsselkäfers *Chlorophanus*. *Z. Naturforsch.* B 11b, 513–524.
- Reichardt, W. (1987). Computation of optical motion by movement detectors. *J. Comp. Physiol. A* 161, 533–547.

---

## Neural Circuit Components of the *Drosophila* OFF Motion Vision Pathway

---

Current Biology Vol 24 No 4  
392

5. Borst, A., and Euler, T. (2011). Seeing things in motion: models, circuits, and mechanisms. *Neuron* 71, 974–994.
6. Fischbach, K., and Dittrich, A. (1989). The optic lobe of *Drosophila melanogaster*. I. A Golgi analysis of wild-type structure. *Cell Tissue Res.* 258, 441–475.
7. Bausenwein, B., Dittrich, A.P.M., and Fischbach, K.F. (1992). The optic lobe of *Drosophila melanogaster*. II. Sorting of retinotopic pathways in the medulla. *Cell Tissue Res.* 267, 17–28.
8. Bausenwein, B., and Fischbach, K.F. (1992). Activity labeling patterns in the medulla of *Drosophila melanogaster* caused by motion stimuli. *Cell Tissue Res.* 270, 25–35.
9. Rister, J., Pauls, D., Schnell, B., Ting, C.Y., Lee, C.H., Sinakevitch, I., Morante, J., Strausfeld, N.J., Ito, K., and Heisenberg, M. (2007). Dissection of the peripheral motion channel in the visual system of *Drosophila melanogaster*. *Neuron* 56, 155–170.
10. Joesch, M., Schnell, B., Raghu, S.V., Reiff, D.F., and Borst, A. (2010). ON and OFF pathways in *Drosophila* motion vision. *Nature* 468, 300–304.
11. Buchner, E., Buchner, S., and Bülthoff, I. (1984). Deoxyglucose mapping of nervous activity induced in *Drosophila* brain by visual movement. *J. Comp. Physiol.* 155, 471–483.
12. Maisak, M.S., Haag, J., Ammer, G., Serbe, E., Meier, M., Leonhardt, A., Schilling, T., Bahl, A., Rubin, G.M., Nern, A., et al. (2013). A directional tuning map of *Drosophila* elementary motion detectors. *Nature* 500, 212–216.
13. Schnell, B., Raghu, S.V., Nern, A., and Borst, A. (2012). Columnar cells necessary for motion responses of wide-field visual interneurons in *Drosophila*. *J. Comp. Physiol. A Neuroethol. Sens. Neural Behav. Physiol.* 198, 389–395.
14. Eichner, H., Joesch, M., Schnell, B., Reiff, D.F., and Borst, A. (2011). Internal structure of the fly elementary motion detector. *Neuron* 70, 1155–1164.
15. Clark, D.A., Bursztyn, L., Horowitz, M.A., Schnitzer, M.J., and Clandinin, T.R. (2011). Defining the computational structure of the motion detector in *Drosophila*. *Neuron* 70, 1165–1177.
16. Joesch, M., Weber, F., Eichner, H., and Borst, A. (2013). Functional specialization of parallel motion detection circuits in the fly. *J. Neurosci.* 33, 902–905.
17. Takemura, S.Y., Bharioke, A., Lu, Z., Nern, A., Vitaladevuni, S., Rivlin, P.K., Katz, W.T., Olbris, D.J., Plaza, S.M., Winston, P., et al. (2013). A visual motion detection circuit suggested by *Drosophila* connectomics. *Nature* 500, 175–181.
18. Takemura, S.Y., Karuppururai, T., Ting, C.-Y., Lu, Z., Lee, C.-H., and Meinertzhagen, I.A. (2011). Cholinergic circuits integrate neighboring visual signals in a *Drosophila* motion detection pathway. *Curr. Biol.* 21, 2077–2084.
19. Braitenberg, V., and Debbage, P. (1974). A regular net of reciprocal synapses in the visual system of the fly, *Musca domestica*. *J. Comp. Physiol.* 90, 25–31.
20. Strausfeld, N.J., and Campos-Ortega, J.A. (1973). The L4 monopolar neurone: a substrate for lateral interaction in the visual system of the fly *Musca domestica* (L.). *Brain Res.* 59, 97–117.
21. Meinertzhagen, I.A., and O'Neil, S.D. (1991). Synaptic organization of columnar elements in the lamina of the wild type in *Drosophila melanogaster*. *J. Comp. Neurol.* 305, 232–263.
22. Rivera-Alba, M., Vitaladevuni, S.N., Mishchenko, Y., Lu, Z., Takemura, S.Y., Scheffer, L., Meinertzhagen, I.A., Chklovskii, D.B., and de Polavieja, G.G. (2011). Wiring economy and volume exclusion determine neuronal placement in the *Drosophila* brain. *Curr. Biol.* 21, 2000–2005.
23. Silies, M., Gohl, D.M., Fisher, Y.E., Freifeld, L., Clark, D.A., and Clandinin, T.R. (2013). Modular use of peripheral input channels tunes motion-detecting circuitry. *Neuron* 79, 111–127.
24. Tuthill, J.C., Nern, A., Holtz, S.L., Rubin, G.M., and Reiser, M.B. (2013). Contributions of the 12 neuron classes in the fly lamina to motion vision. *Neuron* 79, 128–140.
25. Denk, W., Strickler, J.H., and Webb, W.W. (1990). Two-photon laser scanning fluorescence microscopy. *Science* 248, 73–76.
26. Freifeld, L., Clark, D.A., Schnitzer, M.J., Horowitz, M.A., and Clandinin, T.R. (2013). GABAergic lateral interactions tune the early stages of visual processing in *Drosophila*. *Neuron* 78, 1075–1089.
27. Kitamoto, T. (2001). Conditional modification of behavior in *Drosophila* by targeted expression of a temperature-sensitive shibire allele in defined neurons. *J. Neurobiol.* 47, 81–92.
28. Douglass, J.K., and Strausfeld, N.J. (1995). Visual motion detection circuits in flies: peripheral motion computation by identified small-field retinotopic neurons. *J. Neurosci.* 15, 5596–5611.
29. Reiff, D.F., Plett, J., Mank, M., Griesbeck, O., and Borst, A. (2010). Visualizing retinotopic half-wave rectified input to the motion detection circuitry of *Drosophila*. *Nat. Neurosci.* 13, 973–978.
30. Akerboom, J., Chen, T.-W., Wardill, T.J., Tian, L., Marvin, J.S., Mutlu, S., Calderón, N.C., Esposti, F., Borghuis, B.G., Sun, X.R., et al. (2012). Optimization of a GCaMP calcium indicator for neural activity imaging. *J. Neurosci.* 32, 13819–13840.
31. Ting, C.-Y., Gu, S., Guttikonda, S., Lin, T.-Y., White, B.H., and Lee, C.-H. (2011). Focusing transgene expression in *Drosophila* by coupling Gal4 with a novel split-LexA expression system. *Genetics* 188, 229–233.
32. Löhner, R., Godenschwege, T., Buchner, E., and Prokop, A. (2002). Compartmentalization of central neurons in *Drosophila*: a new strategy of mosaic analysis reveals localization of presynaptic sites to specific segments of neurites. *J. Neurosci.* 22, 10357–10367.
33. Robinson, I.M., Ranjan, R., and Schwarz, T.L. (2002). Synaptotagmins I and IV promote transmitter release independently of Ca(2+) binding in the C(2)A domain. *Nature* 418, 336–340.

**Current Biology, Volume 24**

**Supplemental Information**

**Neural Circuit Components of the  
*Drosophila* OFF Motion Vision Pathway**

**Matthias Meier, Etienne Serbe, Matthew S. Maisak, Jürgen Haag, Barry J. Dickson, and Alexander Borst**

---

## Neural Circuit Components of the *Drosophila* OFF Motion Vision Pathway

---

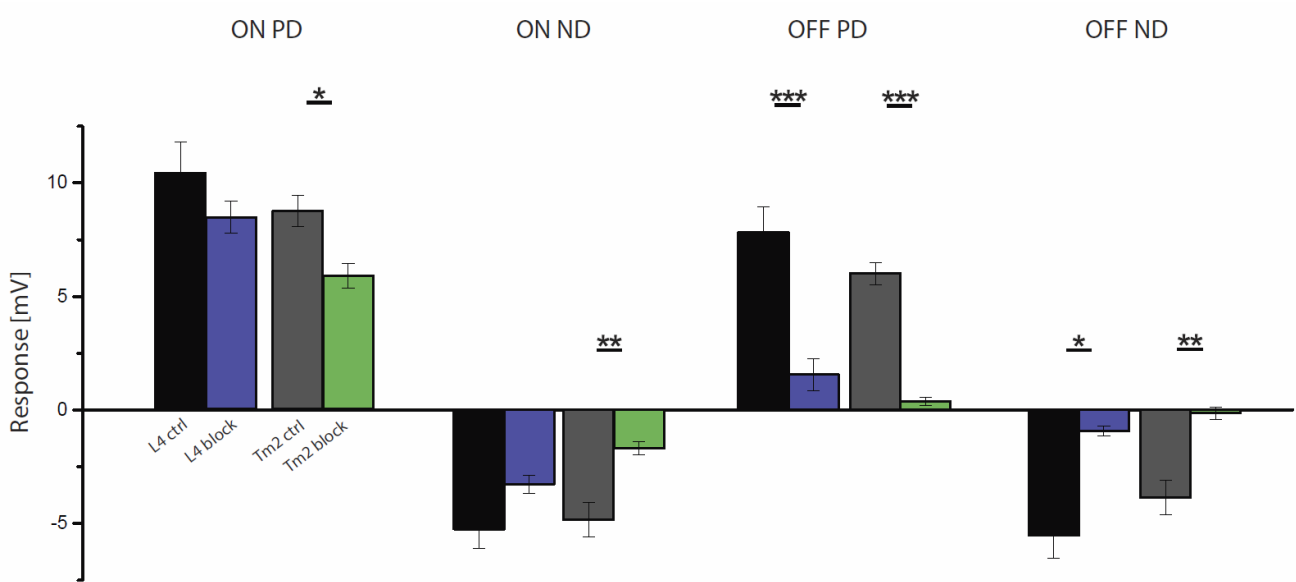


**Figure S1:** Detailed comparison of preferred (PD) and null (ND) direction responses to moving ON (left) and OFF (right) edges between L4 control and L4 block flies, and between Tm2 control and Tm2 block flies. As in Figure 4, data are pooled from HS and VS cells. L4 control data are from 9 cells (4 HS, 5 VS) in 2 flies, L4 block data from 10 cells (3 HS, 7 VS) in 2 flies, Tm2 control data from 14 cells (6 HS, 8 VS) in 8 flies, Tm2 block data from 11 cells (5 HS, 6 VS) in 5 flies. \* $p < 0.05$ , \*\* $p < 0.001$ , \*\*\* $p < 0.0001$ , tested using two-tailed t tests against their controls. Error bars denote +/- SEM. Related to Figure 4.

---

## Neural Circuit Components of the *Drosophila* OFF Motion Vision Pathway

---

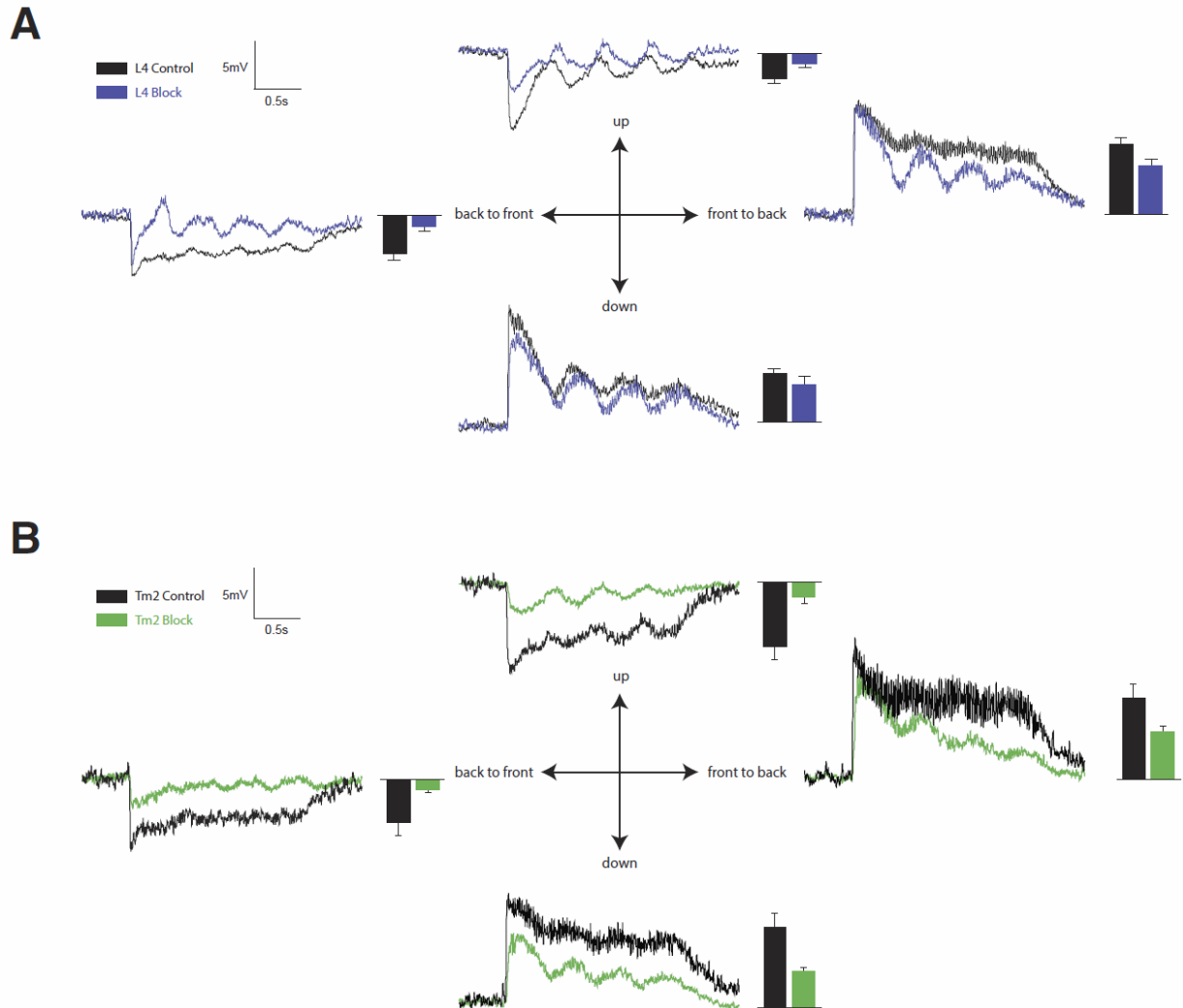


**Figure S2:** Responses to moving gratings of L4 control and L4 block flies (**A**) and of Tm2 control and Tm2 block flies (**B**). Data for horizontal motion are from HS cells, for vertical motion from VS cells. L4 control data are from 40 cells (21 HS, 19 VS) in 15 flies, L4 block data from 31 cells (12 HS, 19 VS) in 12 flies. Tm2 control data are from 14 cells (6 HS, 8 VS) in 7 flies, Tm2 block data from 11 cells (6 VS, 5 HS) in 5 flies. Error bars denote  $\pm$  SEM. Gratings had a spatial wavelength of 30 deg and were moving at 60 deg/s resulting in a temporal frequency of 2 Hz. Related to Figure 4.

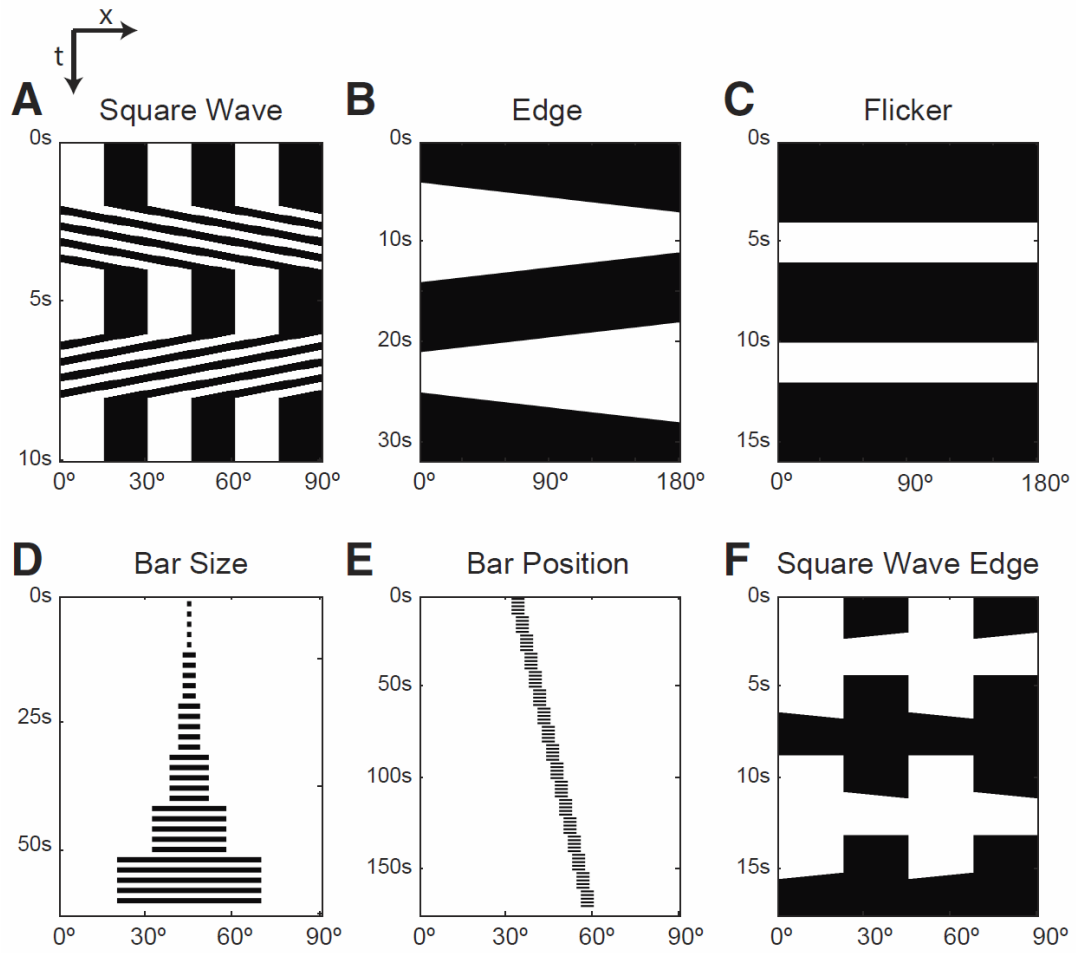


**Figure S3:** Space-time (xt) plots of all visual stimuli used in the study. Related to Figures 2-5.

# Manuscript Nr. 3: A Directional Tuning Map of *Drosophila* Elementary Motion Detectors

Matthew S. Maisak\*, Juergen Haag\*, Georg Ammer, **Etienne Serbe**, Matthias Meier, Aljoscha Leonhardt, Tabea Schilling, Armin Bahl, Gerald M. Rubin, Aljoscha Nern, Barry J. Dickson, Dierk F. Reiff, Elisabeth Hopp, and Alexander Borst

\*equal contribution

## Author Contributions:

M.S.M. and J.H. jointly performed and, together with A.Bo., evaluated all calcium imaging experiments. G.A., E.S. and **M.M.** recorded from tangential cells. A.L., T.S. and A.Ba. performed the behavioral experiments. G.M.R., B.J.D. and A.N. generated the driver lines and characterized their expression pattern. D.F.R. performed preliminary imaging experiments. E.H. helped with programming and developed the PMT shielding for the two-photon microscope. A.Bo. designed the study and wrote the manuscript with the help of all authors.



LETTER

doi:10.1038/nature12320

A directional tuning map of *Drosophila* elementary motion detectors

Matthew S. Maisak<sup>1\*</sup>, Juergen Haag<sup>1\*</sup>, Georg Ammer<sup>1</sup>, Etienne Serbe<sup>1</sup>, Matthias Meier<sup>1</sup>, Aljoscha Leonhardt<sup>1</sup>, Tabea Schilling<sup>1</sup>, Armin Bahl<sup>1</sup>, Gerald M. Rubin<sup>2</sup>, Aljoscha Nern<sup>2</sup>, Barry J. Dickson<sup>3</sup>, Dierk F. Reiff<sup>†</sup>, Elisabeth Hopp<sup>1</sup> & Alexander Borst<sup>1</sup>

The extraction of directional motion information from changing retinal images is one of the earliest and most important processing steps in any visual system. In the fly optic lobe, two parallel processing streams have been anatomically described, leading from two first-order interneurons, L1 and L2, via T4 and T5 cells onto large, wide-field motion-sensitive interneurons of the lobula plate<sup>1</sup>. Therefore, T4 and T5 cells are thought to have a pivotal role in motion processing; however, owing to their small size, it is difficult to obtain electrical recordings of T4 and T5 cells, leaving their visual response properties largely unknown. We circumvent this problem by means of optical recording from these cells in *Drosophila*, using the genetically encoded calcium indicator GCaMP5 (ref. 2). Here we find that specific subpopulations of T4 and T5 cells are directionally tuned to one of the four cardinal directions; that is, front-to-back, back-to-front, upwards and downwards. Depending on their preferred direction, T4 and T5 cells terminate in specific sublayers of the lobula plate. T4 and T5 functionally segregate with respect to contrast polarity: whereas T4 cells selectively respond to moving brightness increments (ON edges), T5 cells only respond to moving brightness decrements (OFF edges). When the output from T4 or T5 cells is blocked, the responses of postsynaptic lobula plate neurons to moving ON (T4 block) or OFF edges (T5 block) are selectively compromised. The same effects are seen in turning responses of tethered walking flies. Thus, starting with L1 and L2, the visual input is split into separate ON and OFF pathways, and motion along all four cardinal directions is computed separately within each pathway. The output of these eight different motion detectors is then sorted such that ON (T4) and OFF (T5) motion detectors with the same directional tuning converge in the same layer of the lobula plate, jointly providing the input to downstream circuits and motion-driven behaviours.

Most of the neurons in the fly brain are dedicated to image processing. The respective part of the head ganglion, called the optic lobe, consists of several layers of neuropile called lamina, medulla, lobula and lobula plate, all built from repetitive columns arranged in a retinotopic way (Fig. 1a). Each column houses a set of identified neurons that, on the basis of Golgi staining, have been described anatomically in great detail<sup>1–5</sup>. Owing to their small size, however, most of these columnar neurons have never been recorded from electrophysiologically. Therefore, their specific functional role in visual processing is still largely unknown. This fact is contrasted by rather detailed functional models about visual processing inferred from behavioural studies and recordings from the large, electrophysiologically accessible output neurons of the fly lobula plate (tangential cells). As the most prominent example of such models, the Reichardt detector derives directional motion information from primary sensory signals by multiplying the output from adjacent photoreceptors after asymmetric temporal filtering<sup>6</sup>. This model makes a number of rather counter-intuitive predictions all of which have been confirmed experimentally (for review, see ref. 7). Yet, the neurons corresponding to most

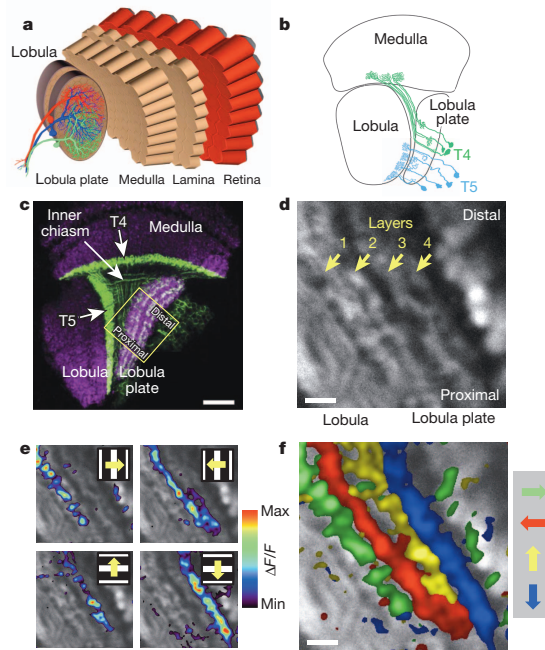


**Figure 1 | Directional tuning and layer-specific projection of T4 and T5 cells.** **a**, Schematic diagram of the fly optic lobe. In the lobula plate, motion-sensitive tangential cells extend their large dendrites over many hundreds of columns. Shown are the reconstructions of the three cells of the horizontal system<sup>22</sup>. **b**, Anatomy of T4 and T5 cells, as drawn from Golgi-impregnated material (from ref. 5). **c**, Confocal image of the Gal4-driver line R42F06, shown in a horizontal cross-section (from ref. 10). Neurons are marked in green (Kir2.1-EGFP labelled), whereas the neuropile is stained in purple by an antibody against the postsynaptic protein Dlg. Scale bar, 20 μm. **d**, Two-photon image of the lobula plate of a fly expressing GCaMP5 under the control of the same driver line R42F06. Scale bar, 5 μm. The size and orientation of the image approximately corresponds to the yellow square in **c**. **e**, Relative fluorescence changes ( $\Delta F/F$ ) obtained during 4-s grating motion along the four cardinal directions, overlaid on the grayscale image. Each motion direction leads to activity in a different layer. Minimum and maximum  $\Delta F/F$  values were 0.3 and 1.0 (horizontal motion), and 0.15 and 0.6 (vertical motion). **f**, Compound representation of the results obtained from the same set of experiments. Scale bar, 5 μm. Results in **e** and **f** represent the data obtained from a single fly averaged over four stimulus repetitions. Similar results were obtained from six other flies.

<sup>1</sup>Max Planck Institute of Neurobiology, 82152 Martinsried, Germany. <sup>2</sup>Janelia Farm Research Campus, Ashburn, Virginia 20147, USA. <sup>3</sup>Institute of Molecular Pathology, 1030 Vienna, Austria. <sup>†</sup>Present address: Institute Biology 1, Albert-Ludwigs University, 79085 Freiburg, Germany. \*These authors contributed equally to this work.

of the circuit elements of the Reichardt detector have not been identified so far. Here, we focus on a set of neurons called T4 and T5 cells (Fig. 1b) which, on the basis of circumstantial evidence, have long been speculated to be involved in motion detection<sup>1,8–10</sup>. However, it is unclear to what extent T4 and T5 cells are directionally selective or whether direction selectivity is computed or enhanced within the dendrites of the tangential cells. Another important question concerns the functional separation between T4 and T5 cells; that is, whether they carry equivalent signals, maybe one being excitatory and the other inhibitory on the tangential cells, or whether they segregate into directional- and non-directional pathways<sup>11</sup> or into separate ON- and OFF-motion channels<sup>12,13</sup>.

To answer these questions, we combined Gal4-driver lines specific for T4 and T5 cells<sup>14</sup> with GCaMP5 (ref. 2) and optically recorded the visual response properties using two-photon fluorescence microscopy<sup>15</sup>. In a first series of experiments, we used a driver line labelling both T4 and T5 cells. A confocal image (Fig. 1c, modified from ref. 10) revealed clear labelling (in green) in the medulla (T4 cell dendrites), in the lobula (T5 cell dendrites), as well as in four distinct layers of the lobula plate, representing the terminal arborizations of the four subpopulations of both T4 and T5 cells. These four layers of the lobula plate can also be seen in the two-photon microscope when the calcium indicator GCaMP5 is expressed (Fig. 1d). After stimulation of the fly with grating motion along four cardinal directions (front-to-back, back-to-front, upwards and downwards), activity is confined to mostly one of the four layers, depending on the direction in which the grating is moving (Fig. 1e). The outcome of all four stimulus conditions can be combined into a single image by assigning a particular colour to each pixel depending on the stimulus direction to which it responded most strongly (Fig. 1f). From these experiments it is clear that the four subpopulations of T4 and T5 cells produce selective calcium signals depending on the stimulus direction, in agreement with previous deoxyglucose labelling<sup>8</sup>. Sudden changes of the overall luminance evokes no responses in any of the layers (field flicker;  $n = 4$  experiments, data not shown). However, gratings flickering in counter-phase lead to layer-specific responses, depending on the orientation of the grating (Supplementary Fig. 1).

The retinotopic arrangement of this input to the lobula plate is demonstrated by experiments where a dark edge was moved within a small area of the visual field only. Depending on the position of this area, activity of T4 and T5 cells is confined to different positions within the lobula plate (Fig. 2a). Consequently, when moving a bright vertical edge horizontally from back to front, activity of T4 and T5 cells is elicited sequentially in layer 2 of the lobula plate (Fig. 2b). These two experiments also demonstrate that T4 and T5 cells indeed signal motion locally. We next investigated the question of where direction selectivity of T4 and T5 cells arises; that is, whether it is already present in the dendrite, or whether it is generated by synaptic interactions within the lobula plate. This question is hard to answer, as the dendrites of both T4 and T5 cells form a dense mesh within the proximal layer of the medulla (T4) and the lobula (T5), respectively. However, signals within the inner chiasm where individual processes of T4 and T5 cells can be resolved in some preparations show a clear selectivity for motion in one over the other directions (Fig. 2c). Such signals are as directionally selective as the ones measured within the lobula plate, demonstrating that the signals delivered from the dendrites of T4 and T5 cells are already directionally selective.

To assess the particular contribution of T4 and T5 cells to the signals observed in the above experiments, we used driver lines specific for T4 and T5 cells, respectively. Applying the same stimulus protocol and data evaluation as in Fig. 1, identical results were obtained as before for both the T4- as well as the T5-specific driver line (Fig. 3a, b). We conclude that T4 and T5 cells each provide directionally selective signals to the lobula plate, in contrast to previous reports<sup>11</sup>. Thus, both T4 and T5 cells can be grouped, according to their preferred direction, into four subclasses covering all four cardinal directions, reminiscent of ON–OFF ganglion cells of the rabbit retina<sup>16</sup>.

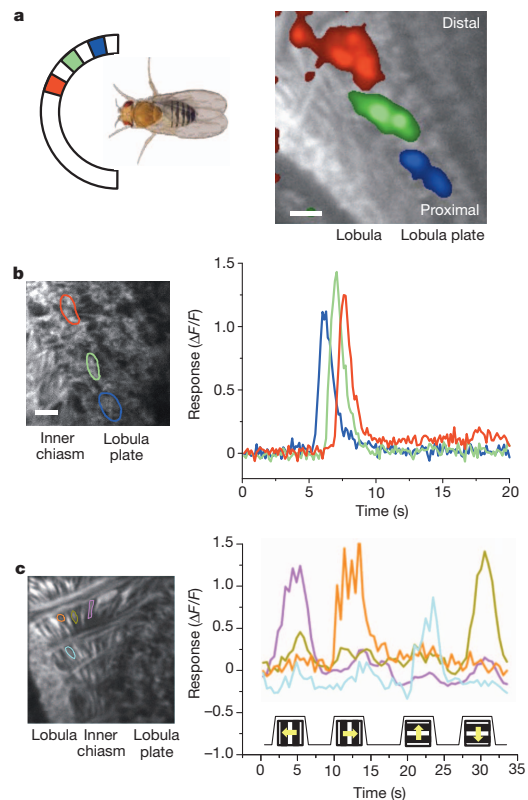


**Figure 2 | Local signals of T4 and T5 cells.** **a**, Retinotopic arrangement of T4 and T5 cells. A dark edge was moving repeatedly from front-to-back within a 15° wide area at different azimuthal positions (left). This leads to relative fluorescence changes at different positions along the proximal–distal axis within layer 1 of the lobula plate (right). Scale bar, 5 μm. Similar results have been obtained in four other flies. **b**, Sequential activation of T4 and T5 cells. A bright edge was moving from back-to-front at 15° s<sup>-1</sup>. Scale bar, 5 μm. Similar results have been obtained in six other flies. **c**, Signals recorded from individual fibres within the inner chiasm (left) reveal a high degree of direction selectivity (right). Scale bar, 5 μm. Similar results were obtained from four other flies, including both lines specific for T4 and T5 cells. Response traces in **b** and **c** are derived from the region of interest encircled in the image with the same colour.

We next addressed whether T4 cells respond differently to T5 cells. To answer this question, we used, instead of gratings, moving edges with either positive (ON edge, brightness increment) or negative (OFF edge, brightness decrement) contrast polarity as visual stimuli. We found that T4 cells strongly responded to moving ON edges, but showed little or no response to moving OFF edges (Fig. 3c). This is true for T4 cells terminating in each of the four layers. We found the opposite for T5 cells. T5 cells selectively responded to moving OFF edges and mostly failed to respond to moving ON edges (Fig. 3d). Again, we found this for T5 cells in each of the four layers. We next addressed whether there are any other differences in the response properties between T4 and T5 cells by testing the velocity tuning of both cell populations by means of stimulating flies with grating motion along the horizontal axis from the front to the back at various velocities covering two orders of magnitude. T4 cells revealed a maximum response at a stimulus velocity of 30° s<sup>-1</sup>, corresponding to a temporal frequency of 1 Hz (Fig. 3e). T5 cell responses showed a similar dependency on stimulus velocity, again with a peak at a temporal frequency of

# A Directional Tuning Map of *Drosophila* Elementary Motion Detectors

RESEARCH LETTER

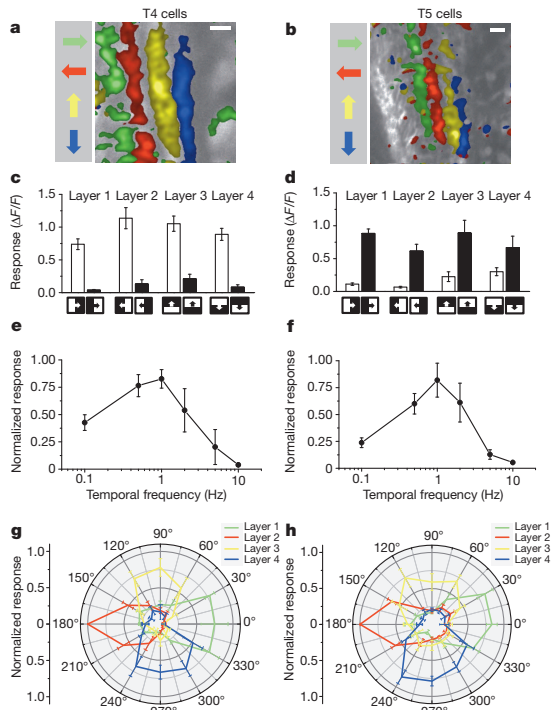


**Figure 3 | Comparison of visual response properties between T4 and T5 cells.** **a, b**, Relative fluorescence changes ( $\Delta F/F$ ) of the lobula plate terminals of T4 (**a**) and T5 (**b**) cells obtained during grating motion along the four cardinal directions. Results represent the data obtained from a single fly each, averaged over two stimulus repetitions. Scale bars, 5  $\mu\text{m}$ . Similar results have been obtained in ten other flies. **c, d**, Responses of T4 (**c**) and T5 (**d**) cells to ON and OFF edges moving along all four cardinal directions. ON (white) and OFF (black) responses within each layer are significantly different from each other, with  $P < 0.005$  except for layers 3 and 4 in T5 cells, where  $P < 0.05$ . **e, f**, Responses of T4 (**e**) and T5 (**f**) cells to gratings moving horizontally at different temporal frequencies. Relative fluorescence changes were evaluated from layer 1 of the lobula plate and normalized to the maximum response before averaging. **g, h**, Responses of T4 (**g**) and T5 (**h**) cells to gratings moving in 12 different directions. Relative fluorescence changes were evaluated from all four layers of the lobula plate normalized to the maximum response before averaging. Data represent the mean  $\pm$  s.e.m. of the results obtained in  $n = 8$  (**c**),  $n = 7$  (**d**),  $n = 6$  (**e**),  $n = 7$  (**f**),  $n = 6$  (**g**) and  $n = 5$  (**h**) different flies. Significances indicated are based on two-sample  $t$ -test.

1 Hz (Fig. 3f). Thus, there is no obvious difference in the velocity tuning between T4 and T5 cells. As another possibility, T4 cells might functionally differ from T5 cells with respect to their directional tuning width. To test this, we stimulated flies with gratings moving into 12 different directions and evaluated the relative change of fluorescence in all four layers of the lobula plate. Using the T4-specific driver line, we found an approximate half width of 60–90° of the tuning curve, with the peak responses in each layer shifted by 90° (Fig. 3g). No decrease of calcium was detectable for grating motion opposite to the preferred direction of the respective layer. When we repeated the experiments using the T5-specific driver line, we found a similar dependence of the relative change of fluorescence on the stimulus direction (Fig. 3h). We conclude that T4 cells have the same velocity and orientation tuning as T5 cells. The only functional difference we were able to detect remains their selectivity for contrast polarity.

Our finding about the different preference of T4 and T5 cells for the polarity of a moving contrast makes the strong prediction that selective

blockade of T4 or T5 cells should selectively compromise the responses of downstream lobula plate tangential cells to either ON or OFF edges. To test this prediction, we blocked the output of either T4 or T5 cells via expression of the light chain of tetanus toxin<sup>17</sup> and recorded the responses of tangential cells via somatic whole-cell patch to moving ON and OFF edges. In response to moving ON edges, strong and reliable directional responses were observed in all control flies (Fig. 4a). However, T4-block flies showed a strongly reduced response to ON edges, whereas the responses of T5-block flies were at the level of control flies (Fig. 4b, c). When we used moving OFF edges, control flies again responded with a large amplitude (Fig. 4d). However, the responses of T4-block flies were at the level of control flies, whereas the responses of T5-block flies were strongly reduced (Fig. 4e, f). These findings are reminiscent of the phenotypes obtained from blocking lamina cells L1 and L2 (ref. 13) and demonstrate that T4 and T5 cells are indeed the motion-coding intermediaries for these contrast polarities on their way to the tangential cells of the lobula plate. Whether the residual responses to ON edges in T4-block flies and to OFF edges in T5-block flies are due to an incomplete signal separation between the two pathways or due to an incomplete genetic block in both fly lines is currently unclear.

To address the question of whether T4 and T5 cells are the only motion detectors of the fly visual system, or whether they represent one cell class, in parallel to other motion-sensitive elements, we tethered flies walking on an air-suspended sphere<sup>18</sup> and stimulated them by ON and OFF edges moving in opposite directions<sup>19</sup>. As in the previous experiments, we blocked T4 and T5 cells specifically by selective expression of the light chain of tetanus toxin. During balanced motion, control flies did not show significant turning responses to either side (Fig. 4g). T4-block flies, however, strongly followed the direction of the moving OFF edges, whereas T5-block flies followed the direction of the moving ON edges (Fig. 4h, i). In summary, the selective preference of T4-block flies for OFF edges and of T5-block flies for ON edges not only corroborates our findings about the selective preference of T4 and T5 cells for different contrast polarities, but also demonstrates that the signals of T4 and T5 cells are indeed the major, if not exclusive, inputs to downstream circuits and motion-driven behaviours.

Almost a hundred years after T4 and T5 cells have been anatomically described<sup>3</sup>, this study reports their functional properties in a systematic way. Using calcium as a proxy for membrane voltage<sup>20</sup>, we found that both T4 and T5 cells respond to visual motion in a directionally selective manner and provide these signals to each of the four layers of the lobula plate, depending on their preferred direction. Both cell types show identical velocity and orientation tuning which matches the one of the tangential cells<sup>21,22</sup>. The strong direction selectivity of both T4 and T5 cells is unexpected, as previous studies had concluded that the high degree of direction selectivity of tangential cells is due to a push-pull configuration of weakly directional input with opposite preferred direction<sup>23,24</sup>. Furthermore, as the preferred direction of T4 and T5 cells matches the preferred direction of the tangential cells branching within corresponding layers, it is currently unclear which neurons are responsible for the null-direction response of the tangential cells. As for the functional separation between T4 and T5 cells, we found that T4 cells selectively respond to brightness increments, whereas T5 cells exclusively respond to moving brightness decrements. Interestingly, parallel ON and OFF motion pathways had been previously postulated on the basis of selective silencing of lamina neurons L1 and L2 (ref. 13). Studies using apparent motion stimuli to probe the underlying computational structure arrived at controversial conclusions: whereas some studies concluded that there was a separate handling of ON and OFF events by motion detectors<sup>12,25,26</sup>, others did not favour such a strict separation<sup>19,27</sup>. The present study directly demonstrates the existence of separate ON and OFF motion detectors, as represented by T4 and T5 cells, respectively. Furthermore, our results anatomically confine the essential processing steps of elementary

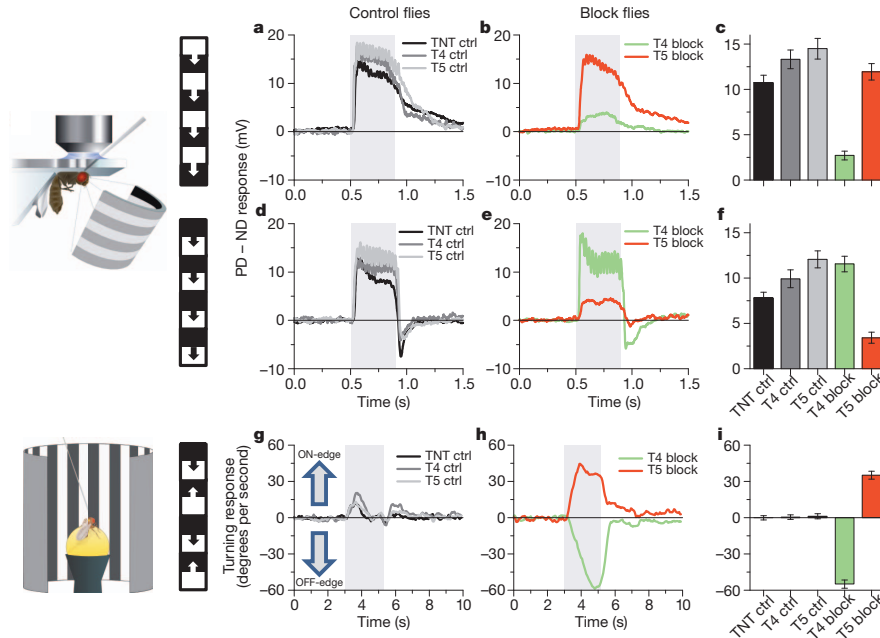


**Figure 4 | Voltage responses of lobula plate tangential cells and turning responses of walking flies to moving ON and OFF edges.** **a, d,** Average time course of the membrane potential in response to preferred direction motion minus the response to null direction motion (PD – ND response) as recorded in three types of control flies (stimulation period indicated by shaded area). **b, e,** Same as in **a, d,** but recorded in T4-block flies (green) and T5-block flies (red). The stimulus pattern, shown to the left, consisted of multiple ON- (**a**) or OFF-edges (**d**). **c, f,** Mean voltage responses (PD – ND) of tangential cells in the five groups of flies. Recordings were done from cells of the vertical<sup>21</sup> and the horizontal<sup>22</sup> system. Because no difference was detected between them, data were pooled. Data comprise recordings from  $n = 20$  (TNT control),  $n = 12$  (T4 control),  $n = 16$  (T5 control),  $n = 17$  (T4 block) and  $n = 18$  (T5 block) cells. In both T4 and T5-block flies, ON and OFF responses are significantly different

from each other with  $P < 0.001$ . In T4-block flies, ON responses are significantly reduced compared to all three types of control flies, whereas in T5-block flies, OFF responses are significantly reduced, both with  $P < 0.001$ . **g,** Average time course of the turning response of three types of control flies to ON and OFF edges moving simultaneously to opposite directions (stimulation period indicated by shaded area). **h,** Same as in **g,** but recorded from T4-block flies (green) and T5-block flies (red). **i,** Mean turning tendency ( $\pm$ s.e.m.) during the last second of the stimulation period averaged across all flies within each group. Data comprise average values obtained in  $n = 12$  (TNT controls),  $n = 11$  (T4 controls),  $n = 13$  (T4 block) and  $n = 12$  (T5 block) flies. Values of T4 and T5-block flies are highly significantly different from zero with  $P < 0.001$ . Significances indicated are based on two-sample  $t$ -test.

motion detection—that is, asymmetric temporal filtering and non-linear interaction—to the neuropile between the axon terminals of lamina neurons L1 and L2 (ref. 28) and the dendrites of directionally selective T4 and T5 cells (Supplementary Fig. 2). The dendrites of T4 and T5 cells might well be the place where signals from neighbouring columns interact in a nonlinear way, similar to the dendrites of starburst amacrine cells of the vertebrate retina<sup>29</sup>.

**METHODS SUMMARY**

**Flies.** Flies used in calcium imaging experiments (Figs 1–3) had the following genotypes: T4/T5 line ( $w^-; +/+; UAS-GCaMP5, R42F06-GAL4/UAS-GCaMP5, R42F06-GAL4$ ), T4 line ( $w^-; +/+; UAS-GCaMP5, R54A03-GAL4/UAS-GCaMP5, R54A03-GAL4$ ), T5 line ( $w^-; +/+; UAS-GCaMP5, R42H07-GAL4/UAS-GCaMP5, R42H07-GAL4$ ). Flies used in electrophysiological and behavioural experiments (Fig. 4) had identical genotypes of the following kind: TNT control flies ( $w^+/w^+; UAS-TNT-E/UAS-TNT-E; +/+$ ), T4 control flies ( $w^+/w^-; +/+; VT37588-GAL4/+$ ), T5 control flies ( $w^+/w^-; +/+; R42H07-GAL4/+$ ), T4-block flies ( $w^+/w^-; UAS-TNT-E/+; VT37588-GAL4/+$ ), T5-block flies ( $w^+/w^-; UAS-TNT-E/+; R42H07-GAL4/+$ ).

**Two-photon microscopy.** We used a custom-built two-photon laser scanning microscope<sup>29</sup> equipped with a  $\times 40$  water immersion objective and a mode locked Ti:sapphire laser. To shield the photomultipliers from the stimulus light, two separate barriers were used: the first was placed directly over the LEDs, the second extended from the fly holder over the arena. Images were acquired at a resolution of  $256 \times 256$  pixels and a frame rate of 1.87 Hz, except where indicated, using ScanImage software<sup>30</sup>.

**Electrophysiology.** Recordings were established under visual control using a Zeiss Microscope and a  $\times 40$  water immersion objective.

**Behavioural analysis.** The locomotion recorder was custom-designed according to ref. 18. It consisted of an air-suspended sphere floating in a bowl-shaped sphere holder. Motion of the sphere was recorded by two optical tracking sensors.

**Visual stimulation.** For calcium imaging and electrophysiological experiments, we used a custom-built LED arena covering  $180^\circ$  and  $90^\circ$  of the visual field along the horizontal and the vertical axis, respectively, at  $1.5^\circ$  resolution. For the behavioural experiments, three 120-Hz LCD screens formed a U-shaped visual arena with the fly in the centre, covering  $270^\circ$  and  $114^\circ$  of the visual field along the horizontal and the vertical axes, respectively, at  $0.1^\circ$  resolution.

**Data evaluation.** Data were evaluated off-line using custom-written software (Matlab and IDL).

**Full Methods** and any associated references are available in the online version of the paper.

Received 16 April; accepted 20 May 2013.

1. Bausenwein, B., Dittrich, A. P. M. & Fischbach, K. F. The optic lobe of *Drosophila melanogaster* II. Sorting of retinotopic pathways in the medulla. *Cell Tissue Res.* **267**, 17–28 (1992).
2. Akerboom, J. et al. Optimization of a GCaMP calcium indicator for neural activity imaging. *J. Neurosci.* **32**, 13819–13840 (2012).
3. Cajal, S. R. & Sanchez, D. *Contribucion al conocimiento de los centros nerviosos de los insectos* (Imprenta de Hijos de Nicholas Moja, 1915).
4. Strausfeld, N. J. *Atlas of an Insect Brain* (Springer, 1976).
5. Fischbach, K. F. & Dittrich, A. P. M. The optic lobe of *Drosophila melanogaster*. I. A Golgi analysis of wild-type structure. *Cell Tissue Res.* **258**, 441–475 (1989).

# A Directional Tuning Map of *Drosophila* Elementary Motion Detectors

## RESEARCH LETTER

- Reichardt, W. Autocorrelation, a principle for the evaluation of sensory information by the central nervous system. In *Sensory Communication* (ed. Rosenblith, W. A.) 303–317 (MIT Press and John Wiley & Sons, 1961).
- Borst, A., Haag, J. & Reiff, D. F. Fly motion vision. *Annu. Rev. Neurosci.* **33**, 49–70 (2010).
- Buchner, E., Buchner, S. & Buelthoff, I. Deoxyglucose mapping of nervous activity induced in *Drosophila* brain by visual movement. 1. Wildtype. *J. Comp. Physiol. A* **155**, 471–483 (1984).
- Strausfeld, N. J. & Lee, J. K. Neuronal basis for parallel visual processing in the fly. *Vis. Neurosci.* **7**, 13–33 (1991).
- Schnell, B., Raghu, V. S., Nern, A. & Borst, A. Columnar cells necessary for motion responses of wide-field visual interneurons in *Drosophila*. *J. Comp. Physiol. A* **198**, 389–395 (2012).
- Douglass, J. K. & Strausfeld, N. J. Visual motion-detection circuits in flies: Parallel direction- and non-direction-sensitive pathways between the medulla and lobula plate. *J. Neurosci.* **16**, 4551–4562 (1996).
- Franceschini, N., Riehle, A. & Le Nestour, A. Directionally selective motion detection by insect neurons. In *Facets of Vision* (ed. Stavenga, H.) 360–390 (Springer, 1989).
- Joesch, M., Schnell, B., Raghu, S. V., Reiff, D. F. & Borst, A. ON and OFF pathways in *Drosophila* motion vision. *Nature* **468**, 300–304 (2010).
- Pfeiffer, B. D. *et al.* Tools for neuroanatomy and neurogenetics in *Drosophila*. *Proc. Natl. Acad. Sci. USA* **105**, 9715–9720 (2008).
- Denk, W., Strickler, J. H. & Webb, W. W. Two-photon laser scanning fluorescence microscopy. *Science* **248**, 73–76 (1990).
- Oyster, C. W. & Barlow, H. B. Direction-selective units in rabbit retina: distribution of preferred directions. *Science* **155**, 841–842 (1967).
- Sweeney, S. T., Broadie, K., Keane, J., Niemann, H. & O’Kane, C. J. Targeted expression of tetanus toxin light chain in *Drosophila* specifically eliminates synaptic transmission and causes behavioral defects. *Neuron* **14**, 341–351 (1995).
- Seelig, J. D. *et al.* Two-photon calcium imaging from head-fixed *Drosophila* during optomotor walking behavior. *Nature Methods* **7**, 535–540 (2010).
- Clark, D. A., Bursztyn, L., Horowitz, M. A., Schnitzer, M. J. & Clandinin, T. R. Defining the computational structure of the motion detector in *Drosophila*. *Neuron* **70**, 1165–1177 (2011).
- Egelhaaf, M. & Borst, A. Calcium accumulation in visual interneurons of the fly: Stimulus dependence and relationship to membrane potential. *J. Neurophysiol.* **73**, 2540–2552 (1995).
- Joesch, M., Plett, J., Borst, A. & Reiff, D. F. Response properties of motion-sensitive visual interneurons in the lobula plate of *Drosophila melanogaster*. *Curr. Biol.* **18**, 368–374 (2008).
- Schnell, B. *et al.* Processing of horizontal optic flow in three visual interneurons of the *Drosophila* brain. *J. Neurophysiol.* **103**, 1646–1657 (2010).
- Borst, A. & Egelhaaf, M. Direction selectivity of fly motion-sensitive neurons is computed in a two-stage process. *Proc. Natl. Acad. Sci. USA* **87**, 9363–9367 (1990).
- Single, S., Haag, J. & Borst, A. Dendritic computation of direction selectivity and gain control in visual interneurons. *J. Neurosci.* **17**, 6023–6030 (1997).
- Eichner, H., Joesch, M., Schnell, B., Reiff, D. F. & Borst, A. Internal structure of the fly elementary motion detector. *Neuron* **70**, 1155–1164 (2011).
- Joesch, M., Weber, F., Eichner, H. & Borst, A. Functional specialization of parallel motion detection circuits in the fly. *J. Neurosci.* **33**, 902–905 (2013).
- Egelhaaf, M. & Borst, A. Are there separate ON and OFF channels in fly motion vision? *Vis. Neurosci.* **8**, 151–164 (1992).
- Takemura, S. Y., Lu, Z. & Meinertzhagen, I. A. Synaptic circuits of the *Drosophila* optic lobe: the input terminals to the medulla. *J. Comp. Neurol.* **509**, 493–513 (2008).
- Euler, T., Detwiler, P. B. & Denk, W. Directionally selective calcium signals in dendrites of starburst amacrine cells. *Nature* **418**, 845–852 (2002).
- Pologruto, T. A., Sabatini, B. L. & Svoboda, K. ScanImage: Flexible software for operating laser scanning microscopes. *Biomed. Eng. Online* **2**, 13 (2003).

Supplementary Information is available in the online version of the paper.

**Acknowledgements** We thank L. Looger, J. Simpson, V. Jayaraman and the Janelia GECI team for making and providing us with the GCaMP5 flies before publication; J. Plett for designing and engineering the LED arena; C. Theile, W. Essbauer and M. Sauter for fly work; and A. Mauss, F. Gabbiani and T. Bonhoeffer for critically reading the manuscript. This work was in part supported by the Deutsche Forschungsgemeinschaft (SFB 870). M.S.M., G.A., E.S., M.M., A.L., A.Ba and A.Bo are members of the Graduate School of Systemic Neurosciences.

**Author Contributions** M.S.M. and J.H. jointly performed and, together with A.Bo., evaluated all calcium imaging experiments. G.A., E.S. and M.M. recorded from tangential cells. A.L., T.S. and A.Ba. performed the behavioural experiments. G.R., B.D. and A.N. generated the driver lines and characterized their expression pattern. D.F.R. performed preliminary imaging experiments. E.H. helped with programming and developed the PMT shielding for the two-photon microscope. A.Bo. designed the study and wrote the manuscript with the help of all authors.

**Author Information** Reprints and permissions information is available at [www.nature.com/reprints](http://www.nature.com/reprints). The authors declare no competing financial interests. Readers are welcome to comment on the online version of the paper. Correspondence and requests for materials should be addressed to A.Bo. ([borst@neuro.mpg.de](mailto:borst@neuro.mpg.de)).

## METHODS

**Flies.** Flies were raised on standard cornmeal-agar medium at 25 °C and 60% humidity throughout development on a 12 h light/12 h dark cycle. For calcium imaging, we used the genetically encoded single-wavelength indicator GCaMP5, variant G, with the following mutations: T302L, R303P and D380Y (ref. 2). Expression of GCaMP5 was directed by three different Gal4 lines, all from the Janelia Farm collection<sup>14</sup>. Flies used in calcium imaging experiments (Figs 1–3) had the following genotypes: T4/T5 line ( $w^-/+;$  *UAS-GCaMP5,R42F06-GAL4/UAS-GCaMP5,R42F06-GAL4*), T4 line ( $w^-/+;$  *UAS-GCaMP5,R54A03-GAL4/UAS-GCaMP5,R54A03-GAL4*), T5 line ( $w^-/+;$  *UAS-GCaMP5,R42H07-GAL4/UAS-GCaMP5,R42H07-GAL4*). All driver lines were generated by the methods described in ref. 14 and were identified by screening a database of imaged lines, followed by reimaging of selected lines<sup>31</sup>. As homozygous for both the Gal4-driver and the *UAS-GCaMP5* genes, T4 flies also showed some residual expression in T5 cells, and T5 flies also in T4 cells. This unspecific expression, however, was in general less than 25% of the expression in the specific cells. Flies used in electrophysiological and behavioural experiments (Fig. 4) had identical genotypes of the following kind: TNT control flies ( $w^+/w^+;$  *UAS-TNT-E/UAS-TNT-E;*  $+/+$ ), T4 control flies ( $w^+/w^+;$   $+/+$ ; *VT37588-GAL4/+;*), T5 control flies ( $w^+/w^+;$   $+/+$ ; *R42H07-GAL4/+;*), T4-block flies ( $w^+/w^+;$  *UAS-TNT-E/+;* *VT37588-GAL4/+;*), T5-block flies ( $w^+/w^+;$  *UAS-TNT-E/+;* *R42H07-GAL4/+;*). *UAS-TNT-E* flies were derived from the Bloomington Stock Center (stock no. 28837) and *VT37588-Gal4* flies were derived from the VDRC (stock no. 205893). Before electrophysiological experiments, flies were anaesthetized on ice and waxed on a Plexiglas holder using bees wax. The dissection of the fly cuticle and exposure of the lobula plate were performed as described previously (for imaging experiments, see ref. 32; for electrophysiology, see ref. 21). Flies used in behavioural experiments were taken from 18 °C just before the experiment and immediately cold-anaesthetized. The head, the thorax and the wings were glued to a needle using near-ultraviolet bonding glue (Sinfony Opaque Dentin) and strong blue LED light (440 nm, dental curing-light, New Woodpecker).

**Two-photon microscopy.** We used a custom-built two-photon laser scanning microscope<sup>33</sup> equipped with a  $\times 40$  water immersion objective (0.80 NA, IR-Achroplan; Zeiss). Fluorescence was excited by a mode locked Ti:sapphire laser (<100 fs, 80 MHz, 700–1,020 nm; pumped by a 10 W CW laser; both Mai Tai; Spectraphysics) with a DeepSee accessory module attached for dispersion compensation control resulting in better pulse compression and fluorescence at the target sample. Laser power was adjusted to 10–20 mW at the sample, and an excitation wavelength of 910 nm was used. The photomultiplier tube (H10770PB-40, Hamamatsu) was equipped with a dichroic band-pass mirror (520/35, Brightline). Images were acquired at a resolution of  $256 \times 256$  pixels and a frame rate of 1.87 Hz, except in Fig. 2 (7.5 Hz), using the ScanImage software<sup>30</sup>.

**Electrophysiology.** Recordings were established under visual control using a  $\times 40$  water immersion objective (LumplanF, Olympus), a Zeiss microscope (Axiotech vario 100, Zeiss), and illumination (100 W fluorescence lamp, hot mirror, neutral density filter OD 0.3; all from Zeiss). To enhance tissue contrast, we used two polarization filters, one located as an excitation filter and the other as an emission filter, with slight deviation on their polarization plane. For eye protection, we additionally used a 420-nm LP filter on the light path.

**Behavioural analysis.** The locomotion recorder was custom-designed according to ref. 18. Briefly, it consists of an air-suspended sphere floating in a bowl-shaped sphere holder. A high-power infrared LED (800 nm, JET series, 90 mW, Roithner Electronics) is located in the back to illuminate the fly and the sphere surface. Two optical tracking sensors are equipped with lens and aperture systems to focus on the sphere behind the fly. The tracking data are processed at 4 kHz internally, read out via a USB interface and processed by a computer at  $\approx 200$  Hz. This allows real-time calculation of the instantaneous rotation axis of the sphere. A third camera (GRAS-20S4M-C, Point Grey Research) is located in the back which is essential for proper positioning of the fly and allows real-time observation and video recording of the fly during experiments.

**Visual stimulation.** For calcium imaging and electrophysiological experiments, we used a custom-built LED arena that allowed refresh rates of up to 550 Hz and 16 intensity levels. It covered  $180^\circ$  ( $1.5^\circ$  resolution) and  $90^\circ$  ( $1.5^\circ$  resolution) of the visual field along the horizontal and the vertical axis, respectively. The LED arena was engineered and modified based upon ref. 34. The LED array consists of  $7 \times 4$  individual TA08-81GWA dot-matrix displays (Kingbright), each harbouring  $8 \times 8$  individual green (568 nm) LEDs. Each dot-matrix display is controlled by an ATmega168 microcontroller (Atmel) combined with a ULN2804 line driver (Toshiba America) acting as a current sink. All panels are in turn controlled via an I2C interface by an ATmega128 (Atmel)-based main controller board, which reads in pattern information from a compact flash (CF) memory card. Matlab was used for programming and generation of the patterns as well as for sending the serial command sequences via RS-232 to the main controller board. The

luminance range of the stimuli was  $0.5\text{--}33 \text{ cd m}^{-2}$ . For the calcium imaging experiments, two separate barriers were used to shield the photomultipliers from the stimulus light coming from the LED arena. The first was a spectral filter with transparency to wavelengths  $>540$  nm placed directly over the LEDs (ASF SFG 10, Microchemicals). The second was a layer of black PVC extending from the fly holder over the arena. Square wave gratings had a spatial wavelength of  $30^\circ$  of visual angle and a contrast of 88%. Unless otherwise stated, they were moving at  $30^\circ \text{ s}^{-1}$ . Edges had the same contrast and were also moving at  $30^\circ \text{ s}^{-1}$ . For the experiments shown in Figs 1, 2b and 3, each grating or edge motion was shown twice within a single sweep, resulting in a total of eight stimulation periods. Each stimulus period lasted 4 s, and subsequent stimuli were preceded by a 3-s pause. In the experiment shown in Fig. 2a, a dark edge of 88% contrast was moved for 1 s at  $15^\circ \text{ s}^{-1}$  from the front to the back at three different positions ( $22^\circ$ ,  $44^\circ$ ,  $66^\circ$ , from frontal to lateral). At each position, edge motion was repeated 15 times. For the experiment shown in Fig. 2b, a bright edge of 88% contrast was moving at  $15^\circ \text{ s}^{-1}$  from the back to the front, and images were acquired at a frame rate of 7.5 Hz. For the experiments shown in Figs 3e, f, all six stimulus velocities were presented once within one sweep, with the stimulus lasting 4 s, and different stimuli being separated by 2 s. In the experiments shown in Figs 3g, h, a single sweep contained all 12 grating orientations with the same stimulus and pause length as above. For the electrophysiology experiments (Fig. 4a–f), multiple edges were used as stimuli moving simultaneously at  $50^\circ \text{ s}^{-1}$ . To stimulate cells of horizontal system (HS cells), a vertical, stationary square-wave grating with  $45^\circ$  spatial wavelength was presented. For ON-edge motion, the right (preferred direction, PD) or the left edge (null direction, ND) of each light bar started moving until it merged with the neighbouring bar. For OFF-edge motion, the right or the left edge of each dark bar was moving. To stimulate cells of the vertical system (VS cells), the pattern was rotated by  $90^\circ$  clockwise. For the behavioural experiments (Fig. 4g–i), three 120-Hz LCD screens (Samsung 2233 RZ) were vertically arranged to form a U-shaped visual arena ( $w = 31 \text{ cm} \times d = 31 \text{ cm} \times h = 47 \text{ cm}$ ) with the fly in the centre. The luminance ranged from 0 to  $131 \text{ cd m}^{-2}$  and covered large parts of the flies' visual field (horizontal,  $\pm 135^\circ$ ; vertical,  $\pm 57^\circ$ ; resolution,  $<0.1^\circ$ ). The three LCD screens were controlled via NVIDIA 3D Vision Surround Technology on Windows 7 64-bit allowing a synchronized update of the screens at 120 frames per second. Visual stimuli were created using Panda3D, an open-source gaming engine, and Python 2.7, which simultaneously controlled the frame rendering in Panda3D, read out the tracking data and temperature and streamed data to the hard disk. The balanced motion stimulus consisted of a square-wave grating with  $45^\circ$  spatial wavelength and a contrast of 63%. Upon stimulation onset, dark and bright edges moved into opposite directions at  $10^\circ \text{ s}^{-1}$  for 2.25 s. This stimulation was performed for both possible edge directions and two initial grating positions shifted by half a wavelength, yielding a total of four stimulus conditions.

**Data evaluation.** Data were evaluated off-line using custom-written software (Matlab and IDL). For the images shown in Figs 1e, f, 2a and 3a, b, the raw image series was converted into four images representing the relative fluorescence change during each direction of grating motion:  $(\Delta F/F)_{\text{stim}} = (F_{\text{stim}} - F_{\text{ref}})/F_{\text{ref}}$ . The image representing the stimulus fluorescence ( $F_{\text{stim}}$ ) was obtained by averaging all images during stimulation; the image representing the reference fluorescence ( $F_{\text{ref}}$ ) was obtained by averaging three images before stimulation. Both images were smoothed using a Gaussian filter of 10 pixel half-width. For the images shown in Figs 1f and 3a, b,  $\Delta F/F$  images were normalized by their maximum value. Then, a particular colour was assigned to each pixel according to the stimulus direction during which it reached maximum value, provided it passed a threshold of 25%. Otherwise, it was assigned to background. The response strength of each pixel was coded as the saturation of that particular colour. For the data shown in Figs 2b, c and 3c–h, the raw image series was first converted into a  $\Delta F/F$  series by using the first three images as reference. Then, a region was defined within a raw image, and average  $\Delta F/F$  values were determined within that region for each image, resulting in a  $\Delta F/F$  signal over time. Responses were defined as the maximum  $\Delta F/F$  value reached during each stimulus presentation minus the average  $\Delta F/F$  value during the two images preceding the stimulus. For the bar graphs shown in Fig. 4c, f, the average voltage responses during edge motion ( $0.45 \text{ s}$ ) along the cell's preferred (PD) and null direction (ND) were calculated. For each recorded tangential cell, the difference between the PD and the ND response was determined, and these values were averaged across all recorded cells. The data shown in Fig. 4g, h were obtained from the four stimulus conditions by averaging the turning responses for the two starting positions of the grating and calculating the mean difference between the turning responses for the two edge directions. For the bar graph shown in Fig. 4i, the average turning response of each fly during the last second of balanced motion stimulation was calculated. These values were averaged across all recorded flies within each genotype.

# A Directional Tuning Map of *Drosophila* Elementary Motion Detectors

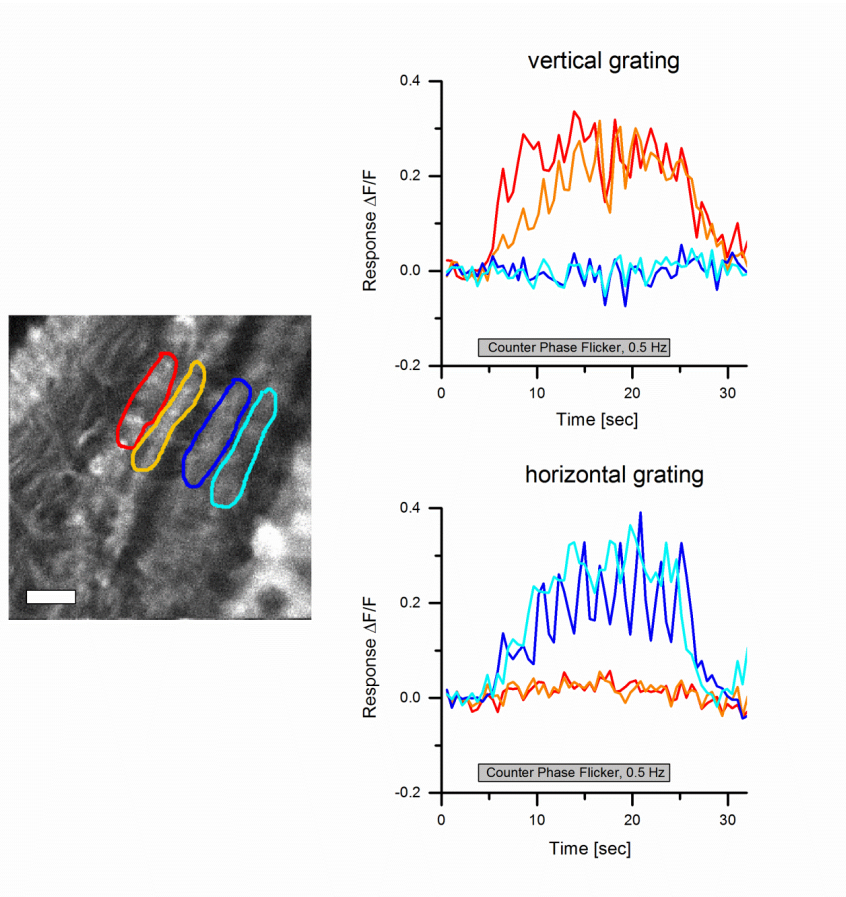
---

## RESEARCH LETTER

31. Jenett, A. *et al.* A Gal4-driver line resource for *Drosophila* neurobiology. *Cell Rep.* **2**, 991–1001 (2012).
32. Reiff, D. F., Plett, J., Mank, M., Griesbeck, O. & Borst, A. Visualizing retinotopic half-wave rectified input to the motion detection circuitry of *Drosophila*. *Nature Neurosci.* **13**, 973–978 (2010).
33. Euler, T. *et al.* Eyecup scope—optical recording of light stimulus-evoked fluorescence signals in the retina. *Pflüger Arch.* **457**, 1393–1414 (2009).
34. Reiser, M. B. & Dickinson, M. H. A modular display system for insect behavioral neuroscience. *J. Neurosci. Methods* **167**, 127–139 (2008).

SUPPLEMENTARY INFORMATION

doi:10.1038/nature12320



**Supplemental Fig.1** Responses of T4 and T5 cells to counter-phase flicker. Square-wave gratings (15 deg spatial wavelength and 88% contrast) with vertical (top) and horizontal (bottom) orientation were phase-shifted every second by 180 deg for 20 seconds. Response traces are derived from the region of interest encircled in the image to the left with the same color from a single stimulation period. T4 and T5 cells in layers 1 and 2 only respond to the vertical grating, cells in layers 3 and 4 selectively respond to the horizontal grating. Similar results were obtained in n=4 flies. Scale bar = 5  $\mu$ m. Together with the missing response of T4 and T5 cells to full-field flicker, these findings suggest that T4 and T5 cells receive input signals from neurons with different orientation tuning, depending on whether they respond to motion along the horizontal (layers 1 and 2) or the vertical (layers 3 and 4) axis<sup>1,2</sup>.

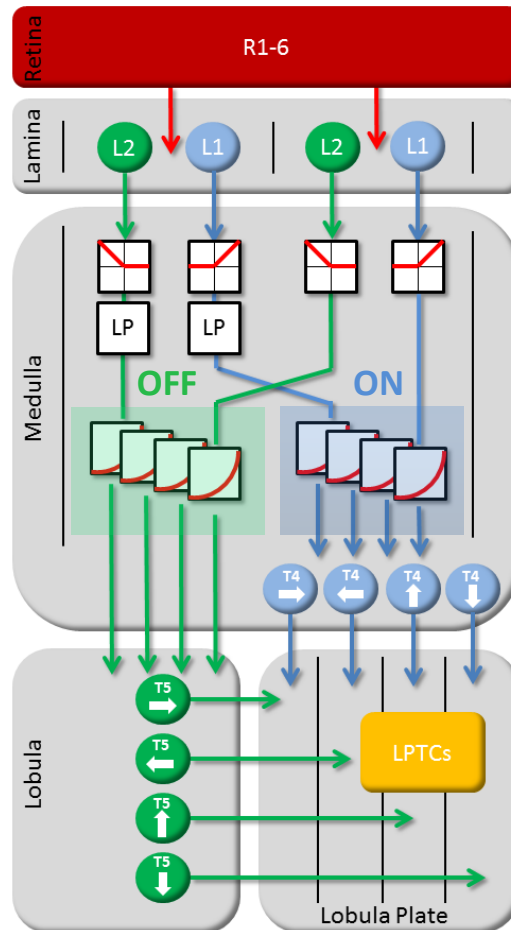
1 Pick, B. & Buchner, E. Visual movement detection under light- and dark-adaptation in the fly, *Musca domestica*. *J. Comp. Physiol.* **134**, 45-54 (1979).

2 Srinivasan, M.V. & Dvorak, D.R. Spatial processing of visual information in the movement-detecting pathway of the fly. *J. Comp. Physiol.* **140**, 1-23 (1980).



# A Directional Tuning Map of *Drosophila* Elementary Motion Detectors

RESEARCH SUPPLEMENTARY INFORMATION



**Supplemental Fig.2** Circuit diagram of the fly elementary motion detector. Visual input from photoreceptors R1-6 is split into parallel pathways, L1 and L2, at the level of the lamina. Two neighboring columns are shown. The outputs from both L1 and L2 are half-wave rectified, such that downstream elements carry information about ON (L1-pathway) and OFF (L2-pathway) signals separately. After temporal low-pass filtering ('LP') the signals from one column, they interact in a supra-linear way with the instantaneous signals derived from the other column. This interaction takes place, separately in both pathways, along all four cardinal directions. Directionally selective signals are carried via T4 and T5 cells to the four layers of the lobula plate where T4 and T5 cells with the same preferred direction converge again on the dendrites of the tangential cells ('LPTCs').

# Manuscript Nr. 4: Optogenetic and Pharmacologic Dissection of Feedforward Inhibition in *Drosophila* Motion Vision

Alex S. Mauss, Matthias Meier, **Etienne Serbe**, and Alexander Borst

## Author Contributions:

A.S.M. and A.B. designed research; A.S.M., M.M., and **E.S.** performed research; A.B. contributed unpublished reagents/analytic tools; A.S.M., M.M., **E.S.**, and A.B. analyzed data; A.S.M. and A.B. wrote the paper.

## Optogenetic and Pharmacologic Dissection of Feedforward Inhibition in *Drosophila* Motion Vision

Alex S. Mauss, Matthias Meier, Etienne Serbe, and Alexander Borst

Max-Planck-Institute of Neurobiology, 82152 Martinsried, Germany

Visual systems extract directional motion information from spatiotemporal luminance changes on the retina. An algorithmic model, the Reichardt detector, accounts for this by multiplying adjacent inputs after asymmetric temporal filtering. The outputs of two mirror-symmetrical units tuned to opposite directions are thought to be subtracted on the dendrites of wide-field motion-sensitive lobula plate tangential cells by antagonistic transmitter systems. In *Drosophila*, small-field T4/T5 cells carry visual motion information to the tangential cells that are depolarized during preferred and hyperpolarized during null direction motion. While preferred direction input is likely provided by excitation from T4/T5 terminals, the origin of null direction inhibition is unclear. Probing the connectivity between T4/T5 and tangential cells in *Drosophila* using a combination of optogenetics, electrophysiology, and pharmacology, we found a direct excitatory as well as an indirect inhibitory component. This suggests that the null direction response is caused by feedforward inhibition via yet unidentified neurons.

**Key words:** *Drosophila*; feedforward inhibition; motion vision; optogenetics; pharmacology; synaptic connectivity

### Introduction

The perception of dynamically changing visual images derives from time-varying brightness changes projected onto a 2D array of photoreceptors. To extract higher order features that are not explicitly encoded at the level of individual inputs, signals from each point in space need to be processed by downstream parallel circuits. An important question is how the direction of local image motion is detected, a process that requires the comparison of signals from at least two neighboring photoreceptors in time. An algorithmic model, the Reichardt detector, accounts for this by multiplying adjacent inputs after asymmetric temporal filtering (Hassenstein and Reichardt, 1956; Borst and Euler, 2011). A functional unit comprises two mirror-symmetrical half detectors tuned to opposite directions. Their outputs are thought to be subtracted on the dendrites of motion-sensitive cells by antagonistic neurotransmitter systems.

Much of our knowledge about the functional organization of such a neural circuit has emerged from studies in flies (Borst et al.,

2010), where large tangential cells in the lobula plate (LPTCs) display direction-selective responses: depolarization during motion along their preferred direction and hyperpolarization during motion along the opposite/null direction. Two pathways, corresponding to separate ON and OFF channels, convey signals from photoreceptors to the LPTCs (Joesch et al., 2010, 2013; Eichner et al., 2011; Maisak et al., 2013), and their behavioral relevance has been investigated in great detail (Rister et al., 2007; Clark et al., 2011; Bahl et al., 2013; Maisak et al., 2013; Silies et al., 2013; Tuthill et al., 2013). The presumed outputs of these pathways are arrays of columnar T4 and T5 cells that are therefore prime candidates to represent the last processing stage of the antagonistic half detectors. In support of this notion, genetically silencing T4/T5 eliminates all motion sensitivity in LPTCs (Schnell et al., 2012). Moreover, both cell types carry direction-selective  $Ca^{2+}$  signals but differ in their preference for edge polarity (Maisak et al., 2013). In the lobula plate, individual T4/T5 axons segregate into four layers according to their tuning: cells selective for front-to-back motion target layer 1, those selective for back-to-front layer 2, cells tuned to upward motion terminate in layer 3, and those tuned to downward motion in layer 4 (Maisak et al., 2013). The planar dendrites of LPTCs are generally, though not exclusively, restricted to individual layers that match the T4/T5 cells' preferred direction (Hausen, 1982, 1984; Hengstenberg et al., 1982). Therefore, LPTCs likely obtain their preferred direction input by integrating excitation from T4/T5 terminals over large receptive fields. However, the synaptic origin of null direction inhibition in LPTCs is unknown.

We studied the functional connectivity of the lobula plate in *Drosophila* by optogenetically stimulating T4/T5 cells while recording the synaptic responses in LPTCs electrophysiologically. Combining this approach with intersectional genetics and pharmacology we found that LPTCs receive excitatory cholinergic

Received Sept. 13, 2013; revised Dec. 13, 2013; accepted Dec. 31, 2013.

Author contributions: A.S.M. and A.B. designed research; A.S.M., M.M., and E.S. performed research; A.B. contributed unpublished reagents/analytic tools; A.S.M., M.M., E.S., and A.B. analyzed data; A.S.M. and A.B. wrote the paper.

The authors declare no competing financial interests.

This work was supported by the Max-Planck-Society and the CRC 870 of the Deutsche Forschungsgemeinschaft. Preparatory experiments were carried out at the Marine Biological Laboratory (Woods Hole, MA), funded by a Grass Fellowship (A.S.M.). We are greatly indebted to Gerald Rubin, Aljoscha Nern, and Barry Dickson for generously sending us driver lines before publishing. We would also like to thank Bettina Schnell for teaching A.S.M. lobula plate tangential cell recordings; Chi-Hon Lee, Stefan Pulver, and Andreas Prokop for kindly providing fly strains; Johannes Plett for advice on the LED arena; and Wolfgang Essbauer, Christian Theile, Renate Gleich, Dieter Mauss, and the MPI workshop for excellent technical support. We are grateful to Alexander Arenz, Armin Bahl, and Jürgen Haag for critically reading this manuscript.

Correspondence should be addressed to Alex S. Mauss, Max-Planck-Institute of Neurobiology, 82152 Martinsried, Germany. E-mail: amauss@neuro.mpg.de.

DOI:10.1523/JNEUROSCI.3938-13.2014

Copyright © 2014 the authors 0270-6474/14/342254-10\$15.00/0

# Optogenetic and Pharmacologic Dissection of Feedforward Inhibition in *Drosophila* Motion Vision

Mauss et al. • Feedforward Inhibition in Fly Motion Vision

J. Neurosci., February 5, 2014 • 34(6):2254–2263 • 2255

input from both T4 and T5. Importantly, optogenetic activation of T4/T5 cells also elicits delayed indirect synaptic inhibition. We propose that LPTC dendrites indeed receive their preferred direction input from correspondingly tuned T4/T5 cell terminals in the same lobula plate layer. Their null direction input, however, likely arises from T4/T5 cells with opposite direction tuning terminating in the adjacent layer by feedforward inhibition via yet unidentified local interneurons.

## Materials and Methods

**Fly stocks.** Flies were raised at 25°C and 60% humidity on standard cornmeal agar medium at a 12 h light/dark cycle. The following fly strains were used: T4/T5-specific driver lines from the Howard Hughes Medical Institute Janelia Farm (Pfeiffer et al., 2008) and IMP Vienna stock collections (generously provided by Gerald Rubin and Barry Dickson) *R42F06-Gal4* on third chromosome (T4+T5), *R42F06-p65-AD* on second (T4+T5), and *VT37588-Gal4* on third (T4; Maisak et al., 2013); *Cha-DBD* on third (courtesy of Chi-Hon Lee; Gao et al., 2008); *UAS-Channelrhodopsin2-H134R-mCherry* on second (*UAS-ChR2-H134R*, courtesy of Stefan Pulver; Nagel et al., 2005; Pulver et al., 2009; Mattis et al., 2012); *norPA<sup>7</sup>* on X (dysfunctional phototransduction mutant; Hotta and Benzer, 1970); *UAS-mCD8-GFP* on second (courtesy of Barry Dickson); *UAS-synaptotagmin-HA* on second (*UAS-syt-HA*, courtesy of Andreas Prokop; Löhr et al., 2002; Robinson et al., 2002); and *UAS-stinger-GFP* on second. The genotypes of flies used in our experiments are as follows, in order of appearance in the Results section: (1) *w<sup>-</sup>*; *UAS-stinger-GFP/+*; *R42F06-Gal4/+*, (2) *w<sup>-</sup>*; *UAS-syt-HA*, *UAS-mCD8-GFP/+*; *R42F06-Gal4/+*, (3) *w<sup>-</sup>*; *UAS-ChR2-H134R*; *R42F06-Gal4*, (4) *w<sup>-</sup>*; *UAS-ChR2-H134R*; *VT37588-Gal4*, (5) *w<sup>-</sup>*; *R42F06-p65-AD*, *UAS-ChR2-H134R/R42F06-p65-AD*; *Cha-DBD*, (6) *w<sup>-</sup>*; +; *R42F06-Gal4* (control without ChR2 expression), (7) *norPA<sup>7</sup>*; *UAS-ChR2-H134R*; *R42F06-Gal4*, (8) *norPA<sup>7</sup>*; *UAS-ChR2-H134R*; *VT37588-Gal4*, and (9) *wild-type Canton-S*.

**Immunohistochemistry and confocal imaging.** For immunostainings brains of 1- to 2-d-old female flies were dissected in PBS, fixed for 30–40 min in PBS/4% paraformaldehyde (PFA) at room temperature, and washed in PBS/0.5% Triton X-100 (PBT). Preparations were blocked for 2 h in PBT/5% NGS, incubated for 1–2 d at 4°C with primary antibodies and 2–3 d with secondary antibodies (5% normal goat serum added to antibody solutions). Primary and secondary antibodies used for T4/T5 > GFP, *sytHA* flies (genotype 2) were as follows: rabbit anti-GFP (1:1000; Torrey Pines Biolabs) + Alexa Fluor 488 goat anti-rabbit (1:500), rat anti-HA (1:50; Roche) + Alexa Fluor 568 goat anti-rat (1:500), and mouse anti-bruchpilot (1:25; NC82, Developmental Studies Hybridoma Bank) + Alexa Fluor 633 goat anti-mouse (1:500). Primary and secondary antibodies used for T4/T5 > *stinger-GFP* flies (genotype 1) were as follows: mouse anti-ChAT (1:1000; courtesy of P. Salvaterra; Takagawa and Salvaterra, 1996) + Alexa Fluor 568 goat anti-mouse (1:200), and rabbit anti-vGAT (1:200; courtesy of D. Kranz; Fei et al., 2010) + Alexa Fluor 568 goat anti-rabbit (1:200). All secondary antibodies were from Invitrogen. Brains were mounted (IMM; ibidi) and optically sectioned with a Leica SP5 confocal laser scanning microscope. To quantify anti-ChAT-positive and anti-vGAT-positive T4/T5 cells, respectively, two nonoverlapping optical sections from two brains for each staining were used for analysis. A total number of 2717 somata for anti-ChAT and 2503 somata for anti-vGAT were evaluated.

To verify ChR2-H134R-mCherry expression specificity and strength with the different driver lines we dissected brains from female flies (1 d after eclosion, genotypes as used in physiological experiments) in PBS (pH 7.4, 280 mOsmol/kg). Brains were fixed at room temperature for 30 min in PBS/4% PFA and an additional 10 min in PBS/4% PFA/0.1% Triton X-100. After three and two washing steps in PBT and PBS, respectively, brains were mounted (IMM; ibidi) and optically sectioned in the horizontal plane with a Leica SP5 confocal laser scanning microscope using 568 nm excitation and a step size of 1 μm. Identical procedures and confocal settings were applied throughout to compare relative signal intensities between different driver lines. For documentation, single sections were processed in ImageJ 1.46r (National Institutes of Health,

Bethesda, Maryland), pseudocolored using the “Fire” lookup table, and images assembled in Adobe Photoshop CS5.

**Cell counts.** A software-aided manual counting strategy was used to estimate T4/T5 cell numbers in confocal stacks (step size 1 μm) generated from brains expressing nuclear-targeted stinger-GFP with a T4/T5-specific driver line (*UAS-stinger-GFP/+*; *R42F06-Gal4/+*). While scrolling through a stack at two orthogonal views distinctly colored spheres were incrementally anchored to centers of individual nuclei. Thus, cells were only counted once and omitted nuclei could easily be detected.

**Electrophysiology.** For all experiments 20- to 30-h-old female flies kept at 25°C were used, except for neurotransmitter injections where flies were 7–30 h old. For optogenetic experiments, yeast paste containing 1 mM all-*trans*-retinal (ATR, R2500; Sigma Aldrich) was fed to freshly eclosed flies. Preparation and recording conditions were modified from Joesch et al. (2008) and Maimon et al. (2010). Flies were anesthetized on ice and attached to a Plexiglas holder with the head bent down using melted beeswax. The holder was placed underneath a recording chamber with a magnet so that the back of the fly's head was accessible through a 1 mm slit in the bottom of the chamber consisting of thin foil. The head was gently attached to the slit edges on one side with melted beeswax. Under external solution, a window was cut into the head capsule on the other side with a hypodermic needle. Further dissection and recordings were performed under a Zeiss Axiotech vario microscope equipped with polarized light contrast and epifluorescence. Under polarized light contrast, the glial sheath was digested locally by applying a stream of 0.5 mg/ml Collagenase IV (Gibco) through a cleaning micropipette (~5 μm opening). Whole-cell recordings were established with patch electrodes of 5–8 MΩ resistance. We used a BA-1S bridge amplifier (npi Electronics) to record in current-clamp, low-pass filtered at 3 kHz, and digitized signals at 10 kHz via an analog/digital converter (PCI-DAS6025; Measurement Computing). All physiological data were acquired in MATLAB (R2010b; Mathworks) using the data acquisition toolbox. Normal external solution contained the following (in mM): 103 NaCl, 3 KCl, 5 TES, 10 trehalose, 10 glucose, 3–7 sucrose, 26 NaHCO<sub>3</sub>, 1 NaH<sub>2</sub>PO<sub>4</sub>, 1.5 CaCl<sub>2</sub>, and 4 MgCl<sub>2</sub>, pH 7.3–7.35, 280–290 mOsmol/kg. Zero Ca<sup>2+</sup>/high Mg<sup>2+</sup> external solution contained the following (in mM): 66 NaCl, 22 Na-glucuronate, 3 KCl, 5 TES, 10 trehalose, 5 glucose, 25 NaHCO<sub>3</sub>, 1 NaH<sub>2</sub>PO<sub>4</sub>, and 20 MgCl<sub>2</sub>, pH 7.3–7.35, 280 mOsmol/kg. External solution was carbonygenated (95% O<sub>2</sub>/5% CO<sub>2</sub>) and, except for α-bungarotoxin (α-BTX) experiments, constantly perfused over the preparation at 2 ml/min. Internal solution, adjusted to pH 7.26 with 1N KOH, contained the following: 140 K-aspartate, 10 HEPES, 4 Mg-ATP, 0.5 Na-GTP, 1 EGTA, 1 KCl, and 0.1 Alexa Fluor 488 hydrazide salt (265 mOsmol/kg). Dye-filled cells included for analyses were VS and HS cells, identified by visual response profile (not possible in blind *norPA<sup>7</sup>* mutant flies) and morphology. Apart from visual direction tuning, no discernible differences were observed for VS and HS cells in all assays.

**Optogenetic stimulation.** During electrophysiological recordings, wide-field light pulses for optogenetic stimulation were delivered via the epifluorescence light path of the microscope through a 40×/0.8 NA water-immersion objective (LUMPlan FI; Olympus). As a light source, a Lambda DG-4 Plus wavelength switcher (Sutter) with a 300 mW Xenon Arc lamp was connected to the illumination port of the microscope via a liquid light guide. Attenuating the output of the DG-4 was achieved by offsetting the output galvanometer. The output for each setting was measured with a power meter (Thorlabs PM100D) under the 40× objective in air. Taking into account the field of illumination under water immersion, the light intensity per area on the specimen was estimated, as given in the Results section and figures. Light stimuli were triggered via the data acquisition software with voltage steps (~500 μs delay to light onset according to the manufacturer and own measurements using a photodiode). A stimulus trial consisted of eight 2 ms light pulses interleaved by 5 s. For analysis, responses to the eight light pulses were averaged for each experimental condition and time point. All values in the text are given as mean ± SEM.

**Pharmacology.** Aqueous stock solutions were prepared from the following antagonists at the following concentrations: 10 mM methyllyca-

# Optogenetic and Pharmacologic Dissection of Feedforward Inhibition in *Drosophila* Motion Vision

2256 • J. Neurosci., February 5, 2014 • 34(6):2254–2263

Mauss et al. • Feedforward Inhibition in Fly Motion Vision

conitine (MLA; Sigma M168), 100 mM mecamylamine (MEC; Sigma M9020) and 1 mM  $\alpha$ -BTX (Tocris Bioscience 2133). Picrotoxinin (PTX; Sigma P8390) was dissolved in dimethylsulfoxide at 50 mM. For experiments,  $\alpha$ -BTX was added directly to the bath with perfusion switched off. All other compounds were diluted in external solution to concentrations given in the results section and perfused over the preparation at 2 ml/min.

**Neurotransmitter pressure injection.** All neurotransmitters were dissolved in dH<sub>2</sub>O at 50 mM (glutamate) or 100 mM (acetylcholine, GABA; all from Sigma; stocks kept aliquoted at  $-20^{\circ}\text{C}$ ), diluted at day of experiment in external solution to 1 mM with additional 10  $\mu\text{M}$  Alexa Fluor 488 hydrazide (Invitrogen), and back-loaded into patch pipettes ( $\sim 1 \mu\text{m}$  tip diameter). The Alexa 488/neurotransmitter-filled pipettes were connected via a holder and rubber tube to a pressure-injection system (FemtoJet; Eppendorf) that was triggered via the MATLAB data acquisition software. During recordings of LPTCs, the neurotransmitter-filled pipettes were carefully positioned by a micromanipulator toward Alexa 488-filled LPTC dendrites in the lobula plate under epifluorescence illumination and electrophysiological responses to brief puffs of neurotransmitters (generally 100 ms) were monitored. Once robust responses remained stable for 5–10 min, a protocol was started during which responses to visual motion stimulation and transmitter puffs were probed continuously every 1–2.5 min while antagonists were washed in and out via the perfusion system. Ejection of Alexa 488/neurotransmitter solution from pipettes was controlled in regular intervals under epifluorescence. For each cell and time point, the average responses to five consecutive pressure pulses at intervals of 5 s were analyzed. Responses were quantified by subtracting the integrated voltage deviations during 1 s before stimulus trigger from 1 s following stimulus trigger. This was done separately for positive and negative values. For each cell and experiment, all positive and negative integrals were normalized either to positive baseline values for acetylcholine injections or negative baseline values for GABA and glutamate injections. All values in the text are given as mean  $\pm$  SEM.

## Results

### T4/T5 cell numbers suggest eight distinct functional subtypes

T4/T5 cells represent the major small-field motion-sensitive input elements to the lobula plate and are required for both preferred direction excitation and null direction inhibition of LPTCs (Schnell et al., 2012). Golgi impregnations have identified eight anatomical types (Fischbach and Dittrich, 1989) and Ca<sup>2+</sup> imaging data have categorized T4/T5 cells into eight functional subgroups: T4 and T5 cells are selective for moving positive and negative contrast changes, respectively, but are otherwise individually tuned to the same four cardinal directions of motion (Maisak et al., 2013). This provides evidence that T4 and T5 cells convey equivalent motion information to the lobula plate. We aimed to determine whether apart from their anatomy and visual response properties the T4/T5 cells could be further functionally subdivided, for instance, into two antagonistic sets implementing different transmitter systems. We reasoned that the total number of T4 and T5 cells divided by approximately 750 ommatidia of a *Drosophila* eye would yield the number of T4/T5 cells per column and therefore the maximum number of different functional subtypes repeated across the retinotopic array. To analyze T4/T5 cell

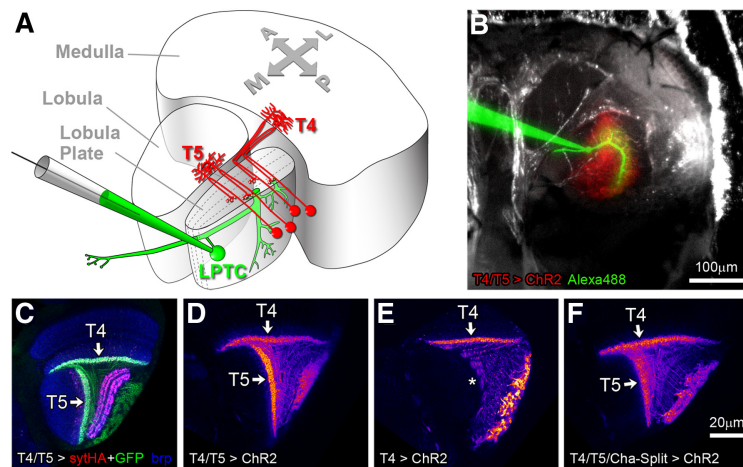


**Figure 1.** Probing synaptic connectivity between T4/T5 and LPTCs. **A**, Schematic to illustrate anatomical layout of fly visual neuropils medulla, lobula, and lobula plate. One LPTC of the vertical system (VS) is shown in green with recording electrode; the dendrites arborize in layer 4 of the lobula plate. Examples of two T4 and two T5 cells are depicted in red that receive input onto their dendrites in the medulla and lobula, respectively. Individual terminals providing synaptic input to the lobula plate are located either in layer 3 or 4. Equivalent cells innervating layers 1 and 2 are omitted. **A**, anterior; **P**, posterior; **M**, medial; **L**, lateral. **B**, View on a preparation from posterior onto the back of the head (right hemisphere). T4/T5 cells express mCherry-tagged ChR2–H134R (red). A VS cell is filled via a patch electrode with a fluorescent dye (green). **C–F**, Single confocal images of horizontally sectioned *Drosophila* brains. **C**, Immunostaining of GFP (green) and the presynaptic marker synaptotagmin-HA (sytHA, red) expressed in T4 and T5 cells, bruchpilot (brp) is labeled in blue for neuropil reference. sytHA clearly demarcates the four synaptic layers in the lobula plate. **D–F**, ChR2–H134R–mCherry expression using three driver lines as used for optogenetic experiments. **D**, T4 and T5 cells; **E**, T4 cells only; **F**, cholinergic T4 and T5 cells.

numbers we expressed a nuclear GFP marker using a T4/T5-specific Gal4 line, generated confocal stacks of optic lobes, and counted nuclei manually with the aid of a custom-made tracking software. Our analyses yielded a total number of  $5264 \pm 433$  (SD) T4 and T5 cells ( $N = 4$ ). If a set of T4/T5 cells were represented by every retinotopic unit this would indicate a number of approximately seven cells per column, approximating eight. Taking into account that a small fraction of cells might have escaped from analysis or that numbers might be reduced toward the edges of the visual field, this result is well in agreement with an electron microscopy study that has identified four T4 cells per medulla column each projecting to one of the four different lobula plate layers (Takemura et al., 2013). In the light of these findings we interpret our result such that in general for each ommatidium each of the four lobula plate layers is innervated by one T4 and one T5 terminal only, both tuned to the same direction of visual motion but individually specialized for moving contrast increments and decrements, respectively.

### Probing synaptic connectivity between T4/T5 and LPTCs

T4 and T5 cells receive synaptic input on their dendrites located in the medulla and lobula, respectively, and convey signals to the lobula plate where they are thought to connect to LPTC dendrites via chemical synapses (Fig. 1A,C; Strausfeld and Lee, 1991). Making use of specific T4/T5 driver lines (Fig. 1B–F) we set out to probe the underlying connectivity by optically stimulating T4/T5-expressing Channelrhodopsin2–H134R–mCherry while recording the synaptic responses in LPTCs by whole-cell patch clamp (Fig. 1A,B). Applying 2 ms blue light pulses at  $\sim 3 \text{ mW mm}^{-2}$  (472 nm center wavelength, 30 nm bandwidth) to T4/T5 > ChR2 brains resulted in a fast excitatory peak (latency  $5.4 \pm 0.4 \text{ ms}$  after onset of stimulus trigger) followed by an

# Optogenetic and Pharmacologic Dissection of Feedforward Inhibition in *Drosophila* Motion Vision

Mauss et al. • Feedforward Inhibition in Fly Motion Vision

J. Neurosci., February 5, 2014 • 34(6):2254–2263 • 2257

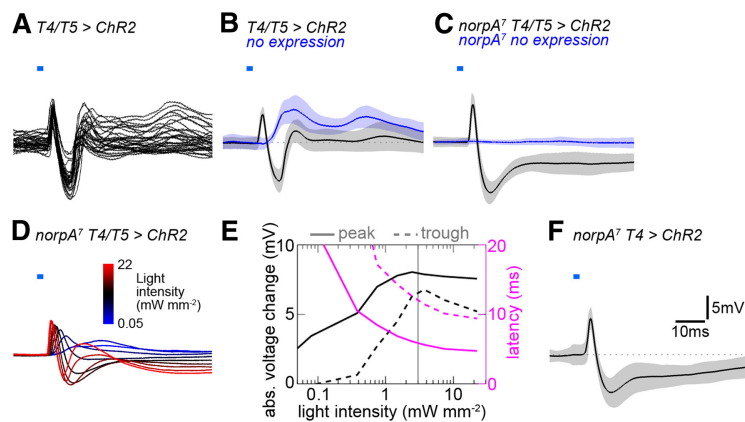


**Figure 2.** Synaptic LPTC responses to optogenetic T4/T5 cell stimulation. **A**, Individual voltage traces of LPTCs ( $N = 4$ ) responding to optogenetic stimulation of T4 and T5 cells ( $T4/T5 > ChR2$ ;  $n = 32$  stimuli total). Optic stimuli consisted of 2 ms wide-field light flashes delivered through the microscope objective onto the preparation with a center wavelength and bandwidth of 472/30 nm and an intensity of  $\sim 3$  mW mm $^{-2}$ . LPTCs respond with initial biphasic voltage deflections consisting of a fast depolarization and a subsequent hyperpolarization. **B**, Average of the same traces as in **A** in black, with SD as shaded area. The blue trace is the response of LPTCs in control flies (Gal4 only) to the same stimulus ( $N = 4$ ), showing the retina input only. **C**, Same as **B**, but with blind flies homozygously carrying the *norpA7* mutation (black,  $N = 7$ ; blue,  $N = 4$ ). **D**, Same condition as for black trace in **C**, but with light intensity varied between 0.05 and 22 mW mm $^{-2}$  ( $N = 8$ , SD omitted for clarity). **E**, Responses were quantified and plotted as absolute (abs.) amplitudes (black) and latencies (magenta) of peak maxima (solid lines) and trough minima (dashed lines). The vertical gray line at 3 mW mm $^{-2}$  denotes the approximate light intensity for all other optogenetic experiments except for *T4/T5/Cha-Split* flies. **F**, Optogenetic stimulation of T4 cells only (*norpA7 T4 > ChR2*; 3 mW mm $^{-2}$ ,  $N = 5$ ) evokes a biphasic voltage response in LPTCs that is comparable to the joint T4/T5 cell stimulation.

inhibitory trough ( $\Delta 11.2 \pm 0.2$  ms) and a second smaller excitatory peak ( $\Delta 16.3 \pm 1.2$  ms). The time course of the response was highly reproducible as shown for four cells and a total number of 32 stimuli (Fig. 2A). Figure 2B (black trace) depicts the average of the same trials with the shaded area indicating the SD. A concern was the unintended stimulation of photoreceptors by the optogenetic light stimulus. To characterize visual artifacts we applied blue light pulses to control flies without expression (*T4/T5-Gal4* only) and observed an excitatory response in all preparations starting with a latency of 8 ms and peaking at  $\Delta 15.5 \pm 1.7$  ms (Fig. 2B, blue trace). The relatively slow time course and long latency of the retina artifact suggests that the initial biphasic depolarizing and hyperpolarizing potential changes in *T4/T5 > ChR2*-expressing flies are caused by synaptic input from optogenetically stimulated T4/T5 cells to LPTCs with the second excitatory peak being evoked by visual input. To further isolate the optogenetic from the retina components we performed experiments in flies without functional phototransduction (*norpA7*: phospholipase C mutated; Hotta and Benzer, 1970). As expected, *norpA7*-mutant flies without ChR2 expression did not show a response to blue light pulses at the level of LPTCs (Fig. 2C, blue trace). Repeating the same stimulation in the mutant background with additional ChR2 expression in T4/T5 lead to an initial biphasic response as in visually intact flies (Fig. 2C, black trace; latency excitatory peak:  $\Delta 5.4 \pm 0.4$  ms, inhibitory trough:  $\Delta 11.7 \pm 0.9$  ms). This result demonstrates that the biphasic response is generated exclusively by optogenetic T4/T5 stimulation. It also supports the notion that the formation of visual circuits in flies is largely independent of sensory experience (Karmeier et al., 2001; Hiesinger et al., 2006). Differences between visually intact and blind flies were only discernible  $>8$  ms after stimulus onset in that LPTCs in *norpA* mutants presumably due to the lack of visual input showed a sustained modest hyperpolarization with a time constant of 0.1 s (Fig. 2, compare B and C, black traces).

We next investigated the dependence of the optogenetic response on varying stimulus intensities to obtain a quantitative description of the underlying input-output relationship (Fig. 2D,E). Several features became apparent: (1) inhibition had a higher threshold than excitation; (2) the amplitudes increased approximately proportional to the logarithm of the stimulus intensity over a wide range; (3) the latency of the excitatory peak was approximately half of that for the inhibitory trough, a ratio that remained fairly stable across a wide range of intensities; and (4) at high light intensities the voltage progression became triphasic (not quantified).

Since we measured the LPTC responses to stimulation of both T4 and T5 cells at the same time the question arises in how far the two cell types might be differentially connected to LPTCs. We made use of a specific Gal4 line to optogenetically stimulate exclusively T4 cells (Figs. 1E, 2F). LPTC recordings show a biphasic response to 2 ms blue light flashes that is very similar to the joint T4/T5 stimulation at comparable light intensities (Fig. 2, compare C, black trace and F; latency excitatory peak:  $\Delta 5.9 \pm 0.4$  ms, inhibitory trough:  $\Delta 13.3 \pm 1.3$  ms). Due to the lack of a sufficiently selective driver line we were not able to perform corresponding experiments with T5 cells. However, the identical effects of our optogenetic T4 and T4/T5 stimulation argue that both cell types are synaptically connected to LPTCs in similar ways and that the initial sharp EPSP arises by direct excitation of LPTCs by both T4 and T5 terminals. This is to be expected because T4 and T5 cells are individually tuned to moving ON and OFF edges, respectively (Maisak et al., 2013), while LPTCs reliably depolarize in response to both visual stimuli.

The delayed hyperpolarization in LPTCs is less straightforward to explain and might be caused by one of the following mechanisms, which we will further address below: (1) direct synaptic inhibition by T4/T5 cells (slower than direct excitation); (2) feedforward inhibition via an additional cell type between T4/T5 and LPTCs; (3) LPTC intrinsic mechanisms, for instance, depolarization-triggered opening of hyperpolarizing conductances; or (4) feedback inhibition postsynaptic of LPTCs.

## T4/T5 cells are primarily cholinergic

Acetylcholine is the primary excitatory neurotransmitter in insect CNS. It is reasonable to assume that at least a substantial fraction of T4/T5 releases acetylcholine onto LPTCs since those express nicotinic cholinergic receptors (nAChRs), depolarize in response to acetylcholine and its agonist carbachol (Brotz and Borst, 1996; Raghu et al., 2009), and receive excitatory preferred direction input, which is eliminated when T4 and T5 cells are genetically silenced (Schnell et al., 2012). However, LPTCs also receive inhibitory null direction input, which is presumably GABAergic (Brotz and Borst, 1996; Single et al., 1997; Raghu et al., 2007). Moreover, genetic expression data and histochemistry have indicated that T4 and T5 cells might also secrete GABA, glutamate, and/or aspartate as neurotransmitters (Strausfeld et

# Optogenetic and Pharmacologic Dissection of Feedforward Inhibition in *Drosophila* Motion Vision

2258 • J. Neurosci., February 5, 2014 • 34(6):2254–2263

Mauss et al. • Feedforward Inhibition in Fly Motion Vision

al., 1995; Sinakevitch and Strausfeld, 2004; Raghu and Borst, 2011). We therefore asked whether T4/T5 cells employ neurotransmitters other than acetylcholine. First, we took an intersectional genetic approach (“Split Gal4”; Luan et al., 2006) to exclude potential noncholinergic T4/T5 cells from ChR2 expression. We targeted two functional domains (AD and DBD) both required for UAS activation independently to T4/T5 (*R42F06-p65-AD*) and cholinergic cells (*Cha-DBD*; Gao et al., 2008), respectively, by two different regulatory elements. Thus, functional transcription factor to activate *UAS-ChR2*

is reconstituted only in the intersection of the two expression patterns, i.e., in cholinergic T4 and T5 cells. It should be noted that in contrast to the other experimental backgrounds only a single copy of ChR2 was included because homozygous animals were not viable. Confocal images reveal that the resulting expression (*T4/T5-p65-AD + Cha-DBD = T4/T5/Cha-Split > ChR2-H134R-mCherry*) is generally weaker but otherwise not obviously different compared with *T4/T5 > ChR2* (Fig. 1D,F). Notably, optic stimulation of *T4/T5/Cha-Split > ChR2* brains (with higher intensities to compensate for weak expression:  $\sim 30 \text{ mW mm}^{-2}$ ) resulted in initial biphasic synaptic responses in LPTCs that were quite similar to the responses seen when driving ChR2 with *T4/T5-Gal4* (compare Figs. 3A, 2B, black trace). Second, we expressed a nuclear reporter (stinger-GFP) using the T4/T5-specific driver line and stained brains with an antibody against choline acetyltransferase (ChAT). Confocal imaging of optic lobes revealed that 99.2% cells labeled with stinger-GFP colocalized with anti-ChAT (Fig. 3B,B'). We also labeled GABAergic neurons in brains of the same genotype with an antibody against vesicular GABA transporter (vGAT). The vast majority (97.6%) of stinger-GFP-labeled cells was clearly vGAT negative (Fig. 3C,C'). Therefore, assuming that T4/T5 cells transmit a single fast neurotransmitter, we conclude that T4/T5 cells are not GABAergic but instead primarily cholinergic.

## Pharmacologic profile of lobula plate tangential cells

The data so far strongly suggest that T4/T5 cells represent a homogenous group with respect to their cholinergic transmitter phenotype. Therefore, the biphasic effect observed in the LPTC membrane potential upon T4/T5 stimulation must arise by mechanisms postsynaptic of T4/T5 terminals. One possibility might be the existence of antagonistic cholinergic receptors expressed in LPTC dendrites, since both excitatory and inhibitory acetylcholine-gated channels have been documented in invertebrates (Pfeiffer-Linn and Glantz, 1989; Dent, 2010). However, this scenario seems unlikely because acetylcholine and its agonist carbachol elicit strong depolarizations but no hyperpolarizations in LPTCs in *Calliphora* and *Drosophila* (Brotz and Borst, 1996; Raghu et al., 2009). We aimed to confirm and extend these findings by dissecting the direct and indirect effects of neurotransmitters pharmacologically. To this end, we pressure injected neurotransmitters via micropipettes into the lobula plate while simultaneously recording from LPTCs. In agreement with the previous studies, injection of 1 mM acetylcholine generated strong excitatory peaks in LPTCs (Fig. 4A–C, white arrows;  $+10.9 \pm 0.7 \text{ mV}$ ,  $N = 18$ ). In 17/18 cases, the excitation was followed by a clear hyperpolarizing response smaller in amplitude ( $-1.9 \pm 0.27 \text{ mV}$ ,  $N = 18$ ) but with a prolonged time course

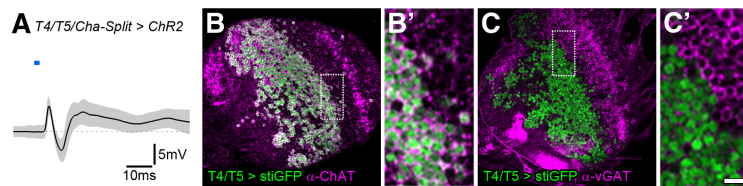


**Figure 3.** T4 and T5 cells are primarily cholinergic. **A**, Optogenetic stimulation of exclusively cholinergic T4/T5 cells leads to initial depolarization and subsequent hyperpolarization in LPTCs (Split-Gal4 approach: *T4/T5-p65-AD + Cha-DBD > ChR2*;  $30 \text{ mW mm}^{-2}$ ,  $N = 8$ ), comparable to T4 and T4/T5 cell stimulation as in Figure 2. The following second excitatory peak is likely caused by retina input. **B–C'**, Confocal images of immunostained *T4/T5-Gal4 > UAS-sti-GFP*-expressing brains reveal that the vast majority of T4/T5 cells are (**B, B'**; 2696/2717:99.2%) positive for ChAT and (**C, C'**; 2444/2503:97.6%) negative for vGAT. Scale bars: **B, C**, 20  $\mu\text{m}$ ; for enlarged insets (**B', C'**) 5  $\mu\text{m}$ .

(Fig. 4A–C, black arrows), reminiscent of the T4/T5 optogenetic stimulation effect albeit on a longer timescale due to the slower stimulus delivery. To quantify these effects relative to each other we divided the negative by the positive stimulus-evoked response integral (see Material and Methods) and obtained a relationship of  $-0.84 \pm 0.16$ . We then performed acetylcholine injection experiments under conditions where synaptic transmission is silenced (Fig. 4D;  $N = 7$ , external solution without  $\text{Ca}^{2+}$  and with high  $\text{Mg}^{2+}$  concentration). We found excitatory responses comparable to the condition with intact synaptic transmission ( $+13.5 \pm 1.1 \text{ mV}$ ). However, hyperpolarization was almost absent ( $-0.3 \pm 0.08 \text{ mV}$ ) and averaged integrated responses relative to excitation amounted to a significantly smaller value ( $-0.1 \pm 0.02$ ) compared with the normal condition (Wilcoxon rank sum test,  $-0.84 \pm 0.16$  vs  $-0.1 \pm 0.02$ ;  $p = 0.001$ ). These results demonstrate that acetylcholine injection evokes a direct depolarizing and an indirect hyperpolarizing response in LPTCs. Moreover, this outcome corroborates the notion that alone acetylcholine release from optogenetically stimulated T4/T5 might underlie the biphasic response in LPTCs. We went on to explore the sensitivity of LPTCs to two other prevalent neurotransmitters. Both pressure-applied GABA and glutamate elicited pronounced inhibitory potential changes (Fig. 4E–H) suggesting that both GABA- and glutamate-gated chloride channels (Cleveland, 1996; Hosie et al., 1997) are expressed in LPTCs.

Next, we used the pressure-injection assay to establish specificity and effectiveness of available cholinergic and GABAergic antagonists. We consider this strategy essential because neurotoxins can display a considerable degree of cross-reactivity particularly for the functionally diverse group of phylogenetically related pentameric ionotropic receptors in insects (Bai et al., 1992; Barbara et al., 2005; Dent, 2010). We thus combined acetylcholine pressure injection into the lobula plate with patch-clamp recordings from LPTCs and bath perfusion of the nicotinic antagonists MLA,  $\alpha$ -BTX (both competitive), and MEC (non-competitive). We found that 1  $\mu\text{M}$  MLA was most effective and irreversibly eliminated all acetylcholine responses within 10–15 min after administering the drug (Fig. 4A–A'). MEC was less potent and reduced both depolarizing and hyperpolarizing responses at a concentration of 100  $\mu\text{M}$  to 9 and 5%, respectively, with a similar time course (Fig. 4B–B'). This effect, however, was reversible (110% for depolarization and 80% for hyperpolarization) after washing for  $\sim 40 \text{ min}$  ( $N = 7$ ; Fig. 4B', dashed trace). Depolarization in response to acetylcholine was also blocked by 10  $\mu\text{M}$   $\alpha$ -BTX (30%) within 40 min (Fig. 4C–C'). The longer time course is presumably due to the much larger molecular weight of the  $\alpha$ -BTX peptide compared with the other compounds or the different delivery (see Material and Methods). Notably, in con-

# Optogenetic and Pharmacologic Dissection of Feedforward Inhibition in *Drosophila* Motion Vision

Mauss et al. • Feedforward Inhibition in Fly Motion Vision

J. Neurosci., February 5, 2014 • 34(6):2254–2263 • 2259

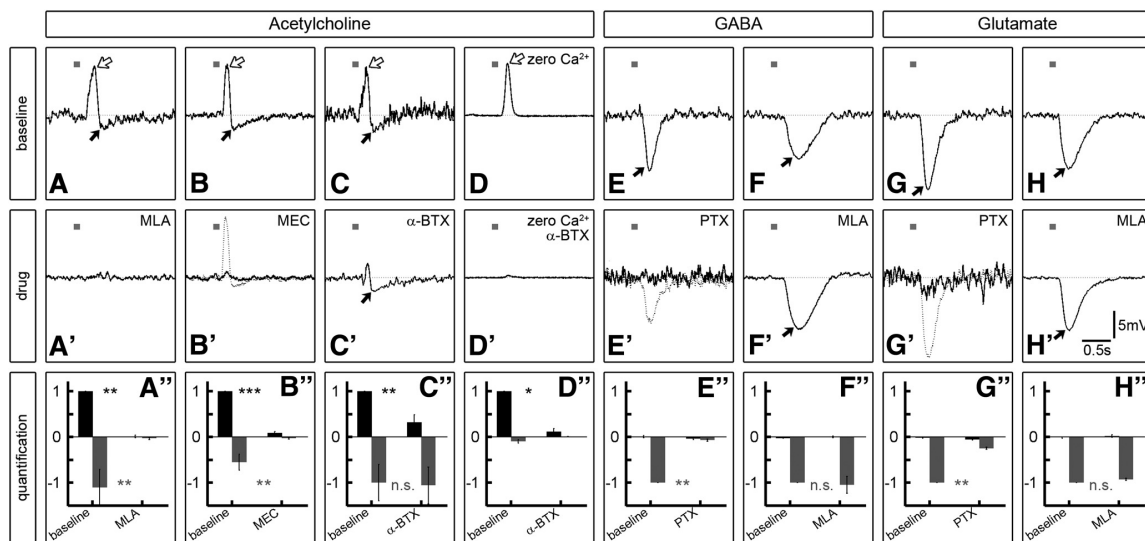


**Figure 4.** Responses to neurotransmitter injections and pharmacologic profile of LPTCs. *A–H*, Representative average voltage traces from single LPTCs in response to five neurotransmitter pressure injections onto the dendrites in the lobula plate are shown (100 ms pulses indicated by small gray bars, neurotransmitters at 1 mM concentration indicated at the top). *A–C*, Acetylcholine injection evokes an initial depolarizing peak (white arrow) and a subsequent hyperpolarization (black arrow) in LPTCs. *D*, In conditions where synaptic transmission is silenced (zero  $\text{Ca}^{2+}$ , high  $\text{Mg}^{2+}$  concentration in external solution) depolarization is still present while hyperpolarization is almost completely absent. *E–H*, Both GABA and glutamate injection leads to strong hyperpolarization in all cells recorded. *A'–H'*, Responses from the same cells after application of the indicated antagonists: (*A'*) 15 min 1  $\mu\text{M}$  MLA, (*B'*) 15 min 100  $\mu\text{M}$  MEC, (*C' + D'*) 40 min 10  $\mu\text{M}$   $\alpha$ -BTX, (*E' + G'*) 10–15 min 25  $\mu\text{M}$  PTX, (*F' + H'*) 25 min 1  $\mu\text{M}$  MLA. The dashed traces in *B'*, *E'*, and *G'* denote responses after 30–60 min wash following MEC or PTX treatment. MLA and  $\alpha$ -BTX effects could not be washed out effectively. *A''–H''*, Responses of individual cells were quantified as positive (black bars) and negative integrals (gray bars; the period 1 s before the stimulus was used as a baseline and subtracted away from the response 1 s after the stimulus; error bars denote SEM) normalized to the baseline depolarization for acetylcholine and baseline hyperpolarization for GABA and glutamate. *A''*,  $N = 5$ , *B''*,  $N = 8$ , *C''*,  $N = 5$ , *D''*,  $N = 4$ , *E''*,  $N = 5$ , *F''*,  $N = 2$ , *G''*,  $N = 5$ , *H''*,  $N = 2$ . Two-tailed Wilcoxon rank-sum test: n.s., Not significant;  $p > 0.3$ ;  $*p < 0.05$ ;  $**p \leq 0.01$ ;  $***p < 0.001$ .

trast to MLA and MEC,  $\alpha$ -BTX did not significantly change the indirect inhibitory effect of acetylcholine, which remained at 106% of baseline level. Because insect nAChR subunits are known to substantially differ in their sensitivity to  $\alpha$ -BTX (Thany et al., 2007, 2010) this result indicates that  $\alpha$ -BTX-sensitive receptors might be expressed on LPTCs while  $\alpha$ -BTX-insensitive receptors are located on another cell type also activated by acetylcholine and providing inhibitory input to LPTCs. We confirmed that the hyperpolarizing component in LPTCs in response to acetylcholine in presence of  $\alpha$ -BTX is indeed indirect, since, as for the baseline, it is absent in conditions where synaptic release is prevented (Fig. 4*D–D'*).

We then tested the noncompetitive GABA receptor antagonist PTX in combination with GABA injection onto LPTC dendrites. As expected, 25  $\mu\text{M}$  PTX effectively reduced the hyperpolarizing GABA response to 7% (Fig. 4*E–E'*; recovery 90% after 50–60 min wash; Fig. 4*E'*, dashed trace). As a control, we confirmed that the cholinergic antagonist MLA did not have any effect on GABA-evoked hyperpolarization, which remained reliably at baseline levels throughout drug treatment (Fig. 4*F–F'*). Since glutamate also produces hyperpolarizing conductances in LPTCs in our assay, we wanted to test a potential blocking action of PTX on those. Indeed, PTX reduced glutamate responses to 25% (Fig. 4*G–G'*; recovery 86% after 30–60 min wash; Fig. 4*G'*, dashed trace) indicating that PTX does not selectively block GABA-gated receptors but also other ligand-gated chloride channels in insects, in line with previous accounts (Rohrbough and Broadie, 2002; Barbara et al., 2005; Liu and Wilson, 2013). As in combination with GABA, MLA had no discernible effect on the LPTC responses to glutamate (Fig. 4*H–H'*).

## Feedforward inhibition from T4/T5 to LPTCs

The experiments above established that T4/T5 cells are cholinergic and that pressure-applied acetylcholine elicits monosynaptic depolarizing responses in LPTCs. Hence, acetylcholine release from T4/T5 cells most likely directly excites tangential cells. In contrast, the inhibitory component of the biphasic synaptic response in LPTCs upon optogenetic T4/T5 stimulation is probably indirectly elicited by yet unidentified inhibitory neurons. To further demonstrate this point, we compared LPTC responses to optogenetic stimulation of T4/T5 cells before and after the application of the cholinergic antagonists characterized above. Since the action of pharmacologic substances build up rather slowly *in vivo* we wanted to control for unspecific changes of the synaptic response in LPTCs over time, for instance, caused by synaptic depletion. However, we observed that the biphasic LPTC response did not substantially change at least over 50 individual stimulations and 40 min recording time (Fig. 5*A*, the black trace represents average baseline responses, the red trace recordings from the same cells 40 min later). Next, we combined T4/T5 stimulation with bath application of the potent and specific cholinergic antagonist MLA. Indeed, in full agreement with indirect synaptic inhibition, both the excitatory and the inhibitory responses were almost completely eliminated within 15 min after applying the drug (Fig. 5*B*, red trace). We then combined T4/T5 stimulation with the less potent cholinergic antagonist MEC (Fig. 5*C*). Now, the inhibitory component was abolished but a slowed excitatory component remained. Like in the acetylcholine pressure application assay, effects of MEC were largely reversible (data not shown). The residual excitation in presence of MEC with absent inhibition could mean that cholinergic receptors on



# Optogenetic and Pharmacologic Dissection of Feedforward Inhibition in *Drosophila* Motion Vision

2260 • J. Neurosci., February 5, 2014 • 34(6):2254–2263

Mauss et al. • Feedforward Inhibition in Fly Motion Vision

LPTCs are less affected by MEC than receptors on the putative inhibitory neuron type. The existence of nAChRs that differ in their sensitivity to MEC has, for instance, been suggested in cockroach DUM neurons (Courjaret and Lapied, 2001). Alternatively, regardless of nicotinic receptor properties, the putative inhibitory interneurons might have a higher threshold to become activated by T4/T5 cells than the LPTCs. The latter explanation is supported by experiments in which reduced light intensities were applied to optogenetically stimulate T4/T5 cells ( $<0.5$  mW mm<sup>2</sup>). Similar to MEC treatment, low light intensities resulted in slow and predominantly depolarizing responses in LPTCs (Fig. 2*D,E*). We wondered how the biphasic response would be affected by the more selective drug  $\alpha$ -BTX. As expected, the excitatory peak was effectively reduced (Fig. 5*D*, red trace). However, the IPSP was virtually unchanged similar to the result obtained by acetylcholine injection into the lobula plate (Fig. 4*C–C'*). This finding demonstrates that T4/T5-mediated inhibition in LPTCs does not require a preceding depolarization in those and thus rules out LPTC-intrinsic depolarization-triggered processes and feedback inhibition downstream of LPTCs. This conclusion is also supported by direct stimulation of ChR2-expressing tangential cells, which produced strong depolarizations without following hyperpolarizing troughs ( $N = 3$ , data not shown). Given that at least 10 nAChR subunits are encoded by the *Drosophila* genome (Jones and Sattelle, 2010), and expressed in various combinations in the optic lobe (Takemura et al., 2011), our experiments point toward a more complex connectivity between T4/T5 and LPTCs than just a direct cholinergic synapse. Rather, T4 and T5 cells additionally activate a yet unidentified cell type potentially expressing  $\alpha$ -BTX-insensitive receptors, which in turn supplies inhibition to LPTCs.

Furthermore, we also combined optogenetic T4/T5 stimulation with bath perfusion of PTX (Fig. 5*E*). LPTCs responded with depolarizations of rise time kinetics similar to the baseline but with enhanced peak amplitude. Importantly, fully in agreement with an indirect inhibitory synaptic connection from T4/T5 to the LPTCs, PTX strongly delayed and reduced hyperpolarizing effects of T4/T5 optogenetic stimulation. Since hyperpolarizing responses of LPTCs to both GABA and glutamate injection could be blocked by PTX (Fig. 4*E',G'*) this indicates that the postulated inhibitory cell type could be either GABAergic or glutamatergic.

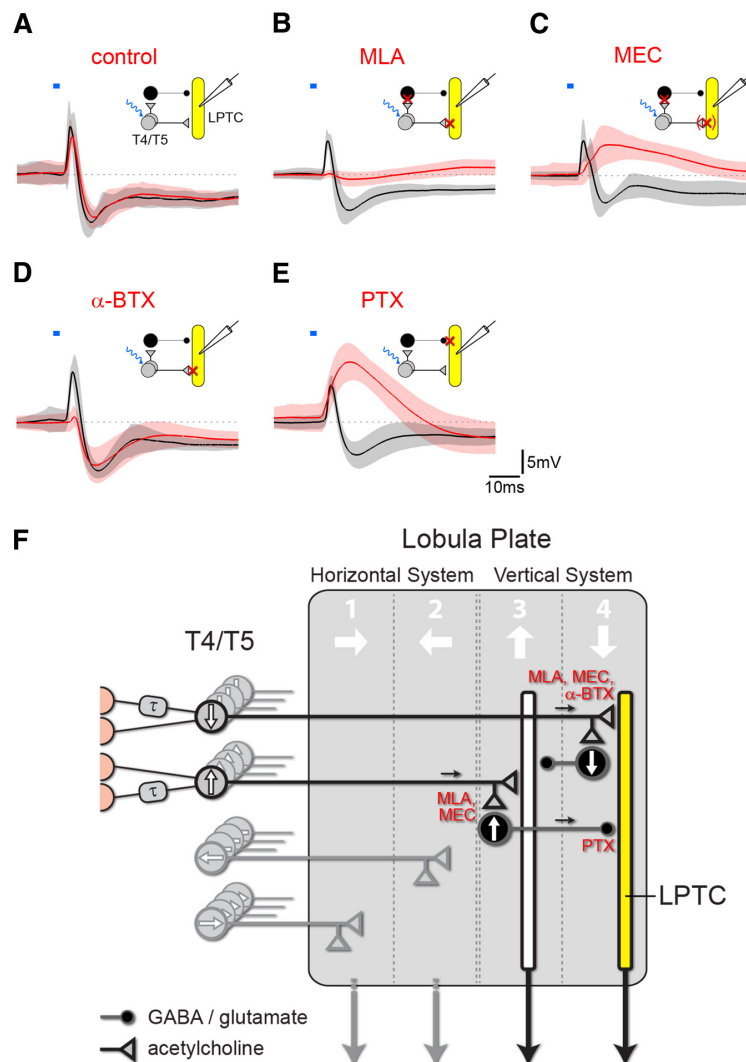


**Figure 5.** Effects of neurotransmitter antagonists on T4/T5-mediated synaptic potentials in LPTCs. **A**, Biphasic LPTC voltage response to optogenetic T4/T5 cell stimulation ( $T4/T5 > ChR2$ ; 2 ms 472/30 nm at  $\sim 3$  mW mm<sup>-2</sup>) over at least 50 individual stimulations and 40 min recording time ( $N = 5$ ; black, baseline; red, the same cells 40 min later). Amplitude and dynamics have not obviously changed over time. **B–E**, Responses of LPTCs (same genotype and stimulation) before (black trace) and after (red trace) indicated drug application (1  $\mu$ M MLA:  $N = 5$ , 15 min; 100–200  $\mu$ M MEC:  $N = 4$ , 15 min; 10  $\mu$ M  $\alpha$ -BTX:  $N = 6$ , 40 min; 25  $\mu$ M PTX:  $N = 7$ , 15 min). The schematic insets illustrate the connectivity supported by the data between T4/T5 and LPTCs with a direct excitatory connection and an inhibitory indirect arm. Synaptic targets of the individual antagonists are indicated with red crosses. The bracketed cross for MEC treatment indicates a potentially incomplete block. **F**, Connectivity model of the lobula plate that incorporates results from this study as well as previously published data (see Discussion). T4 and T5 cells terminate in one of four lobula plate layers according to their direction tuning where they directly connect to LPTC dendrites (yellow) in the same layer via cholinergic synapses and thus provide preferred direction excitation. T4 and T5 cells with opposite tuning terminate in the adjacent layer and provide feedforward null direction input to the same LPTC via putative GABAergic or glutamatergic inhibitory neurons. The inferred synaptic blocking sites of the antagonists (red) are indicated.

## Discussion

The visual ganglia of insects have been powerful model systems to address questions related to visual processing and circuit function largely because of experimental accessibility and the existence of individually identifiable neurons (Borst, 2009; Borst et al., 2010; Fotowat and Gabbiani, 2011; Homberg et al., 2011). However, due to the intricate connectivity and small sizes of most

# Optogenetic and Pharmacologic Dissection of Feedforward Inhibition in *Drosophila* Motion Vision

Mauss et al. • Feedforward Inhibition in Fly Motion Vision

J. Neurosci., February 5, 2014 • 34(6):2254–2263 • 2261

visual interneurons detailed circuit information has been difficult to establish. Here, we present a strategy to probe functional synaptic connectivity between identified neurons in *Drosophila* by combining optogenetic stimulation, electrophysiology, and pharmacology. The outcome of this work reveals a new synaptic processing stage in the fly motion vision circuitry.

Our experiments have established that wide-field visual motion-sensitive lobula plate tangential cells receive fast excitation when T4/T5 cells are optogenetically stimulated. We have shown that the excitatory input is cholinergic because it can be effectively blocked by selective nicotinic antagonists. The short latency of the optogenetic response (<3 ms after light onset; not taking into account the delay caused by ChR2-H134R opening kinetics) suggests that this excitatory cholinergic connection of T4/T5 cells onto LPTCs is most likely direct, well in agreement with functional, light microscopy and ultrastructure data (Fischbach and Dittrich, 1989; Strausfeld and Lee, 1991; Schnell et al., 2012; Maisak et al., 2013). Moreover, all T4/T5 somata are labeled by a choline acetyltransferase-specific antibody and acetylcholine pressure injection onto LPTC dendrites also elicits strong excitatory peaks in conditions where synaptic release is blocked (zero  $\text{Ca}^{2+}$ /high  $\text{Mg}^{2+}$ ). These optogenetic and pressure injection paradigms provide opportunities to explore synaptic ligand-gated receptors and their pharmacologic profiles on the level of individually identifiable neurons. In *Drosophila*, 10 nAChR subunits have been identified but their individual properties are not well understood largely because heterologous expression of functional insect nAChRs has been exceedingly difficult (Sattelle et al., 2005; Thany et al., 2007; Jones and Sattelle, 2010; Millar and Lansdell, 2010). LPTCs have been proposed to express  $\text{D}\alpha 7$  nAChR subunits (Raghu et al., 2009) that are candidates to form channels of an  $\alpha$ -BTX-sensitive type (Thany et al., 2007). In line with this view, depolarizing responses to acetylcholine and carbachol can be largely eliminated by  $\alpha$ -BTX (Fig. 4D–D'); Brotz and Borst, 1996). Somewhat surprisingly, however, in  $\text{D}\alpha 7$ -mutant flies visual responses in LPTCs are largely unaltered and a fluorophore-conjugated  $\alpha$ -BTX probe still binds to LPTC dendrites (Raghu et al., 2009) suggesting that other  $\alpha$ -BTX-sensitive subunits can substitute for  $\text{D}\alpha 7$  absence. It remains to be seen whether the cholinergic receptors are of heteromeric or homomeric types. Transcript profiling of individual LPTCs could help to assign nicotinic subunit composition to identified neurons (Takemura et al., 2011) and perhaps also reveal post-transcriptional modifications that might further functionally diversify receptors in a cell-specific manner (Sattelle et al., 2005). This approach in combination with whole-cell recordings, optogenetic stimulation, neurotransmitter injection, and genetic manipulation would open up this system for detailed analyses of the pharmacologic properties of nicotinic and other channels at the level of individual subunits and functional domains.

In addition to direct excitation, both optogenetic stimulation of T4/T5 cells and acetylcholine pressure injection onto LPTC dendrites elicit delayed hyperpolarization. This inhibitory component is indirect because it can be eliminated by the cholinergic antagonists MLA and MEC (Figs. 4A–A', B–B', 5B, C) and because it is absent for acetylcholine injection when synaptic transmission is blocked (Fig. 4D). We therefore propose that cholinergic T4/T5 cells excite yet unidentified local interneurons, which supply inhibition to LPTCs. Such putative local interneurons might express acetylcholine receptors of an  $\alpha$ -BTX-insensitive type because this neurotoxin had no effect on inhibition evoked by optogenetic T4/T5 cell stimulation and acetylcholine injection (Figs. 4C–C', 5D). What is the functional

significance of the T4/T5 cell-mediated direct excitation and indirect inhibition onto LPTCs? During visual stimulation, LPTCs receive two kinds of inputs: excitation tuned to their preferred direction and inhibition tuned to the opposite/null direction. Since T4/T5 cells have been identified to represent the motion-sensitive input elements to the lobula plate (Schnell et al., 2012; Maisak et al., 2013; Takemura et al., 2013) three scenarios seemed conceivable to underlie preferred and null direction responses in LPTCs. (1) T4/T5 cells convey signals to LPTCs via a single neurotransmitter with graded positive and negative release modulations from a spontaneous level, similar to photoreceptor terminals. (2) Synaptic connections between T4/T5 and LPTCs comprise two antagonistic types, for instance, implementing different transmitter systems mediating oppositely tuned excitation and inhibition. In line with this model T4 and T5 cells have been suggested to release acetylcholine, GABA, glutamate, and aspartate as neurotransmitters (Strausfeld et al., 1995; Sinakevitch and Strausfeld, 2004; Raghu and Borst, 2011; Raghu et al., 2011). (3) Excitatory output from T4/T5 cells is partly sign inverted and fed forward to LPTCs by inhibitory cells in a direction-specific manner. Possibility 1 appears highly unlikely on the basis of current injections in LPTCs during visual motion stimulation (Borst et al., 1995, 2010; Joesch et al., 2008). These experiments reveal that the synaptic currents underlying preferred and null direction responses are mediated by different synaptic receptors because the responses have markedly different reversal potentials. As for the remaining possibilities, previous data (Fischbach and Dittrich, 1989; Maisak et al., 2013; Takemura et al., 2013) and our cell counts indicate eight functional types of T4/T5 per retinotopic column: each tuned to one of two contrast polarities and one of the four cardinal directions of motion. This number is difficult to reconcile with the second model, because it would require a further subdivision of T4/T5 cells according to transmitter profile. Moreover, individual LPTC dendrites generally do not anatomically overlap with T4/T5 terminals tuned to the LPTC's null direction. Rather, our results clearly support the third possibility because, as we have shown, all T4/T5 cells are in fact cholinergic and supply direct excitation and indirect inhibition to LPTCs.

We thus favor a model where LPTC dendrites receive cholinergic input during preferred direction motion from T4/T5 terminals in one layer of the lobula plate where they overlap, and input from the neighboring layer conveyed by yet unidentified inhibitory cells during null direction motion (Fig. 5F). Furthermore, the postulated inhibitory neurons might additionally inhibit presynaptic T4/T5 terminals in the adjacent layer and thereby antagonize excitatory inputs to tangential cells both presynaptically and postsynaptically at the same time. Such a wiring would constitute a recurrent inhibitory motive and potentially explain why optogenetic stimulation of all T4/T5 cells with high intensities generates a triphasic voltage progression in tangential cells (Fig. 2D, red trace). In line with this idea, prolonged optogenetic T4/T5 cell stimulation evokes membrane potential oscillations in tangential cells (data not shown). The transmitter used by neurons responsible for null direction inhibition has been suggested to be GABA. This conclusion is primarily based on experiments in which PTX has been used to block inhibition (Schmid and Bülthoff, 1988; Egelhaaf et al., 1990; Brotz and Borst, 1996; Single et al., 1997). However, we have found that LPTCs respond with hyperpolarization both to GABA and to glutamate injection, and that both responses can be blocked by PTX. These results challenge the notion that GABA underlies the null direction responses in LPTCs and suggest glutamate as another candidate neurotransmitter that should be taken into consideration.

# Optogenetic and Pharmacologic Dissection of Feedforward Inhibition in *Drosophila* Motion Vision

2262 • J. Neurosci., February 5, 2014 • 34(6):2254–2263

Mauss et al. • Feedforward Inhibition in Fly Motion Vision

The identification of the neurons underlying null direction inhibition will be required for the verification of the underlying neurotransmitter system and to complete the suggested wiring model of the lobula plate. Previous anatomical studies might provide an entry point. Fischbach and Dittrich (1989), Raghu et al. (2011, 2013), and Raghu and Borst (2011) describe cells such as Tlp, Lpi, and Y neurons, which arborize in more than one lobula plate layer but also in other neuropils and are therefore not immediately persuasive to fulfill the postulated role. Additional anatomical analyses and identification of novel cell types might therefore be necessary. Genetic control over the postulated inhibitory neurons would facilitate the study of the integration and functional implications of antagonistic preferred and null direction inputs on tangential cells. Depending on the anatomical and physiological properties of the postulated inhibitory cells some null direction-specific processing might occur. For instance, while ON and OFF motion vision pathways likely converge first at the level of the tangential cells during preferred direction motion (Maisak et al., 2013), it remains to be determined whether null direction ON and OFF motion signals are perhaps integrated in the inhibitory neurons presynaptic to tangential cells.

## References

- Bahl A, Ammer G, Schilling T, Borst A (2013) Object tracking in motion-blind flies. *Nat Neurosci* 16:730–738. [CrossRef Medline](#)
- Bai D, Erdbrugger H, Breer H, Sattelle DB (1992) Acetylcholine receptors of thoracic dorsal midline neurones in the cockroach, *Periplaneta americana*. *Arch Insect Biochem Physiol* 21:289–301. [CrossRef Medline](#)
- Barbara GS, Zube C, Rybak J, Gauthier M, Grünwald B (2005) Acetylcholine, GABA and glutamate induce ionic currents in cultured antennal lobe neurons of the honeybee, *Apis mellifera*. *J Comp Physiol A Neuroethol Sens Neural Behav Physiol* 191:823–836. [CrossRef Medline](#)
- Borst A (2009) *Drosophila's* view on insect vision. *Curr Biol* 19:R36–R47. [CrossRef Medline](#)
- Borst A, Euler T (2011) Seeing things in motion: models, circuits, and mechanisms. *Neuron* 71:974–994. [CrossRef Medline](#)
- Borst A, Egelhaaf M, Haag J (1995) Mechanisms of dendritic integration underlying gain control in fly motion-sensitive interneurons. *J Comput Neurosci* 2:5–18. [CrossRef Medline](#)
- Borst A, Haag J, Reiff DF (2010) Fly motion vision. *Annu Rev Neurosci* 33:49–70. [CrossRef Medline](#)
- Brotz TM, Borst A (1996) Cholinergic and GABAergic receptors on fly tangential cells and their role in visual motion detection. *J Neurophysiol* 76:1786–1799. [Medline](#)
- Clark DA, Bursztyl L, Horowitz MA, Schnitzer MJ, Clandinin TR (2011) Defining the computational structure of the motion detector in *Drosophila*. *Neuron* 70:1165–1177. [CrossRef Medline](#)
- Cleland TA (1996) Inhibitory glutamate receptor channels. *Mol Neurobiol* 13:97–136. [CrossRef Medline](#)
- Courjaret R, Lapiet B (2001) Complex intracellular messenger pathways regulate one type of neuronal alpha-bungarotoxin-resistant nicotinic acetylcholine receptors expressed in insect neurosecretory cells (dorsal unpaired median neurons). *Mol Pharmacol* 60:80–91. [Medline](#)
- Dent JA (2010) The evolution of pentameric ligand-gated ion channels. *Adv Exp Med Biol* 683:11–23. [CrossRef Medline](#)
- Egelhaaf M, Borst A, Pils B (1990) The role of GABA in detecting visual motion. *Brain Res* 509:156–160. [CrossRef Medline](#)
- Eichner H, Joesch M, Schnell B, Reiff DF, Borst A (2011) Internal structure of the fly elementary motion detector. *Neuron* 70:1155–1164. [CrossRef Medline](#)
- Fei H, Chow DM, Chen A, Romero-Calderón R, Ong WS, Ackerson LC, Maidment NT, Simpson JH, Frye MA, Krantz DE (2010) Mutation of the *Drosophila* vesicular GABA transporter disrupts visual figure detection. *J Exp Biol* 213:1717–1730. [CrossRef Medline](#)
- Fischbach KF, Dittrich A (1989) The optic lobe of *Drosophila melanogaster*. I. A Golgi analysis of wild-type structure. *Cell Tissue Res* 258:441–475.
- Fotowat H, Gabbiani F (2011) Collision detection as a model for sensory-motor integration. *Annu Rev Neurosci* 34:1–19. [CrossRef Medline](#)
- Gao S, Takemura SY, Ting CY, Huang S, Lu Z, Luan H, Rister J, Thum AS, Yang M, Hong ST, Wang JW, Odenwald WF, White BH, Meinertzhagen IA, Lee CH (2008) The neural substrate of spectral preference in *Drosophila*. *Neuron* 60:328–342. [CrossRef Medline](#)
- Hassenstein B, Reichardt W (1956) Systemtheoretische Analyse der Zeit-, Reihenfolgen- und Vorzeichenbewertung bei der Bewegungsperzeption des Rüsselkäfers *Chlorophanus*. *Z Naturforsch* 11b:513–524.
- Hausen K (1982) Motion sensitive interneurons in the optomotor system of the fly I. The horizontal cells: structure and signals. *Biol Cybernet* 45:143–156. [CrossRef](#)
- Hausen K (1984) The lobula-complex of the fly: structure, function and significance in visual behaviour. In: *Photoreception vision invertebrates*, NATO ASI Series, Vol 74, pp 523–559. New York: Springer.
- Hengstenberg R, Hausen K, Hengstenberg B (1982) The number and structure of giant vertical cells (VS) in the lobula plate of the blowfly *Calliphora erythrocephala*. *J Comp Physiol A Neuroethol Sens Neural Behav Physiol* 149.
- Hiesinger PR, Zhai RG, Zhou Y, Koh TW, Mehta SQ, Schulze KL, Cao Y, Verstreken P, Clandinin TR, Fischbach KF, Meinertzhagen IA, Bellen HJ (2006) Activity-independent prespecification of synaptic partners in the visual map of *Drosophila*. *Curr Biol* 16:1835–1843. [CrossRef Medline](#)
- Homberg U, Heinze S, Pfeiffer K, Kinoshita M, el Jundi B (2011) Central neural coding of sky polarization in insects. *Philos Trans R Soc Lond B Biol Sci* 366:680–687. [CrossRef Medline](#)
- Hosie AM, Aronstein K, Sattelle DB, French-Constant RH (1997) Molecular biology of insect neuronal GABA receptors. *Trends Neurosci* 20:578–583. [CrossRef Medline](#)
- Hotta Y, Benzer S (1970) Genetic dissection of the *Drosophila* nervous system by means of mosaics. *Proc Natl Acad Sci U S A* 67:1156–1163. [CrossRef Medline](#)
- Joesch M, Plett J, Borst A, Reiff DF (2008) Response properties of motion-sensitive visual interneurons in the lobula plate of *Drosophila melanogaster*. *Curr Biol* 18:368–374. [CrossRef Medline](#)
- Joesch M, Schnell B, Raghu SV, Reiff DF, Borst A (2010) ON and OFF pathways in *Drosophila* motion vision. *Nature* 468:300–304. [CrossRef Medline](#)
- Joesch M, Weber F, Eichner H, Borst A (2013) Functional specialization of parallel motion detection circuits in the fly. *J Neurosci* 33:902–905. [CrossRef Medline](#)
- Jones AK, Sattelle DB (2010) Diversity of insect nicotinic acetylcholine receptor subunits. *Adv Exp Med Biol* 683:25–43. [CrossRef Medline](#)
- Karmeier K, Tabor R, Egelhaaf M, Krapp HG (2001) Early visual experience and the receptive-field organization of optic flow processing interneurons in the fly motion pathway. *Vis Neurosci* 18:1–8. [CrossRef Medline](#)
- Liu WW, Wilson RI (2013) Glutamate is an inhibitory neurotransmitter in the *Drosophila* olfactory system. *Proc Natl Acad Sci U S A* 110:10294–10299. [CrossRef Medline](#)
- Löhr R, Godenschwege T, Buchner E, Prokop A (2002) Compartmentalization of central neurons in *Drosophila*: a new strategy of mosaic analysis reveals localization of presynaptic sites to specific segments of neurites. *J Neurosci* 22:10357–10367. [Medline](#)
- Luan H, Peabody NC, Vinson CR, White BH (2006) Refined spatial manipulation of neuronal function by combinatorial restriction of transgene expression. *Neuron* 52:425–436. [CrossRef Medline](#)
- Maimon G, Straw AD, Dickinson MH (2010) Active flight increases the gain of visual motion processing in *Drosophila*. *Nat Neurosci* 13:393–399. [CrossRef Medline](#)
- Maisak MS, Haag J, Ammer G, Serbe E, Meier M, Leonhardt A, Schilling T, Bahl A, Rubin GM, Nern A, Dickson BJ, Reiff DF, Hopp E, Borst A (2013) A directional tuning map of *Drosophila* elementary motion detectors. *Nature* 500:212–216. [CrossRef Medline](#)
- Mattis J, Tye KM, Ferenczi EA, Ramakrishnan C, O'Shea DJ, Prakash R, Gunaydin LA, Hyun M, Fenko LE, Gradinaru V, Yizhar O, Deisseroth K (2012) Principles for applying optogenetic tools derived from direct comparative analysis of microbial opsins. *Nat Methods* 9:159–172. [Medline](#)
- Millar NS, Lansdell SJ (2010) Characterisation of insect nicotinic acetylcholine receptors by heterologous expression. *Adv Exp Med Biol* 683:65–73. [CrossRef Medline](#)
- Nagel G, Brauner M, Liewald JF, Adeishvili N, Bamberg E, Gottschalk A (2005) Light activation of channelrhodopsin-2 in excitable cells of *Caenorhabditis elegans* triggers rapid behavioral responses. *Curr Biol* 15:2279–2284. [CrossRef Medline](#)

# Optogenetic and Pharmacologic Dissection of Feedforward Inhibition in *Drosophila* Motion Vision

Mauss et al. • Feedforward Inhibition in Fly Motion Vision

J. Neurosci., February 5, 2014 • 34(6):2254–2263 • 2263

- Pfeiffer BD, Jenett A, Hammonds AS, Ngo TT, Misra S, Murphy C, Scully A, Carlson JW, Wan KH, Lavery TR, Mungall C, Svirskas R, Kadonaga JT, Doe CQ, Eisen MB, Celniker SE, Rubin GM (2008) Tools for neuroanatomy and neurogenetics in *Drosophila*. *Proc Natl Acad Sci U S A* 105:9715–9720. [CrossRef Medline](#)
- Pfeiffer-Linn C, Glantz RM (1989) Acetylcholine and GABA mediate opposing actions on neuronal chloride channels in crayfish. *Science* 245:1249–1251. [CrossRef Medline](#)
- Pulver SR, Pashkovski SL, Hornstein NJ, Garrity PA, Griffith LC (2009) Temporal dynamics of neuronal activation by Channelrhodopsin-2 and TRPA1 determine behavioral output in *Drosophila* larvae. *J Neurophysiol* 101:3075–3088. [CrossRef Medline](#)
- Raghu SV, Borst A (2011) Candidate glutamatergic neurons in the visual system of *Drosophila*. *PLoS One* 6:e19472. [CrossRef Medline](#)
- Raghu SV, Joesch M, Borst A, Reiff DF (2007) Synaptic organization of lobula plate tangential cells in *Drosophila*: gamma-aminobutyric acid receptors and chemical release sites. *J Comp Neurol* 502:598–610. [CrossRef Medline](#)
- Raghu SV, Joesch M, Sigrist SJ, Borst A, Reiff DF (2009) Synaptic organization of lobula plate tangential cells in *Drosophila*: Dalpha7 cholinergic receptors. *J Neurogenet* 23:200–209. [CrossRef Medline](#)
- Raghu SV, Reiff DF, Borst A (2011) Neurons with cholinergic phenotype in the visual system of *Drosophila*. *J Comp Neurol* 519:162–176. [CrossRef Medline](#)
- Raghu SV, Claussen J, Borst A (2013) Neurons with GABAergic phenotype in the visual system of *Drosophila*. *J Comp Neurol* 521:252–265. [CrossRef Medline](#)
- Rister J, Pauls D, Schnell B, Ting CY, Lee CH, Snakevitch I, Morante J, Strausfeld NJ, Ito K, Heisenberg M (2007) Dissection of the peripheral motion channel in the visual system of *Drosophila melanogaster*. *Neuron* 56:155–170. [CrossRef Medline](#)
- Robinson IM, Ranjan R, Schwarz TL (2002) Synaptotagmins I and IV promote transmitter release independently of Ca(2+) binding in the C(2)A domain. *Nature* 418:336–340. [CrossRef Medline](#)
- Rohrbough J, Broadie K (2002) Electrophysiological analysis of synaptic transmission in central neurons of *Drosophila* larvae. *J Neurophysiol* 88:847–860. [Medline](#)
- Sattelle DB, Jones AK, Sattelle BM, Matsuda K, Reenan R, Biggin PC (2005) Edit, cut and paste in the nicotinic acetylcholine receptor gene family of *Drosophila melanogaster*. *Bioessays* 27:366–376. [CrossRef Medline](#)
- Schmid A, Bülthoff H (1988) Using neuropharmacology to distinguish between excitatory and inhibitory movement detection mechanisms in the fly *Calliphora erythrocephala*. *Biol Cybernet* 59:71–80. [CrossRef](#)
- Schnell B, Raghu SV, Nern A, Borst A (2012) Columnar cells necessary for motion responses of wide-field visual interneurons in *Drosophila*. *J Comp Physiol A* 198:389–395. [CrossRef Medline](#)
- Silies M, Gohl DM, Fisher YE, Freifeld L, Clark DA, Clandinin TR (2013) Modular use of peripheral input channels tunes motion-detecting circuitry. *Neuron* 79:111–127. [CrossRef Medline](#)
- Sinakevitch I, Strausfeld NJ (2004) Chemical neuroanatomy of the fly's movement detection pathway. *J Comp Neurol* 468:6–23. [CrossRef Medline](#)
- Single S, Haag J, Borst A (1997) Dendritic computation of direction selectivity and gain control in visual interneurons. *J Neurosci* 17:6023–6030. [Medline](#)
- Strausfeld NJ, Lee JK (1991) Neuronal basis for parallel visual processing in the fly. *Vis Neurosci* 7:13–33. [CrossRef Medline](#)
- Strausfeld NJ, Kong A, Milde JJ, Gilbert C, Ramaiah L (1995) Oculomotor control in calliphorid flies: GABAergic organization in heterolateral inhibitory pathways. *J Comp Neurol* 361:298–320. [CrossRef Medline](#)
- Tagakawa K, Salvaterra P (1996) Analysis of choline acetyltransferase protein in temperature sensitive mutant flies using newly generated monoclonal antibody. *Neurosci Res* 24:237–243. [CrossRef Medline](#)
- Takemura SY, Bharioke A, Lu Z, Nern A, Vitaladevuni S, Rivlin PK, Katz WT, Olbris DJ, Plaza SM, Winston P, Zhao T, Horne JA, Fetter RD, Takemura S, Blazek K, Chang LA, Ogundeyi O, Saunders MA, Shapiro V, Sigmund C, et al. (2013) A visual motion detection circuit suggested by *Drosophila* connectomics. *Nature* 500:175–181. [CrossRef Medline](#)
- Takemura SY, Karuppudurai T, Ting CY, Lu Z, Lee CH, Meinertzhagen IA (2011) Cholinergic circuits integrate neighboring visual signals in a *Drosophila* motion detection pathway. *Curr Biol* 21:2077–2084. [CrossRef Medline](#)
- Thany SH (2010) Electrophysiological studies and pharmacological properties of insect native nicotinic acetylcholine receptors. *Adv Exp Med Biol* 683:53–63. [CrossRef Medline](#)
- Thany SH, Lenaers G, Raymond-Delpech V, Sattelle DB, Lapied B (2007) Exploring the pharmacological properties of insect nicotinic acetylcholine receptors. *Trends Pharmacol Sci* 28:14–22. [CrossRef Medline](#)
- Tuthill JC, Nern A, Holtz SL, Rubin GM, Reiser MB (2013) Contributions of the 12 neuron classes in the fly lamina to motion vision. *Neuron* 79:128–140. [CrossRef Medline](#)

# Manuscript Nr. 5: Neural Mechanisms for *Drosophila* Contrast Vision

Armin Bahl, **Etienne Serbe**, Matthias Meier, Georg Ammer, and Alexander Borst

## Author Contributions:

A.Ba. and A.Bo. designed the study. **E.S.** and M.M. performed electrophysiological recordings. G.A. provided the Mi1, Tm3, and Mi1/Tm3-Gal4 lines and did the immunostainings. A.Ba. built the behavioral setup, programmed the visual stimuli, performed the behavioral experiments, and analyzed the data. A.Ba. wrote the paper with help from the other authors.

# Neuron

## Neural Mechanisms for *Drosophila* Contrast Vision

### Highlights

- Flies are susceptible to contrast illusions in the same way as human observers
- Contrast and motion computations are carried out in parallel pathways
- Medulla cells Mi1 and Tm3 form a center-surround antagonism for contrast computation
- Signals from the motion and contrast pathways converge again in the lobula plate

### Authors

Armin Bahl, Etienne Serbe, Matthias Meier, Georg Ammer, Alexander Borst

### Correspondence

arminbahl@fas.harvard.edu

### In Brief

Bahl et al. employ optical illusions in behavioral experiments in *Drosophila* to investigate mechanisms and neuronal correlates of spatial contrast computation. They find that spatial contrast and motion cues are computed largely in parallel and that both pathways eventually converge.



Bahl et al., 2015, *Neuron* 88, 1240–1252  
December 16, 2015 ©2015 Elsevier Inc.  
<http://dx.doi.org/10.1016/j.neuron.2015.11.004>

CellPress

Neural Mechanisms for *Drosophila* Contrast VisionArmin Bahl,<sup>1,2,\*</sup> Etienne Serbe,<sup>1</sup> Matthias Meier,<sup>1</sup> Georg Ammer,<sup>1</sup> and Alexander Borst<sup>1</sup><sup>1</sup>Max Planck Institute of Neurobiology, Am Klopferspitz 18, 82152 Martinsried, Germany<sup>2</sup>Present address: Department of Molecular and Cell Biology, Harvard University, 16 Divinity Avenue, Cambridge, MA 02138, USA\*Correspondence: [arminbahl@fas.harvard.edu](mailto:arminbahl@fas.harvard.edu)<http://dx.doi.org/10.1016/j.neuron.2015.11.004>

## SUMMARY

Spatial contrast, the difference in adjacent luminance values, provides information about objects, textures, and motion and supports diverse visual behaviors. Contrast computation is therefore an essential element of visual processing. The underlying mechanisms, however, are poorly understood. In human psychophysics, contrast illusions are means to explore such computations, but humans offer limited experimental access. Via behavioral experiments in *Drosophila*, we find that flies are also susceptible to contrast illusions. Using genetic silencing techniques, electrophysiology, and modeling, we systematically dissect the mechanisms and neuronal correlates underlying the behavior. Our results indicate that spatial contrast computation involves lateral inhibition within the same pathway that computes motion of luminance increments (ON pathway). Yet motion-blind flies, in which we silenced downstream motion-sensitive neurons needed for optomotor behavior, have fully intact contrast responses. In conclusion, spatial contrast and motion cues are first computed by overlapping neuronal circuits which subsequently feed into parallel visual processing streams.

## INTRODUCTION

Computation of spatial contrast, the local difference in adjacent luminance values, allows animals to distinguish between figure and ground, to detect edges, and to visually adapt to the dynamic range of the current visual scene. Despite the importance of such computations for a wide range of visual behaviors, the mechanisms underlying spatial contrast computation are not well-understood in any organism. Optical illusions elicit visual perceptions that differ from physical reality and can serve as a tool in psychophysical experiments to explore how the brain computes. For example, when a gray bar of uniform luminance is embedded in a gradient background, humans perceive a brightness gradient within the bar, which indicates that human brightness estimation is based on relative rather than absolute luminance (Adelson, 2000). Such illusions are static and require the experimental subject to report its perception. Hence, they are difficult to use in other species. Motion illusions, however, often elicit behavioral responses and can be transferred to sim-

ple model organisms (Bülthoff and Götz, 1979; Eichner et al., 2011; Tuthill et al., 2011). A motion illusion based on spatial contrast computation, the contrast motion illusion, has recently been described in human psychophysics (Shapiro and Hamburger, 2007). Here, several dark stripes are embedded in a gradient background which is dark on the left and bright on the right end. When all stripes brighten simultaneously, humans report illusory motion to the right (see [Movie S1](#) available online). The contrast motion illusion is thought to rest on similar principles as another type of contrast illusion known as the single-field contrast asynchrony illusion (Shapiro et al., 2004): A single stripe is embedded in a dark or in a bright background. When an identical sinusoidal luminance change is applied to the stripe, humans report that the modulations are out of phase for the different background conditions ([Movie S2](#)). This indicates that humans perceive temporal variations of spatial contrast rather than luminance. Responses to such contrast stimuli cannot be explained by classical models of motion vision based on spatio-temporal correlation of luminance (Shapiro et al., 2005). Alternatively, it was hypothesized that rectified center-surround filters compute spatial contrast and further integrate such cues in higher visual centers. However, detailed systematic dissections of the computational mechanisms are missing, and very little is known about potential neuronal circuits involved.

In order to investigate visual processing at the cellular level, humans offer limited experimental access. In contrast, other species, such as the fruit fly *Drosophila melanogaster*, provide various tools for such a purpose. *Drosophila* has a set of innate and robust visual behaviors and can be genetically modified. The anatomy and connectivity of the visual system is well-known (Fischbach and Dittrich, 1989; Takemura et al., 2013) and is accessible via electrophysiology (Behnia et al., 2014; Joesch et al., 2008). The visual system is arranged in a retinotopic manner and forms several neuropils for visual processing ([Figure 1A](#)). Photoreceptor input from R1–R6 provides direct or indirect signals to lamina neurons L1–L5 ([Figures 1B and S1A](#)). Subsequently, L1/L5 and L2/L3/L4 form separate visual pathways specialized for motion computation of luminance increments (ON pathway) and decrements (OFF pathway), respectively (Clark et al., 2011; Eichner et al., 2011; Joesch et al., 2010; 2013; Maisak et al., 2013; Meier et al., 2014; Strother et al., 2014). Connectomics has revealed potential components of both pathways, namely Mi1 and Tm3 within the ON pathway and Tm1, Tm2, Tm4, and Tm9 within the OFF pathway (Shinomiya et al., 2014; Takemura et al., 2013). Neurons in the two pathways converge onto T4 and T5 neurons (Bausenwein et al., 1992), which are the first direction-selective elements in the fly visual system and which are selective for motion of

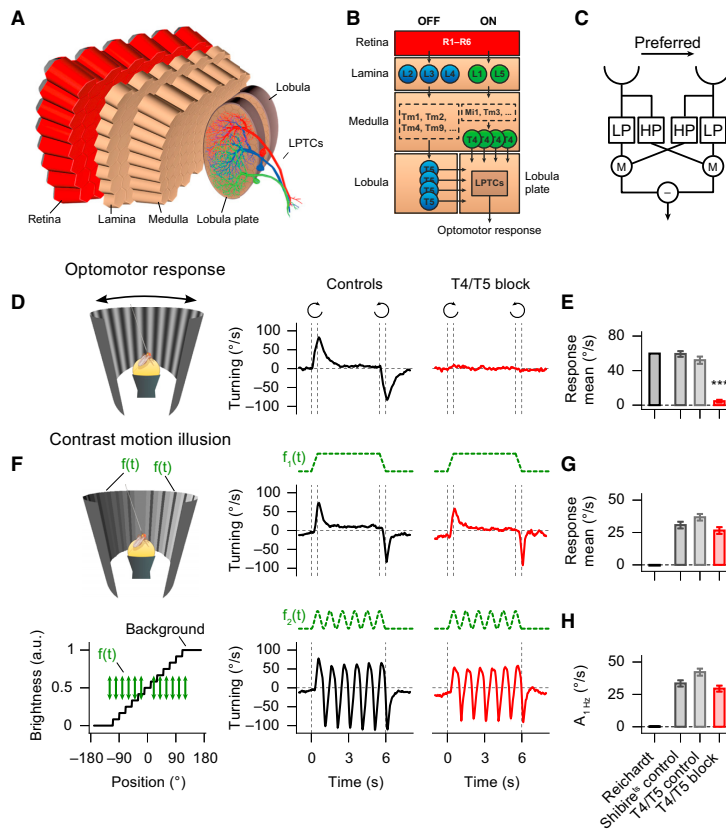


**Figure 1. Control and Motion-blind Flies Respond to Contrast Motion Illusions**

(A and B) Schematic of the fly's optic lobe and its cellular composition within the ON (green) and OFF (blue) pathways.

(C) Hassenstein-Reichardt detector with preferred direction to the right.

(D) Experiment with full-field moving sine-grating. Motion direction and stimulus on- and offset are illustrated by circular arrows and vertical dashed lines.

(E) Quantification of the optomotor response (response to clockwise motion minus that to counterclockwise motion divided by two; averaged between 0.1 and 1.1 s after stimulus onset) of the Hassenstein-Reichardt detector simulation and of the experimental groups.

(F) Contrast motion illusion. Several vertical stripes are embedded in a stepped luminance gradient background (black trace in bottom part) and simultaneously change luminance according to  $f_1(t)$  or  $f_2(t)$  (green arrows and green dashed time traces).

(G) Quantification of the response to the contrast motion illusion with stripe luminance dynamics according to  $f_1(t)$  (response to luminance increment minus that to luminance decrement divided by two; averaged between 0.1–1.1 s after stimulus onset) of the Hassenstein-Reichardt detector simulation and of the experimental groups.

(H) Quantification of the response for luminance dynamics according to  $f_2(t)$  (1 Hz amplitude of the Fourier-transformed response during stimulation) of the Hassenstein-Reichardt detector simulation and of the experimental groups.

Data represent mean  $\pm$  SEM with  $n = 12$ –13 flies per group.  $p$  values based on a two-sided Welch's  $t$  test, comparing T4/T5 block flies with both control groups (\*\* $p < 0.001$ ;  $p = 0.26$  in G;  $p = 0.25$  in H). Detailed statistics in Table S1A. Hassenstein-Reichardt detector simulation result in black, shibire<sup>ts</sup> flies in dark gray, T4/T5 control flies in light gray and T4/T5 block flies in (D) and (F) are pooled from both control groups.

brightness increments and decrements, respectively (Maisak et al., 2013). Mi1 and Tm3 have been proposed to provide temporally different and spatially offset inputs to the T4 dendrite, giving rise to its direction-selectivity (Behnia et al., 2014; Take-mura et al., 2013). Furthermore, Mi1 and Tm3 were recently shown to also be functionally involved in the computation of motion of brightness increments (Ammer et al., 2015). Eventually, T4 and T5 neurons converge onto lobula plate tangential cells (Figures S1B and S1C) and render vertical system cells and horizontal system cells direction-selective for motion along the vertical and horizontal axis, respectively. Genetic silencing of T4 and T5 neurons abolishes direction-selective responses in lobula plate tangential cells (Schneil et al., 2012). Moreover, in behavioral experiments, flies are motion-blind and no longer show an optomotor response (Bahl et al., 2013). Various aspects of fly motion vision can be modeled by the Hassenstein-Reichardt detector (Hassenstein and Reichardt, 1956). In this model, luminance signals from two neighboring ommatidia are differently filtered in time and subsequently multiplied. Subtracting the output of a mirror-symmetric detector subunit leads to fully

opponent direction-selective responses (Figure 1C). Computation of visual cues other than motion, such as color (Morante and Desplan, 2008) or spatial contrast, are less explored in flies.

In this paper, we employ contrast illusions as a tool to study spatial contrast computation in *Drosophila*. We use tethered flies walking on an air-suspended ball in a virtual environment. Throughout the paper, we measure fly turning speed in response to various kinds of visual stimuli, which allows quantitative comparisons of the behavior and systematic dissections of the underlying computational mechanisms. In order to identify neuronal correlates, we use the GAL4-UAS system (Brand and Perrimon, 1993) to genetically target specific subsets of neurons for silencing synaptic transmission via temperature-sensitive shibire (shibire<sup>ts</sup>) (Kitamoto, 2001; Pfeiffer et al., 2012).

**RESULTS**

**Flies Respond to Contrast Motion Illusions**

In a first set of control experiments, we tested behavioral performance to full-field sine-grating motion (Figure 1D). As expected,



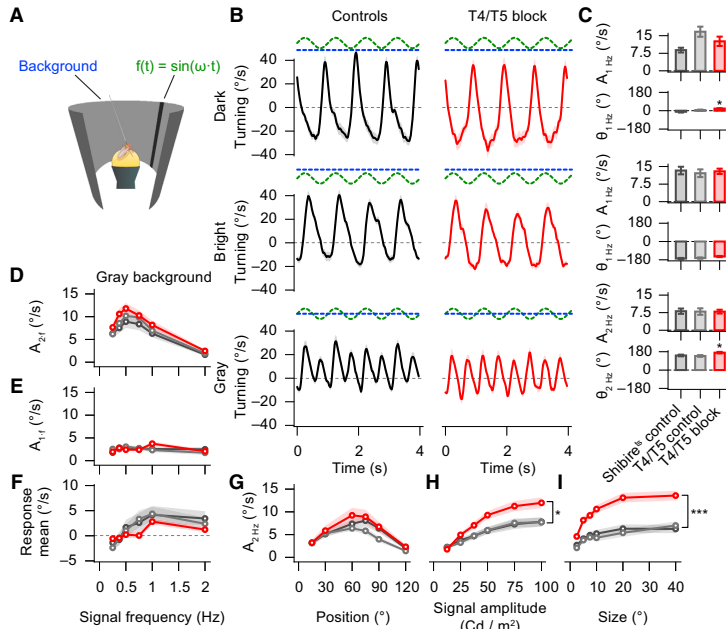


**Figure 2. Control and Motion-Blind Flies Respond to Single-Field Contrast Asynchrony Illusions**

(A) A single nonmoving vertical stripe on the right side of the fly flickers sinusoidally in luminance with frequency  $\omega$  on a uniform background. (B) Responses for 1 Hz stripe flicker (identical in all conditions; green dashed lines) on three different backgrounds (dark, bright, and gray; blue dashed lines). (C) Quantification of amplitude  $A$  and phase  $\Theta$  of the 1 Hz or 2 Hz response components. (D–F) Quantification of the response amplitudes (2- $f$  and 1- $f$  components) and the response mean to stripes flickering at different frequencies on a gray background. (G–I) Quantification of 2 Hz amplitude response components to a 1 Hz flickering stripe on a gray background when varying stripe position, signal amplitude, or size. All stimuli lasted for 10 s, the last 9 s were analyzed. Only the last 4 s are illustrated in (B). Data represent mean  $\pm$  SEM with  $n = 12$ –14 flies per group.  $p$  values based on a two-sided Welch’s  $t$  test, comparing T4/T5 block flies with both control groups ( $*p < 0.05$ ;  $***p < 0.001$ ;  $p = 0.18, 0.69,$  and  $0.99$  for response amplitudes for the different background conditions, respectively, and  $p = 0.10$  for response phase for the bright background in C). Detailed statistics in Table S1B. *Shibire<sup>ts</sup>* flies in dark gray, T4/T5 control flies in light gray, T4/T5 block flies in red. Raw time traces for control flies (black) in (B) are pooled from both control groups.

control flies responded with a robust optomotor response, a behavior predicted by the Hassenstein-Reichardt detector (Figures 1D and 1E). Next, we tested the contrast motion illusion as used in human psychophysics (Shapiro and Hamburger, 2007) (Figure 1F): several stripes are embedded in a stepped luminance gradient. We applied identical luminance dynamics to the stripes. The stimulus is designed such that luminance change is symmetric around the fly and, therefore, potential directed turning responses toward luminance change average out. Moreover, the local stripe environment is symmetric in luminance, and hence pairwise local comparisons, as performed by the Hassenstein-Reichardt detector, cancel out as well. We tested two luminance dynamics for the stripes: first, stripe luminance increased, remained bright for a few seconds, and then decreased again. Second, stripe luminance oscillated sinusoidally at 1 Hz. As expected, the Hassenstein-Reichardt detector predicted no turning response for both stimuli (Figures 1G and 1H). However, control flies robustly responded to the contrast motion illusion: when the background was dark on the left and bright on the right end, a luminance increase elicited turning to the right and a luminance decrease turning to the left. For the 1 Hz luminance oscillations, control flies responded with a robust 1 Hz oscillatory turning response. Notably, response strengths were similar to those observed for the optomotor response, and turning directions matched the direction of illusory motion reported by human observers (Shapiro and Hamburger, 2007).

Since the observed responses to the contrast motion illusion cannot be explained by the Hassenstein-Reichardt detector,

we developed two alternative hypotheses which could explain the result. First, the behavior might be a side effect of potentially unexplored interactions within the motion pathway. Second, it might be controlled by an independent visual pathway dedicated to the computation of spatial contrast. In order to test both hypotheses, we used a driver line which selectively labels T4 and T5 neurons, allowing us to silence synaptic transmission from these cells via *shibire<sup>ts</sup>*. T4/T5 block flies are completely motion-blind and lack an optomotor response (Bahl et al., 2013) (Figures 1D and 1E). Yet, when we tested the contrast motion illusion, such flies responded with exactly the same magnitude and direction as control flies (Figures 1F–1H). In conclusion, spatial contrast and motion computations seem to be carried out in parallel visual pathways.

**Flies Respond to Single-Field Contrast Asynchronies**

In order to gain a better understanding of the computational mechanisms underlying spatial contrast computation in the fly brain, we further investigated behavioral responses to another type of contrast illusion known as the single-field contrast asynchrony illusion (Shapiro et al., 2004). In particular, this stimulus allows us to investigate whether flies respond to signed or unsigned (absolute) spatial contrast, which is not possible with the global contrast motion illusion. We presented flies with a single vertical stripe in the right visual field and modulated the stripe luminance sinusoidally at 1 Hz (Figure 2A). Such a stimulus contains two components, flicker of luminance and flicker of relative spatial luminance (spatial contrast flicker). The luminance flicker

dynamics remain independent of background light levels but the spatial contrast flicker is background-dependent. To explore responses to spatial contrast flicker, we varied background light levels. When the stripe was presented against a dark background, control and T4/T5 block flies responded with 1 Hz turning speed oscillations of large amplitude with the same phase as the stimulus (Figures 2B and 2C). In contrast, when the stripe was presented against a bright background, control and T4/T5 block flies still responded with 1 Hz turning speed oscillations but responses were shifted in phase by 180°. Interestingly, an intermediate gray background led to 2 Hz turning speed oscillations, following the 2 Hz absolute spatial contrast dynamics of the flickering stripe. In summary, the observed behaviors rely on the computation of unsigned spatial contrast and are largely independent of T4 and T5 neurons, both in terms of amplitude and phase. These findings provide further evidence that spatial contrast computations are carried out in a T4/T5-independent visual circuit.

We further characterized the response oscillation amplitude to different parameters of a flickering stripe on a gray background (Figures 2D–2I). We first varied stimulus frequency. For all tested frequencies, control and T4/T5 block flies responded with turning speed oscillations of the frequency of the spatial contrast flicker (2-f component of the response), with the strongest response for 0.5 Hz signals (Figure 2D). The 1-f response component, corresponding to the luminance dynamics, however was small (Figure 2E) and response averages over time were close to zero (Figure 2F). The latter result is in contrast to previous findings which suggested that flickering stripes elicit strong directed turning toward the stimulus (Bahl et al., 2013; Pick, 1974). We further characterized responses as function of azimuthal position, signal amplitude, and size. For both control and T4/T5 block flies, responses were strongest for stripes located at ~70° (Figure 2G), became stronger with increasing signal amplitude (Figure 2H), and increased for stripe sizes up to 20°, after which the response saturated (Figure 2I).

The amount of luminance flicker increases with stripe size. Spatial contrast flicker however only occurs at the boundary of the flickering stripe and remains independent of size once the stripe exceeds the receptive field of the underlying neuronal elements. Interestingly, T4/T5 block flies responded stronger than control flies for large signal amplitudes and for large stripe sizes (Figures 2H and 2I). This suggests that luminance flicker, analyzed via T4/T5 cells, can reduce the responsiveness of the circuit performing spatial contrast computation.

#### Receptive Field Properties of Spatial Contrast Computation

In further experiments, we wanted to better characterize the spatial receptive field properties of the contrast response. To this end, we used counterphase flicker (Movie S3) which provide contrast flicker covering a large extent of the visual field. Such stimuli do not contain any net-motion and the average luminance in the area of stimulation remains constant. Hence, counterphase flicker allow characterization of the contrast system in isolation. We presented stimuli within a unilateral circular window on the right side of the fly and varied spatial frequency and orientation (Figure 3A).

As a control experiment, we first characterized responses to moving sine-gratings. As expected, control flies turned right and left for front-to-back and back-to-front motion, respectively, with comparable absolute amplitudes (Figure 3B). When we tested different spatial frequencies, motion responses in control flies decreased for high spatial frequencies and even inverted for spatial frequencies larger than 0.1 cycles per degree ( $\lambda = 10^\circ$ ) but no tuning was apparent for low spatial frequencies (Figures 3C and 3E). The response reduction and inversion for high spatial frequencies is due to the resolution of the *Drosophila* eye (~5°) (Götz, 1964). Next, we presented grating motion along different axes and quantified direction-selectivity (Figures 3D and 3E). As expected, control flies were able to discriminate motion direction well and did not respond with horizontal turning to motion along the vertical axis. Irrespective of spatial frequency or direction, T4/T5 block flies did not respond to any of the motion stimuli (Figures 3B–3E).

We next tested counterphase flicker. The luminance at each point was modulated at 1 Hz, resulting in a 2 Hz modulation of the absolute spatial contrast (Movie S3). If flies follow changes in absolute spatial contrast, they should respond with a 2 Hz oscillation in turning speed. Indeed, this was the case for both control and T4/T5 block flies (Figure 3F). Quantification of the response to different spatial frequencies revealed a clear tuning peak at a spatial frequency of 0.5 cycles per degree ( $\lambda = 20^\circ$ ) (Figures 3G and 3I). Such band-pass properties are reminiscent of a spatial antagonism involving center-surround receptive fields, which indicates that lateral inhibition is involved in the computation of spatial contrast. In order to characterize the receptive field isotropy of the contrast system, we quantified turning responses to differently oriented counterphase flicker (Figures 3H and 3I). We found that responses of control and T4/T5 block flies were strongly orientation-tuned. Interestingly, counterphase flicker along the vertical axis also elicited small responses and the orientation tuning curves were shifted by ~30°. This shift corresponds to a 30° backward-tilted pattern and is probably due to the position of the flies which walk slightly upward on the ball.

Responses to orientations perpendicular to the preferred orientation were almost zero for control flies but still present in T4/T5 block flies. It is known that counterphase flicker elicits depolarization in T4/T5 neurons (Maisak et al., 2013). T4 and T5 cells then target lobula plate tangential cells as well as lobula plate intrinsic inhibitory interneurons (Mauss et al., 2015). If the contrast and motion pathways converge in later processing stages, the latter cells might then actively suppress contrast responses along the vertical axis, improving counterphase flicker orientation tuning in control flies.

In summary, the observed spatial frequency and orientation tuning properties suggest a mechanism for contrast computation which involves lateral inhibition. T4 and T5 neurons are not required for such computations.

#### Identification of Neuronal Elements of Contrast Computation

Having found that unilateral counterphase flicker elicit robust contrast responses, we next used this stimulus to screen for neuronal elements underlying contrast computation. To maximize stimulus strength, we presented a vertically oriented sine-

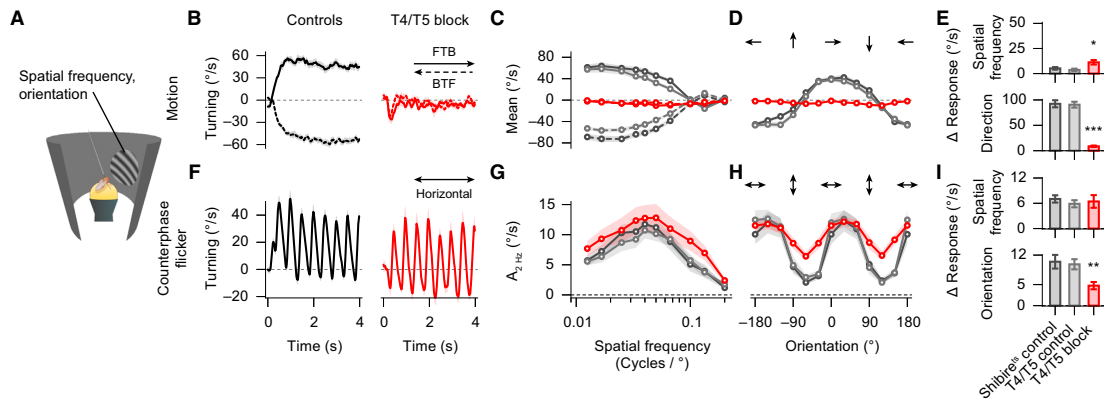


**Figure 3. Characterization of Receptive Field Properties of Motion and Contrast Systems**

(A) A circular window is shown on the right side of the fly in which a sine-grating moves or flickers in counterphase with different spatial frequencies or orientations. (B) Example traces for horizontal front-to-back motion (FTB; solid lines) and back-to-front motion (BTF; dashed lines).

(C and D) Spatial frequency and orientation tuning for motion.

(E) Quantification of spatial frequency tuning (difference between maximal absolute response and that for the smallest spatial frequency) and direction-selectivity (difference between maximal absolute response and that of motion in the opposite direction).

(F) Example traces for the counterphase flicker stimulus.

(G and H) Spatial frequency and orientation tuning curves of the 2 Hz response component.

(I) Quantification of spatial frequency tuning (difference between maximal absolute response and that for the smallest spatial frequency) and orientation tuning (difference between maximal absolute response and that for counterphase flicker in perpendicular orientation).

All stimuli lasted for 10 s, the last 9 s were analyzed, and the first 4 s are illustrated in (B) and (FF). Data represent mean  $\pm$  SEM with  $n = 12$ –14 flies per group.  $p$  values based on a two-sided Welch's  $t$  test, comparing T4/T5 block flies with both control groups (\* $p < 0.05$ ; \*\* $p < 0.01$ ; \*\*\* $p < 0.001$ ;  $p = 0.75$  for the spatial frequency tuning in I). Detailed statistics in Table S1C. Shibire<sup>ts</sup> flies in dark gray, T4/T5 control flies in light gray, T4/T5 block flies in red. Raw time traces for control flies (black) in (B) and (F) are pooled from both control groups.

grating in a rectangular window on the right side of the fly. The sine-grating either moved front-to-back or back-to-front along the horizontal axis with a temporal frequency of 1 Hz or it flickered in counterphase, providing a 2 Hz spatial contrast flicker (Figures 4A and 4B). As expected, control flies followed the direction of stimulus motion (Figure 4C) and responded robustly to counterphase flicker with strong 2 Hz oscillatory turning responses (Figure 4D), as previously described (Figures 3B and 3F). We tested ten different Gal4 driver lines, labeling cells in the lamina, medulla, and lobula (Figures S2A and S2B), and quantified optomotor behavior (Figure 4E) and responses to counterphase flicker (Figure 4F) for control and block flies. All flies had a comparable walking speed of around 1 cm/s (Figure S2D).

First, we tested the optomotor response in flies with silenced lamina neurons L1–L5. Surprisingly, we did not find response reductions when blocking L1 or L2. This can be attributed to the fact that the ON or OFF motion pathways receive redundant signals when stimulated with sine-grating motion (Joesch et al., 2010; Silles et al., 2013; Tuthill et al., 2013). Nevertheless, we found small but significant decreases when blocking L3 or L5 and an unexpected mild increase in the response when silencing L4. Next, we quantified responses to the counterphase flicker: Blocking output of L1 led to a strong reduction of the contrast response. Blocking L2, L3, or L5 however showed no significant phenotypes. Notably, silencing L4 almost doubled the response strength, suggesting that L4 not only modulates elements for

motion computation (Meier et al., 2014), but also affects the contrast computation circuit.

These experiments indicated that the ON pathway seems to be the key player for contrast computation. In order to test for its sufficiency, we next silenced the output of L2, L3, and L4 at the same time, abolishing all input channels into the OFF pathway. We did not find a reduction of the contrast response even though further analysis indicated that the triple lamina block is functional (Figure S3). This finding provides evidence that the ON pathway alone can compute spatial contrast.

We next tested medulla interneurons Mi1 and Tm3 which are known to be the major postsynaptic elements to L1 (Takemura et al., 2013). We first tested motion responses: Mi1 block flies showed a mild, but significant, optomotor response reduction. In contrast, using two different driver lines for Tm3, we found that silencing Tm3 output did not alter the response. Blocking the output of Mi1 and Tm3 together, using a driver line which labels both neuron types (revealed by stochastic GFP-labeling; Figures S2A and S2C), led to a strong response reduction of ~50% compared to controls. Because L1-silenced flies did not show such a phenotype, this finding suggests that further lamina input to Mi1 or Tm3 play a role in motion computation, such as L3 (Silles et al., 2013; Takemura et al., 2013). As expected, silencing T4 and T5 neurons abolished optomotor behavior completely (Figures 4C and 4E).

When testing counterphase flicker, Mi1-silenced flies showed a response reduction tendency, and blocking Tm3 output led to

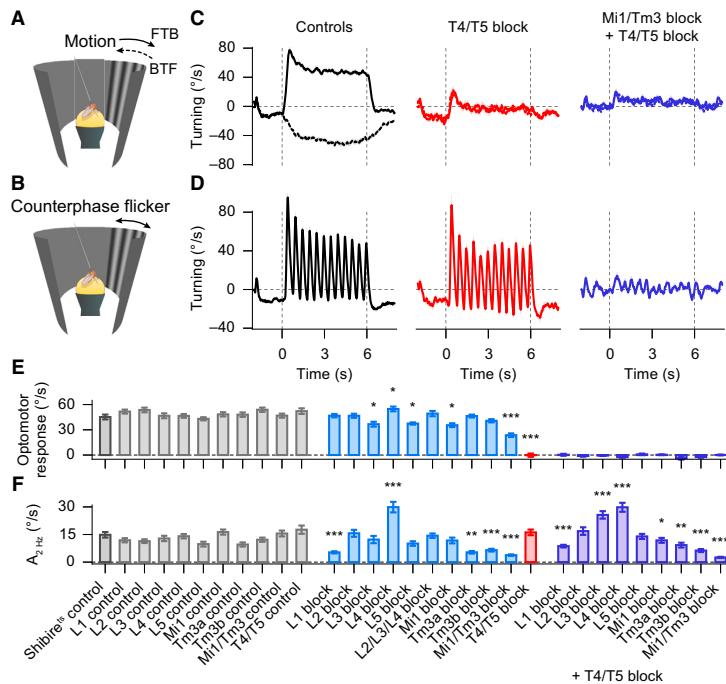


**Figure 4. Mi1 and Tm3 Neurons Are Key Neuronal Elements of Contrast Computation**

(A and B) A vertical oriented sine-grating either moves front-to-back (FTB), back-to-front (BTF; dashed lines), or flickers in counterphase in a rectangular window on the right side of the fly.

(C and D) Example traces of control, T4/T5 block, and combined Mi1/Tm3 block + T4/T5 block flies. Vertical gray dashed lines indicate onset and offset of the stimulus.

(E) Quantification of the optomotor response (response to front-to-back motion minus response to back-to-front motion divided by two; averaged from 2 to 6 s).

(F) Quantification of the response to counterphase flicker (2 Hz response amplitude component of the Fourier-transformed signal from 2 to 6 s).

Data represent mean  $\pm$  SEM with  $n = 14\text{--}19$  flies per group.  $p$  values based on a two-sided Welch's  $t$  test, comparing the group of block flies with respective control groups (for example, L1 block with L1 control and *shibire<sup>ts</sup>* control; groups with combined lamina or medulla block + T4/T5 block (right side) were compared only to the T4/T5 block group; \* $p < 0.05$ ; \*\* $p < 0.01$ ; \*\*\* $p < 0.001$ ). Detailed statistics in Tables S4 and S5. Expression patterns and list of genotypes in Figures S2A–S2C. *Shibire<sup>ts</sup>* control flies in dark gray, Gal4 control flies in light gray, lamina and medulla block flies in blue, T4/T5 block flies in red, and combined lamina or medulla block + T4/T5 block flies in violet. Raw time traces for control flies (black) in (C) and (D) are pooled from *shibire<sup>ts</sup>* control, T4/T5 control, and Mi1/Tm3 control flies. See Figures 1A, 1B, and S1A for schematics of cell types and locations.

a strong response reduction comparable to that found in L1-silenced flies. Since blocking Tm3 left some residual response intact, we tested the combined Mi1/Tm3 block flies and found that responses to counterphase flicker were almost completely abolished in these flies. Yet, when blocking T4/T5, contrast responses remained fully intact (Figures 4D and 4F), as found previously (Figures 3F–3I).

L1, Mi1, and Tm3 are part of the ON pathway for motion vision which converges onto T4 cells (Takemura et al., 2013). In order to determine whether these cells act directly on the contrast response or indirectly through T4, we repeated the screen in a T4/T5 block background. Moreover, working in such a simplified visual circuit makes it easier to interpret a particular phenotype when silencing neurons upstream to T4 and T5. As expected, the optomotor response remained abolished for flies in which lamina or medulla neurons were blocked in addition to T4 and T5 (Figure 4E). When analyzing responses to counterphase flicker, we found that blocking L1 led to a strong response reduction while silencing L3 or L4 increased the response strength, and blocking L2 or L5 did not have a significant effect (Figure 4F). Blocking Mi1 led to a small, but significant, response reduction and blocking Tm3 strongly reduced the response. We also combined the Mi1/Tm3 block with the T4/T5 block and found that such flies no longer responded at all to the counterphase flicker (Figures 4D and 4F). We conclude that medulla interneurons Mi1 and Tm3 act directly on the contrast response, and not via T4/T5, and that the response is modulated by L3 and L4.

Mi1 and Tm3 neurons are thought to provide temporally different and spatially offset signals to the dendrites of T4 neurons for computing motion direction of luminance increments (Behnia et al., 2014; Takemura et al., 2013). The optomotor response reduction we observed when Mi1 and Tm3 were jointly silenced is in agreement with previous findings (Ammer et al., 2015) which indicated an important role of these neurons in fly motion vision. Our data further suggest that Mi1 and Tm3 are also key elements for spatial contrast computation. In addition to targeting T4 neurons, Mi1 and Tm3 project onto yet unidentified neurons which function in parallel to T4 cells. In summary, thus, motion and contrast computations are carried out by shared neuronal circuit elements within the ON pathway and, subsequently, visual processing streams diverge.

**Mi1 and Tm3 Neurons Form a Center-Surround Antagonism**

We found that responses to counterphase flicker were spatial frequency-tuned, which suggested that the underlying neuronal system uses lateral inhibition for contrast computation (Figures 3G and 3I). Taking away lateral inhibition should decrease responses to intermediate spatial frequency but should increase the response strength to large spatial frequencies, in particular to homogeneous field flicker. Such a differential effect allows distinguishing lateral inhibition from localized inhibition as silencing a cell involved in localized inhibition should affect responses to all spatial frequencies equally. Our experiments

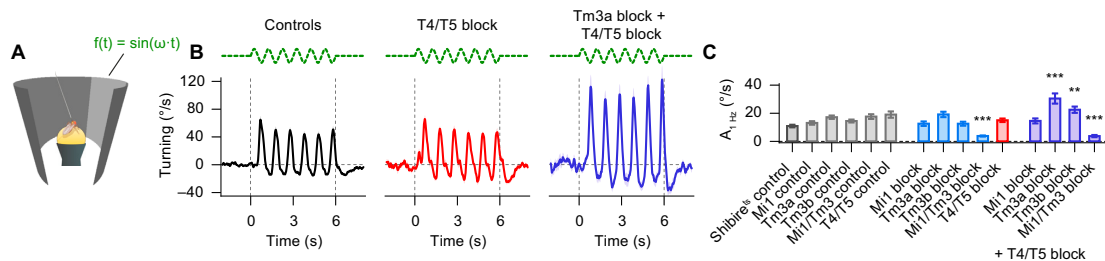


**Figure 5. Tm3 Cells Provide Lateral Inhibition**

(A) A large field sinusoidal 1 Hz luminance flicker (green dashed lines) on a gray background is presented on the right side.

(B) Example response traces for control, T4/T5 block and combined Tm3a block + T4/T5 block flies.

(C) Response quantification (1 Hz response amplitude component of the Fourier-transformed signal from 2 to 6 s).

Data represent mean  $\pm$  SEM with  $n = 14$ – $19$  flies per group.  $p$  values based on a two-sided Welch's  $t$  test, comparing the group of block flies with respective control groups (groups with combined lamina or medulla block + T4/T5 block were compared only to the T4/T5 block group; \*\* $p < 0.01$ ; \*\*\* $p < 0.001$ ). Detailed statistics in Table S1D. Shibire<sup>ts</sup> control flies in dark gray, Gal4 control flies in light gray, lamina and medulla block flies in blue, T4/T5 block flies in red, and combined lamina or medulla block + T4/T5 block flies in violet. Raw time traces for control flies (black) in (B) are pooled from shibire<sup>ts</sup> control, T4/T5 control, and Tm3a control flies. See Figures 1A, 1B, and S1A for schematics of cell types and locations.

show that silencing Mi1 or Tm3 leads to a reduced responsiveness to counterphase flicker of intermediate spatial frequency ( $\lambda = 20^\circ$ ; Figure 4F). To test for responses to large spatial frequency flicker, we presented flies with a wide 1 Hz homogeneously flickering region on the right side (Figure 5A). We observed that the turning speed of control and T4/T5 block flies followed the luminance dynamics of the stimulus: Flies turned right for luminance decrease and left for luminance increase (Figures 5B and 5C). Blocking Mi1 or Tm3, with intact T4 and T5, had no effect on the behavior, and silencing Mi1 in a T4/T5-blocked background did not change the behavior either. However, silencing Tm3 together with T4 and T5 cells almost doubled the response amplitude. In contrast, blocking Mi1 and Tm3 at the same time abolished responses to field flicker completely (Figure 5C). These findings, together with our previous silencing experiments (Figure 4F), suggest that Mi1 and Tm3 neurons form a center-surround antagonism for the computation of spatial contrast. In this arrangement, Tm3 cells provide lateral inhibition, not localized inhibition.

The fact that the Tm3 block phenotype was only visible when T4 and T5 neurons were additionally silenced suggests an interesting interplay between the motion and contrast circuit: Since Tm3 is connected to T4 (Takemura et al., 2013), Tm3 output likely modulates T4 responses to field flicker. In turn, T4 and T5 output can reduce the responsiveness of the contrast system using mechanisms discussed previously (Figures 2H, 2I, 3H, and 3I). Hence, silencing only Tm3 might show no phenotype in the response to field flicker because an increased flicker sensitivity in the contrast system is compensated by an increased flicker sensitivity in the motion system.

#### Contrast Illusions in Mi1/Tm3-Silenced Flies

Having identified Mi1 and Tm3 as the key players shaping response dynamics to counterphase and homogeneous field flicker (Figures 4 and 5), we wondered whether such flies also show deficits when presented with contrast illusions (Figures 1F–1H and 2). We first stimulated Mi1/Tm3-silenced flies with

full-field sine-grating motion and found a reduction of the optomotor response (Figures 6A and 6B). The effect was smaller compared to our previous findings (Figure 4E), since we used bilateral motion stimuli here, likely leading to a response saturation. When presenting the contrast motion illusion (Figure 1F) to Mi1/Tm3 block flies, turning responses were completely abolished (Figures 6C and 6D). This finding suggests that the contrast motion illusion is mediated by spatial contrast computations within the ON pathway. Subsequently, neurons postsynaptic to Mi1/Tm3 globally integrate these contrast cues and control behavior.

We also tested Mi1/Tm3 block flies with the single-field contrast asynchrony illusion (compare Figures 2A–2C, 6E, and 6F). The response amplitude to a flickering stripe on a dark background was not different to that of control flies. Yet, when the background was bright or gray, response amplitudes were strongly reduced (Figures 6E and 6F). Moreover, we compared response phases for the dark and bright background condition and found that responses were still in antiphase to one another. However, turning speed oscillations for the two background conditions were shifted in phase by  $\sim 90^\circ$  compared to controls. The same was true for Mi1/Tm3 block flies in a T4/T5 block background (Figure S4).

We also performed spatial frequency tuning experiments in Mi1/Tm3 block flies (Figures 6G and 6H). To our surprise, we found that for low spatial frequencies, control and Mi1/Tm3 block flies showed weak but identical responses to counterphase flicker. Only for intermediate spatial frequencies, control flies had a much stronger contrast response.

These experiments indicated that beside the Mi1/Tm3-dependent local spatial contrast system, another Mi1/Tm3-independent contrast system exists which operates on larger spatial scales, perhaps globally. To directly test this hypothesis, we slightly modified the single-field contrast asynchrony stimulus and now only varied the background luminance locally around the 1 Hz flickering stripe (Figure S5A). The rest of the arena was gray. Hence, the global light levels remain approximately

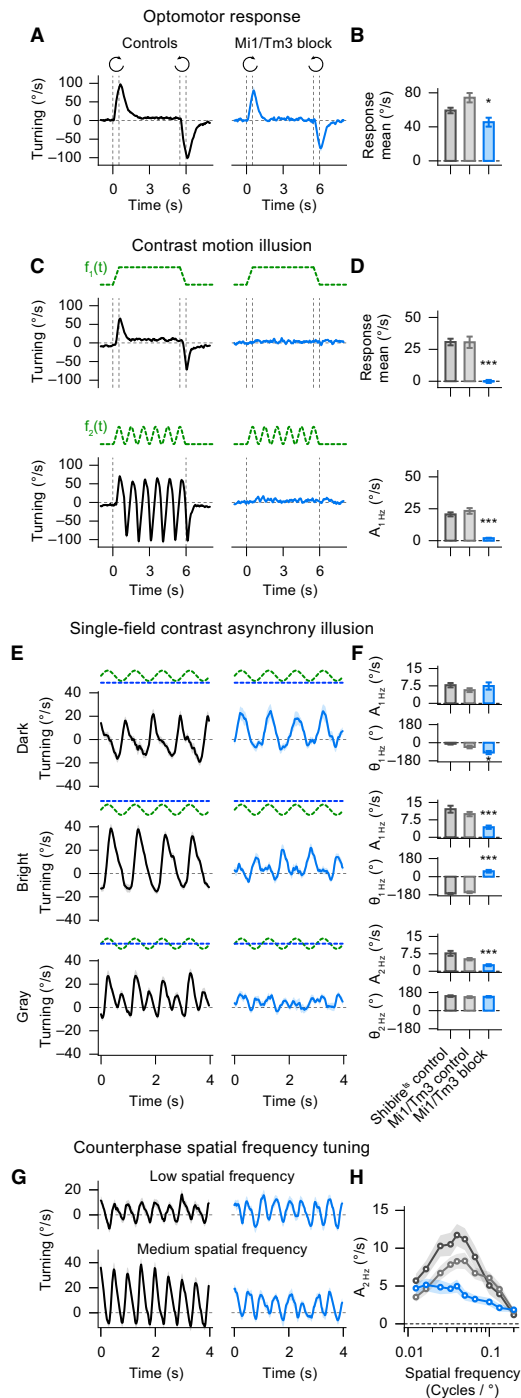


**Figure 6. Mi1/Tm3-Silenced Flies Lack Responses to Contrast Illusions**

(A and B) Responses of control and Mi1/Tm3 block flies to full-field sine-grating motion (= optomotor response) and quantification (see Figures 1D and 1E for comparison).

(C and D) Responses to contrast motion illusions with stripe luminance profiles  $f_1(t)$  and  $f_2(t)$  (green dashed lines) and quantification (see Figures 1F–1H for comparison).

(E and F) Responses to the single-field contrast asynchrony illusion and quantification (see Figures 2A–2C for comparison; green dashed lines represent the sinusoidal luminance modulation of the single vertical stripe, blue dashed lines represent background luminances dark, bright, and gray).

(G and H) Example traces for the counterphase flicker stimulus with low ( $\lambda = 80^\circ$ ) and intermediate ( $\lambda = 25^\circ$ ) spatial frequency and quantification of the 2 Hz response components.

Data represent mean  $\pm$  SEM with  $n = 12$ –13 flies per group.  $p$  values based on a two-sided Welch's  $t$  test, comparing Mi1/Tm3 block flies with both control groups ( $^*p < 0.001$ ;  $^{***}p < 0.001$ ;  $p = 0.85$  for the amplitude of the 1 Hz response component for the dark background condition, and  $p = 0.78$  for the phase of the 2 Hz response component for the gray background condition in F). Detailed statistics in Table S2A. Shibire<sup>ts</sup> flies in dark gray, Mi1/Tm3 control flies in light gray, Mi1/Tm3 block flies in blue. Raw time traces for control flies (black) in (A), (C), (E), and (G) are pooled from both control groups.

gray for any local background luminance. If a Mi1/Tm3-independent global contrast system exists, Mi1/Tm3 block flies should respond, independently of local background light levels, with a 2 Hz contrast response as the flickering stripe is compared to global gray background light levels. When we tested the new stimulus, control flies behaved as before (compare Figures 2B, 2C, S5B, and S5C), indicating that the local contrast system is the dominating one. Mi1/Tm3 block flies however responded with a weak 2 Hz response that was independent of local background luminance (Figure S5B–S5D), providing evidence for the existence of a global contrast system.

In summary, the observed residual turning responses in Mi1/Tm3-silenced flies (Figures 6E–6H) are likely mediated by another, weaker, subsystem which analyzes spatial contrast on a global scale.

**Output Elements of the Circuit for Spatial Contrast Computation**

Next, we wanted to identify the output elements of the contrast computation circuit. As neurons with major input from both Mi1 and Tm3, other than T4, have not yet been identified (Takemura et al., 2013), we could not proceed further with our strategy of characterizing circuit elements based on their behavioral phenotype when silenced. Since membrane depolarization in lobula plate tangential cells elicits an optomotor response (Haikala et al., 2013), we wondered whether the membrane voltage of these cells might also reflect the contrast responses we observed in the behavioral experiments. In order to test this hypothesis, we performed electrophysiological whole-cell patch clamp recordings from these neurons, stimulated flies with motion and counterphase flicker, and silenced synaptic output of either T4 and T5, or Mi1, Tm3, T4, and T5, as in the behavioral experiments.

When stimulated with motion along the vertical axis of a horizontally oriented sine-grating, lobula plate vertical system cells responded in a direction-selective manner (Figures 7A and 7B).

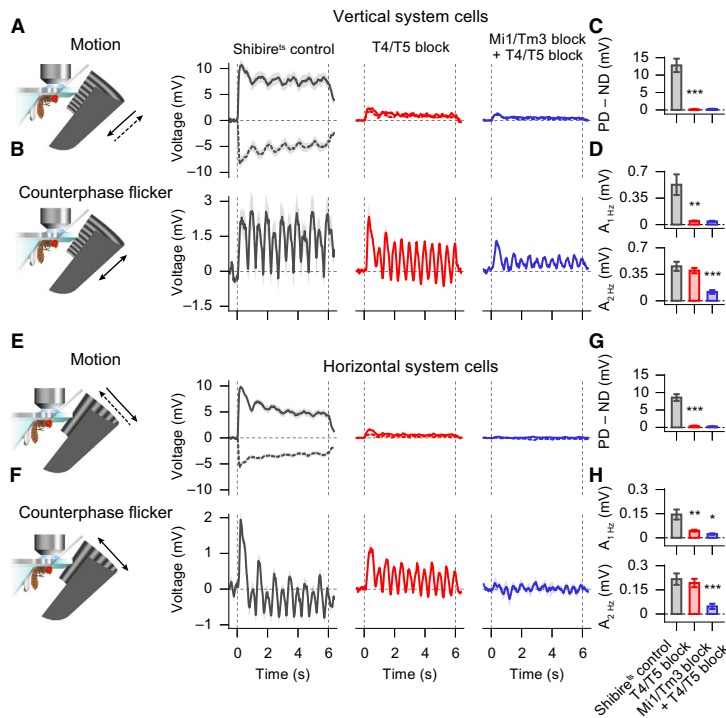


**Figure 7. Lobula Plate Tangential Cell Membrane Voltage Reflects Spatial Contrast Dynamics of Counterphase Flicker**

(A and B) Vertical system cell responses to a horizontally oriented sine-grating moving downward (PD, solid lines), upward (ND, dashed lines), or flickering in counterphase (2 Hz spatial contrast flicker).

(C and D) Quantification of the motion responses (mean of PD-ND) and of the 1 Hz and 2 Hz amplitude components of the Fourier-transformed responses to the counterphase flicker.

(E-H) Same as in (A)-(D), but for a vertically oriented sine-grating which moves along the horizontal axis or flickers in counterphase. Data represent mean  $\pm$  SEM with  $n = 4-11$  cells per group (of two to eight flies per group), analyzed from 1-6 s after stimulus onset.  $p$  values based on a two-sided Welch's  $t$  test, comparing shibire<sup>ts</sup> control flies with T4/T5 block flies and T4/T5 block flies with combined Mi1/Tm3 block + T4/T5 block flies ( $p < 0.05$ ;  $**p < 0.01$ ;  $***p < 0.001$ ;  $p = 0.42$  and  $p = 0.59$  for the amplitudes of the 2 Hz response component of the T4/T5 block in D and H, respectively). Detailed statistics in Table S2C. Shibire<sup>ts</sup> flies in dark gray, T4/T5 block flies in red, combined Mi1/Tm3 block + T4/T5 block flies in violet. See Figures 1A, 1B, and S1 for schematics of cell types and locations.

As expected from previous studies (Schnell et al., 2012), motion responses were completely abolished when blocking T4 and T5. Blocking Mi1 and Tm3 in addition did not change responses further. Next, we stimulated flies with counterphase flicker of the same orientation, providing 1 Hz local luminance flicker and 2 Hz spatial contrast flicker. We observed complex oscillatory voltage dynamics in control flies (Figure 7C) which contained both a 1 Hz and a 2 Hz component (Figure 7D). Hence, vertical system cells integrate both the 1 Hz luminance dynamics of counterphase flicker as well as its 2 Hz spatial contrast dynamics. When we tested T4/T5 block flies, the neurons' voltage dynamics were much simpler: While the 1 Hz component was completely abolished, the 2 Hz response component remained unchanged and when silencing Mi1/Tm3 together with T4/T5, the 2 Hz response component was strongly decreased as well. In further experiments, we also recorded from lobula plate horizontal system cells and presented sine-gratings with vertical orientation (Figure 7E). We obtained essentially the same results as we did in vertical system cells (Figures 7E-7H). Because no motion and contrast responses were detectable in flies with silenced Mi1, Tm3, T4, and T5, we also tested full-field flicker (Figure S6). In these flies, we still found robust voltage responses to such stimuli, indicating that even more visual processing pathways arrive at the lobula plate (Schnell et al., 2012) and that the recorded neurons were functionally intact.

From these experiments, we conclude that lobula plate tangential cells not only collect direction-selective input from

T4 and T5; they also receive signals from another, unidentified, visual pathway which computes spatial contrast. This pathway requires Mi1 and Tm3 to be functional and bypasses T4 and T5. Hence, spatial contrast and motion cues converge in the lobula plate where they shape visuomotor behavior together. Such interactions could also explain the smaller contrast responses in control flies compared to that of T4/T5 block flies which we observed in some of the behavioral experiments (Figures 2H, 2I, 3H, 3I, and 5C).

### Modeling

Our experiments revealed that contrast responses rely on the change of absolute spatial contrast. In particular, when spatial contrast decreases on the right side, flies turn right, when it increases, flies turn left (Figures 2 and 3). Based on these experimental findings, we developed a minimal computational model which could reproduce our results.

Spatial contrast can be computed by taking the difference between adjacent luminance values, i.e., by lateral inhibition,

$$S_{i,rel} = S_i - 0.5 \cdot (S_{i-1} + S_{i+1}),$$

where  $S_i$  describes signals of an ommatidium at location  $i$ . The change in absolute spatial contrast can then be described by a full-wave rectification followed by a high-pass filter:

$$R_i = -HP(\text{abs}(S_{i,rel})).$$

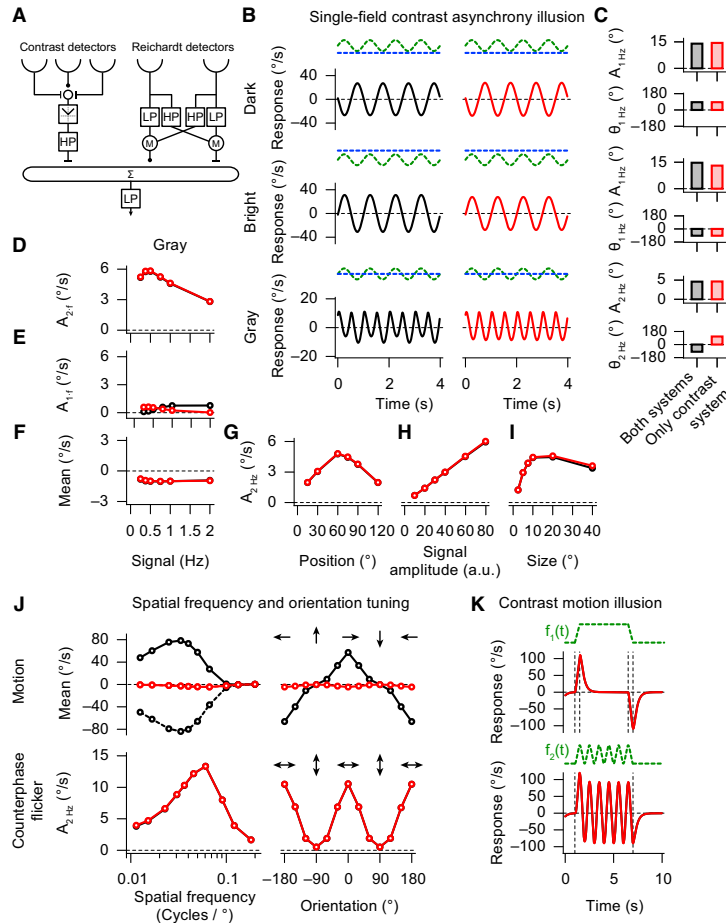


**Figure 8. A Simple Computational Model Reproduces Contrast Responses Observed in the Behavioral Experiments**

(A) Model structure of contrast detectors combined with Hassenstein-Reichardt detectors. We use an array of these detectors, weighted according to the function in Figure 2G. (B and C) Responses to the single-field contrast asynchrony illusion for different backgrounds (blue dashed lines) and quantification of amplitude  $A$  and phase  $\theta$  of the 1 Hz and 2 Hz response components (green dashed lines illustrate sinusoidal 1 Hz flicker of the vertical stripe). See Figures 2A–2C for comparison. (D–I) Responses as a function of stripe flicker frequency, position, signal amplitude, and size (Figure 2D–2I for comparison). (J) Variation of spatial frequency and orientation of a sine-grating which moves (upper part) or flickers in counterphase (bottom part) in a circular window on the right side. See Figure 3 for comparison. (K) Responses to the contrast motion illusion for vertical stripe luminance profiles  $f_1(t)$  and  $f_2(t)$ , as in Figures 1F–1H. Black and red traces are simulation results from the complete model (contrast + Hassenstein-Reichardt detectors; corresponds to control flies) and from a model in which motion responses were blocked (only contrast detector; corresponds to T4/T5 block flies), respectively.

the response oscillation were only slightly different compared to those measured experimentally (compare Figures 8C and 2C). Next, we varied the position, the signal amplitude, and the size of the flickering stripe on a gray background. As expected, the model reproduced the position dependency because positional weighting was an intrinsic component of the model construction. Moreover, the model showed a linear dependency on the signal amplitude (Figure 8H), which is expected from the model structure. Our model also reproduced the other experimental findings which were not used for its design. The model reproduced the shape of the size dependency and even predicted a small reduction for larger sizes under control conditions (compare Figures 8I and 2I). We also probed the spatial receptive field properties of the model (Figure 8J) and obtained very similar results as observed in our experiments (Figure 3). Finally, we presented the contrast motion illusion to our model (Figure 8K): The model faithfully reproduced both the direction and the amplitude of the response for both stripe luminance profiles as seen in our experiments (Figures 1F–1H). The negative arm of the Hassenstein-Reichardt detector was minimally weighted less than the positive arm (Eichner et al., 2011), which is the reason why simulated control flies have slightly different contrast responses to stripe flicker and counterphase flicker than simulated block flies.

In summary, using a single set of parameters, the simple model reproduced our experimental results astonishingly well,

This equation can be translated into a simple detector model diagram (Figure 8A). We modeled motion detectors as classical Hassenstein-Reichardt detectors (Hassenstein and Reichardt, 1956). The output of an array of both types of detectors was locally weighted and summated according to the position-dependent function found in our experiments (Figure 2G). A final low-pass filter mimicked the inertia of the motor system. We presented the model with exactly the same visual stimuli as used in the behavioral experiments. We then tested the model under two conditions, the complete model (both systems = simulating control flies) and the model without Hassenstein-Reichardt detectors (only contrast system = simulating T4/T5 block flies).

The model reproduced the antiphasic turning response oscillations for the flickering stripe under the dark and bright background conditions, respectively, as well as the frequency doubling when the background was gray (Figures 8B–8D). Moreover, we observed a small 1 Hz component in the response in the complete model (Figures 8B and 8E). The phase and the mean of



both qualitatively and quantitatively. We conclude that spatial contrast computation in the fly visual system is based on lateral inhibition followed by full-wave rectification and high-pass filtering. The resulting spatial contrast signals are then globally integrated in a similar fashion as local motion cues.

As our experimental findings indicate that Mi1 and Tm3 neurons are required for both spatial contrast computation and for motion vision (Figures 4 and 6), we also wanted to know to what extent a more detailed model, incorporating such a circuit overlap, can account for our results (Figure S7). The detailed model is based on separate pathways for brightness increments (ON pathway) and for brightness decrements (OFF pathway). Within each pathway, motion is computed by independent polarity-specific Hassenstein-Reichardt detectors (Eichner et al., 2011). We extended the ON pathway by a stage for the computation of absolute spatial contrast, as done in the less complex model (Figure 8). Simulation of the model under different conditions (control condition = full model; T4/T5 block = only the contrast system; Mi1/Tm3 block = only the OFF pathway) revealed a qualitative and quantitative match to most of our experimental data. This shows that overlapping circuitry in the ON pathway can account for spatial contrast computation as well as for motion computation.

As suggested by our experiments, apart from computing local spatial contrast, flies also have a system for the computation of spatial contrast on a global scale (Figures 6C–6H and S5). We incorporated such a system in our detailed model by taking signals from photoreceptors minus the global average luminance level followed by full-wave rectification and high-pass filtering (Figure S8). Interestingly, the model now reproduced the residual responses to the single-field contrast asynchrony illusion (compare Figures 6E and 6F with Figures S8B and S8C), the counterphase spatial frequency tuning experiment (compare Figures 6G, 6H, and S8J) and the lack of responses to the contrast motion illusion (compare Figures 6C, 6D, and S8K) under Mi1/Tm3 block conditions (only the OFF pathway and the system for global contrast computation intact). This close agreement between modeling and experiments provides further evidence that a Mi1/Tm3-independent contrast system operating on a larger spatial scale can account for the residual responses seen in Mi1/Tm3 block flies (Figure 6).

## DISCUSSION

In this paper, we studied contrast computation in *Drosophila*. We employed two types of contrast illusions, the contrast motion illusion and the single-field contrast asynchrony illusion, as a tool to explore the underlying circuit mechanisms. Testing the first type of illusion, we found that flies responded with a turning response along the direction of illusory motion as perceived by humans (Shapiro and Hamburger, 2007) (Figures 1F–1H). Moreover, when testing the second type of illusion, flies responded to the flickering spatial contrast rather than to its flickering luminance (Figure 2), a phenomenon which is also observed in human psychophysics (Shapiro et al., 2004). Genetic silencing of the essential elements of motion computation, T4 and T5, left responses to contrast stimuli largely unaffected. This suggested

that spatial contrast and motion computations are implemented in different visual pathways. Further behavioral analysis revealed that lateral inhibition is involved in the computation, resulting in spatial frequency and orientation tuning of contrast responses (Figure 3). Using counterphase flicker as a stimulus which elicits robust responses to spatial contrast change, we identified the lamina neuron L1 and its postsynaptic partners Mi1 and Tm3 to be essential for contrast computation (Figure 4D). Moreover, silencing the output of both Mi1 and Tm3 at the same time, completely abolished responses to the contrast motion illusion and reduced, or even inverted, responses to the single-field contrast asynchrony illusion (Figures 6C–6F). These results held also true when blocking T4 and T5 in combination with Mi1 and Tm3 (Figures 4D and S2).

Notably, connectomics (Takemura et al., 2013) and electrophysiological recordings (Behnia et al., 2014) revealed small receptive fields for Mi1 and larger receptive fields for Tm3. Both neuron types provide spatially offset and temporally different input to the T4 dendrite in order to shape its direction-selectivity (Behnia et al., 2014; Takemura et al., 2013). In agreement with previous silencing experiments (Ammer et al., 2015), our experiments provide further behavioral evidence for an important role of Mi1 and Tm3 in motion vision because Mi1/Tm3-silenced flies show a reduced optomotor response (Figures 4C, 6A, and 6B). We identified Tm3 to be important for lateral inhibition during contrast computation (Figure 5), but lateral inhibition is not apparent in electrophysiological recordings from Tm3 (Behnia et al., 2014). Hence, lateral inhibition ought to be further downstream. Taking these findings and our modeling results (Figure 8) into account, we suggest that Mi1 provides excitatory input and Tm3 surround inhibition to neurons other than T4 in order to compute spatial contrast. We speculate that a similar circuit motif might also be found on the T4 dendrite (Behnia et al., 2014; Takemura et al., 2013), forming the basis for orientation-selective responses described for these cells (Fisher et al., 2015; Maisak et al., 2013).

Using electrophysiological recordings, we found voltage oscillations in lobula plate tangential cells that correlate with the contrast dynamics of counterphase flicker (Figure 7). Blocking T4 and T5 cells left the response intact, but silencing additionally Mi1 and Tm3 neurons abolished the response. Hence, contrast cues converge on the level of the lobula plate, bypassing T4 and T5. Tm3 is known to synapse also in the lobula (Fischbach and Dittrich, 1989) (Figures S1A, S2A, and S2C), which could be the area where spatial contrast cues are integrated and then transmitted into the lobula plate.

Nevertheless, the identification of a membrane voltage representation of contrast computation does not necessarily imply that lobula plate tangential cells control the behavioral responses we observed. The responses to counterphase flicker might simply be a reflection of other, unidentified, neurons within the highly interconnected network of lobula plate tangential cells (Haag and Borst, 2001, 2002, 2004; Schnell et al., 2010). Moreover, the contrast system might provide signals to neurons in the lobula as well. In order to identify such elements, it will be required to explore further postsynaptic partners of Mi1 and Tm3, and probe the response properties of lobula plate neurons, after silencing such cells.

In conclusion, spatial contrast and motion computation in the fly brain share some of the neuronal circuit elements, pre- and postsynaptic to T4 cells. Such a circuit design suggests that computation of contrast provides important auxiliary signals which assist or further shape direction-selective responses in lobula plate tangential cells. Such cues could, for example, equilibrate motion responses to local variations of contrast, shape motion response to edges or bars (Bahl et al., 2013), improve orientation or spatial frequency tuning, or realize figure-ground discrimination (Egelhaaf, 1985). Our identification of the mechanisms and neuronal elements of spatial contrast computation opens the door for further behavioral, genetic, anatomical, and physiological dissections of these interactions and might help to elucidate the functional relevance of spatial contrast computation, and the associated contrast illusions, in flies and, perhaps, even humans.

#### EXPERIMENTAL PROCEDURES

Behavioral experiments were performed as described previously (Bahl et al., 2013). Briefly, tethered flies were walking on an air-suspended ball in a monitor-based virtual environment. Temperature was precisely controlled. In the electrophysiological experiments, control and block flies were heat-shocked for one hour before the experiments. The recording protocol was as described previously (Joesch et al., 2008). Immunostainings and stochastic flip-outs (Figures S2A and S2C) were performed as previously described (Nern et al., 2015; Yu et al., 2010). For statistical analysis, we use a two-sided Welch's t test throughout the paper. In order to average circular phase angles and to determine their variance, we applied circular operators. Statistical tests were performed between both genetic controls and block flies (*shibire*<sup>ts</sup> and Gal4 control versus block) and the larger p value determined significance:  $p^* < 0.05$ ,  $p^{**} < 0.01$ , and  $p^{***} < 0.001$ . For the simulations, we used movies of  $360 \times 180$  pixels at 60 Hz as model stimuli which were rendered from cylindrical projections of the same stimuli used in the experiments. Simulations were carried out according to the models shown in Figures 8A, S7A, and S8A. See Supplemental Experimental Procedures for detailed methods.

#### SUPPLEMENTAL INFORMATION

Supplemental Information includes eight figures, six tables, three movies, and Supplemental Experimental Procedures and can be found with this article at <http://dx.doi.org/10.1016/j.neuron.2015.11.004>.

#### AUTHOR CONTRIBUTIONS

A.Ba. and A.Bo. designed the study. E.S. and M.M. performed electrophysiological recordings. G.A. provided the Mi1, Tm3, and Mi1/Tm3-Gal4 lines and did the immunostainings. A.Ba. built the behavioral setup, programmed the visual stimuli, performed the behavioral experiments, and analyzed the data. A.Ba. wrote the paper with help from the other authors.

#### ACKNOWLEDGMENTS

We are grateful to Romina Kutlesa and Christian Theille for superb technical assistance with the behavioral experiments and fly work, and to Aljoscha Leonhardt for many valuable discussions. We also wish to thank Aljoscha Nern and Gerald M. Rubin for providing the T4/T5 split-Gal4 line and stochastic flippase, and Aljoscha Leonhardt, Alison Barker, Alexander Arenz, and Anna Schützenberger for critically reading the manuscript.

Received: April 13, 2015  
Revised: September 24, 2015  
Accepted: October 28, 2015  
Published: December 3, 2015

#### REFERENCES

- Adelson, E.H. (2000). Lightness perception and lightness illusions. In *The New Cognitive Neurosciences*, Second Edition, M. Gazzaniga, ed. (Cambridge, MA: MIT Press), pp. 339–351.
- Ammer, G., Leonhardt, A., Bahl, A., Dickson, B.J., and Borst, A. (2015). Functional specialization of neural input elements to the *Drosophila* ON motion detector. *Curr. Biol.* 25, 2247–2253.
- Bahl, A., Ammer, G., Schilling, T., and Borst, A. (2013). Object tracking in motion-blind flies. *Nat. Neurosci.* 16, 730–738.
- Bausenwein, B., Dittrich, A.P., and Fischbach, K.F. (1992). The optic lobe of *Drosophila melanogaster*. II. Sorting of retinotopic pathways in the medulla. *Cell Tissue Res.* 267, 17–28.
- Behnia, R., Clark, D.A., Carter, A.G., Clandinin, T.R., and Desplan, C. (2014). Processing properties of ON and OFF pathways for *Drosophila* motion detection. *Nature* 512, 427–430.
- Brand, A.H., and Perrimon, N. (1993). Targeted gene expression as a means of altering cell fates and generating dominant phenotypes. *Development* 118, 401–415.
- Bülthoff, H., and Götz, K.G. (1979). Analogous motion illusion in man and fly. *Nature* 278, 636–638.
- Clark, D.A., Bursztyn, L., Horowitz, M.A., Schnitzer, M.J., and Clandinin, T.R. (2011). Defining the computational structure of the motion detector in *Drosophila*. *Neuron* 70, 1165–1177.
- Egelhaaf, M. (1985). On the neuronal basis of figure-ground discrimination by relative motion in the visual system of the fly. I. Behavioural constraints imposed on the neuronal network and the role of the optomotor system. *Biol. Cybern.* 52, 123–140.
- Eichner, H., Joesch, M., Schnell, B., Reiff, D.F., and Borst, A. (2011). Internal structure of the fly elementary motion detector. *Neuron* 70, 1155–1164.
- Fischbach, K.F., and Dittrich, A. (1989). The optic lobe of *Drosophila melanogaster*. I. A Golgi analysis of wild-type structure. *Cell Tissue Res.* 258, 441–475.
- Fisher, Y.E., Silies, M., and Clandinin, T.R. (2015). Orientation selectivity sharpens motion detection in *Drosophila*. *Neuron* 88, 390–402.
- Götz, K.G. (1964). Optomotorische Untersuchung des visuellen Systems einiger Augenmutanten der Fruchtfliege *Drosophila*. *Kybernetik* 2, 77–92.
- Haag, J., and Borst, A. (2001). Recurrent network interactions underlying flow-field selectivity of visual interneurons. *J. Neurosci.* 21, 5685–5692.
- Haag, J., and Borst, A. (2002). Dendro-dendritic interactions between motion-sensitive large-field neurons in the fly. *J. Neurosci.* 22, 3227–3233.
- Haag, J., and Borst, A. (2004). Neural mechanism underlying complex receptive field properties of motion-sensitive interneurons. *Nat. Neurosci.* 7, 628–634.
- Haikala, V., Joesch, M., Borst, A., and Mauss, A.S. (2013). Optogenetic control of fly optomotor responses. *J. Neurosci.* 33, 13927–13934.
- Hassenstein, B., and Reichardt, W. (1956). Systemtheoretische Analyse der Zeit, Reihenfolgen und Vorzeichenbewertung bei der Bewegungserkennung des Rüsselkäfers *Chlorophanus*. *Z. Naturforsch. B* 11, 513–524.
- Joesch, M., Plett, J., Borst, A., and Reiff, D.F. (2008). Response properties of motion-sensitive visual interneurons in the lobula plate of *Drosophila melanogaster*. *Curr. Biol.* 18, 368–374.
- Joesch, M., Schnell, B., Raghu, S.V., Reiff, D.F., and Borst, A. (2010). ON and OFF pathways in *Drosophila* motion vision. *Nature* 468, 300–304.
- Joesch, M., Weber, F., Eichner, H., and Borst, A. (2013). Functional specialization of parallel motion detection circuits in the fly. *J. Neurosci.* 33, 902–905.
- Kitamoto, T. (2001). Conditional modification of behavior in *Drosophila* by targeted expression of a temperature-sensitive *shibire* allele in defined neurons. *J. Neurobiol.* 47, 81–92.
- Maisak, M.S., Haag, J., Ammer, G., Serbe, E., Meier, M., Leonhardt, A., Schilling, T., Bahl, A., Rubin, G.M., Nern, A., et al. (2013). A directional tuning map of *Drosophila* elementary motion detectors. *Nature* 500, 212–216.

- Mauss, A.S., Pankova, K., Arenz, A., Nern, A., Rubin, G.M., and Borst, A. (2015). Neural circuit to integrate opposing motions in the visual field. *Cell* 162, 351–362.
- Meier, M., Serbe, E., Maisak, M.S., Haag, J., Dickson, B.J., and Borst, A. (2014). Neural circuit components of the *Drosophila* OFF motion vision pathway. *Curr. Biol.* 24, 385–392.
- Morante, J., and Desplan, C. (2008). The color-vision circuit in the medulla of *Drosophila*. *Curr. Biol.* 18, 553–565.
- Nern, A., Pfeiffer, B.D., and Rubin, G.M. (2015). Optimized tools for multicolor stochastic labeling reveal diverse stereotyped cell arrangements in the fly visual system. *Proc. Natl. Acad. Sci. USA* 112, E2967–E2976.
- Pfeiffer, B.D., Truman, J.W., and Rubin, G.M. (2012). Using translational enhancers to increase transgene expression in *Drosophila*. *Proc. Natl. Acad. Sci. USA* 109, 6626–6631.
- Pick, B. (1974). Visual flicker induces orientation behaviour in the fly *Musca*. *Z. Naturforsch. C* 29, 310–312.
- Schnell, B., Joesch, M., Forstner, F., Raghu, S.V., Otsuna, H., Ito, K., Borst, A., and Reiff, D.F. (2010). Processing of horizontal optic flow in three visual interneurons of the *Drosophila* brain. *J. Neurophysiol.* 103, 1646–1657.
- Schnell, B., Raghu, S.V., Nern, A., and Borst, A. (2012). Columnar cells necessary for motion responses of wide-field visual interneurons in *Drosophila*. *J. Comp. Physiol. A Neuroethol. Sens. Neural Behav. Physiol.* 198, 389–395.
- Shapiro, A.G., and Hamburger, K. (2007). Last but not least. *Perception* 36, 1104–1107.
- Shapiro, A.G., D'Antona, A.D., Charles, J.P., Belano, L.A., Smith, J.B., and Shear-Heyman, M. (2004). Induced contrast asynchronies. *J. Vis.* 4, 459–468.
- Shapiro, A.G., Charles, J.P., and Shear-Heyman, M. (2005). Visual illusions based on single-field contrast asynchronies. *J. Vis.* 5, 764–782.
- Shinomiya, K., Karuppururai, T., Lin, T.-Y., Lu, Z., Lee, C.-H., and Meinertzhagen, I.A. (2014). Candidate neural substrates for off-edge motion detection in *Drosophila*. *Curr. Biol.* 24, 1062–1070.
- Silies, M., Gohl, D.M., Fisher, Y.E., Freifeld, L., Clark, D.A., and Clandinin, T.R. (2013). Modular use of peripheral input channels tunes motion-detecting circuitry. *Neuron* 79, 111–127.
- Strother, J.A., Nern, A., and Reiser, M.B. (2014). Direct observation of ON and OFF pathways in the *Drosophila* visual system. *Curr. Biol.* 24, 976–983.
- Takemura, S.-Y., Bharioke, A., Lu, Z., Nern, A., Vitaladevuni, S., Rivlin, P.K., Katz, W.T., Olbris, D.J., Plaza, S.M., Winston, P., et al. (2013). A visual motion detection circuit suggested by *Drosophila* connectomics. *Nature* 500, 175–181.
- Tuthill, J.C., Chiappe, M.E., and Reiser, M.B. (2011). Neural correlates of illusory motion perception in *Drosophila*. *Proc. Natl. Acad. Sci. USA* 108, 9685–9690.
- Tuthill, J.C., Nern, A., Holtz, S.L., Rubin, G.M., and Reiser, M.B. (2013). Contributions of the 12 neuron classes in the fly lamina to motion vision. *Neuron* 79, 128–140.
- Yu, J.Y., Kanai, M.I., Demir, E., Jefferis, G.S.X.E., and Dickson, B.J. (2010). Cellular organization of the neural circuit that drives *Drosophila* courtship behavior. *Curr. Biol.* 20, 1602–1614.

Neuron, Volume 88

**Supplemental Information**

**Neural Mechanisms for *Drosophila* Contrast Vision**

Armin Bahl, Etienne Serbe, Matthias Meier, Georg Ammer, and Alexander Borst

## SUPPLEMENTAL EXPERIMENTAL PROCEDURES

### FLIES

Flies were raised on standard cornmeal-agar medium on a 12h light/12h dark cycle and 60% humidity for the entire period of development. For the first seven days of development, flies were kept at 25 °C and then transferred to 18 °C. In experiments, we only used female flies aged ~1 day. We used the following driver lines: L1-splitGal4 (OK371-AD, ort-C1-3-DBD), L2-Gal4 (21D), L3-Gal4 (VT40568), L4-Gal4 (VT40547), L5-splitGal4 (R21A05-AD; R31H09-DBD), Mi1-Gal4 (VT7747), Tm3a-Gal4 (R12C11), Tm3b-Gal4 (R13E12), Mi1/Tm3-Gal4 (VT0465), T4/T5-splitGal4 (R59E08-AD; R42F06-DBD), T4/T5-Gal4 (R42F06). These lines were either crossed to wild type Canton S flies or to 20xUAS-shibire<sup>ts</sup> flies (Pfeiffer et al., 2012), resulting in the genotypes presented in Figure S2B.

### ELECTROPHYSIOLOGY

The glial sheet was digested locally by application of a stream of 0.5 mg/ml collagenase IV (GIBCO) through a cleaning micropipette (5 µm opening) under polarized light contrast. Then, somata of lobula plate tangential cells were whole-cell patched. We identified vertical and horizontal system cells based on their directional tuning properties (control flies), cell body location and resting membrane potential (block flies). For visual stimulation, we used a LED arena covering ±90° in azimuth and ±48° in elevation. Patterns had a spatial wavelength of  $\lambda = 22.5^\circ$  and 100% contrast (maximal luminance 75 cd/m<sup>2</sup>). Recordings were performed at 2 kHz, the signal was then downsampled to 50 Hz and 2–4 trials were averaged per cell. Further analysis was performed as in the behavioral experiments.

### IMMUNOHISTOCHEMISTRY

Primary antibodies used were rabbit polyclonal anti-GFP (1:2000, Torri Pines) and mouse anti-nc82 (1:25, Developmental Studies Hybridoma Bank). We used the following secondary antibodies: goat anti-rabbit Alexa-488 and goat anti-mouse Alexa-633 (both 1:500, Invitrogen). Brains were mounted in Vectashield (Vectalabs) and optically sectioned in the horizontal plane with a Leica SP5 confocal microscope. For documentation, single sections were processed in ImageJ 1.46r (NIH). For stochastic labeling of cells in the VT0465-Gal4 line, we used a weak flippase which sparsely removes an FRT-flanked stop cassette and thereby allows Gal4-driven expression of a GFP reporter (Nem et al., 2015).

### BEHAVIORAL EXPERIMENTS

We used six independent setups (almost identical to those presented in Bahl et al. 2013) for visual stimulation and to record fly locomotion. All monitors were equilibrated in brightness and contrast. We applied the same temperature protocol in all behavioral experiments: Temperature was kept at 25 °C for the first 5 min and then, within 10 min, raised to 34 °C. The sine-grating in Figure 1D had a spatial wavelength of  $\lambda = 20^\circ$ , 60% contrast and moved at a velocity of 20 °/s. In the contrast motion illusion, we used a stepped gradient background (20° wide steps) ranging from luminance 0–100 cd/m<sup>2</sup>. Twelve 5° wide vertical stripes were superimposed within the centers of the background steps. The luminance of these stripes varied from 9–45 cd/m<sup>2</sup> according to the functions illustrated in Figure 1F. In Figures 2A–F and 6E–F, we used a single 10° wide vertical stripe located at 70° in azimuth. The luminance of the stripe varied sinusoidally (1 Hz) from 4–57 cd/m<sup>2</sup>. In Figure 2G–I, only the illustrated parameters were varied, the other parameters were as in Figure 2B (gray background) but in Figure 2I, the stripe was centered at 80° in azimuth. The uniformly dark, bright, and gray backgrounds had luminances of 1.3, 27, and 86 cd/m<sup>2</sup>, respectively. The sine pattern in Figures 3 and 6G,H had a contrast of 60%. Stimuli were shown in a circular window (radius = 40°) positioned at 90° in azimuth and 0° in elevation. Stimuli in Figure 4 were shown within a 70° wide rectangular window located at 90° in azimuth and full elevation. The sine-grating had a spatial wavelength of  $\lambda = 20^\circ$  and 60% contrast. Field flicker (Figure 5) was shown within the same window and varied from 4–57 cd/m<sup>2</sup> in luminance. The rest of the visual field for stimuli in Figures 3, 4 and 5 was gray (27 cd/m<sup>2</sup>). The size of the local background around the flickering stripe in Figure S5 was 30°, the rest of the arena was gray (27 cd/m<sup>2</sup>). Otherwise the stimulus was as in Figure 2A. The spatial phase of all sine-gratings (Figures 1A, 3, 4,

6A) was chosen randomly before each trial. In all behavioral experiments, we additionally presented exact mirror-symmetrical versions of the stimuli.

For each experiment, fly locomotion was sampled for ~90 min at 4 kHz and data was subsequently downsampled to 50 Hz. We then picked a trial range during which the average walking speed in each trial was above 0.5 cm/s. Trials were then averaged. Experiments not having at least 9 of such trials were discarded. Further, responses to all stimuli and to their mirror-symmetrical versions were subtracted from another and divided by two, which removed potential turning biases and improved data quality. Finally, we applied a first order low-pass filter ( $\tau = 40$  ms). The resulting data was then analyzed by averaging or via Fourier transform within a specific time range. In the Fourier-transformed signal, we picked the frequency of interest and calculated its amplitude and phase. For each stimulus, we then averaged these values and calculated the standard error of the mean (s.e.m.) over flies.

### STATISTICS

The Welch's t-test is a variant of Student's t-test and does not require equal variances ([https://en.wikipedia.org/wiki/Welch%27s\\_t\\_test](https://en.wikipedia.org/wiki/Welch%27s_t_test)). T-values were calculated as

$$t = \frac{\bar{X}_1 - \bar{X}_2}{\sqrt{\frac{s_1^2}{N_1} + \frac{s_2^2}{N_2}}},$$

where  $\bar{X}_i$ ,  $s_i^2$  and  $N_i$  are population mean, variance, and size of group  $i$ , respectively. We used the Welch-Satterthwaite equation to calculate degrees of freedom:

$$df = \frac{\left(\frac{s_1^2}{N_1} + \frac{s_2^2}{N_2}\right)^2}{\frac{s_1^4}{N_1^2 \cdot (N_1 - 1)} + \frac{s_2^4}{N_2^2 \cdot (N_2 - 1)}}.$$

In order to work with circular variables (response phases), we used the following circular operators to calculate mean ( $\bar{\alpha}$ ) and variance ( $s_\alpha^2$ ) of the values:

$$\bar{\alpha} = \arg \left( \sum_{j=1}^N \exp(i \cdot \alpha_j) \right),$$

$$s_\alpha^2 = -2 \cdot \log \left( \frac{1}{N} \cdot \left| \sum_{j=1}^N \exp(i \cdot \alpha_j) \right| \right).$$

To obtain the numerator in the Welch's t test, we determined the smallest difference of angular means:

$$(\bar{\alpha}_1 - \bar{\alpha}_2 + \pi) \text{ modulo } 2\pi - \pi.$$

### MODELING

In the first step, frames were spatially convolved with a 2D Gaussian kernel of isotropic  $\sigma = 1.75^\circ$  and then fed into an array of  $90 \times 45$   $4^\circ$ -spaced input elements. For input elements on the left visual hemisphere, the Hassenstein-Reichardt detector had a mirror-symmetrical structure. All filters in the input stage had the same time constants of  $\tau = 100$  ms. Lateral inhibition in the contrast detector along the horizontal axis was calculated as

$$R_i = S_i - 0.5 \cdot (S_{i-1} + S_{i+1}),$$

where  $S_i$  is the central input element. Output weighting of the contrast detector was 20, of the positive arm of the Hassenstein-Reichardt detector 0.15 and of the negative arm 0.147. Output of all detectors was then summated according to the weighting function

$$w(x) = \exp\left(-\frac{x^2}{2 \cdot 60^2}\right) - 0.9 \cdot \exp\left(-\frac{x^2}{2 \cdot 40^2}\right),$$

approximating the function in Figure 2G, and values along the y-axis were summated. For simplicity, all motion and contrast detectors were weighted with the same function, as done in previous modeling studies (Bahl et al., 2013). In the left visual hemisphere, output signals were multiplied by  $-1$ . The resulting signal was then low-pass filtered ( $\tau = 300$  ms). All filters were of first-order and implemented according to [https://en.wikipedia.org/wiki/Low-pass\\_filter](https://en.wikipedia.org/wiki/Low-pass_filter) and [https://en.wikipedia.org/wiki/High-pass\\_filter](https://en.wikipedia.org/wiki/High-pass_filter), respectively. The high-pass filter in the input stage take away signal means completely and, for example, reduce a sinusoidal 1 Hz input signal to 50 % in amplitude and produce a phase shift of around  $0.3 \cdot \pi$ .

In the detailed models (Figures S7 and S8), the DC component was 40% of the photoreceptor signal and the half-wave rectification in the OFF pathway was shifted by +80. The weight for the spatial contrast detector in the ON pathway was 30, for the positive and negative arms of the Hassenstein-Reichardt detectors 0.1 and 0.098, respectively. The output weight of the global contrast system was either 0 (Figure S7) or 2 (Figure S8). All other parameter were as in the less complex model.

The output weights, the DC component and the shift in the OFF rectification (only in the detailed models) were the only free model parameters and were adjusted by hand. Time constants were approximately the same as in previous modeling studies (Eichner et al., 2011) and were not optimized.

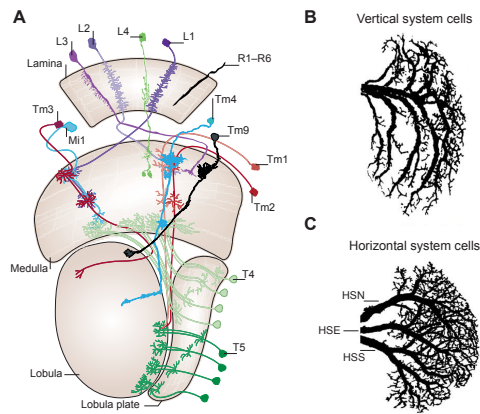


**Figure S1, related to Figure 1. Cellular Schematic of the Fly Optic Lobe and Morphology of Lobula Plate Tangential Cells**

(A) Cellular schematic of the fly optic lobe. See corresponding abstract schematic in Figure 1A,B for comparison. (B,C) Anatomy of five of the six vertical system cells and of the three horizontal system cells in *Drosophila*. Both cell types reside in the lobula plate and receive input from T4 and T5 neurons. The scheme in (A) was modified from Borst, 2014. The images of lobula plate tangential cells in (B,C) are taken from Rajashekhar and Shamprasad, 2004. Cell sizes not to scale.



# Neural Mechanisms for *Drosophila* Contrast Vision

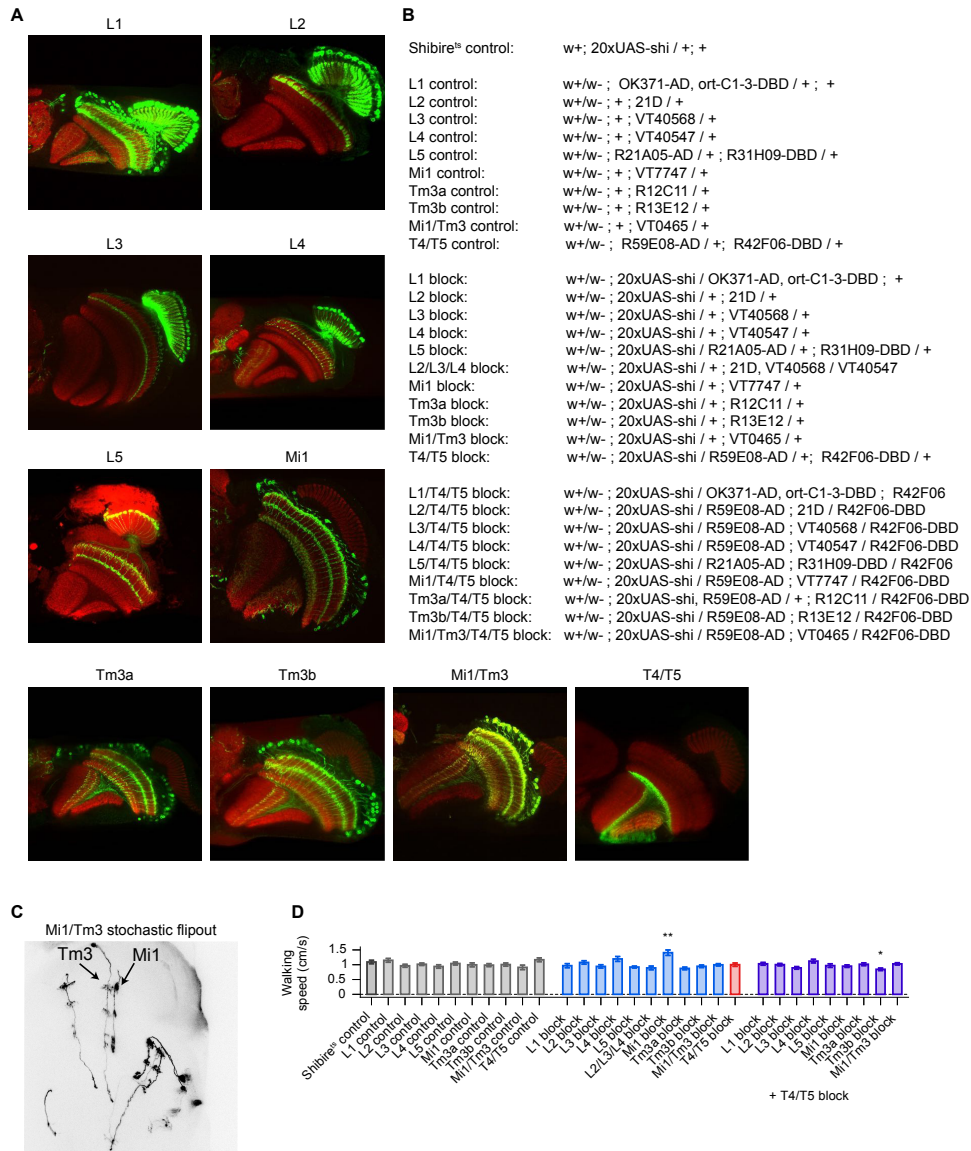


**Figure S2, related to Figures 4, 5, S3, and S4. Expression Patterns, Genotypes, and Walking Speed**

(A) GFP expression pattern of GAL4 driver lines. Horizontal sections of the optic lobe. (B) Genotypes used in the experiments. (C) Stochastic GFP labeling of neurons in the VT0465 Gal4 line. Flipouts of several Mi1 and Tm3 cells are distinguishable. In addition to these cells, we occasionally found weak expression in unidentified Mi and Dm cells. (D) Walking speed (averaged over same trial range as used for quantification of turning speeds and over all stimuli). Data represent mean  $\pm$  s.e.m with  $n = 14-19$  flies per group. P-values based on a two-sided Welch's t test, comparing the group of block flies with respective control groups (for example, L1 block with L1 control and shibire<sup>ts</sup> control; groups with combined lamina or medulla block + T4/T5 block (right side) were compared only to the T4/T5 block group;  $P^* < 0.05$ ;  $P^{**} < 0.01$ ). Detailed statistics in Table S6. Shibire<sup>ts</sup> control flies in dark gray, Gal4 control flies in light gray, lamina and medulla block flies in blue, T4/T5 block flies in red, and combined lamina or medulla block + T4/T5 block flies in violet.

## Neural Mechanisms for *Drosophila* Contrast Vision

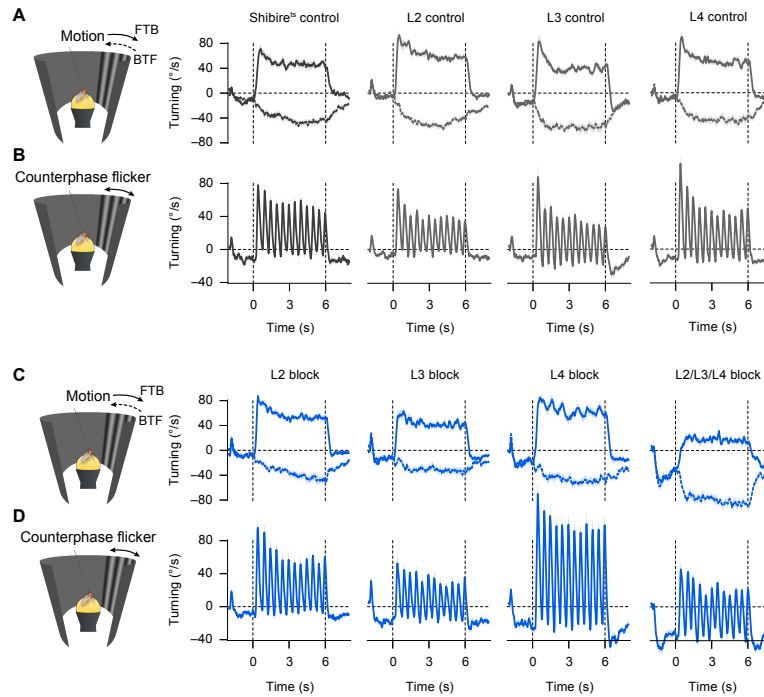


**Figure S3, related to Figure 4. Raw Time Traces for OFF Pathway Lamina Blocks**

(A,B) Responses of control flies to motion and counterphase flicker. (C,D) Responses of L2, L3, L4 and combined L2/L3/L4 block flies to motion and counterphase flicker. L2/L3/L4 block flies strongly turn away from stationary patterns ( $\approx 40$  °/s). For motion and counterphase flicker, all responses were shifted to negative values. This effect was not found in any of the controls or in any of the flies where L2, L3, or L4 cells were blocked independently. Even though we do not understand these dynamics, it shows that the triple lamina block works. For quantification, we calculated the optomotor response by subtracting front-to-back and back-to-front motion responses and by determining the 2 Hz response amplitude to counterphase flicker. Hence, a shift of the traces to negative values is not seen in the quantification in Figure 4E,F. Vertical gray dashed lines indicate on- and offset of the stimulus. Shibire<sup>®</sup> control flies in dark gray, Gal4 control flies in light gray, lamina block flies in blue. Data represent mean  $\pm$  s.e.m with  $n = 14$ – $19$  flies per group. Same flies as in Figure 4.

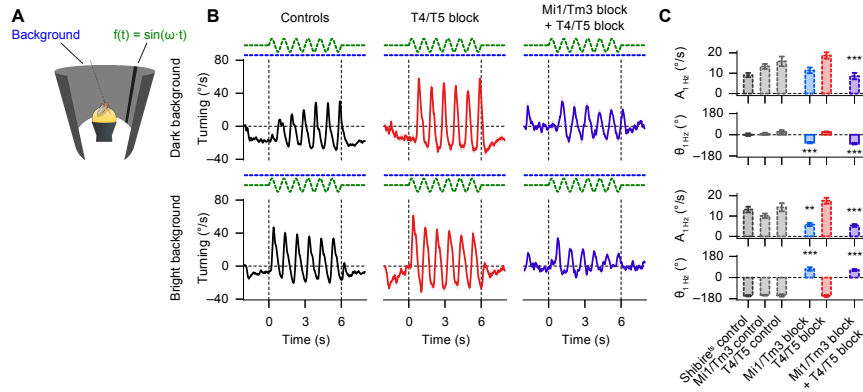


**Figure S4, related to Figure 6. Single-field Contrast Illusion in Mi1/Tm3 Block Flies**

(A) Same as in Figure 2A. (B) Fly turning responses for 1 Hz stripe flicker (identical in the two conditions; green dashed line) on two different backgrounds (dark and bright; blue dashed line). (C) Quantification of response amplitude  $A$  and phase  $\theta$ . Data represent mean  $\pm$  s.e.m with  $n = 14-19$  flies per group. Same flies as in Figures 4 and 5. P-values based on a two-sided Welch's t test, comparing the group of block flies with respective control groups (Mi1/Tm3 block with Mi1/Tm3 control and shibire<sup>ts</sup> control; The combined Mi1/Tm3 block + T4/T5 block (right side) was compared only to the T4/T5 block group;  $P^{**} < 0.01$ ;  $P^{***} < 0.001$ ). Detailed statistics in Table S2B. Expression patterns and list of genotypes in Figure S2A-C. Shibire<sup>ts</sup> control flies in dark gray, Gal4 control flies in light gray, Mi1/Tm3 block flies in blue, T4/T5 block flies in red, and combined Mi1/Tm3 block + T4/T5 block flies in violet. Raw time traces for control flies (black) in (C,D) are pooled from shibire<sup>ts</sup> control, T4/T5 control and Mi1/Tm3 control flies.

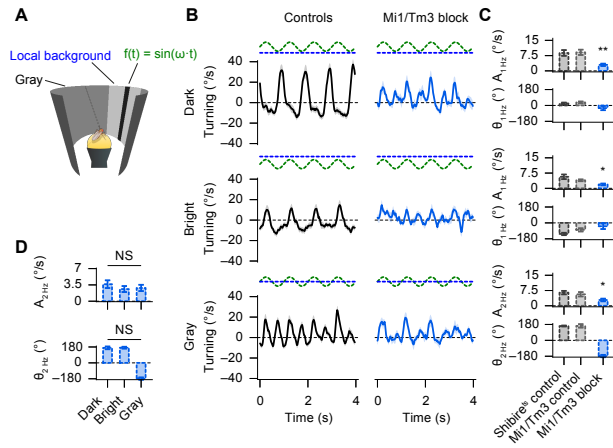


**Figure S5, related to Figure 6. Single-Field Contrast Asynchrony Illusion with Local Background Variation in Mi1/Tm3 Block Flies**

(A) The global background is gray for all conditions. Varied is the local background (dark, bright, and gray; blue dashed line) surrounding the  $\omega = 1$  Hz flickering stripe (identical in all conditions; green dashed line). Compare with stimuli in Figures 2A and 6E where global background luminance is varied. (B,C) Fly turning responses for the three local background conditions and quantification of response amplitude  $A$  and phase  $\Theta$ . (D) Quantification of the 2 Hz response component for the three local background conditions for Mi1/Tm3 block flies. Data represent mean  $\pm$  s.e.m with  $n = 8-12$  flies per group. P-values based on a two-sided Welch's t test, comparing Mi1/Tm3 block flies with both control groups ( $P^* < 0.05$ ;  $P^{**} < 0.01$ ). Statistics in (D) was done by pairwise comparing responses between the different conditions. None of these combinations was statistically different. Detailed statistics in Table S3. Shibire<sup>ts</sup> control flies in dark gray, Mi1/Tm3 control flies in light gray, Mi1/Tm3 block flies in blue. Raw time traces for control flies (black) in (B) are pooled from shibire<sup>ts</sup> control and Mi1/Tm3 control flies.

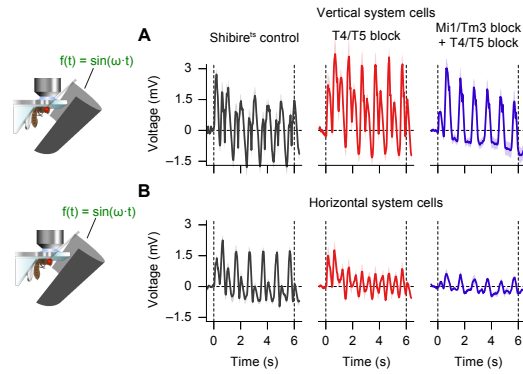


**Figure S6, related to Figure 7. Responses of Lobula Plate Tangential Cells to Full Field Flicker**

(A,B) Responses of vertical system and horizontal system cells to 1 Hz full field flicker. Data represent mean  $\pm$  s.e.m with  $n = 4-11$  cells per group (of 2-8 flies per group). Same flies and cells as in Figure 7. Shibire<sup>ts</sup> flies in dark gray, T4/T5 block flies in red, combined Mi1/Tm3 block + T4/T5 block flies in violet. See Figure S1B,C for illustration of the recorded neurons.

# Neural Mechanisms for *Drosophila* Contrast Vision

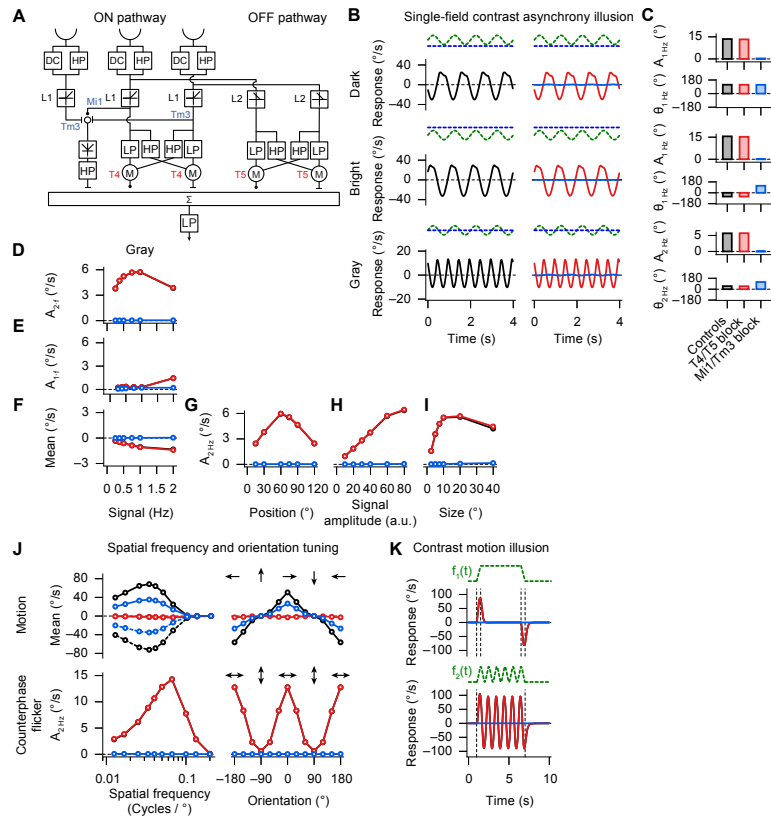


**Figure S7, related to Figure 8. Detailed Model with Contrast Computation within the ON Pathway**

(A) Detailed model with two pathways computing motion from brightness increments (ON pathway) and brightness decrements (OFF pathway). See Eichner et al., 2011. Within the ON pathway, lateral inhibition by Tm3 neurons and central excitation by Mi1 neurons are used to compute local spatial contrast (compare with Figure 8A). T4 and T5 neurons represent the output of the Hassenstein-Reichardt detectors in the two motion pathways. (B,C) Model responses for the single-field contrast asynchrony illusion (same stimulus as in Figures 2A–C and 6E–F) and quantification of amplitude  $A$  and phase  $\Theta$ . (D–I) Quantification of responses to varying signal frequency, position, amplitude, and stripe size. (J) Model responses for motion and counterphase flicker spatial frequency and orientation tuning (same stimulus as in Figure 3). (K) Model responses for the contrast motion illusion (same stimulus as in Figures 1F–H and 6C,D). Control conditions (full model) in black. T4/T5 block (model without Hassenstein-Reichardt detectors) in red. Mi1/Tm3 block (only OFF motion pathway intact) in blue.

# Neural Mechanisms for *Drosophila* Contrast Vision

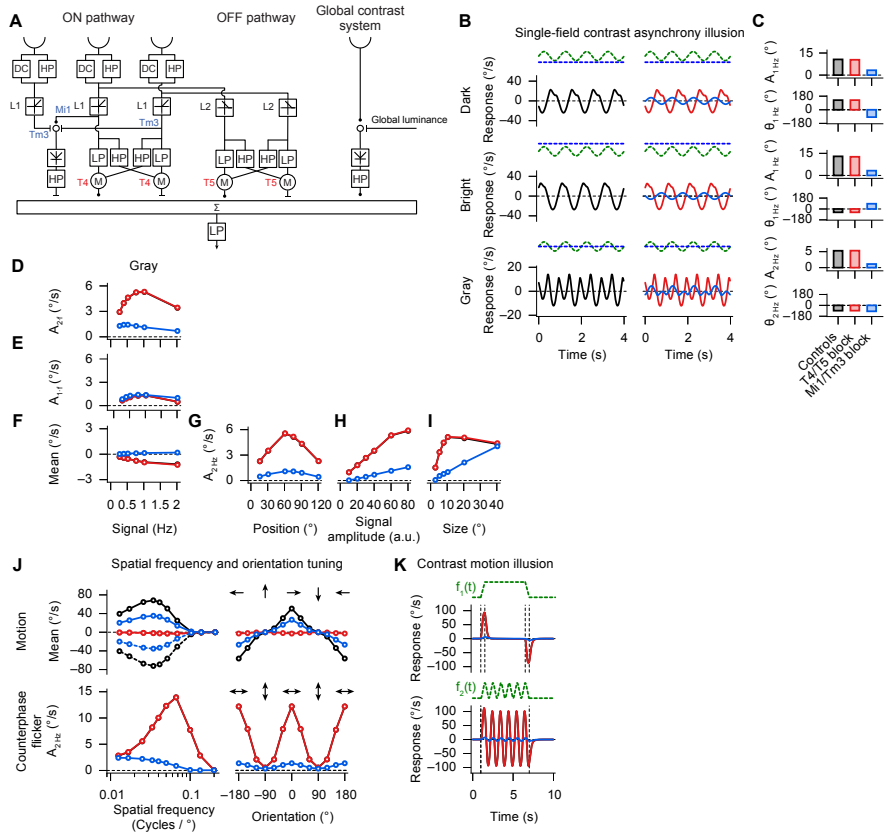


**Figure S8, related to Figure 8. Detailed Model with Local Contrast Computation within the ON Pathway and an Additional Pathway for Global Contrast Computation**  
 (A–K) Same as in Figure S7 but with an additional pathway for global contrast computation. Control conditions (full model) in black. T4/T5 block (model without Hassenstein-Reichardt detectors) in red. Mi1/Tm3 block (only OFF motion pathway and global contrast pathway intact) in blue.

# Neural Mechanisms for *Drosophila* Contrast Vision

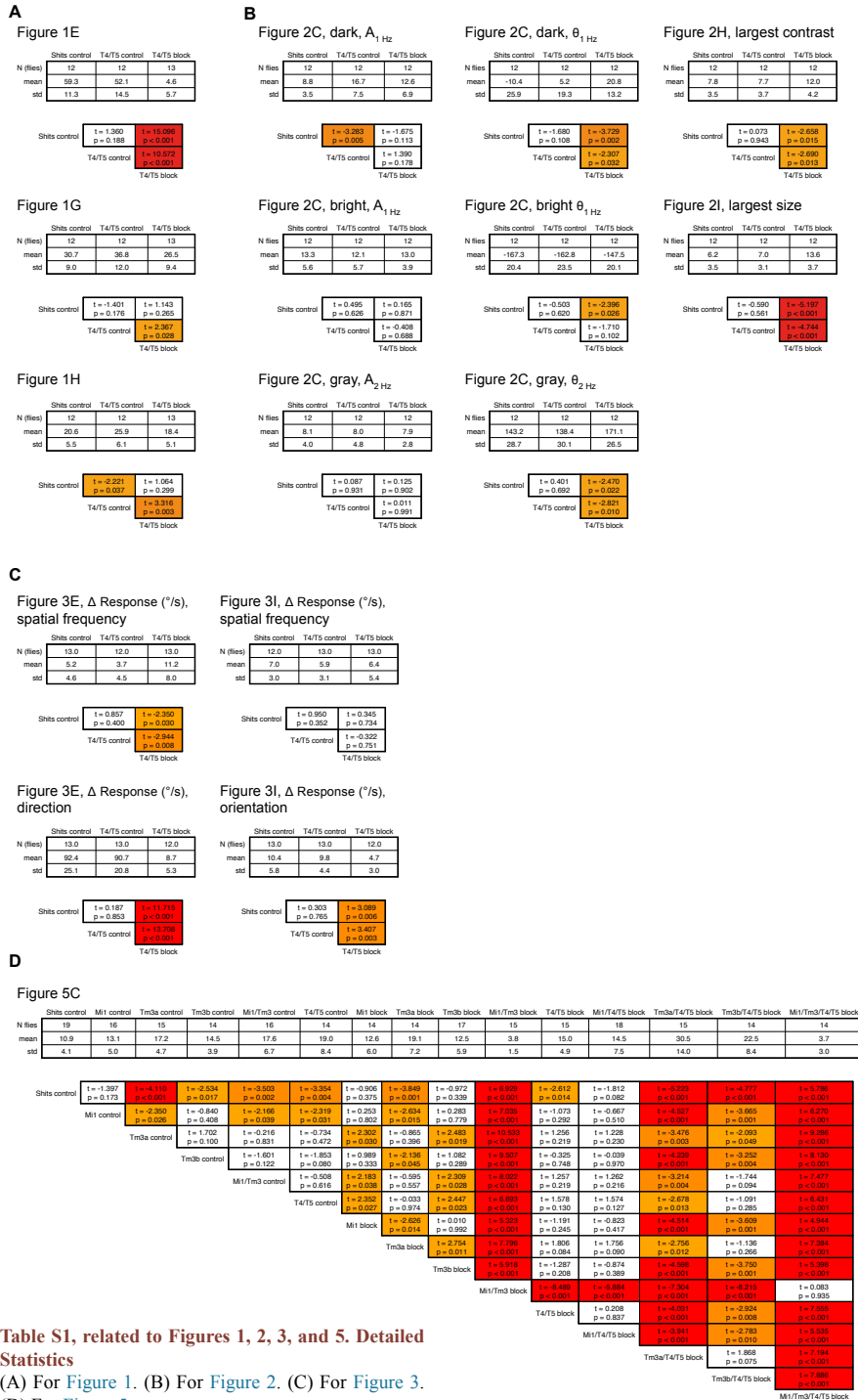


**Table S1, related to Figures 1, 2, 3, and 5. Detailed Statistics**  
 (A) For Figure 1. (B) For Figure 2. (C) For Figure 3. (D) For Figure 5.



# Neural Mechanisms for *Drosophila* Contrast Vision

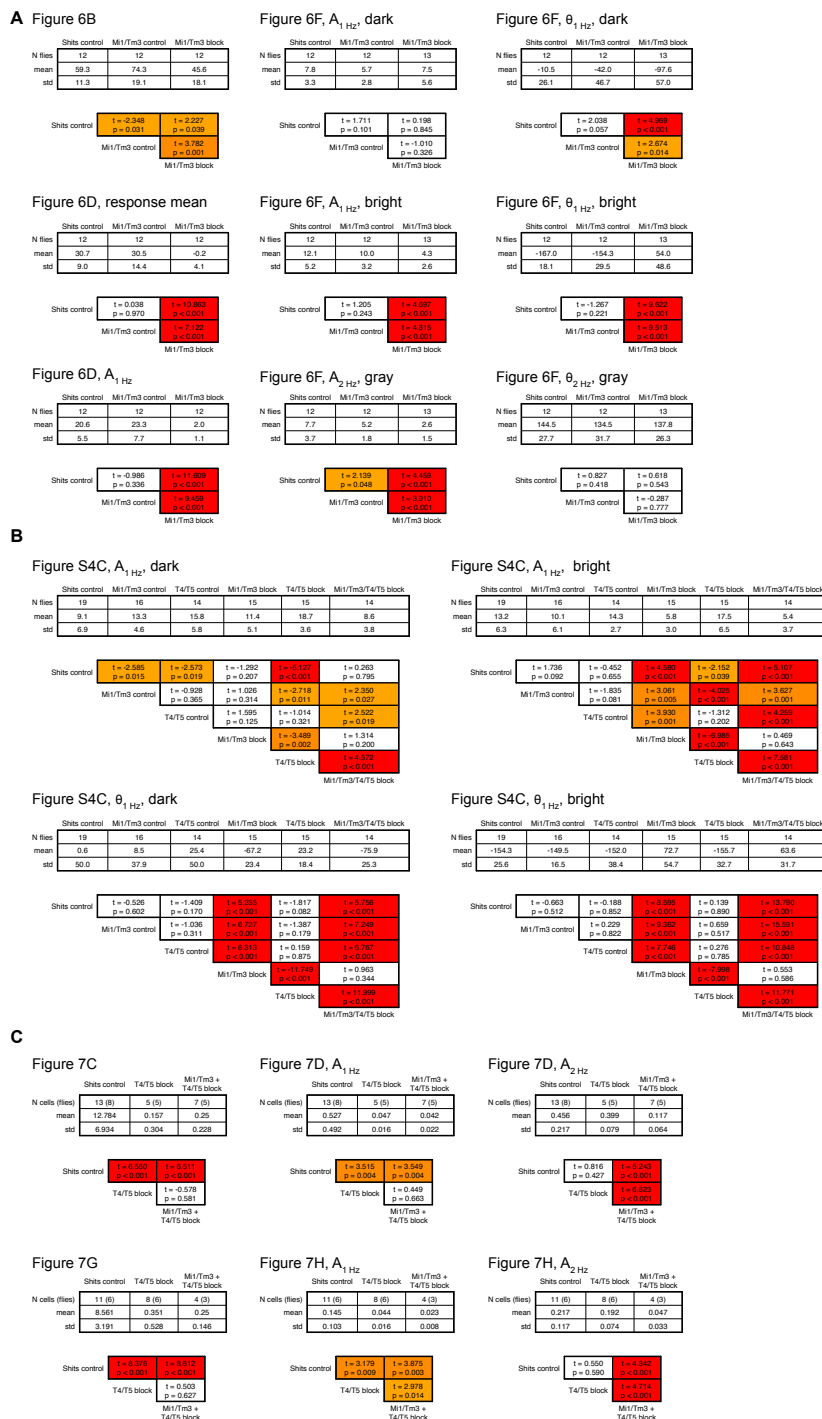


Table S2, related to Figures 6, S4, and 7. Detailed Statistics (A) For Figure 6. (B) For Figure S4. (C) For Figure 7.

# Neural Mechanisms for *Drosophila* Contrast Vision

**A**

**Figure S5C,  $A_1$  Hz, dark**

	Shits control	Mi1/Tm3 control	Mi1/Tm3 block
N files	10	12	8
mean	8.8	9.1	3.0
std	4.5	4.5	1.7

Shits control	$t = -0.165$ $p = 0.871$	$t = 3.810$ $p = 0.002$
Mi1/Tm3 control	$t = 4.205$ $p < 0.001$	

**Figure S5C,  $\theta_1$  Hz, dark**

	Shits control	Mi1/Tm3 control	Mi1/Tm3 block
N files	10	12	8
mean	22.6	34.1	-30.0
std	32.7	38.5	67.1

Shits control	$t = -0.761$ $p = 0.455$	$t = 2.032$ $p = 0.071$
Mi1/Tm3 control	$t = 2.440$ $p = 0.034$	

**Figure S5D,  $A_2$  Hz, Mi1/Tm3 block**

	Dark	Bright	Gray
N files	8	8	8
mean	3.7	2.7	2.8
std	2.3	1.8	1.9

Dark	$t = 1.840$ $p = 0.093$	$t = 0.385$ $p = 0.706$
Bright	$t = -0.382$ $p = 0.559$	

**Figure S5C,  $A_1$  Hz, bright**

	Shits control	Mi1/Tm3 control	Mi1/Tm3 block
N files	10	12	8
mean	5.7	3.9	1.9
std	3.6	1.6	1.3

Shits control	$t = 1.294$ $p = 0.189$	$t = 2.039$ $p = 0.011$
Mi1/Tm3 control	$t = 3.132$ $p = 0.005$	

**Figure S5C,  $\theta_1$  Hz, bright**

	Shits control	Mi1/Tm3 control	Mi1/Tm3 block
N files	10	12	8
mean	-125.3	-75.2	-38.3
std	43.0	64.2	89.1

Shits control	$t = -2.023$ $p = 0.059$	$t = 2.535$ $p = 0.031$
Mi1/Tm3 control	$t = -1.119$ $p = 0.285$	

**Figure S5D,  $\theta_2$  Hz, Mi1/Tm3 block**

	Dark	Bright	Gray
N files	8	8	8
mean	170.1	172.1	-177.9
std	45.0	30.2	35.4

Dark	$t = -0.104$ $p = 0.918$	$t = -0.577$ $p = 0.574$
Bright	$t = 0.582$ $p = 0.569$	

**Figure S5C,  $A_2$  Hz, gray**

	Shits control	Mi1/Tm3 control	Mi1/Tm3 block
N files	10	12	8
mean	5.5	5.5	2.8
std	2.7	3.8	1.9

Shits control	$t = 0.594$ $p = 0.559$	$t = 2.311$ $p = 0.034$
Mi1/Tm3 control	$t = 2.190$ $p = 0.043$	

**Figure S5C,  $\theta_2$  Hz, gray**

	Shits control	Mi1/Tm3 control	Mi1/Tm3 block
N files	10	12	8
mean	162.5	162.8	-177.9
std	18.4	68.1	38.4

Shits control	$t = -0.063$ $p = 0.951$	$t = -1.330$ $p = 0.214$
Mi1/Tm3 control	$t = -0.767$ $p = 0.453$	

Table S3, related to Figure S5. Detailed Statistics  
(A) For Figure S5.

# Neural Mechanisms for *Drosophila* Contrast Vision

A

Figure 4E

	ChR1 control	L1 control	L2 control	L3 control	L4 control	L5 control	MI control	TnCh control	MI/TnCh control	T4/T5 control	L1 block	L2 block	L3 block	L4 block	L5 block	L2,L3,L4 block	MI block	TnCh block	TnCh block	MI/TnCh block	T4/T5 block	L1/T4/T5 block	L2/T4/T5 block	L3/T4/T5 block	L4/T4/T5 block	L5/T4/T5 block	MI/T4/T5 block	TnCh/T4/T5 block	TnCh/T4/T5 block	MI/TnCh/T4/T5 block	
<b>Mean</b>	39	10	16	14	14	16	36	36	36	36	18	18	18	18	18	18	36	36	36	36	36	36	36	36	36	36	36	36	36	36	
<b>SE</b>	12.7	9.7	15.9	11.0	8.4	7.0	15.1	10.2	9.7	9.6	12.6	8.2	9.7	12.3	11.0	9.2	11.8	8.4	6.5	8.3	9.7	4.9	3.2	1.8	2.7	3.5	2.0	5.8	3.0	1.9	
<b>Statistics</b>	$t=11.719$ $p<0.0001$	$t=0.044$ $p=0.959$	$t=0.000$ $p=1.000$	$t=0.000$ $p=1.000$	$t=0.000$ $p=1.000$	$t=0.000$ $p=1.000$	$t=0.000$ $p=1.000$	$t=0.000$ $p=1.000$	$t=0.000$ $p=1.000$	$t=0.000$ $p=1.000$	$t=0.000$ $p=1.000$	$t=0.000$ $p=1.000$	$t=0.000$ $p=1.000$	$t=0.000$ $p=1.000$	$t=0.000$ $p=1.000$	$t=0.000$ $p=1.000$	$t=0.000$ $p=1.000$	$t=0.000$ $p=1.000$	$t=0.000$ $p=1.000$	$t=0.000$ $p=1.000$	$t=0.000$ $p=1.000$	$t=0.000$ $p=1.000$	$t=0.000$ $p=1.000$	$t=0.000$ $p=1.000$	$t=0.000$ $p=1.000$	$t=0.000$ $p=1.000$	$t=0.000$ $p=1.000$	$t=0.000$ $p=1.000$	$t=0.000$ $p=1.000$	$t=0.000$ $p=1.000$	$t=0.000$ $p=1.000$

Table S4, related to Figure 4. Detailed Statistics (A) For Figure 4E.





### SUPPLEMENTAL REFERENCES

Borst, A. (2014). Fly visual course control: behaviour, algorithms and circuits. *Nat. Rev. Neurosci.* 15, 590–599.

Rajashekhar, K.P., and Shamprasad, V.R. (2004). Golgi analysis of tangential neurons in the lobula plate of *Drosophila melanogaster*. *J. Biosci.* 29, 93–104.

# Manuscript Nr. 6: **Asymmetry of *Drosophila* ON and OFF motion detectors enhances real-world velocity estimation**

Aljoscha Leonhardt\*, Georg Ammer\*, Matthias Meier, **Etienne Serbe**, Armin Bahl, and Alexander Borst

\*equal contribution

## Author Contributions:

A.L., G.A. and A.Bo. designed the study. A.L. performed behavioral experiments, associated data analysis and all modeling work. G.A., M.M., and **E.S.** performed electrophysiological experiments. G.A. performed calcium imaging. A.L. and G.A. analyzed physiological data. A. Ba. designed the behavioral apparatuses and performed behavioral experiments. A.L. wrote the manuscript with help from all of the authors.

## Asymmetry of *Drosophila* ON and OFF motion detectors enhances real-world velocity estimation

Aljoscha Leonhardt<sup>1,3</sup>, Georg Ammer<sup>1,3</sup>, Matthias Meier<sup>1</sup>, Etienne Serbe<sup>1</sup>, Armin Bahl<sup>1,2</sup> & Alexander Borst<sup>1</sup>

The reliable estimation of motion across varied surroundings represents a survival-critical task for sighted animals. How neural circuits have adapted to the particular demands of natural environments, however, is not well understood. We explored this question in the visual system of *Drosophila melanogaster*. Here, as in many mammalian retinas, motion is computed in parallel streams for brightness increments (ON) and decrements (OFF). When genetically isolated, ON and OFF pathways proved equally capable of accurately matching walking responses to realistic motion. To our surprise, detailed characterization of their functional tuning properties through *in vivo* calcium imaging and electrophysiology revealed stark differences in temporal tuning between ON and OFF channels. We trained an *in silico* motion estimation model on natural scenes and discovered that our optimized detector exhibited differences similar to those of the biological system. Thus, functional ON-OFF asymmetries in fly visual circuitry may reflect ON-OFF asymmetries in natural environments.

Motion cues resulting from movement through space constitute an important source of information about the external world, supporting course stabilization, navigation or tracking of landmarks<sup>1</sup>. Biological motion detectors have evolved in environments of astounding complexity. Visual landscapes from which animals derive such cues are cluttered and produce rapidly fluctuating signals. Exploiting a priori knowledge about scene features is therefore critical for organisms to reliably extract the spatiotemporal correlations that indicate motion. Basic statistical properties such as the shape of power spectra are known to be conserved between natural scenes<sup>2–4</sup>. Higher order features such as textures, edges or contrast distributions yield additional cues and exhibit consistent statistics across visual environments. Examples of neural adaptation to natural scene statistics abound, operating at various levels of visual processing hierarchies<sup>5–7</sup>.

Segregated processing of positive (ON) and negative (OFF) changes in sensory magnitude is a common trait among modalities ranging from olfaction to motion detection in the insect and mammalian visual systems<sup>1,8,9</sup>. Splitting time-varying signals into two streams, covering opposite directions of change, is thought to confer various advantages to sensory circuits. For instance, ON-OFF systems maximize information transfer when resources are constrained<sup>8</sup>. In the case of motion detection, the ON-OFF split may drastically simplify the biophysical implementation of operations such as sign-correct multiplication<sup>10,11</sup>.

Luminance distributions in real-world environments are heavily asymmetric with regard to positive and negative contrast<sup>2,12</sup>. Visual systems take this into account: in the mammalian retina, for example, more ganglion cells are dedicated to processing negative than positive spatial contrast, consistent with naturally encountered skewness<sup>13</sup>. Theoretical studies on motion detection have proposed that, in ON-OFF asymmetric environments, higher order correlations carry valuable

information about scene motion<sup>14</sup>. Indeed, flies and humans alike appear to be capable of extracting higher order cues<sup>12,15</sup>, suggesting that both apply this strategy for motion estimation. However, little is known about the neural mechanism by which either visual system gains access to higher order correlations.

As a result of the availability of powerful genetic tools and extensive connectomic<sup>16,17</sup> as well as functional<sup>18–24</sup> characterizations, knowledge about the neural substrate of *Drosophila* motion detectors has grown exponentially in recent years<sup>9</sup>. Briefly, signals impinging on the photoreceptors are split into two polarity-specific channels, with one processing brightness increases (from L1 to T4 via at least Mi1 and Tm3) and the other processing brightness decreases (from L2, L3 and L4 to T5 via Tm1, Tm2, Tm4 and Tm9). Local ON and OFF motion signals are then extracted on the dendrites of T4 and T5, respectively, in a manner that is well explained by the Hassenstein-Reichardt correlation model<sup>9,11,21</sup>. Large tangential cells in the lobula plate pool these signals and influence behavioral output<sup>1,9,25,26</sup>.

Given the ON-OFF asymmetries encountered in natural environments, we set out to determine how the specific features of natural scenes have shaped ON and OFF motion detectors in the fly visual system. In contradistinction to previous studies, we were able to directly assess the behavioral performance of neural pathways by isolating them genetically. We found that asymmetries of natural environments had direct correspondence in tuning asymmetries of the fly motion detection system.

### RESULTS

#### ON and OFF motion detectors reliably estimate velocity

Flies react to visual wide-field motion by turning with the environment<sup>1,19,27</sup>. During navigation, this optomotor response stabilizes the animal's course in the face of external perturbations or internal noise.

<sup>1</sup>Max Planck Institute of Neurobiology, Martinsried, Germany. <sup>2</sup>Present address: Department of Molecular and Cell Biology, Harvard University, Cambridge, Massachusetts, USA. <sup>3</sup>These authors contributed equally to this work. Correspondence should be addressed to A.L. (leonhardt@neuro.mpg.de).

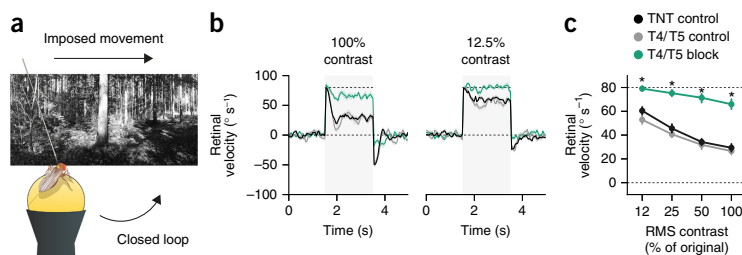
Received 19 November 2015; accepted 29 January 2016; published online 29 February 2016; doi:10.1038/nn.4262



# Asymmetry of *Drosophila* ON and OFF motion detectors enhances real-world velocity estimation

## ARTICLES

**Figure 1** Flies stabilize their path in naturalistic environments using a combination of ON and OFF motion detectors. (a) Illustration of behavioral setup. Tethered flies walk in a virtual closed-loop environment. During certain time periods, their trajectories are perturbed externally. (b) Path stabilization under different contrast conditions. Retinal velocity describes environment rotation relative to the fly's eye. During epochs shaded in gray, a constant rotation bias of  $80^\circ \text{ s}^{-1}$  was added. Upper dashed line indicates imposed velocity. Control flies (TNT control in black,  $N = 19$ ;



T4/T5 control in gray,  $N = 12$ ) reduced the imposed retinal velocity effectively whereas T4/T5 block flies (in green,  $N = 13$ ) did not. Left, unmodified image contrast. Right, artificial reduction of root-mean-square (RMS) contrast to 12.5% of initial value. Exact genotypes are listed in **Supplementary Table 1**. (c) Quantification of stabilization performance across contrasts. Retinal velocity was averaged between 2 and 3 s. Dashed lines correspond to zero and full correction of the perturbation. Shaded areas around traces and vertical bars signify bootstrapped 68% confidence intervals around the mean. Asterisks indicate significant differences of block flies from both genotype controls after Bonferroni-corrected two-tailed  $t$  tests ( $*P < 0.05$ ); exact test statistics are reported in **Supplementary Table 2**.

Any deviation from a straight path results in retinal flow that is counteracted by matching direction and, ideally, velocity of perceived drift through locomotion. Responses of behaving fruit flies and wide-field motion-sensitive neurons to simplified motion stimuli such as sinusoidal gratings have been studied extensively<sup>27,28</sup>. Tethered flying flies placed in such artificial environments do indeed correct for externally applied biases<sup>29</sup>. However, flies generally solve this problem in vastly more complex environments. So far, nothing is known about the quantitative extent of their ability to perform path stabilization in naturalistic contexts.

We addressed this question by allowing tethered flies to stabilize their walking trajectories in virtual environments. To cover many possible surroundings, we generated a library of panoramic images spanning the entire visual field of the fly. Randomly selected images were projected onto a virtual cylinder whose orientation was controlled in closed loop through the angular trajectory of flies walking on an air-suspended ball (**Fig. 1a**). In addition, we superimposed fixed-velocity rotations and recorded the relative motion between the fly and its environment. Our approach therefore simulated translation-free walking through a distant visual scene in the presence of external course perturbations. As expected, control flies actively reduced retinal slip speed by rotating in the direction of and with similar velocity as their visual environment (**Fig. 1b**). A combination of neural, motor and setup-intrinsic delays resulted in characteristic over- and undershoots on the order of hundreds of milliseconds, trailing both onset and offset of the motion bias. Notably, control flies rarely achieved a retinal velocity of zero, which would indicate full compensation of the involuntary rotation.

Although combined synaptic silencing of cell types T4 and T5 abolishes behavioral and electrophysiological sensitivity to grating motion<sup>27,30</sup>, it is unclear whether naturalistic stimuli can provide additional cues exploited by secondary circuits. When we used Gal4-controlled<sup>31</sup> expression of the light chain of tetanus toxin<sup>32</sup> (TNT) to genetically disrupt synaptic output of all T4 and T5 cells, which are known to implement local motion detection<sup>21,27,30</sup>, we discovered a marked impairment of stabilization performance. This was the case across the full range of artificially reduced image contrasts tested (**Fig. 1b,c**). The effect did not stem from gross motor defects; the flies' walking speed was at control level (**Supplementary Fig. 1**). Contrast reductions also negatively affected the stabilization ability of control flies. This replicated a previously described property of motion-sensitive lobula plate tangential cells in a behavioral setting: response gain of these cells is diminished for natural images artificially reduced in contrast<sup>33</sup>. In summary, we found that flies actively

stabilized their path in complex visual scenes and that T4 and T5 cells were necessary neural elements for this feedback behavior.

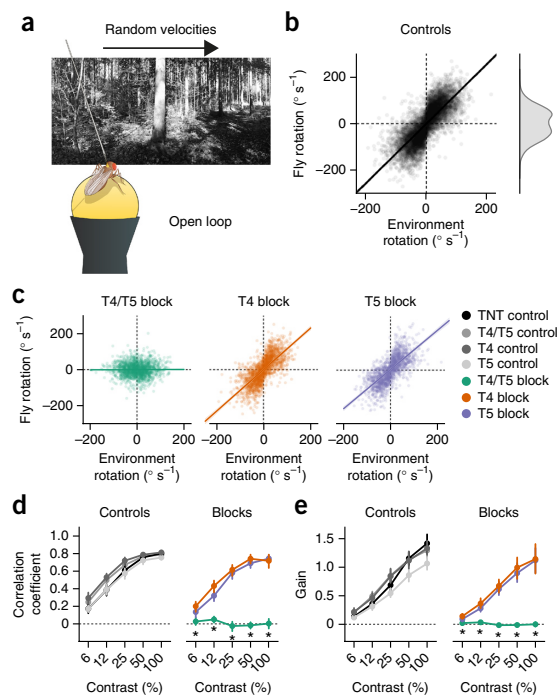
Previous work confirmed that T4 and T5 cells are predominantly sensitive to motion defined by luminance increases and decreases, respectively<sup>21</sup>. Full-field motion of naturalistic scenes, especially at large viewing distances and in cluttered environments, creates a rich gamut of both ON and OFF motion. Arrays of ON or OFF detectors may therefore be equally capable of reporting the direction and velocity of realistic global motion. However, nothing is known about the individual contributions of ON and OFF detectors to velocity estimation in such contexts. Moreover, the transformation from stimulus velocity to response strength for all read-outs of the fly motion system is highly sensitive to geometrical features of the stimulus: the fly motion detector is generally not a pure speedometer<sup>1,9</sup>. Even though most gain regimes would eventually lead to stabilization, the optomotor response should ideally match true retinal velocity to correct the fly's course quickly and efficiently<sup>29</sup>. Indeed, tangential cells exhibit a linear and reliable velocity-response curve when stimulated with natural images as opposed to periodic stimuli such as gratings<sup>33</sup>. We sought to test whether this is reflected by optomotor behavior.

To this end, we assessed *Drosophila*'s behavioral ability to track scene velocity in open loop (**Fig. 2a**). Velocity-response curves were stochastically probed by presenting randomly chosen images moving at constant velocities drawn from a Gaussian distribution on each individual trial. Estimation performance was then defined as the linear correlation between environment rotation and average turning response of the fly. A correlation coefficient of  $r = 1.0$  indicates a perfectly reliable linear mapping of global motion onto behavioral response across all scenes, as would be required of a functional speedometer. Following visual stimulation, flies responded with robust turning responses that increased until stimulus offset and decayed right after (**Supplementary Fig. 2**). To our surprise, control flies performed the velocity estimation task exceedingly well (**Fig. 2b**). For our image set, individual flies reached correlation coefficients above 0.8 across hundreds of trials. Not all behavioral complexity was captured by the linear model: trials with turning responses close to  $0^\circ \text{ s}^{-1}$ , for instance, were rare (**Fig. 2b**). However, several effects suggested that our simplified measure was indeed valid. First, as anticipated, flies with disrupted T4 and T5 activity exhibited correlation coefficients and response gain close to zero (**Fig. 2c–e**). Second, the correlation coefficients of control flies were heavily decreased by the reduction of image contrast (**Fig. 2d**). This reflected increasing task difficulty at the lower end of the contrast spectrum. Third,

# Asymmetry of *Drosophila* ON and OFF motion detectors enhances real-world velocity estimation

ARTICLES

**Figure 2** ON and OFF channels are equally capable of estimating the velocity of natural scenes. **(a)** Sketch of experimental approach. Flies were subjected to a set of natural images rotating at random velocities drawn from a Gaussian distribution (s.d. =  $50^\circ \text{ s}^{-1}$ ) in open loop. **(b)** Velocity estimation performance of control flies. Each dot represents the average rotational response for one trial at full contrast. Trials were pooled across flies of all control groups ( $n = 1,936$  trials from  $N = 13$  TNT control flies,  $n = 1,879/N = 12$  for T4/T5 control,  $n = 2,070/N = 13$  for T4 control,  $n = 1,331/N = 12$  for T5 control); the linear fit is for illustrative purposes only. The shaded curve to the right shows a kernel density estimate of rotational responses. **(c)** Velocity estimation performance of block flies, displayed as in **b** ( $n = 1,755/N = 11$  for T4/T5 block,  $n = 1,976/N = 12$  for T4 block,  $n = 1,778/N = 12$  for T5 block). **(d)** Quantification of velocity estimation performance across artificially modified image contrasts. Performance was measured as the Pearson correlation between environment rotation and integrated response. Although T4/T5 block flies were strongly impaired at all contrasts, silencing T4 or T5 individually had no measurable effect on estimation performance. **(e)** Quantification of response gain across contrast range. Gain was measured as the slope of a linear regression model mapping environmental rotation onto rotational response. Vertical bars signify bootstrapped 68% confidence intervals around the mean. Asterisks indicate significant differences for block flies from both Gal4 and UAS controls after Bonferroni-corrected two-tailed *t* tests ( $*P < 0.05$ ); exact test statistics are reported in **Supplementary Table 3**.



we once again found a contrast-dependent decrease of response gain as determined by the slope of a linear fit (**Fig. 2e**). It should be noted that these gain values depend on the choice of averaging window. For this reason, and because control systems tend to overcompensate in the absence of feedback, large gain values in open loop do not necessarily entail full compensation in closed loop (**Fig. 1c**).

To determine potentially differential contributions of ON and OFF detectors to velocity estimation in naturalistic contexts, we then silenced only T4 or T5 using TNT. In a previous study using the same lines<sup>21</sup>, we found that blocking T4 or T5 led to a strongly reduced ability to detect bright or dark edges, respectively, at both the electrophysiological and behavioral level. In stark contrast to these effects, we found no impairment of velocity estimation for our naturalistic image set. Correlation coefficients for both T4 block and T5 block flies were not substantially different from control groups, even at low contrast levels (**Fig. 2c,d** and **Supplementary Fig. 2**). Finally, we alternatively quantified estimation performance as the root-mean-square error of a Bayesian estimator trained on the behavioral data, the results of which supported similar conclusions (**Supplementary Fig. 3**).

Taken together, we found that combined silencing of T4 and T5 completely abolished flies' ability to track the velocity of global motion in naturalistic scenes. Notably, ON and OFF channels appeared to be redundant for this task. Either was sufficient to recapitulate naturalistic behavior.

## Tuning properties of ON and OFF channels are asymmetric

Given that ON and OFF channels seemed equally capable of performing reliable velocity estimation across various visual scenes, it is plausible to assume that they share temporal tuning properties. Previous studies reported comparable temporal frequency optima for sinusoidal gratings<sup>21</sup>. Calcium imaging, however, lacks the temporal resolution required for a precise characterization of pathway kinetics. Moreover, considering the polarity specialization of T4 and T5, we sought to characterize the channels using pure ON or OFF stimuli as opposed to sinusoidal gratings defined equally by brightness increments and decrements.

First, we confirmed that T4 and T5 respond exclusively to bright and dark edges, respectively. The T4 driver line used for imaging

in a previous study<sup>21</sup> showed marginal coexpression in T5 cells; the converse applied to the T5 driver line. Our earlier work had revealed minor sensitivity for OFF edges in T4 cells as well as small responses for ON edges in T5 cells, measured in the confines of the lobula plate, where both cell types intermingle. We speculated that this was a result of either Gal4 coexpression or actual physiological crosstalk between ON and OFF circuitry. Moreover, a physiological characterization of T4 input elements suggests that T4 should only be mildly selective for ON motion<sup>24</sup>. To conclusively decide between the alternatives, we performed two-photon calcium imaging using a combined T4 and T5 line in conjunction with the calcium reporter GCaMP6f<sup>34</sup> (**Fig. 3a**). Separation of T4 and T5 signals was then achieved by restricting the region of interest to the cells' dendrites in the medulla or lobula, respectively (**Fig. 3b**). Dendrites showed strong calcium increases following visual edge stimulation that were perfectly polarity specific (**Fig. 3c,d**). This allowed us to characterize the temporal tuning properties of T4 and T5 by means of highly time-resolved electrophysiological recordings from downstream cells.

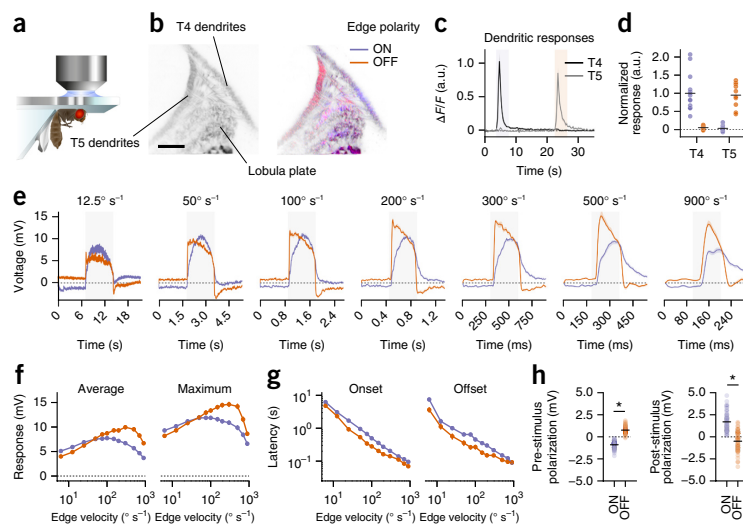
We determined velocity tuning curves for ON and OFF edges moving at speeds spanning two orders of magnitude by recording from the large-field motion-sensitive cells of the horizontal and vertical systems<sup>9,28</sup> in the lobula plate. These cells are the primary recipients of feedforward ON and OFF signals, receiving direct input from T4 and T5 for stimuli moving in preferred direction and indirect inhibitory input via lobula plate interneurons for null direction motion<sup>30,35</sup>. Cells depolarized when stimulated with ON or OFF edge motion along their preferred direction. Unexpectedly, tuning curves as well as general kinetics differed substantially between ON and OFF (**Fig. 3e**). Both channels showed increasing response strength up to a certain velocity, after which responses fell off (**Fig. 3f**). For ON edges, however, this peak was located at approximately  $100^\circ \text{ s}^{-1}$ , whereas OFF responses reached their maximum at edge velocities of  $\sim 300^\circ \text{ s}^{-1}$ . This held true

# Asymmetry of *Drosophila* ON and OFF motion detectors enhances real-world velocity estimation

## ARTICLES

**Figure 3** Physiological characterization of ON and OFF channels reveals tuning asymmetries.

(a) Schematic of preparation used for two-photon calcium imaging and patch-clamp recordings from lobula plate tangential cells (LPTCs). (b) Left, two-photon image of GCaMP6f expression in T4 and T5 cells. Scale bar represents 10  $\mu\text{m}$ . Right, representative T4 and T5 activity during ON (blue) or OFF (red) edge stimulation overlaid onto left-hand image. Activity was confined to T4 or T5 dendrites, depending on edge polarity. (c) Relative fluorescence ( $\Delta F/F$ ) across time for regions of interest centered on either T4 (black,  $N = 14$ ) or T5 (gray,  $N = 10$ ) dendrites. (d) Quantification of responses as averages over edge presentation period indicated by shaded areas in c. (e) Average responses of LPTCs for ON and OFF edges moving at a range of velocities in preferred direction. Time axes are scaled differently. Shaded area indicates edge presentation and covers visual field traversal ( $90^\circ$ ) at the specified velocity. Vertical and horizontal system cells from wild-type flies were pooled ( $n = 70$  from  $N = 43$  flies). (f) Velocity tuning curves for ON and OFF edges based on either average or maximum response during full stimulation period. (g) Response kinetics for ON and OFF edges on logarithmic scale. (h) Static properties averaged across velocities. Dots represent individual observations and black bars indicate group averages. Vertical bars and shaded areas signify bootstrapped 68% confidence intervals around the mean. Asterisks indicate significant differences between ON and OFF after two-tailed  $t$  tests ( $*P < 0.05$ ). Exact test statistics are reported in **Supplementary Table 4**.



regardless of whether we quantified average or maximum voltage. Moreover, both onset and offset latencies were larger for ON edges than for OFF edges across the full range of velocities tested (Fig. 3g). We also observed a constant polarization that closely reflected surround luminance (Fig. 3h); for instance, the field illumination preceding the onset of an OFF edge led to steady-state depolarization of the cell, which gave way to hyperpolarization after the dark edge had traveled through the fly's visual field (Fig. 3e). In a second set of experiments, we examined whether such differential pre-stimulus polarization could explain the observed ON-OFF asymmetries. Flies were presented with edges starting from an intermediate background luminance that was equal for both polarities (Supplementary Fig. 4a). Notably, edge velocity tuning curves were not affected by this alteration, whereas differences in onset kinetics vanished (Supplementary Fig. 4b,c). This suggests that luminance adaptation has a strong effect on the dynamics of tangential cell responses, but does not influence temporal tuning.

In summary, we observed strongly differential velocity tuning for ON and OFF pathways, with the former responding maximally to slower velocities than the latter. To determine whether the observed tuning differences are behaviorally relevant, we performed balanced motion experiments on walking flies. Multiple resetting ON and OFF edges distributed across the visual field moved simultaneously in opposite directions over several seconds<sup>19,21,23</sup> (Fig. 4a). This was done for a large velocity range and offered a behavioral read-out of the weighting between ON and OFF pathways. Here, a turning tendency of zero implies equal ON and OFF responses. Consistent with electrophysiological results, we found that the balance between ON and OFF responses was clearly modulated by edge velocity (Fig. 4b). At low speeds, ON responses dominated the overall turning behavior and control flies continuously rotated in the direction of bright edges (Fig. 4c). At higher velocities, this turning tendency was reversed, indicating dominant OFF responses. ON and OFF were only completely in balance at an edge velocity of around  $80^\circ \text{ s}^{-1}$ . To test whether these imbalances also occur at the transient time scales dominating walking behavior,

we then shortened the stimulus duration to 500, 250 or 100 ms. These opposing edge pulses produced robust responses whose amplitude diminished with decreasing stimulus length. Notably, all tuning curves had shapes that were comparable to the steady-state condition (Supplementary Fig. 5).

We also performed blocking experiments using this assay (Fig. 4c). Removing T4 and T5 from the circuit resulted in abolished turning tendencies across all velocities. For individual blocks, we recovered effects whose general direction had been described before<sup>21</sup>: T4 block flies always rotated in the direction of OFF edges and T5 block flies consistently followed motion of ON edges (Fig. 4b). Notably, these block effects were most pronounced at different velocities. For T4 block flies, the curve peaked at  $160^\circ \text{ s}^{-1}$ . For T5 block flies, the maximum was found at  $80^\circ \text{ s}^{-1}$ . This roughly confirmed the edge tuning curves from tangential cell recordings (Fig. 3f) under the assumption that each individual block was reasonably complete, leaving only one pathway intact. From this, we generated linear predictions for wild-type behavior. *Post hoc* tuning curves were calculated by either subtracting edge tuning curves measured as average voltage or summing the behavioral curves of T4 block and T5 block flies (Fig. 4d). Both models successfully predicted response signs and approximate zero crossing of control flies, corroborating the notion that tangential cells combine T4 and T5 signals in an approximately linear regime and then control turning behavior directly.

Despite their comparable performance during naturalistic velocity estimation, the ON and OFF pathways represented by T4 and T5 are tuned to different velocity regimes at both the electrophysiological and behavioral level. We next explored whether this tuning asymmetry is critical for their estimation fidelity.

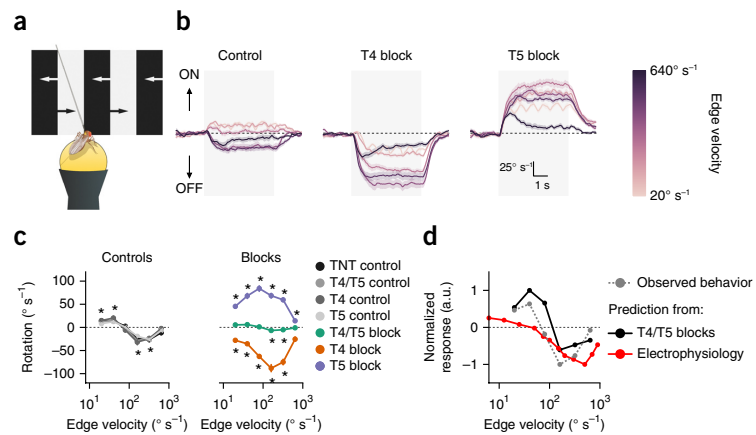
### Optimized detectors are ON-OFF asymmetric

The *Drosophila* motion detection system is well described by a two-quadrant ON-OFF detector: the combination of two motion detectors, one processing only ON signals akin to the physiological T4 channel and one processing only OFF signals akin to the physiological

# Asymmetry of *Drosophila* ON and OFF motion detectors enhances real-world velocity estimation

ARTICLES

**Figure 4** Asymmetry between ON and OFF channels persists at the behavioral level. (a) Schematic drawing of balanced motion stimulus with ON and OFF edges simultaneously moving into opposite directions at various velocities. (b) Rotational responses for TNT control flies as well as T4 and T5 block flies. Trace color indicates velocity of edges. Positive responses are syndirectional with ON edge motion; negative responses follow OFF edge motion. Gray-shaded area denotes epoch during which edges were moving. T4 and T5 block flies are consistently biased away from the disrupted polarity. For control flies, the dominant polarity changes with velocity. (c) Quantification of turning responses averaged over stimulation period (3 to 7 s;  $N = 12$  for TNT control,  $N = 12$  for T4/T5 control,  $N = 12$  for T4 control,  $N = 13$  for T5 control,  $N = 12$  for T4/T5 block,  $N = 15$  for T4 block,  $N = 14$  for T5 block). For controls, asterisks indicate responses that are significantly different from zero ( $*P < 0.05$ ). For block genotypes, asterisks indicate significant differences from both corresponding Gal4 and UAS controls (Bonferroni-corrected  $t$  tests,  $*P < 0.05$ ). (d) Comparison of observed control tuning curves (gray) with tuning curves linearly predicted from either the sum of behavioral T4 block and T5 block tuning curves (black) or the difference between electrophysiologically determined ON and OFF tuning curves (red; Fig. 3). Vertical bars and shaded areas surrounding traces signify bootstrapped 68% confidence intervals around the mean. Exact test statistics are reported in **Supplementary Table 5**.



T5 channel<sup>10</sup>. Each subunit then computes motion according to the well-established Hassenstein-Reichardt correlation model based on the multiplication of differentially filtered, spatially separated signals<sup>11</sup>. Counter-intuitively, such models are capable of explaining complex phenomena such as the reverse-phi effect observed for motion accompanied by contrast reversals<sup>10,19,36</sup>. Critical for this is the inclusion of a weighted tonic signal (DC component) in addition to the high-pass signal modeling processing in lamina monopolar cells. Parameters for the model are generally chosen such that the ON and OFF subunits of the detector remain symmetric<sup>10,19</sup>. Our results concerning edge velocity tuning, however, speak in favor of asymmetric tuning. Moreover, work on natural scenes has repeatedly shown that realistic environments are strongly asymmetric with regard to ON and OFF<sup>2,12,13</sup>. What does an ON-OFF detector look like that is tuned to naturalistic environments?

Various estimation objectives may be prioritized, depending on the given task<sup>29,37</sup>. For this study, we operationalized detector fitness analogously to previous studies<sup>12</sup> and equivalently to our own behavioral experiments as the linear correlation between the velocity of a rigidly translating natural image and time-averaged detector output. Given that Hassenstein-Reichardt detectors directly explain many aspects of fly optomotor behavior<sup>1,9</sup>, and considering that flies achieve extremely high correlation values in the corresponding experimental setting (Fig. 2), this seemed to be a sensible target for the model. We optimized by exhaustively scanning the parameter space spanned by low-pass filter time constant and DC component of simplified ON and OFF detectors (Fig. 5a). This was done in a cross-validated manner. We chose a small set of parameters for optimization in which ON-OFF asymmetries had been observed previously. Our own results on edge tuning (Fig. 3e,f) indicated that there were large temporal tuning differences between ON and OFF pathways. Physiological characterization of medulla interneurons Mi1 and Tm3 for T4 as well as Tm1 and Tm2 for T5 has revealed distinct differences with regard to the strength of DC signals present at the input of motion detectors<sup>24</sup>. Thus, we looked for combinations of low-pass filter time constants and DC weightings that would maximize velocity estimation performance of isolated ON and OFF detectors for a large

set of natural scenes from the van Hateren image database<sup>6</sup>. Velocities were drawn from a Gaussian distribution whose width was based on turning speed distributions determined in our closed-loop experiments. Optimized parameters were modulated in physiologically plausible ranges; all other settings were chosen based on previous modeling work<sup>10</sup> and not tuned for any particular result.

The resulting fitness landscape as a function of low-pass time constant and DC component was smooth and strongly asymmetric with respect to ON and OFF (Fig. 5b). Indeed, when we extracted the parameter sets that maximized fitness for independent ON and OFF detectors, we found that optimal settings were ON-OFF asymmetric with respect to both parameters (Fig. 5c). Specifically, the best time constants for ON detectors were larger than those achieving maximum correlation for OFF detectors. The best DC weights had higher values for ON detectors than for OFF detectors and opposite signs (Fig. 5c).

To ascertain whether parameter asymmetry improved velocity estimation over that achieved by symmetric models, we compared equally weighted combinations of independently optimized ON and OFF detectors to optimized detectors that were constrained to be symmetric. The cross-validated performance improvement was small but significant ( $t(98) = 4.08$ ,  $P < 0.001$ ), suggesting that detector asymmetry is an advantageous strategy (Fig. 5d). The differences between ON and OFF parameters of optimal asymmetric models were substantial (Fig. 5e). We therefore looked for functional disparities between the average optimized models. Simulated temporal frequency tuning curves for sinusoidal gratings were highly similar, with slightly shifted response optima (Fig. 5f). The asymmetric and the symmetric model also produced comparable output for a dynamically moving grating (Fig. 5g). When we simulated edge velocity tuning curves as we had measured experimentally (Figs. 3 and 4), the symmetric model exhibited identical tuning for ON and OFF edges, as was expected from identical temporal parameters. Our asymmetric model, however, correctly replicated the shift between optima for ON and OFF edges with the detector being tuned to higher OFF than ON edge velocities (Fig. 5h). In addition, the asymmetric model predicted a difference in overall strength between ON and

# Asymmetry of *Drosophila* ON and OFF motion detectors enhances real-world velocity estimation

## ARTICLES

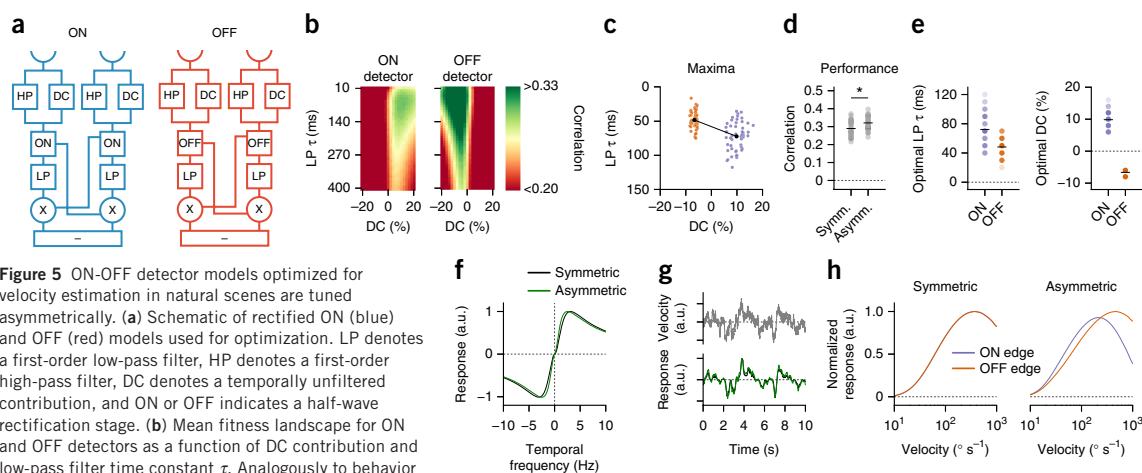


**Figure 5** ON-OFF detector models optimized for velocity estimation in natural scenes are tuned asymmetrically. **(a)** Schematic of rectified ON (blue) and OFF (red) models used for optimization. LP denotes a first-order low-pass filter, HP denotes a first-order high-pass filter, DC denotes a temporally unfiltered contribution, and ON or OFF indicates a half-wave rectification stage. **(b)** Mean fitness landscape for ON and OFF detectors as a function of DC contribution and low-pass filter time constant  $\tau$ . Analogously to behavior (Fig. 2d), estimation performance was measured as the Pearson correlation between input velocity and average detector output. **(c)** Distribution of optimized parameters. Each dot represents the best parameter set found for either ON (blue) or OFF (red) detectors on a given training image set ( $N = 50$  folds; points are jittered for clarity). Black dots mark the center of the ON and OFF parameter clouds. **(d)** Cross-validated performance of detectors. Optimal ON and OFF detectors are linearly combined (asymmetric detectors), tested on images not seen during training and compared with ON-OFF detectors optimized under the additional constraint of ON-OFF symmetry. The difference was significant after a two-tailed  $t$  test ( $N = 50/50$ ,  $t(98) = 4.08$ ,  $*P < 0.001$ ). **(e)** Comparison of parameters for asymmetric detectors from **c**. **(f)** Temporal tuning of optimized symmetric and asymmetric detector. **(g)** Responses of optimized symmetric and asymmetric detector to a sinusoidal grating drifting with Gaussian velocity profile. **(h)** Simulated ON and OFF edge velocity tuning curves (with peaks for the asymmetric model at  $230$  and  $480^\circ \text{ s}^{-1}$ , respectively). Dots represent individual results and black bars indicate group averages.

OFF edge responses (Fig. 3f) even though subunits were summed at equal gain. The modeled edge optima occurred at higher velocities than those we had determined experimentally. As optimized parameters for the detectors depended on the s.d. of the distribution from which test velocities were drawn, their absolute scale was

somewhat arbitrary; conditional on behavioral state, turning speed distributions may differ substantially. The direction of the asymmetry, however, was consistent with experimental findings.

We then determined natural image features necessary for asymmetries to appear in tuned ON-OFF detectors. To this end, we repeated the optimization procedure for image sets in which we had manipulated specific statistical properties. First, for the unaltered set, the best asymmetric ON and OFF detectors showed large differences for both low-pass time constant, as well as absolute DC level (Fig. 6a). Second, we randomized the phase structure of every image, thereby removing all higher level features such as textures or edges, as well as making scenes largely ON-OFF symmetric<sup>13</sup>, while retaining the typical power spectrum of natural scenes. Here, the asymmetry of time constants disappeared (Fig. 6b). Third, we artificially reinstated the natural luminance distribution in phase-randomized images (Fig. 6c). This manipulation rescued the time constant asymmetry, suggesting that a skewed luminance distribution is the critical constraint forcing filter

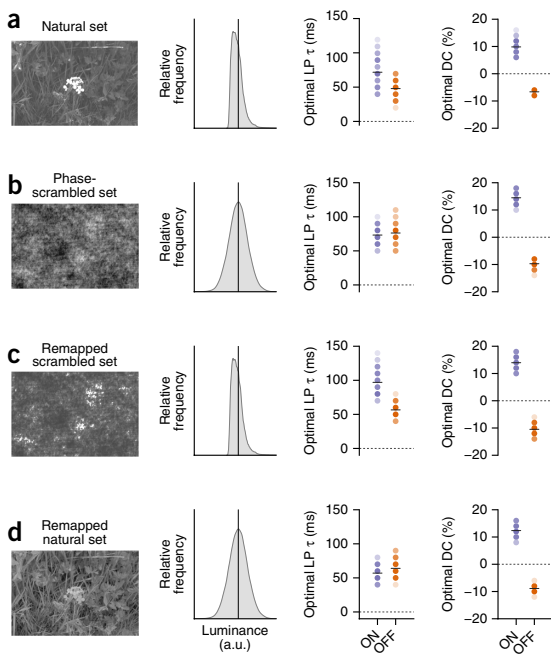
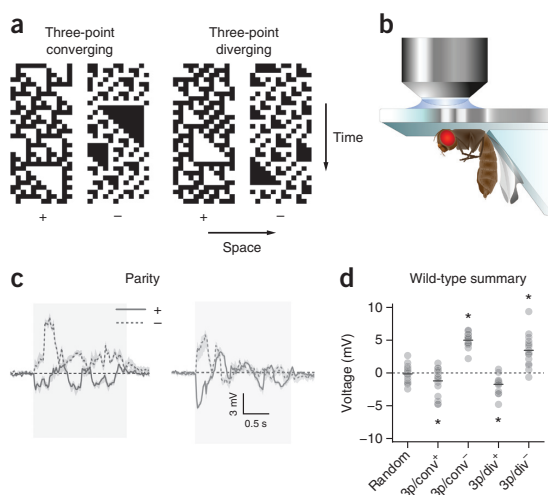


**Figure 6** Luminance asymmetry in natural scenes is critically responsible for asymmetry of ON-OFF parameters in optimized motion detector. **(a–d)** Left, example picture from image set used for optimization. Middle, kernel density estimate of pixel luminance distribution for example picture. The vertical line indicates average image luminance. Right-hand panels, optimized parameters for ON (blue) and OFF (red) detector trained on corresponding image set. **(a)** Unmodified image set used for earlier optimizations (Fig. 5). **(b)** Phase-scrambled image set in which the phase structure of each image was replaced by that of a random image, effectively rendering the luminance distribution symmetric. **(c)** Luminance-remapped image set in which the luminance distribution of natural images was remapped onto phase-scrambled images. **(d)** Luminance-remapped image set in which the luminance distribution of phase-scrambled images was remapped onto natural images. Dots represent individual observations and black bars indicate group averages ( $N = 50$  cross-validations for all image sets). No significance tests were performed in this figure.

**Figure 7** LPTCs are sensitive to higher order correlation stimuli. (a) Space-time plots of glider stimuli used to probe LPTC sensitivity to triple correlations. (b) Schematic drawing of *in vivo* electrophysiology preparation and setup. (c) Average responses to full-field three-point glider stimulation of pooled vertical and horizontal system cells ( $n = 16$  cells from  $N = 12$  flies). Gray shaded area shows duration of stimulus presentation. Shaded areas surrounding traces signify bootstrapped 68% confidence intervals around the mean. (d) Quantification of integrated responses (averaged over the first second of stimulus presentation); “3p/conv” or “3p/div” indicate three-point converging or diverging glider orientation, respectively, and superscript the stimulus parity. All recordings were done in wild-type Canton S flies. Depicted responses are the difference between glider presentation in preferred and null direction. Dots represent individual observations and black bars show group averages. Asterisks indicate significant differences from zero after two-tailed  $t$  tests ( $*P < 0.05$ ); exact test statistics are reported in **Supplementary Table 6**.



properties to diverge between ON and OFF channels. Finally, replacing the skewed luminance distribution of natural images with a symmetric one again abolished the temporal tuning differences (Fig. 6d). Notably, the DC asymmetry did not depend on higher order statistics of the stimulus. This particular tuning difference may be advantageous for ON-OFF detectors regardless of image statistics.

Taken together, our optimization findings demonstrate that, in realistic environments, the ON and OFF channels of motion detectors that were optimal under our criterion were tuned asymmetrically. The specific parameters that best estimated motion in natural scenes reproduced tuning properties of the biological fly motion detector we determined experimentally. At no point did we use our previous experimental findings as a constraint during optimization; the procedure arrived at this specific asymmetry independently.

### Higher-order motion sensitivity derives from ON-OFF asymmetry

Theoretical considerations indicate that spatiotemporal correlations of orders higher than two become informative indicators of visual motion in environments that are ON-OFF asymmetric<sup>14</sup>. Hassenstein-Reichardt detectors exclusively capture two-point correlations. Experimental work, however, confirmed that *Drosophila* responds to triple correlations<sup>12</sup>. This suggests that such correlations are either computed explicitly by secondary circuits or implicitly extracted by detectors that treat ON and OFF motion differentially. We assessed whether an asymmetric detector can account for *Drosophila*'s sensitivity to higher order motion.

First, we tested whether tangential cells respond to higher order motion cues given that these neurons receive their primary direction-selective input from T4 and T5 (ref. 30). We made use of previously characterized three-point glider stimuli<sup>12,15</sup> (Fig. 7a), which enforce the mean sign of correlations across three spatiotemporal points. They have four possible forms: converging or diverging, depending on their spatiotemporal orientation, and either positive or negative parity. Notably, they are guaranteed to contain on average zero

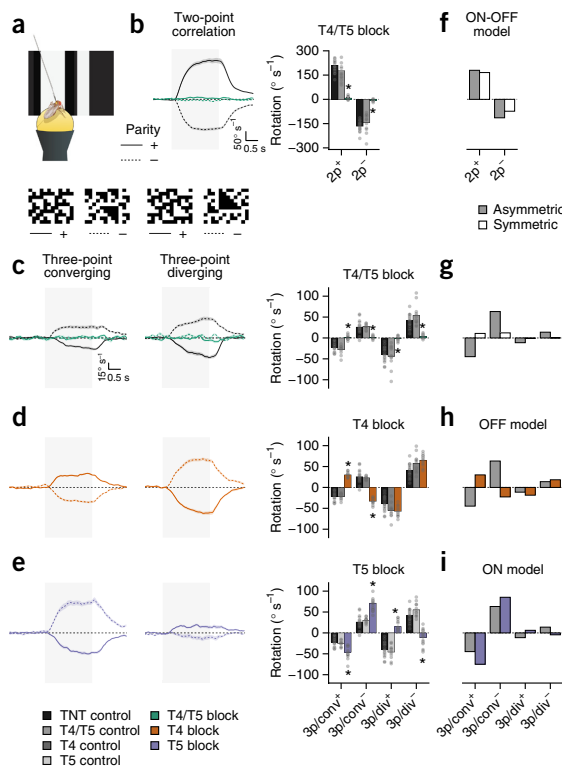


**Figure 8** Behavioral sensitivity to higher order correlations depends on T4 and T5 and is predicted by an asymmetric ON-OFF model. (a) Illustration of behavioral experiment. (b) Two-point glider responses. Left, average response traces for two-point glider stimuli. Here, as in all following panels, the gray shaded area indicates stimulus presentation. Right, rotational responses for two-point gliders representing phi and reverse-phi motion are abolished in T4/T5 block flies. (c) Control flies respond to three-point gliders in a specific pattern. Blocking T4 and T5 in conjunction eliminates these responses completely. (d, e) Silencing T4 or T5 modulates responses by reversing rotation for converging or diverging gliders, respectively. (f) Asymmetric and symmetric models account for two-point glider responses. (g) Only the asymmetric model correctly predicts three-point glider responses of control flies. (h, i) Simulating individual T4 and T5 blocks in the asymmetric ON-OFF model by setting the gain for either ON (red) or OFF (blue) channel to zero replicates the behavioral effects. Shaded areas surrounding traces signify bootstrapped 68% confidence intervals around the mean. Dots represent individual flies and bars show group averages. Asterisks indicate significant differences of block flies from both Gal4 and UAS controls after Bonferroni-corrected two-tailed  $t$  tests ( $N = 18$  for TNT control,  $N = 12$  for T4/T5 control,  $N = 12$  for T4 control,  $N = 12$  for T5 control,  $N = 14$  for T4/T5 block,  $N = 13$  for T4 block,  $N = 17$  for T5 block;  $*P < 0.05$ ). Exact test statistics are reported in **Supplementary Table 7**.

© 2016 Nature America, Inc. All rights reserved. npg

# Asymmetry of *Drosophila* ON and OFF motion detectors enhances real-world velocity estimation

## ARTICLES

directed two-point correlations, allowing the isolated characterization of responses to higher order motion. When we recorded from tangential cells of both the horizontal and vertical system (Fig. 7b), they responded to single instantiations of three-point gliders with complex dynamics (Fig. 7c). Their time-averaged voltage signals replicated the response pattern observed for behaving flies<sup>12</sup> (Fig. 7d). Given that fly locomotion is thought to reflect integrated tangential cell responses<sup>26</sup>, the combination of T4 and T5 thus appeared to be sufficient for higher order motion sensitivity.

We then examined the necessity of T4 and T5 for three-point glider responses. Tethered walking flies were presented with a complete set of two-point and three-point gliders (Fig. 8a). Next, we silenced T4 and T5 in isolation as well as simultaneously. For control flies, turning responses to two-point correlations were as expected for standard phi and reverse-phi stimuli: flies turned strongly in the direction of positive correlations (positive glider parity) and reversed this tendency for negative correlations (negative glider parity; Fig. 8b). Blocking T4 and T5 in conjunction completely abolished sensitivity to all two-point gliders. This is, to the best of our knowledge, the first demonstration that reverse-phi motion, defined by spatiotemporal anti-correlations, depends on the combined activity of ON and OFF motion detectors<sup>10,19,36</sup>. We then replicated the previously reported behavioral response pattern for three-point gliders<sup>12</sup>. Flies in which both T4 and T5 were silenced failed to respond to any of the higher order motion stimuli, indicating that T4 and T5 are also necessary for motion detection beyond two-point correlations (Fig. 8c). Blocking T4 or T5 in isolation had no effect on two-point responses (Supplementary Fig. 6a–c). We were, however, surprised to find that isolated T4 or T5 blocks resulted in particular three-point glider phenotypes. Silencing the ON pathway specifically reversed the flies' turning tendency for converging gliders while slightly boosting diverging glider responses (Fig. 8d). For OFF block flies, the opposite pattern emerged (Fig. 8e).

Finally, we probed our symmetric and asymmetric detector models for higher order motion sensitivity. Both produced comparable two-point glider responses (Fig. 8f). For three-point gliders, both detectors generated nonzero output, but only the asymmetric model qualitatively matched the pattern we observed in our electrophysiological experiments as well as in walking flies (Fig. 8g). Notably, when evaluating detector responses to individual glider instantiations, we found complex and strongly fluctuating responses that resembled tangential cell responses (Supplementary Fig. 6d,g). Responses became smooth and regular only after integration of many repetitions (Fig. 7 and Supplementary Fig. 6e,f,h,i). We then simulated T4 or T5 silencing by setting ON or OFF gain to zero. These models reliably predicted the specific response reversals (Fig. 8h,i) observed in behavior (Fig. 8d,e). We therefore posit that T4 and T5 are capable of extracting triple correlations on their own. ON and OFF edges have been found to contain a particular combination of triple correlations<sup>12</sup>. The reverse also held: three-point gliders elicited strong signals of opposite sign in pure ON or OFF detectors (Fig. 8d,e,h,i). Only if the pathways were perfectly symmetric did these responses cancel out. If they were asymmetric, as in our optimized detector or the *Drosophila* visual system, then residual responses remained. Our optimized models correctly predicted the sign and relative magnitude of these effects, suggesting that the asymmetries we found *in silico* track the asymmetries of the biological system.

## DISCUSSION

We studied the roles of ON and OFF motion pathways for velocity estimation in natural scenes. *Drosophila* stabilized their walking trajectories in a closed-loop virtual environment whose statistics

resembled those of natural scenes. Genetically silencing cells T4 and T5 rendered flies unable to perform this path correction. In an open-loop setting, flies reliably tracked whole-field motion of naturalistic images. Interrupting the activity of ON or OFF pathways did not affect this capability, suggesting that the two channels subserve redundant functions in information-rich natural scenes. In physiological and behavioral experiments, we found that ON and OFF motion estimators exhibit diverging temporal tuning. When we optimized the estimation performance of an ON-OFF motion detector, we obtained asymmetric models whose temporal tuning properties resembled those found for the biological system. This suggests that *Drosophila* motion detectors are tailored to an ON-OFF asymmetric visual world, with each channel covering the most informative temporal range. In a final set of experiments and without specific tuning of the model, we found that *Drosophila*'s sensitivity to certain types of higher order motion has a straightforward explanation in this framework of differentially tuned pathways.

One could interpret the shifted tuning ranges of T4 and T5 as a solution for maximizing information transfer by avoiding coding redundancy. However, for the asymmetric detector, pathways were optimized independently, forcing both to adequately encode the input velocity distribution. We therefore favor the interpretation that features reliably indicating scene velocity operate on time scales that differ between ON and OFF signals. The skewed luminance distribution of real images (Fig. 6a) offers an intuition for this notion: ON signals are dominated by infrequent and large positive deflections, whereas OFF signals are generally smaller and more regular. As neither RC filters nor lamina cells act as perfect differentiators, these differences plausibly persist at later levels of motion detection, where they may be exploited by appropriately tuned mechanisms<sup>13</sup>. Notably, detector performance was generally better for OFF detectors than for ON detectors (Fig. 5b), possibly reflecting the sparseness of informative ON signals.

During conditioning of detector parameters on natural images, we also optimized the weight of the tonic DC signal. We found nonzero optima for both pathways, as postulated in previous studies on reverse-phi responses<sup>10</sup>. Electrophysiologically, ON pathway interneurons Mi1 and Tm3 did indeed show static responses to absolute brightness levels with the amplitude ratio between high-pass and DC signal qualitatively matching our findings<sup>24</sup>. In contrast to our prediction, OFF intermediaries Tm1 and Tm2 did not exhibit inverted tonic signals. However, other cells presynaptic to T5 still await characterization<sup>17</sup>. How DC signals can be reconciled with our demonstration that T4 and T5 responses are fully polarity specific remains unclear. In particular, theoretical considerations on the basis of the response properties of Mi1 and Tm3 predict sensitivity to OFF edges for T4 (ref. 24). This is not borne out by our experiments (Fig. 3).

Theoretical studies have proposed that responding to higher order correlations allows motion detectors to exploit natural ON-OFF asymmetries<sup>12,14</sup>. The asymmetry between ON and OFF pathways reported here does indeed confer sensitivity to triple correlations. Only under the assumption that ON and OFF steps are processed equally do spurious two-point correlations vanish. However, whether *Drosophila*'s higher order motion responses are an epiphenomenon of detector asymmetries or whether detector asymmetry represents a way of accessing higher order correlations is up for debate. Moreover, it remains to be seen whether the findings at hand generalize to other forms of higher order motion perceived by *Drosophila*<sup>38</sup>.

Our previous characterization of cell types T4 and T5 revealed only minor differences in temporal frequency tuning for gratings<sup>21</sup>. It is currently not well understood how physiological tuning curves for edges and gratings relate to each other. Given the drastically different

# Asymmetry of *Drosophila* ON and OFF motion detectors enhances real-world velocity estimation

## ARTICLES

kinetics of the two stimuli, large ON-OFF differences for one may lead to only small ON-OFF differences for the other. In addition, we suggest that edges provide a better approximation of visual kinetics in the real world than artificial gratings that are periodic as well as constant in mean luminance, contrast and geometry. Moreover, measurements from tangential cells in behaving flies have indicated grating response optima that are shifted toward higher frequencies compared with quiescence<sup>26,39,40</sup>. How this state dependency translates to the tuning for edge velocity is unclear. Indeed, our linear prediction of opposing edge responses from physiological edge tuning underestimates the true crossing point between ON and OFF dominance (Fig. 4d). A shift toward higher preferred velocities, as observed for grating optima, could account for this discrepancy. Notably, our behavioral data demonstrate that basic characteristics of temporal ON-OFF asymmetries are preserved in active flies.

The ON-OFF asymmetry we describe represents one of many examples for the adaptation of sensory systems to the environment in which they evolved<sup>5,6,13,41</sup>. Contrast asymmetries between ON and OFF are a widespread feature shared by most visual niches. It therefore seems probable that the sensory asymmetries found in *Drosophila* are conserved across species. ON-OFF divergence has previously been described for several computations in vertebrate visual systems<sup>42–44</sup>. It will be interesting to examine the effects on optimal tuning exerted by features of the mammalian retina, such as contrast normalization<sup>45</sup>. Finally, motion energy models have been successfully used to explain the psychophysics of motion perception in higher organisms<sup>46</sup>. Given that Hassenstein-Reichardt detectors and motion energy models are generally mathematically equivalent<sup>47</sup>, our optimization results could also emerge for an appropriately rectified ON-OFF motion energy detector.

T4 and T5 are critically involved in behaviors other than the optomotor response. Recently, studies have implicated motion detectors in object fixation<sup>27</sup>, depth perception<sup>48</sup> or looming responses<sup>49</sup>. Given the variety of tasks and resulting visual statistics, optimal tuning needs to be examined under various constraints. Finally, we believe this ecological perspective on biological motion detection could have a decisive role in the continued mapping of the fly visual system. The abundance of information-bearing features in natural visual scenes may necessitate complex filter banks and multi-cell processing stages<sup>17,20,23,50</sup>. Real-world demands will then be critical constraints when assigning function to cells in the *Drosophila* optic lobe.

## METHODS

Methods and any associated references are available in the [online version of the paper](#).

Note: Any Supplementary Information and Source Data files are available in the [online version of the paper](#).

## ACKNOWLEDGMENTS

A. Nern and G.M. Rubin (Janelia Research Campus) generated and kindly provided the splitGal4 line targeting T4 and T5. We are grateful for fly work and behavioral experiments performed by R. Kutlesa, C. Theile and W. Essbauer. We thank A. Arenz and A. Mauss for carefully reading the manuscript, T. Schilling for fly illustrations, and all of the members of the Borst laboratory for extensive discussions. The Bernstein Center for Computational Neuroscience Munich supplied computing resources for our simulations. A.L., G.A., M.M., E.S., A. Bahl and A. Borst are members of the Graduate School for Systemic Neurosciences, Munich.

## AUTHOR CONTRIBUTIONS

A.L., G.A. and A. Borst designed the study. A.L. performed behavioral experiments, associated data analysis and all modeling work. G.A., M.M. and E.S. performed electrophysiological experiments. G.A. performed calcium imaging. A.L. and

G.A. analyzed physiological data. A. Bahl designed the behavioral apparatuses and performed behavioral experiments. A.L. wrote the manuscript with help from all of the authors.

## COMPETING FINANCIAL INTERESTS

The authors declare no competing financial interests.

Reprints and permissions information is available online at <http://www.nature.com/reprints/index.html>.

1. Borst, A. Fly visual course control: behavior, algorithms and circuits. *Nat. Rev. Neurosci.* **15**, 590–599 (2014).
2. Ruderman, D.L. & Bialek, W. Statistics of natural images: Scaling in the woods. *Phys. Rev. Lett.* **73**, 814–817 (1994).
3. Simoncelli, E.P. & Olshausen, B.A. Natural image statistics and neural representation. *Annu. Rev. Neurosci.* **24**, 1193–1216 (2001).
4. Field, D.J. Relations between the statistics of natural images and the response properties of cortical cells. *J. Opt. Soc. Am. A* **4**, 2379–2394 (1987).
5. Laughlin, S. A simple coding procedure enhances a neuron's information capacity. *Z. Naturforsch. C* **36**, 910–912 (1981).
6. van Hateren, J.H. & van der Schaaf, A. Independent component filters of natural images compared with simple cells in primary visual cortex. *Proc. Biol. Sci.* **265**, 359–366 (1998).
7. Yu, Y., Schmid, A.M. & Victor, J.D. Visual processing of informative multipoint correlations arises primarily in V2. *eLife* **4**, e06604 (2015).
8. Gjorgjieva, J., Sompolinsky, H. & Meister, M. Benefits of pathway splitting in sensory coding. *J. Neurosci.* **34**, 12127–12144 (2014).
9. Borst, A. & Helmstaedter, M. Common circuit design in fly and mammalian motion vision. *Nat. Neurosci.* **18**, 1067–1076 (2015).
10. Eichner, H., Joesch, M., Schnell, B., Reiff, D.F. & Borst, A. Internal structure of the fly elementary motion detector. *Neuron* **70**, 1155–1164 (2011).
11. Hassenstein, B. & Reichardt, W. Systemtheoretische Analyse der Zeit-, Reihenfolgen- und Vorzeichenbewertung bei der Bewegungsperzeption des Rüsselkäfers *Chlorophanus*. *Z. Naturforsch. B* **11**, 513–524 (1956).
12. Clark, D.A. et al. Flies and humans share a motion estimation strategy that exploits natural scene statistics. *Nat. Neurosci.* **17**, 296–303 (2014).
13. Ratliff, C.P., Borghuis, B.G., Kao, Y.-H., Sterling, P. & Balasubramanian, V. Retina is structured to process an excess of darkness in natural scenes. *Proc. Natl. Acad. Sci. USA* **107**, 17368–17373 (2010).
14. Fitzgerald, J.E., Katsov, A.Y., Clandinin, T.R. & Schnitzer, M.J. Symmetries in stimulus statistics shape the form of visual motion estimators. *Proc. Natl. Acad. Sci. USA* **108**, 12909–12914 (2011).
15. Hu, Q. & Victor, J.D. A set of high-order spatiotemporal stimuli that elicit motion and reverse-phi percepts. *J. Vis.* **10**, 9.1–9.16 (2010).
16. Takemura, S.-Y. et al. A visual motion detection circuit suggested by *Drosophila* connectomics. *Nature* **500**, 175–181 (2013).
17. Shinomiya, K. et al. Candidate neural substrates for off-edge motion detection in *Drosophila*. *Curr. Biol.* **24**, 1062–1070 (2014).
18. Joesch, M., Schnell, B., Raghu, S.V., Reiff, D.F. & Borst, A. ON and OFF pathways in *Drosophila* motion vision. *Nature* **468**, 300–304 (2010).
19. Clark, D.A., Bursztyn, L., Horowitz, M.A., Schnitzer, M.J. & Clandinin, T.R. Defining the computational structure of the motion detector in *Drosophila*. *Neuron* **70**, 1165–1177 (2011).
20. Silies, M. et al. Modular use of peripheral input channels tunes motion-detecting circuitry. *Neuron* **79**, 111–127 (2013).
21. Maisak, M.S. et al. A directional tuning map of *Drosophila* elementary motion detectors. *Nature* **500**, 212–216 (2013).
22. Meier, M. et al. Neural circuit components of the *Drosophila* OFF motion vision pathway. *Curr. Biol.* **24**, 385–392 (2014).
23. Ammer, G., Leonhardt, A., Bahl, A., Dickson, B.J. & Borst, A. Functional specialization of neural input elements to the *Drosophila* ON motion detector. *Curr. Biol.* **25**, 2247–2253 (2015).
24. Behnia, R., Clark, D.A., Carter, A.G., Clandinin, T.R. & Desplan, C. Processing properties of ON and OFF pathways for *Drosophila* motion detection. *Nature* **512**, 427–430 (2014).
25. Haikala, V., Joesch, M., Borst, A. & Mauss, A.S. Optogenetic control of fly optomotor responses. *J. Neurosci.* **33**, 13927–13934 (2013).
26. Schnell, B., Weir, P.T., Roth, E., Fairhall, A.L. & Dickinson, M.H. Cellular mechanisms for integral feedback in visually guided behavior. *Proc. Natl. Acad. Sci. USA* **111**, 5700–5705 (2014).
27. Bahl, A., Ammer, G., Schilling, T. & Borst, A. Object tracking in motion-blind flies. *Nat. Neurosci.* **16**, 730–738 (2013).
28. Joesch, M., Plett, J., Borst, A. & Reiff, D.F. Response properties of motion-sensitive visual interneurons in the lobula plate of *Drosophila melanogaster*. *Curr. Biol.* **18**, 368–374 (2008).
29. Warzecha, A.-K. & Egelhaaf, M. Intrinsic properties of biological motion detectors prevent the optomotor control system from getting unstable. *Phil. Trans. R. Soc. Lond. B* **351**, 1579–1591 (1996).
30. Schnell, B., Raghu, S.V., Nern, A. & Borst, A. Columnar cells necessary for motion responses of wide-field visual interneurons in *Drosophila*. *J. Comp. Physiol. A Neuroethol. Sens. Neural Behav. Physiol.* **198**, 389–395 (2012).



# Asymmetry of *Drosophila* ON and OFF motion detectors enhances real-world velocity estimation

## ARTICLES

31. Brand, A.H. & Perrimon, N. Targeted gene expression as a means of altering cell fates and generating dominant phenotypes. *Development* **118**, 401–415 (1993).
32. Sweeney, S.T., Broadie, K., Keane, J., Niemann, H. & O’Kane, C.J. Targeted expression of tetanus toxin light chain in *Drosophila* specifically eliminates synaptic transmission and causes behavioral defects. *Neuron* **14**, 341–351 (1995).
33. Straw, A.D., Rainsford, T. & O’Carroll, D.C. Contrast sensitivity of insect motion detectors to natural images. *J. Vis.* **8**, 32.1–32.9 (2008).
34. Chen, T.-W. *et al.* Ultrasensitive fluorescent proteins for imaging neuronal activity. *Nature* **499**, 295–300 (2013).
35. Mauss, A.S. *et al.* Neural circuit to integrate opposing motions in the visual field. *Cell* **162**, 351–362 (2015).
36. Tuthill, J.C., Chiappe, M.E. & Reiser, M.B. Neural correlates of illusory motion perception in *Drosophila*. *Proc. Natl. Acad. Sci. USA* **108**, 9685–9690 (2011).
37. Dror, R.O., O’Carroll, D.C. & Laughlin, S.B. Accuracy of velocity estimation by Reichardt correlators. *J. Opt. Soc. Am. A Opt. Image Sci. Vis.* **18**, 241–252 (2001).
38. Theobald, J.C., Duistermars, B.J., Ringach, D.L. & Frye, M.A. Flies see second-order motion. *Curr. Biol.* **18**, R464–R465 (2008).
39. Jung, S.N., Borst, A. & Haag, J. Flight activity alters velocity tuning of fly motion-sensitive neurons. *J. Neurosci.* **31**, 9231–9237 (2011).
40. Chiappe, M.E., Borst, A. & Jayaraman, V. Walking modulates speed sensitivity in *Drosophila* motion vision. *Curr. Biol.* **20**, 1470–1475 (2010).
41. Dyakova, O., Lee, Y.-J., Longden, K.D., Kiselev, V.G. & Nordström, K. A higher order visual neuron tuned to the spatial amplitude spectra of natural scenes. *Nat. Commun.* **6**, 8522 (2015).
42. Komban, S.J. *et al.* Neuronal and perceptual differences in the temporal processing of darks and lights. *Neuron* **82**, 224–234 (2014).
43. Chichilnisky, E.J. & Kalmar, R.S. Functional asymmetries in ON and OFF ganglion cells of primate retina. *J. Neurosci.* **22**, 2737–2747 (2002).
44. Pandarinath, C., Victor, J.D. & Nirenberg, S. Symmetry breakdown in the ON and OFF pathways of the retina at night: functional implications. *J. Neurosci.* **30**, 10006–10014 (2010).
45. Carandini, M. & Heeger, D.J. Normalization as a canonical neural computation. *Nat. Rev. Neurosci.* **13**, 51–62 (2012).
46. Adelson, E.H. & Bergen, J.R. Spatiotemporal energy models for the perception of motion. *J. Opt. Soc. Am. A* **2**, 284–299 (1985).
47. van Santen, J.P. & Sperling, G. Elaborated Reichardt detectors. *J. Opt. Soc. Am. A* **2**, 300–321 (1985).
48. Schwegmann, A., Lindemann, J.P. & Egelhaaf, M. Depth information in natural environments derived from optic flow by insect motion detection system: a model analysis. *Front. Comput. Neurosci.* **8**, 83 (2014).
49. Schilling, T. & Borst, A. Local motion detectors are required for the computation of expansion flow-fields. *Biol. Open* **4**, 1105–1108 (2015).
50. Burge, J. & Geisler, W.S. Optimal speed estimation in natural image movies predicts human performance. *Nat. Commun.* **6**, 7900 (2015).



# Asymmetry of *Drosophila* ON and OFF motion detectors enhances real-world velocity estimation

## ONLINE METHODS

**Fly strains and genetics.** We raised *Drosophila melanogaster* on cornmeal-agar medium under standard conditions (60% humidity, 18 °C for behavioral and 25 °C for physiology experiments, 12-h light/12-h dark schedule) for the full duration of their developmental cycle. Female flies were used in all experiments. For physiological experiments, we selected flies 5–20 h post-eclosion. Flies in behavioral experiments were 1–3 d old. Behavioral experiments targeting T4 or T5 used the following driver lines, as described previously<sup>21</sup>: T4-Gal4 (VT37588) and T5-Gal4 (R42H07). When targeting T4 and T5 simultaneously, we employed a new, highly specific driver line: T4/T5-splitGal4 (R59E08-AD; R42F06-DBD), kindly provided to us by A. Nern and G.M. Rubin at Janelia Research Campus. For visualization of expression patterns (Supplementary Fig. 1), we crossed driver lines to UAS-mCD8GFP reporter flies. For experiments, Gal4 flies were then crossed to either wild type Canton S flies or UAS-TNT-E flies resulting in Gal4 control or block flies, respectively. Crossing UAS-TNT-E flies to Canton S flies generated UAS control flies. For calcium imaging, we combined two different Gal4 lines (VT25965 and VT37588) that in conjunction expressed at comparable levels in T4 and T5. These were crossed to UAS-GCaMP6f<sup>34</sup> flies. Genotypes derived from these crossings and their aliases as used throughout the text are listed in the supplementary material (Supplementary Table 1).

**Immunohistochemistry.** Antibody stainings (Supplementary Fig. 1) were performed as described previously<sup>51</sup>. We used the following antibodies and dilutions. Primary antibodies: rabbit anti-GFP (Torri Pines, TP401, 1:2,000), mouse anti-nc82 (DSHB, AB\_2314866, 1:25); secondary antibodies: goat anti-rabbit 488 (Invitrogen, A-11008, 1:500), goat anti-mouse 633 (Invitrogen, A-21053, 1:500). Imaging was performed on a SP5 confocal microscope (Leica) at a resolution of 1,024 × 1,024. Images were processed in ImageJ 1.46f (US National Institutes of Health). Single z-slices are shown for horizontal views.

**Behavioral experiments.** We performed behavioral experiments as described previously<sup>21,23,27</sup>. Briefly, tethered flies were placed on an air-suspended polyurethane ball in a virtual environment consisting of three computer screens covering a substantial part of the animal's visual field (approximately 270° in azimuth and 120° in elevation). Experiments were run on six set-ups in parallel; two of them displayed visual stimuli at 120 Hz and the remaining four at 144 Hz with all screens calibrated to display at comparable contrast and brightness. We never observed any differences in behavior between refresh rates. All stimuli were rendered in real-time using the graphics engine Panda3D, allowing visual feedback based on flies' instantaneous walking behavior. Due to high pixel density on all computer screens, stimulus pixel size was well below the resolution limit of *Drosophila*. The immediate surround of the ball was temperature-controlled by means of a closed-loop thermoregulation system. Each experiment used the same temperature protocol: Temperature was kept at 25 °C for the first 5 min and then linearly raised to 34 °C within 10 min.

All behavioral experiments ran for 60–90 min and comprised 50–60 repeated trials, except for open-loop velocity estimation experiments (Fig. 2) that lasted 280 trials. In each trial, we randomized stimulus presentation order. Movement of the ball was tracked at 4 kHz and down-sampled to 20 Hz for offline analysis. For each fly, we manually selected a continuous range of 100–200 (Fig. 2) or 25 trials (other experiments) based on the following criteria: First, the temperature was at a constant 34 °C. Second, the average forward walking speed of the fly was above 0.3 cm s<sup>-1</sup>, indicating healthy locomotion and visual responsiveness. Third, the average turning tendency of the fly was stable and close to 0° s<sup>-1</sup>. These criteria excluded approximately 20% of all flies we measured. During analysis, we averaged traces across trials, resulting in a single walking trace per fly per experimental condition. Where applicable (Figs. 1, 4 and 8, and Supplementary Fig. 5), we then subtracted responses to mirror-symmetric stimulus presentations to minimize the impact of small rotational biases in turning behavior. Traces were filtered using a first-order low-pass filter ( $\tau = 100$  ms). In open-loop experiments (Fig. 2), we generated a regression model for each fly that mapped rotation of the environment to the turning response of the fly (averaged over 1 s after stimulus onset) using least-squares fitting. Response gain was then defined as the slope of this model. The intercepts clustered around 0° s<sup>-1</sup>, indicating trajectories that were on average straight. For additional analysis (Supplementary Fig. 3), we constructed Bayesian decoders that minimize the squared error of their estimates. This was done on a fly-by-fly basis. We first split the data set consisting of pairs of image

velocity and turning response as for the correlation analysis (Fig. 2) into training and test sets at a ratio of 3:1, approximated the posterior distribution through application of Bayes' rule to the joint probability generated from appropriate histograms, and estimated image velocity as the expected value of the posterior for a given response. Finally, we assessed decoding performance of resulting mapping functions by calculating the root-mean-square error after application to the test set. The behavioral data analysis pipeline was implemented in Python 2.7 using pandas 15.1, NumPy 1.6, SciPy 0.15, matplotlib 1.3 and Numba 0.18.

**Electrophysiology.** Electrophysiological *in vivo* patch-clamp recordings from lobula plate tangential cells closely followed previously described protocols<sup>21,22,28</sup>. Recordings were low-pass filtered with a cut-off frequency of 3 kHz and digitized at 10 kHz. Data acquisition was based on Matlab R2011A (MathWorks). We identified cell types based on their response profile when stimulated with moving gratings. In addition, cells were dye-filled and anatomically verified whenever possible.

We visually stimulated flies using a custom-built LED arena spanning approximately 180° in azimuth and 90° in elevation of the fly's visual field with a spatial resolution of 1.5° per individual LED. The LED refresh rate was in the kHz range; stimulus images were then updated with up to 600 Hz. Maximum luminance was 80 cd m<sup>-2</sup>. During offline data analysis, recorded traces were down-sampled to 2 kHz and averaged across 2–5 trials per cell. We randomized the order of stimulus presentation within trials. Cells that did not respond reliably to grating stimulation were excluded from further analysis. Before we extracted response maxima and minima for edge responses (Fig. 3), electrophysiological traces were filtered with a second-order Savitzky-Golay kernel that was 40 samples wide. The electrophysiological data analysis pipeline was implemented in Python 2.7 using pandas 15.1, NumPy 1.6, matplotlib 1.3 and Numba 0.18.

**Calcium imaging.** We employed a custom-built two-photon laser scanning microscope as described previously<sup>21,22</sup>. We prepared flies analogously to electrophysiology experiments. Images were recorded at a resolution of 256 × 128 pixels and a frame rate of 3.74 Hz. Raw images were then converted into relative fluorescence change ( $\Delta F/F$ ) series by using the mean of three frames before stimulation onset as a baseline. For summary images, the resulting images were averaged across time; for time-resolved traces, we defined relevant regions of interest and collapsed signals within the defined borders by averaging across pixels. We used the LED arena described above for visual stimulation. Data acquisition and analysis were performed in Matlab R2011a (MathWorks) using ScanImage 3.8.

**Image sets.** Two image sets were used throughout the study. First, for all behavioral experiments involving natural images, we generated a small library of 60 panoramic images spanning approximately 360° in azimuth using a consumer-grade camera (iPhone 5s; Apple). The resolution of each image was 10,800 × 2,460 pixels. Images were taken in various natural environments covering different visual statistics: woods (30%), open rural spaces (30%), urban landscapes (20%), and laboratories (20%). We used raw images without processing or calibration and converted them to gray scale by averaging across color channels. Critical image statistics such as RMS contrast (that is, the s.d. of pixel values), luminance distribution, and power spectrum were comparable to other scientific image libraries. Second, for all *in silico* experiments, we made use of calibrated images from the van Hateren natural image database<sup>6</sup>. No image category was excluded and we performed no further sorting, yielding 4,167 images at a resolution of 1,536 × 1,024 pixels. One pixel corresponded to one arc minute of visual angle. We normalized the set through subtraction of and division by the mean pixel value for each image<sup>12,45</sup>. Kernel density estimates (Figs. 2 and 6) were generated using a routine in the SciPy library. Gaussian kernels were used, and we determined bandwidth via Silverman's rule.

We scaled the contrast of our in-house image set by subtracting the image's mean luminance, applying the specified multiplicative factor, and then adding the initial mean luminance (Figs. 1 and 2). Phase-scrambling of the van Hateren image set was achieved by performing a Fourier transform, replacing the phase spectrum with that of a Gaussian random image of equal mean luminance, and finally recovering the phase-randomized image via the inverse Fourier transform (Fig. 6b). The luminance-remapped scrambled set was generated by replacing each pixel value of a phase-randomized image with the value corresponding to

# Asymmetry of *Drosophila* ON and OFF motion detectors enhances real-world velocity estimation

the same luminance-ordered rank in the original image (Fig. 6c). Analogously, we generated the luminance-remapped natural set by drawing pixel values from the corresponding phase-scrambled image (Fig. 6d).

**Visual stimuli.** On every trial of the closed-loop course stabilization experiment (Fig. 1), a random image was chosen from our in-house image library and projected onto a virtual cylinder surrounding the fly. In order to cover the visual field without significant distortion, the panorama was mirrored across the fly's elevation axis. Each trial lasted 5 s. The rotational component of the walking trajectory was used as a feedback signal for the azimuthal orientation of the virtual cylinder, effectively giving flies control over their angular orientation relative to the environment. Feedback gain was set to unity. Between 1.5 s and 3.5 s, we additionally rotated the virtual environment at a constant  $80^\circ \text{ s}^{-1}$  in clockwise or counter-clockwise direction. Contrast was scaled in accordance with the procedure described above to 12.5%, 25%, 50% and 100% of the original RMS value.

For open-loop velocity estimation experiments (Fig. 2), images were chosen and projected as above while feedback gain was set to zero. On each trial, a random velocity was drawn from a Gaussian distribution centered at  $0^\circ \text{ s}^{-1}$  with a s.d. of  $50^\circ \text{ s}^{-1}$ . Trials lasted 3.5 s. Between 1.5 s and 2 s, the virtual environment rotated with the constant velocity drawn earlier. The border where the image on the cylinder wrapped around was placed such that it remained in the back of the fly on most trials. Here, we added the 6% contrast condition.

We used single bright and dark edges for characterizing the physiological response properties of ON and OFF channels (Fig. 3). During electrophysiology experiments, we presented edges moving at 12 constant velocities across two orders of magnitude (6.25, 12.5, 25, 50, 75, 100, 150, 200, 300, 500, 700 and  $900^\circ \text{ s}^{-1}$ ). When recording from vertical system or horizontal system cells, edges traveled along the vertical or horizontal axis, respectively, and in the preferred direction of the cell. Edges used during calcium imaging always moved at  $25^\circ \text{ s}^{-1}$  and either downwards or from front to back (no differences between the two directions were observed). Physiology stimuli (Fig. 3) had a Michelson contrast of 100%, starting from either a dark (ON) or bright (OFF) background. For additional experiments (Supplementary Fig. 4), edges started from an equal background luminance of  $10.7 \text{ cd m}^{-2}$ . As the stimulation device only allowed discrete steps, ON edges then had a contrast of 76% and OFF edges a contrast of 100%.

The behavioral balanced motion stimulus resembled previous iterations<sup>19,21,23</sup>. Briefly, we presented flies with a stationary square wave grating that had an initial spatial wavelength of  $45^\circ$  and Michelson contrast of 50%. Each individual trial lasted 9 s. Between 2 s and 7 s, bright and dark edges moved in opposite directions at the same velocity. In contradistinction to previous experiments, we reset the stimulus to the initial state after edges had traversed  $20^\circ$  of visual angle, allowing us to keep stimulus duration fixed regardless of edge velocity. After each reset, we applied a random phase shift in order to minimize the effect of initial grating position relative to the fly. This was done for six velocities (20, 40, 80, 160, 320 and  $640^\circ \text{ s}^{-1}$ ) in clockwise and counter-clockwise direction. Pulse experiments (Supplementary Fig. 5) were performed analogously, with edge movement being limited to the indicated duration (500 ms, 250 ms or 100 ms).

Glider experiments (Figs. 7 and 8) were performed as described previously<sup>12</sup>. Briefly, the visual field was divided into vertical stripes that had an azimuthal extent of  $6^\circ$  (behavior) or  $4.5^\circ$  (electrophysiology). Each bar could either be dark or bright; Michelson contrast for these experiments was 50% (behavior) or 100% (electrophysiology). Initial bars were seeded with a random binary pattern. Depending on the glider, bars were then updated according to the corresponding deterministic rule. The glider update frequency was either 24 Hz (behavior) or 10 Hz (electrophysiology). For electrophysiological experiments, we used a single pre-generated glider sequence. Here, preferred direction was defined as the update direction that would depolarize cells for two-point gliders.

**Modeling.** The ON-OFF detector used in this study (Figs. 5, 6 and 8) was derived from a previously published two-quadrant model<sup>10</sup>. Briefly, we modeled photoreceptor signals as time series with a resolution of 10 ms (for optimization experiments) or 1 ms (for other experiments) per step. Lamina processing was then approximated as the linear sum of a high-pass-filtered signal (first-order RC filter with  $\tau = 250 \text{ ms}$ ) and an unfiltered tonic component (DC) with variable weight. This was followed by a half-wave rectification step. For the pure ON detector, signals were rectified with the threshold set to exactly zero. For the pure OFF detector, the signal was inverted and then rectified with the threshold set to exactly

zero. Further processing was identical for both: The signal was first-order low-pass filtered with variable time constant  $\tau$  and then multiplied with an unfiltered signal from the other spatial location. This was done twice in a mirror-symmetrical fashion, followed by subtraction, yielding a fully opponent direction-selective signal. For the full ON-OFF detector, an ON detector and an OFF detector were summed with equal weight. Unlike previous versions<sup>10</sup>, our simplified detector did not make use of shifted rectification thresholds or unequally weighted detector halves. Outside of natural image experiments, stimuli were rendered at a spatial resolution of  $0.1^\circ$ . We modeled the spatial acceptance profile of photoreceptors as Gaussians with a half-width at maximum of  $5^\circ$ . The symmetric detectors (Figs. 5 and 8) had, by definition, zero DC component and identical filter time constants for the ON and the OFF channel as determined by the optimization procedure. The asymmetric detector had DC components and time constants that were allowed to differ between ON and OFF during optimization.

The detector characterization (Fig. 5) depicts results from a combination of 20 detectors separated by  $6.5^\circ$ . The spatial wavelength of all gratings was  $20^\circ$  with velocity being defined by temporal frequency. Simulations for grating and edge tunings ran for 10 s each; output was averaged across detectors and time. For the velocity profile (Fig. 5g), we used a time series drawn from a Gaussian distribution with s.d. =  $20^\circ \text{ s}^{-1}$  that was first-order low-pass filtered with  $\tau = 500 \text{ ms}$ . Units were discarded for display purposes. Modeled edge stimuli lasted for 15 s, with movement starting after 2 s. The starting condition was fixed at 1.0 and followed by a jump to 1.2 for ON edges or 0.8 for OFF edges. Detector output was averaged for the duration of edge motion, which depended on velocity. We simulated 50 velocities on a logarithmic scale from  $10^\circ \text{ s}^{-1}$  to  $1,000^\circ \text{ s}^{-1}$ . Glider stimuli (Fig. 8) were rendered as idealized signals mapping 21 virtual stripes to the 21 virtual photoreceptors of an array of 20 detectors, without any spatial overlap. The array was seeded with a random combination of binary dark and bright values (arbitrarily defined as 1.0 and 3.0, respectively) and then updated according to previously described rules<sup>12</sup> at a frequency of 5 Hz. Glider simulations ran for 5 s each and were averaged across 500 instantiations and time (Fig. 8f–i). We approximated compressive characteristics of the visuo-motor transformation by multiplying two-point and three-point responses with slightly different gain values ( $2,500^\circ \text{ s}^{-1}$  and  $3,500^\circ \text{ s}^{-1}$ , respectively) when translating detector output into turning tendency. All simulations were implemented in Python 2.7 using NumPy 1.6 and Numba 0.18.

**Detector optimization.** Optimization of detector models was based on an exhaustive cross-validated search on a two-dimensional parameter grid. We generated 50 random training-to-test splits from the 4,167 images of the van Hateren data set with a training-to-test ratio of 4:1. All images received a luminance bias of 3.0 and were clipped at zero in order to ensure that only positive signals arrived at detector inputs while keeping mean values constant. The optimization procedure was then performed independently for each training fold.

We scanned a parameter space comprising  $40 \times 21$  combinations of low-pass time constants (from 10 to 400 ms in 10-ms steps) and DC contribution (from  $-20\%$  to  $+20\%$  in 2% steps). For each parameter set, three detectors with the corresponding parameter settings were simulated: a pure ON detector, a pure OFF detector, and a symmetric ON-OFF detector where ON and OFF channels used the same parameters. Fitness of a given detector was determined as follows, based on previous studies<sup>12</sup> and analogously to behavioral experiments (Fig. 2): on each iteration, we drew a random image from the training set and a random velocity from a Gaussian distribution centered at zero with s.d. =  $25^\circ \text{ s}^{-1}$ . We then generated two time series corresponding to a simulated pair of photoreceptors separated by  $6.5^\circ$  traveling across the horizontal middle row of the image at the constant velocity drawn before and for a duration of 1,000 ms. The signals were fed into each of the three detectors. Detector output was averaged across time. We repeated this procedure 50,000 times per parameter set. Detector fitness was then defined as the Pearson correlation between input velocity and average detector output. During testing, we assembled two detectors per test set. The optimal symmetric detector was the best-performing detector constrained to use equal ON and OFF settings and zero DC. The optimal asymmetric detector was the linear combination of the best performing ON detector and the best performing OFF detector. The performance of both was then evaluated on the corresponding test set; here, detector evaluations were repeated 100,000 times. This was done for the natural, phase-scrambled and luminance-remapped image sets.

# Asymmetry of *Drosophila* ON and OFF motion detectors enhances real-world velocity estimation

---

We implemented the optimization procedure in Python 2.7 using NumPy 1.6, SciPy 0.15, Numba 0.18, and IPython 3.0. Parallel operations were distributed across 128 CPUs on a Beowulf cluster consisting of eight physical machines.

**Code availability.** Python and Matlab code used throughout analysis, modeling, and optimization is available upon request to the authors.

**Statistics.** All statistical tests were two-tailed Student's *t* tests at a significance level of 0.05, assuming unequal variance unless stated otherwise. Where necessary, conservative Bonferroni correction was applied in order to correct for multiple hypothesis testing. Normality of data was confirmed visually and not formally tested. We did not predetermine sample sizes using statistical tests, but numbers

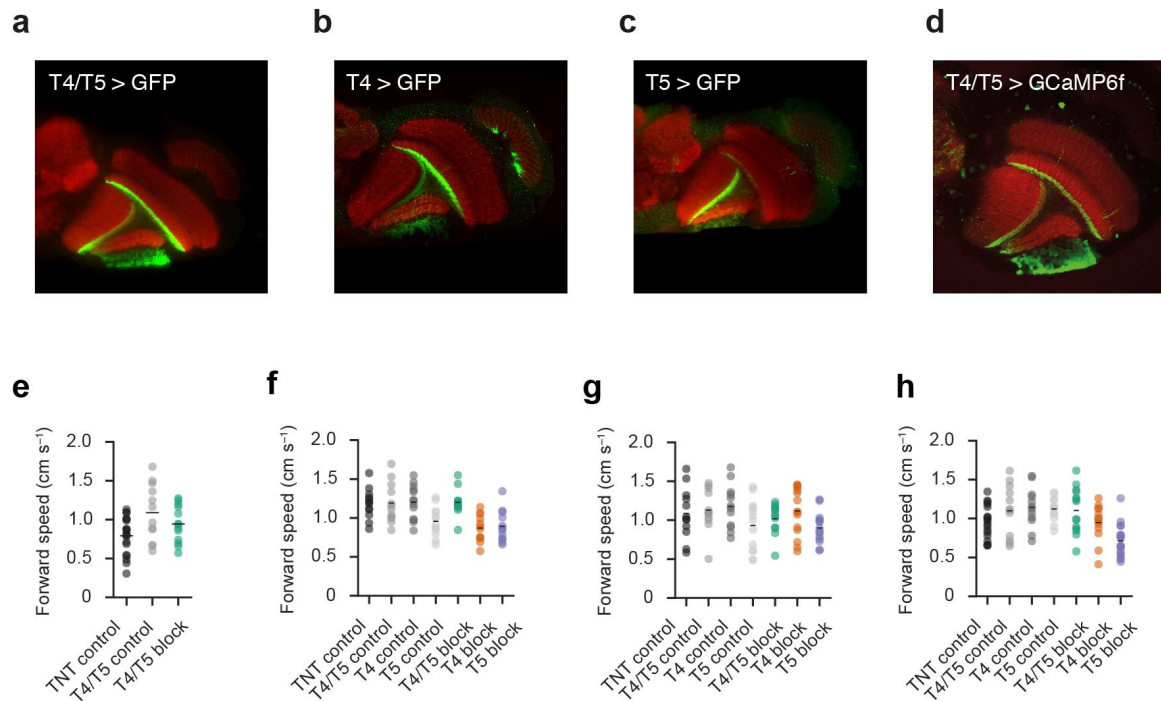
are in line with established work<sup>12,20,21,23,27</sup>. Our confidence intervals were computed according to a bootstrapping procedure based on 1,000 re-samplings of the data set. We did not differentiate levels of significance; only single asterisks are used regardless of *P* value. Statistical procedures were used as implemented in SciPy 0.15. All experiments and data analysis were performed without blinding to conditions or genotypes.

A **Supplementary Methods Checklist** is available.

51. Yu, J.Y., Kanai, M.I., Demir, E., Jefferis, G.S.X.E. & Dickson, B.J. Cellular organization of the neural circuit that drives *Drosophila* courtship behavior. *Curr. Biol.* **20**, 1602–1614 (2010).



## Asymmetry of *Drosophila* ON and OFF motion detectors enhances real-world velocity estimation

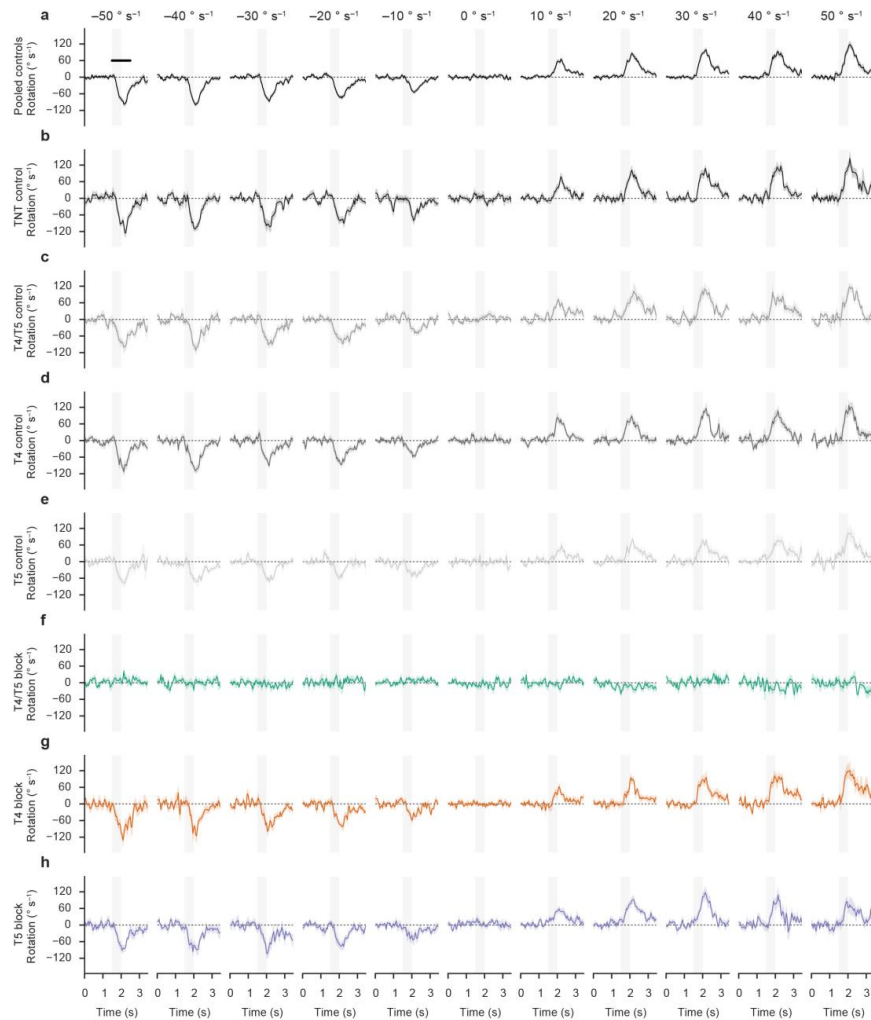


Supplementary Figure 1

### Auxiliary data for Gal4 lines used throughout the study.

(a-d) UAS-mCD8GFP or UAS-GCaMP6f were driven by Gal4 driver lines used throughout the text and visualized using confocal images of the optic lobe. (a) GFP expression of splitGal4 line labeling T4 and T5. (b) GFP expression of Gal4 line labeling T4. (c) GFP expression of Gal4 line labeling T5. (d) GCaMP6f expression of combined Gal4 line labeling T4 and T5. See Online Methods for Gal4 line names and details of the immunohistochemistry procedures. (e-h) Locomotor integrity for each behavioral experiment was quantified as the mean forward velocity across conditions, with values close to control level indicating a general ability to respond to visual stimuli. (e) Walking speeds for closed-loop experiments (Fig. 1). (f) Walking speeds for open-loop experiments (Fig. 2). (g) Walking speeds for opposing edge experiments (Fig. 4). (h) Walking speeds for glider experiments (Fig. 8). Dots represent individual flies. Black bars mark the group mean for each genotype.

# Asymmetry of *Drosophila* ON and OFF motion detectors enhances real-world velocity estimation

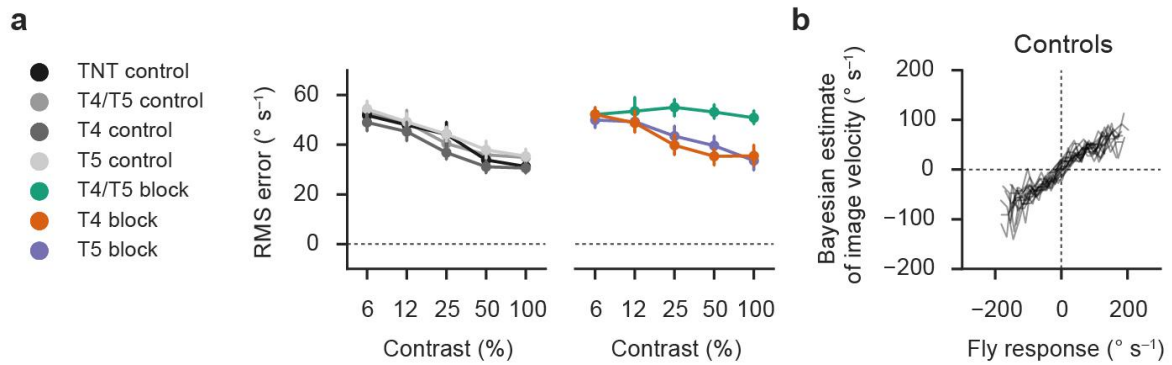


Supplementary Figure 2

## Walking traces for open-loop velocity estimation experiment.

Binned response traces for all genotypes used throughout the stochastic open loop velocity estimation experiment (Fig. 2). In order to generate velocity-specific traces, stimulus velocities were sorted into bins spanning  $5^\circ \text{ s}^{-1}$  centered about the value indicated above each column. The corresponding traces were then averaged for each fly. Shaded areas indicate the bootstrapped 68% confidence interval across flies ( $N$  as in main figure; Fig. 2). Nota bene, traces were not low-pass filtered and the sampling base for each fly decreases with distance from zero velocity due to the stimulus distribution. The black line in the top leftmost panel indicates the period over which we averaged in order to generate responses for main experiment (Fig. 2). See Online Methods for details. (a) Responses for pooled controls as in main experiment (Fig. 2b). (b-h) Responses for individual genotypes.

## Asymmetry of *Drosophila* ON and OFF motion detectors enhances real-world velocity estimation

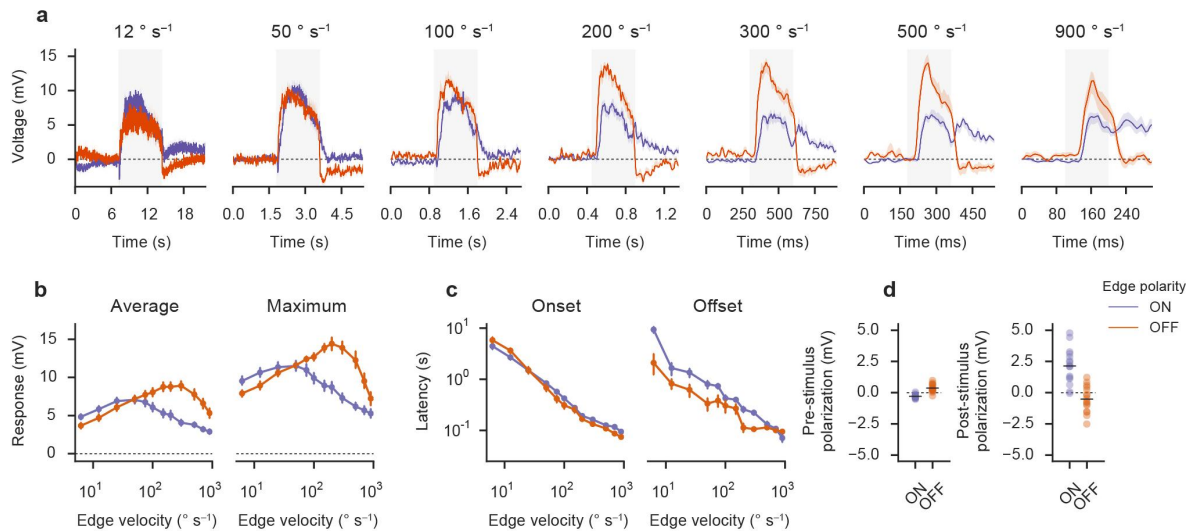


Supplementary Figure 3

### Bayesian analysis of open-loop behavioral data.

Using open-loop behavioral data (Fig. 2), we generated Bayesian decoders according to the procedure outlined in the Online Methods. For details about quantification and subject numbers, refer to main experiment (Fig. 2). (a) Mapping error across image contrast values, quantified as the root-mean-square error after application to the test data set. With higher contrasts, the quality of the estimate improves; this resembles results based on linear correlation. For T4/T5 block flies, the error stays flat. T4 or T5 block cannot be distinguished from wild-type behavior. (b) Visualization of resulting mapping functions, transforming fly responses into Bayesian estimates of input image velocity. Each line corresponds to a single fly. No significance tests were performed.

## Asymmetry of *Drosophila* ON and OFF motion detectors enhances real-world velocity estimation



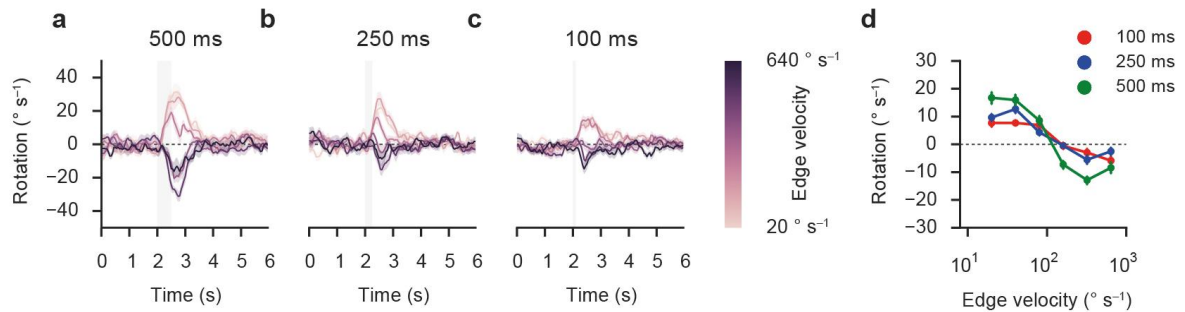
Supplementary Figure 4

### Physiological edge velocity tuning for fixed starting luminance.

Lobula plate tangential cell responses to ON and OFF edges for equalized initial mean luminance ( $N=16$  by pooling 12 vertical system/4 horizontal system cells). See legend of main experiment (Fig. 3) as well as Online Methods for details. (a) Response traces for edges moving at various velocities. Note that the timescale depends on edge velocity. (b) Quantification of velocity tuning. (c) Quantification of response dynamics (with latency being defined as the time to maximal response during stimulation for onset or time to minimal response after stimulation for offset). (d) Quantification of polarization before and after stimulus presentation. No significance tests were performed.



## Asymmetry of *Drosophila* ON and OFF motion detectors enhances real-world velocity estimation

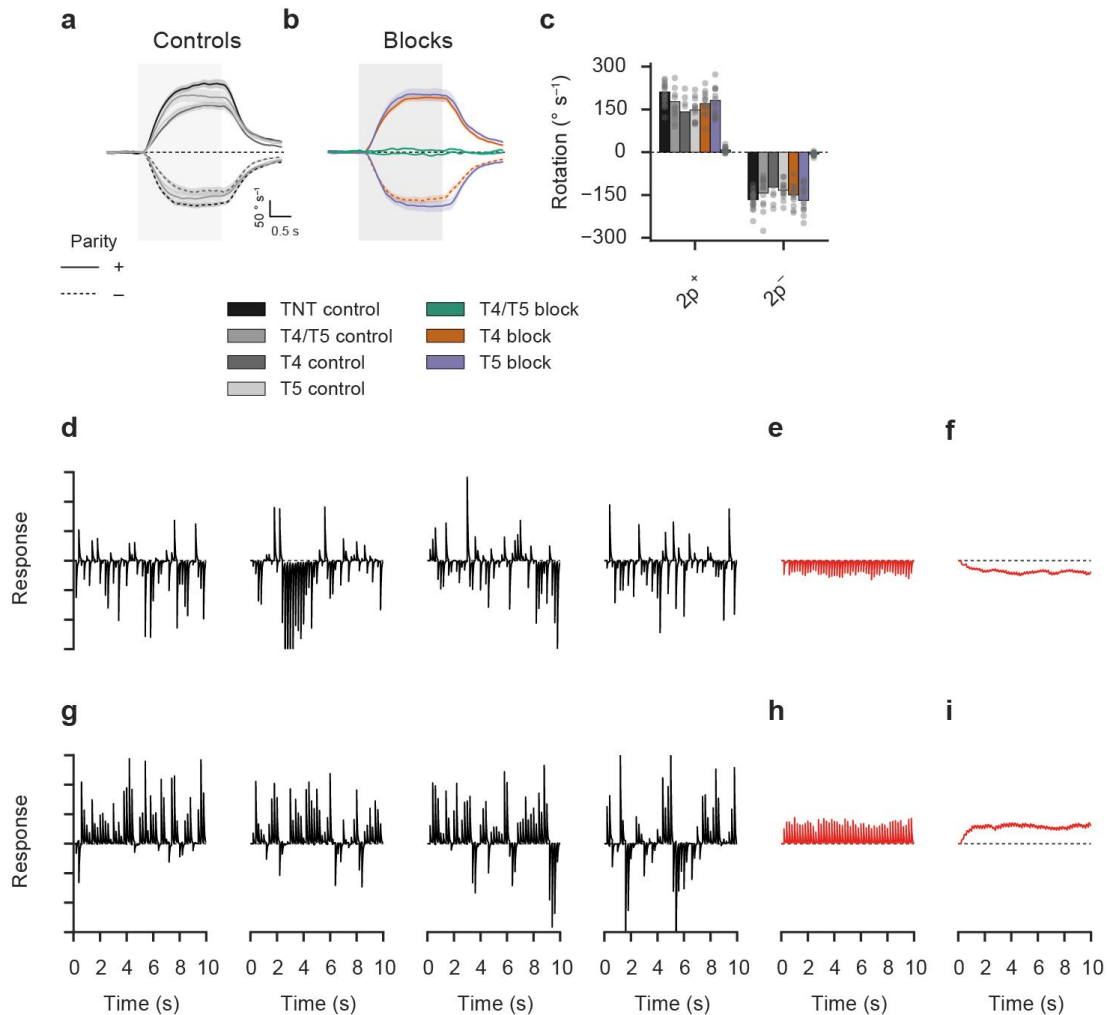


Supplementary Figure 5

### Opposing edge responses for varying stimulus durations.

Presentation and quantification are analogous to main experiment (Fig. 4; see Online Methods and associated legend for details). Depicted flies were T4/T5 control flies. (a-c) Turning responses for edge pulses of 500 ms ( $N=12$ ), 250 ms ( $N=12$ ), and 100 ms ( $N=14$ ) duration, respectively. (d) Quantification of turning responses.

# Asymmetry of *Drosophila* ON and OFF motion detectors enhances real-world velocity estimation



Supplementary Figure 6

## Extended data for higher-order motion experiments and simulations.

(a-c) T4 block flies and T5 block flies show 2-point glider responses at control level. (a) Control responses for 2-point gliders of positive or negative parity. (b) Block fly responses. (c) Summary of average turning tendency. Shaded area indicates stimulation period (see Online Methods and legend of main experiment for details; Fig. 8). (d-i) Time- and instantiation-resolved output of the asymmetric detector for converging 3-point gliders. Black traces are arbitrarily scaled detector responses for five random starting conditions of the pattern. (d) Single traces for positive parity. (e) Average time-resolved output for positive parity across 100 instantiations of the stimulus. (f) Low-pass filtered trace from e (first order with time constant of 500 ms followed by multiplicative scaling with a factor of four, approximating the behavioral response). (g) Single traces for negative parity. (h) Average time-resolved output for negative parity across 100 instantiations of the stimulus. (i) Low-pass filtered and scaled trace from h (procedure as in f).

Asymmetry of *Drosophila* ON and OFF motion detectors enhances real-world velocity estimation

---

Supplementary Table 1

Alias	Genotype	Experiments
<b>T4/T5 block</b>	w <sup>+</sup> /w <sup>-</sup> ; UAS-TNT-E/Gal4-R59E08-AD; +/Gal4-R42F06	Figs. 1, 2, 4, 8, S1, S2, S3, S6
<b>T4/T5 imaging</b>	w <sup>-</sup> ; UAS-GCaMP6f; Gal4-VT25965/Gal4-VT37588	Fig. 3, S1
<b>T4 block</b>	w <sup>+</sup> /w <sup>-</sup> ; UAS-TNT-E/+; +/Gal4-VT37588	Figs. 2, 4, 8, S1, S2, S3, S6
<b>T5 block</b>	w <sup>+</sup> /w <sup>-</sup> ; UAS-TNT-E/+; +/Gal4-R42H07	Figs. 2, 4, 8, S1, S2, S3, S6
<b>TNT control</b>	w <sup>+</sup> /w <sup>-</sup> ; UAS-TNT-E/+; +/+	Figs. 1, 2, 4, 8, S1, S2, S3, S6
<b>T4/T5 control</b>	w <sup>+</sup> /w <sup>-</sup> ; +/Gal4-R59E08-AD; +/Gal4-R42F06	Figs. 1, 2, 4, 8, S1, S2, S3, S5, S6
<b>T4 control</b>	w <sup>+</sup> /w <sup>-</sup> ; +/+; +/Gal4-VT37588	Figs. 2, 4, 8, S1, S2, S3, S6
<b>T5 control</b>	w <sup>+</sup> /w <sup>-</sup> ; +/+; +/Gal4-R42H07	Figs. 2, 4, 8, S1, S2, S3, S6
<b>Canton S</b>	w <sup>+</sup> ; +/+; +/+	Figs. 3, 7, S4

# Asymmetry of *Drosophila* ON and OFF motion detectors enhances real-world velocity estimation

Supplementary Table 2

12.5% contrast			25% contrast		
Genotype		T4/T5 block (n=13)	Genotype		T4/T5 block (n=13)
UAS control	n	19	UAS control	n	19
	t	9.27		t	12.2
	p	2.83e-10		p	3.89e-13
Gal4 control	n	12	Gal4 control	n	12
	t	11.2		t	16.4
	p	1.35e-9		p	3.75e-14

50% contrast			100% contrast		
Genotype		T4/T5 block (n=13)	Genotype		T4/T5 block (n=13)
UAS control	n	19	UAS control	n	19
	t	14.4		t	12.9
	p	4.55e-13		p	3.56e-12
Gal4 control	n	12	Gal4 control	n	12
	t	13.7		t	13.9
	p	1.47e-12		p	3.36e-12

**Extended statistics for Fig. 1.** For each contrast condition, we determined significance by comparing the block group to both control groups (UAS control and Gal4 control) using a two-tailed Student's *t* test. Blocks were declared significantly different if and only if both control groups were significantly different at a level of 0.05. For multiple comparisons, Bonferroni correction was applied. Red fields indicate significant differences after Bonferroni correction. The number indicated by n is the number of individual flies.

# Asymmetry of *Drosophila* ON and OFF motion detectors enhances real-world velocity estimation

Supplementary Table 3

Correlation coefficient (Fig. 2d)

Gain (Fig. 2e)

c = 6.25%	Genotype		T4/T5 block	T4 block	T5 block
			(n=11)	(n=12)	(n=12)
UAS control	n		12	12	12
	t		-3.98	0.673	-0.862
	p		7.06e-4	0.508	0.398
Gal4 control	n		12	13	12
	t		-6.20	-1.95	-0.923
	p		3.89e-6	0.0631	0.368

c = 12.5%	Genotype		T4/T5 block	T4 block	T5 block
			(n=11)	(n=12)	(n=12)
UAS control	n		12	12	12
	t		-9.15	0.968	-1.49
	p		4.05e-8	0.344	0.150
Gal4 control	n		12	13	12
	t		-14.7	-2.38	-1.57
	p		2.86e-12	0.0277	0.130

c = 25%	Genotype		T4/T5 block	T4 block	T5 block
			(n=11)	(n=12)	(n=12)
UAS control	n		12	12	12
	t		-13.2	0.108	-0.545
	p		2.50e-11	0.915	0.591
Gal4 control	n		12	13	12
	t		-19.1	-2.53	0.0875
	p		7.56e-14	0.0198	0.931

c = 50%	Genotype		T4/T5 block	T4 block	T5 block
			(n=11)	(n=12)	(n=12)
UAS control	n		12	12	12
	t		-31.5	-0.499	-2.02
	p		1.42e-17	0.624	0.0608
Gal4 control	n		12	13	12
	t		-28.2	-1.49	-0.832
	p		4.00e-18	0.156	0.415

c = 100%	Genotype		T4/T5 block	T4 block	T5 block
			(n=11)	(n=12)	(n=12)
UAS control	n		12	12	12
	t		-24.0	-1.89	-2.25
	p		4.04e-13	0.0803	0.0362
Gal4 control	n		12	13	12
	t		-22.3	-2.17	-0.458
	p		6.25e-14	0.0495	0.652

c = 6.25%	Genotype		T4/T5 block	T4 block	T5 block
			(n=11)	(n=12)	(n=12)
UAS control	n		12	12	12
	t		-4.13	0.175	-1.34
	p		5.41e-4	0.863	0.193
Gal4 control	n		12	13	12
	t		-5.99	-1.81	-0.987
	p		1.15e-5	0.0853	0.336

c = 12.5%	Genotype		T4/T5 block	T4 block	T5 block
			(n=11)	(n=12)	(n=12)
UAS control	n		12	12	12
	t		-8.66	0.0732	-1.58
	p		5.01e-7	0.942	0.129
Gal4 control	n		12	13	12
	t		-10.5	-1.55	-0.614
	p		9.04e-8	0.136	0.546

c = 25%	Genotype		T4/T5 block	T4 block	T5 block
			(n=11)	(n=12)	(n=12)
UAS control	n		12	12	12
	t		-11.3	-0.161	-0.828
	p		4.18e-8	0.874	0.417
Gal4 control	n		12	13	12
	t		-14.4	-1.82	0.969
	p		2.00e-9	0.0810	0.344

c = 50%	Genotype		T4/T5 block	T4 block	T5 block
			(n=11)	(n=12)	(n=12)
UAS control	n		12	12	12
	t		-19.3	-1.38	-2.35
	p		1.53e-10	0.185	0.0300
Gal4 control	n		12	13	12
	t		-17.3	-0.927	0.328
	p		7.31e-10	0.364	0.747

c = 100%	Genotype		T4/T5 block	T4 block	T5 block
			(n=11)	(n=12)	(n=12)
UAS control	n		12	12	12
	t		-16.0	-1.68	-2.00
	p		1.42e-9	0.110	0.0596
Gal4 control	n		12	13	12
	t		-19.2	-1.23	0.404
	p		4.77e-11	0.235	0.692

**Extended statistics for Fig. 2.** Test details were as in Supplementary Table 2. c denotes contrast. Red fields indicate significant differences after Bonferroni correction. The number indicated by n is the number of individual flies.

# Asymmetry of *Drosophila* ON and OFF motion detectors enhances real-world velocity estimation

---

Supplementary Table 4

Feature		Mean (n=70)	Maximum (n=70)	Onset latency (n=70)	Offset latency (n=70)	Pre-stimulus polarization (n=70)	Post-stimulus polarization (n=70)
ON vs. OFF	t	-7.30	-5.50	5.18	5.63	-17.2	11.1
	p	3.76e-10	6.13e-7	2.13e-6	3.63e-7	1.12e-26	6.10e-17

**Extended statistics for Fig. 3.** We compared response features between ON and OFF edge presentation. Responses were always averaged across velocities and then tested using two-tailed Student's *t* tests at a significance level of 0.05. Red fields indicate significant differences. The number indicated by n is the number of individual cells pooled from vertical and horizontal system cells.

# Asymmetry of *Drosophila* ON and OFF motion detectors enhances real-world velocity estimation

Supplementary Table 5

Difference from zero					Difference from control					
$v = 20 \text{ °/s}$	Genotype	TNT control (n=12)	T4/T5 control (n=13)	T4 control (n=12)	T5 control (n=13)	Genotype	T4/T5 block (n=12)	T4 block (n=15)	T5 block (n=14)	
	versus 0						n	12	12	12
	t	6.36	6.64	5.57	4.90		t	-2.66	-14.9	6.80
	p	5.34e-5	2.39e-5	1.67e-4	3.65e-4		p	0.0143	5.04e-13	1.32e-6
							n	13	12	13
					t	-2.08	-13.5	8.60		
					p	0.0502	2.15e-11	1.27e-7		
$v = 40 \text{ °/s}$	Genotype	TNT control (n=12)	T4/T5 control (n=13)	T4 control (n=12)	T5 control (n=13)	Genotype	T4/T5 block (n=12)	T4 block (n=15)	T5 block (n=14)	
	versus 0						n	12	12	12
	t	4.77	5.88	5.33	6.36		t	-2.20	-13.1	8.85
	p	5.77e-4	7.51e-5	2.40e-4	3.60e-5		p	0.0399	4.12e-12	2.80e-8
							n	13	12	13
					t	-2.90	-12.4	9.65		
					p	8.33e-3	1.26e-10	3.65e-8		
$v = 80 \text{ °/s}$	Genotype	TNT control (n=12)	T4/T5 control (n=13)	T4 control (n=12)	T5 control (n=13)	Genotype	T4/T5 block (n=12)	T4 block (n=15)	T5 block (n=14)	
	versus 0						n	12	12	12
	t	0.703	-0.765	-1.44	0.249		t	-0.324	-11.8	11.3
	p	0.497	0.459	0.178	0.808		p	0.749	1.07e-11	4.30e-10
							n	13	12	13
					t	0.921	-9.70	12.7		
					p	0.367	6.14e-10	1.86e-9		
$v = 160 \text{ °/s}$	Genotype	TNT control (n=12)	T4/T5 control (n=13)	T4 control (n=12)	T5 control (n=13)	Genotype	T4/T5 block (n=12)	T4 block (n=15)	T5 block (n=14)	
	versus 0						n	12	12	12
	t	-4.57	-8.74	-5.78	-7.81		t	3.18	-6.82	12.3
	p	8.02e-4	1.50e-6	1.23e-4	4.78e-6		p	7.32e-3	4.96e-7	7.74e-12
							n	13	12	13
					t	6.02	-5.98	15.0		
					p	1.29e-5	3.56e-6	9.84e-12		
$v = 320 \text{ °/s}$	Genotype	TNT control (n=12)	T4/T5 control (n=13)	T4 control (n=12)	T5 control (n=13)	Genotype	T4/T5 block (n=12)	T4 block (n=15)	T5 block (n=14)	
	versus 0						n	12	12	12
	t	-5.67	-7.97	-5.44	-11.1		t	3.99	-6.06	14.2
	p	1.45e-4	3.93e-6	2.04e-4	1.14e-7		p	9.22e-4	2.95e-6	1.16e-12
							n	13	12	13
					t	4.66	-6.45	19.0		
					p	1.10e-4	1.24e-6	7.84e-15		
$v = 640 \text{ °/s}$	Genotype	TNT control (n=12)	T4/T5 control (n=13)	T4 control (n=12)	T5 control (n=13)	Genotype	T4/T5 block (n=12)	T4 block (n=15)	T5 block (n=14)	
	versus 0						n	12	12	12
	t	-2.50	-1.54	-1.15	-2.64		t	2.25	-2.21	4.54
	p	0.0297	0.149	0.274	0.0216		p	0.0439	0.0368	1.89e-4
							n	13	12	13
					t	1.18	-4.80	5.05		
					p	0.256	1.06e-4	3.73e-5		

**Extended statistics for Fig. 4.** For each velocity condition, we determined significance by comparing control groups to zero or block groups to both corresponding control groups (UAS control and Gal4 control) using a two-tailed Student's t test. Blocks were declared significantly different if and only if both control groups were significantly different at a significance level of 0.05.  $v$  denotes velocity. For multiple comparisons, Bonferroni correction was applied. Red fields indicate significant differences after Bonferroni correction. The number indicated by  $n$  is the number of individual flies.

# Asymmetry of *Drosophila* ON and OFF motion detectors enhances real-world velocity estimation

---

Supplementary Table 6

Stimulus		Random (n=16)	3p/conv/+ (n=16)	3p/conv/- (n=16)	3p/div/+ (n=16)	3p/div/- (n=16)
versus 0	t	-0.426	-2.33	18.4	-5.44	5.73
	p	0.676	0.0341	1.02e-11	6.89e-5	3.98e-5

**Extended statistics for Fig. 7.** We compared glider voltage responses to zero. Responses were tested using two-tailed Student's *t* tests at a significance level of 0.05. Red fields indicate significant differences. The number indicated by n is the number of individual cells pooled across cells from the horizontal and vertical systems.



# Asymmetry of *Drosophila* ON and OFF motion detectors enhances real-world velocity estimation

Supplementary Table 7

		Positive parity			Negative parity					
	Genotype	T4/T5 block (n=14)	T4 block (n=13)	T5 block (n=17)	Genotype	T4/T5 block (n=14)	T4 block (n=13)	T5 block (n=17)		
2-point	UAS control	n	18	18	18	UAS control	n	18	18	
		t	-16.2	-2.41	-1.33		t	21.3	1.29	-0.169
		p	2.17e-12	0.0228	0.194		p	1.43e-14	0.211	0.867
	Gal4 control	n	12	12	12	Gal4 control	n	12	12	
		t	-7.93	1.82	1.54		t	8.08	-1.79	-1.91
		p	5.91e-6	0.0814	0.136		p	5.28e-6	0.0869	0.0679
3-point/conv.	UAS control	n	18	18	18	UAS control	n	18	18	
		t	7.82	16.7	-5.85		t	-6.44	-14.0	6.83
		p	2.73e-8	4.72e-16	1.85e-6		p	3.12e-6	1.30e-13	2.01e-7
	Gal4 control	n	12	12	12	Gal4 control	n	12	12	
		t	8.57	19.3	-5.49		t	-12.4	-23.7	7.00
		p	2.56e-7	2.39e-15	1.11e-5		p	4.45e-10	1.88e-15	1.00e-6
3-point/div.	UAS control	n	18	18	18	UAS control	n	18	18	
		t	8.58	-3.34	10.8		t	-9.25	4.52	-8.51
		p	2.83e-8	2.32e-3	8.68e-12		p	8.57e-9	1.01e-4	1.36e-9
	Gal4 control	n	12	12	12	Gal4 control	n	12	12	
		t	5.36	-0.354	11.4		t	-6.82	0.991	-9.76
		p	1.85e-4	0.727	7.10e-10		p	2.12e-5	0.335	3.33e-10

**Extended statistics for Fig. 8.** Test details were as in Supplementary Table 2. Red fields indicate significant differences after Bonferroni correction. The number indicated by n is the number of individual flies.

# Discussion

To analyze the mechanisms underlying the computation of motion direction, the fly visual system seems to be predestined. The existing knowledge about the connectivity of involved cell candidates, mathematical models and *Drosophila's* abundant genetic toolbox makes it a suitable organism to study this important visual cue. In the publications of this cumulative thesis I probed the necessity and the role of individual circuit elements for detecting the direction of motion. We used two photon calcium imaging to characterize cells' responses properties, silencing and activation experiments to test the influence of single components on lobula plate tangential cell and behavioral responses, and immunohistochemistry to investigate involved neurotransmitters. The key findings in this collection of publications concentrate on T4 and T5 cells and their presynaptic partners. Together with my colleagues in the department, I found that T4 and T5 cells are the first direction-selective cells in the ON and OFF pathway, respectively. Their four subtypes are responsible and essential for the detection of the four cardinal directions of motion. Interestingly, both, T4 as well as T5 cells, receive input from four cell types. I could demonstrate that, in the OFF pathway, all four input cells are required to various degrees. Furthermore, I could show that cells presynaptic to T4 cells are not only involved in ON motion detection but are also required for the computation of contrasts indicating that parallel visual processing streams use shared components. Additionally, I found T4 and T5 cells to forward their signals to lobula plate tangential cells via the excitatory neurotransmitter acetylcholine. Lobula plate tangential cells exhibit different dynamics toward ON and OFF stimulation, which can be reproduced by asymmetric tuning of ON and OFF Reichardt-Hassenstein correlators. This asymmetry parallels ON-OFF asymmetries in natural scenes. Taken together, the publications from the main section could identify the role of individual circuit elements in motion detection, and could pinpoint the computation of direction selectivity in the OFF pathway to the dendrites of T5 cells. Emerging questions and ideas of future experiments with the usage of new techniques will be discussed in the subsequent sections, loosely following the anatomy from the periphery to the central brain.

## ON/OFF Split and ON/OFF Differences

The discovery of the split into two parallel pathways responsible for the detection of ON and OFF motion [101] and the discovery of the anatomical connectivity within a medullary column started to suggest correspondences between neuronal elements on the one hand and elements of the algorithmic model on the other hand. However, synapse numbers and connectivity patterns changed from study to study [74, 88, 89, 103]. Interestingly, both differences and parallels emerged in the architecture of the pathways and in the response properties of the elements. In the lamina, L1 and L2 were first described to represent crucial elements of the ON and OFF pathway, respectively [101]. Later, it was shown that L3 and L4 also contribute to the OFF pathway [99, 104, 109][MS2]. L1, L2 and L3 were proposed to function in modules and, depending of the stimulus nature, feeding into either the ON or the OFF pathway [99, 104]. The role of L5, reciprocally connected to L1, still remains unknown as of today. Noteworthy, L1 and L2 are electrically coupled to each other leading to nearly identical responses [101, 98]. Taken together, the lamina monopolar cells L1-L5 are strongly interconnected but feed into the parallel ON and OFF pathways. Are these pathway interconnections, possibly leading to pathway crosstalk, still present in the medulla? The fact that the complementary ON or OFF responses in lobula plate tangential cells remain unaltered when blocking single elements of one pathway demonstrates that this is not the case [110][MS1]. However, until now, these experiments were only performed for six of the eight cells presynaptic to T4 and T5. Additionally, no chemical synapses could be found between the elements in the medulla of the two pathways [74]. The same holds true for the ON and OFF elementary motion detectors T4 and T5. Neither are they interconnected nor does blocking either of them affect the other pathway [MS3]. Consequently, ON and OFF motion is computed separately but that the pathways share a similar architecture. Four cells, (ON: Mi1, Mi4, Mi9, and Tm3; OFF: Tm1, Tm2, Tm4, and Tm9) receiving input from the lamina, project onto direction-selective T4 and T5 cells, respectively [91, 103]. The dynamics of ON and OFF responses in lobula plate tangential cells, however, differ significantly. Besides displaying a peak response at higher edge velocities, OFF responses are also more confined to the stimulus time window compared to their ON counterpart. That means that OFF responses in lobula plate tangential cells exhibit a faster rise and decay time compared to ON responses over all velocities (example trace in Figure 8A). When presented with edges starting from an intermediate background luminance, differences remained for the velocity tuning curves, but disappeared for the response kinetics [MS6]. Luminance adaptation mechanisms might influence the dynamics of tangential cell responses while leaving the temporal tuning response properties unaltered. Another difference is that a short depolarization precedes the hyperpolarization in lobula plate tangential cells upon ON null direction stimulation. A possible explanation could be an asymmetric involvement of the two pathways in flicker detection, as the ON pathway elements Mi1 and Tm3 represent crucial elements in the detection of local contrast changes [MS5]. Nevertheless, it is important to note that for

the T5 [MS3] as well as for the Tm2/Tm9 block (strongest block in [MS1]) residual OFF responses are still present (Figure 8). This could be due to two factors. Either the used blocking tools result in an incomplete block or the remaining responses are mediated via other cells. In order to test this for the Tm2/Tm9 block, we expressed one or two copies of *shibire<sup>ts</sup>* (Figure 8A and B). With increasing expression level of the blocker, it should be possible to detect differential effects due to incomplete blocking. However, both genotypes exhibit nearly identical response dynamics and amplitudes leading to the notion that inactivating the cells' output with *shibire<sup>ts</sup>* produces a strong OFF motion vision impairment but the residual responses in lobula plate tangential cells are not a result of ineffective blocking. It is very likely that Tm1 and Tm4 elicit the remaining OFF responses. When calculating the mean tangential cell responses over all velocities tested (from 3°/s to 900°/s) the residual OFF responses are comparable to the T5 block (Figure 8C). This does not necessarily mean that these two results are equivalent. T5 blocking experiments were conducted using TNT as a blocking tool, because expressing *shibire<sup>ts</sup>* in T5 cells abolished OFF and reduced ON responses (data not shown). A possible explanation for this result could be the weak co-expression of T4 cells in this T5 Gal4 driver line. Assuming that inactivating neurons with *shibire<sup>ts</sup>* is more effective than with TNT, the small, remaining OFF responses in the T5 TNT block are likely due to incomplete blocking. Another point that speaks in favor of the incomplete T5 block is the work of Schnell et al. [107]. When using a strong and T4/T5 specific GAL4 driver line, lobula plate tangential cell responses are abolished [107]. The expression pattern and level of the GAL4 driver lines are always crucial and have to be examined in great detail. Different inactivation tools can result in various effects. This can be explained by the different mechanisms how they interrupt signaling in the cells. TNT stops synaptic transmission, *shibire<sup>ts</sup>* vesicle re-uptake and KIR constantly hyperpolarizes the cells via the expression of an inward rectifying potassium channel. It is also important to note that TNT and KIR are already active during the development. *Shibire<sup>ts</sup>* on the other hand is only activated when the temperature is raised above the restrictive level. Thus, in order to cover these variances, it would be ideal to test multiple combinations of several driver lines and effectors. Interpreting the results of [MS1] (Tm2/Tm9) and [MS3] (T5), I conclude that residual OFF responses in the Tm2/Tm9 block are due to signaling via Tm1 and Tm4 and that the T5 block is incomplete. In summary, it is possible to see that despite striking similarities in the architecture, the implementation of direction-selective responses could be different for the ON and OFF pathway and that both pathways are operating strictly in parallel after the lamina. Physiology [111] and computational modeling [112][MS3] showed that motion processing of both polarities stays separated and is nonoverlapping. In general, such splitting is thought to enable more efficient coding at lower metabolic cost, as separate pathways can be optimized to their requirements, respectively [113][MS6].

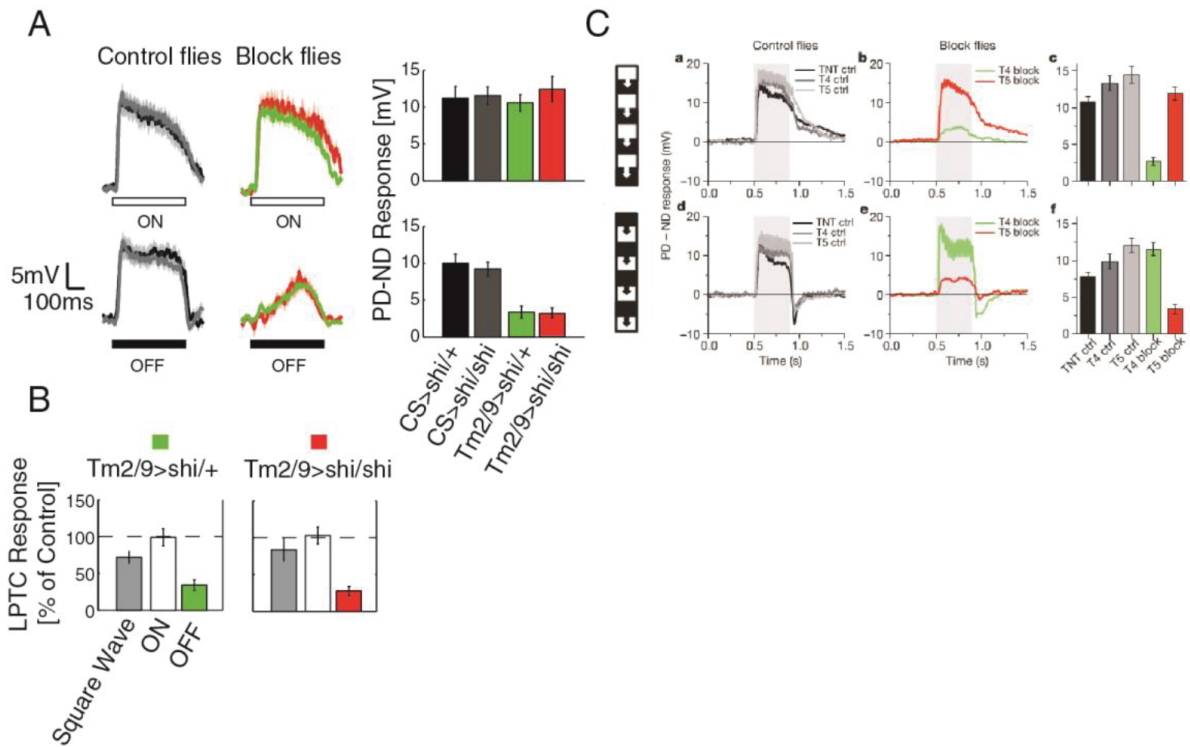


**Figure 8: LPTC Response Dynamics and Block Completion.** (A) Mean LPTC responses to 50°/s stimulation. CS>shi/+ data are from 13 cells (5HS, 8VS) in 5 flies, CS>shi/shi data are from 13 cells (5HS, 8VS) in 5 flies, Tm2/Tm9>shi/+ (green) data are from 12 cells (4HS, 8VS) in 8 flies, and Tm2/Tm9>shi/shi (red) data are from 4 cells (2HS, 2VS) in 2 flies (B) Percent of control responses of the 2 blocking phenotypes over all 9 velocities to square wave, ON edge, and OFF edge stimulation. (C) Mean LPTC responses to 50°/s stimulation of T4 and T5 block flies and their controls (adapted from [MS3]). Errorbars and errorshades indicate +/-SEM.

## T4/T5 as Elementary Motion Detectors

### T5 and its Four Inputs

As mentioned before, I have shown that direction selectivity in the OFF pathway arises on the T5 dendrites via an intricate interplay of four cell types, namely Tm1, Tm2, Tm4, and Tm9. As far as it has been tested, this also seems to be the case in the ON pathway [110]. But how can this be mapped onto current algorithmic models? What possible explanations deliver the response properties of the input elements on the computation of direction selectivity?

The crucial computation of the Hassenstein-Reichardt correlator is the interaction of two spatially separated inputs from which one of them is temporally delayed. How can four cells implement this operation? Several possibilities seem feasible:

- (1) Two pairs of Tm cells could represent the two arms of such an elementary motion detector, jointly performing the filter operation represented by one element of the algorithmic model.
- (2) Two cells (e.g. Tm2 and Tm9) act as the fast and the slow arm of a Hassenstein-Reichardt correlator and the other two cell types function as modulatory or accessory elements.
- (3) The four cell types function in different stimulus regimes (velocity, color, contrast, luminance, or polarization of light) and form several motion detectors with different sensitivities.
- (4) Modifying the structure of existing algorithmic models by implementing four elements as input lines to a direction-selective stage.

Blocking experiments would lead to different results:

For (1), blocking either element would lead to diminished direction-selective motion responses as every element is necessary for a fully operating Hassenstein-Reichardt correlator.

Possibility (2) requires only two of the four input cells. Silencing either of the two arms would abolish motion responses, whereas interrupting the signals of the modulatory elements would influence response kinetics or amplitudes.

Depending on the sensitivity of each input, blocking experiments for (3) would result in impaired visual motion responses for different stimulus conditions.

Supposed that all four elements are implemented on the direction-selective stage via separate motion detectors (4), taking out one of the four input lines would lead to decreased, but not abolished motion responses.

My results [MS1] can rule out the first two possibilities as every Tm cell contributes to the processing of OFF motion but to varying degrees and blocking combinations of two cell types led to further reduced, but never completely abolished OFF responses (e.g. Figure 8A and B). For (3), one can only rule out that individual Tm cells are responsible for the detection of specific velocities as the stimuli I used were constant in luminance

changes, contrast, color, and polarization. However, recent studies deliver evidence that they could be responsive in various stimulus regimes. First, the four Tm cell types could exhibit different spectral sensitivities. The color vision pathway was shown to improve motion detection [114]. Tm2 and Tm9 express histamine gated chloride channels making them putative synaptic partners to color sensitive photoreceptors R7 and R8 that send their projections to the same layers of the medulla where Tm2's and Tm9's dendrites reside [102]. Second, individual Tm cell types could also be differentially tuned to varying luminance or contrast levels. For example, lamina monopolar cells of various hawkmoth species differ anatomically depending on their activity periods [115]. Hawkmoth species that are more active under dim light possess lamina monopolar cells with bigger dendrites spanning more cartridges compared to the species that are active during the day. In *Drosophila*, Tm4 was shown to be multicolumnar [74] making it a potential candidate to pool visual information under dim light conditions. Moreover, Tm9 is a possible candidate for the detection of the overall luminance level. Tm9's activity follows the full field luminance in a tonic fashion. Its peculiar receptive field properties make it difficult to speculate about the exact mechanism as Tm9 is subject to lateral inhibition but also responsive to full field flicker stimulation. An upward shifted Mexican hat receptive field could elicit such size dependent receptive field properties [MS1], but the cellular implementation awaits further electron microscopy reconstructions as the connections within strata via wide-field medullary cells (e.g. Dm cells) were not mapped so far. Tm9's sustained responses, however, make it a possible candidate for the tonic component in a modified 2-quadrant detector [112, 116]. Third, photoreceptors in the dorsal rim of the fly's eye are sensitive toward stimulation with polarized light [117]. Whether the detection of polarized light also influences the motion vision circuitry is not known to date. Taken together, the response property characterization of the four Tm cells covered only a fraction of the stimulus parameter space [MS1]. Hence, depending on the stimulus nature, differential sensitivities of individual Tm cell types could shift their contribution to direction-selective responses in T5 cells. Consequently, it is necessary to expand the stimulus set including additional regimes and to add more naturalistic features.

In order to modify the Hassenstein-Reichardt correlator that could implement four input lines it is necessary to introduce the Barlow-Levick detector (BLD). Compared to the Hassenstein-Reichardt correlator, this elementary motion detector uses a division (e.g. shunting inhibition) as non-linear stage where the temporally delayed and direct line coincide. Even though all four Tm cells were described to be cholinergic (excitatory), one can not rule out the presence of inhibition, which may be implemented via the co-expression of a second neurotransmitter in one of the Tm cells or via a more complex mechanism than just the monosynaptic contact of the Tm cells to T5 [91]. As the Barlow-Levick detector also consists of two lines, a parallel implementation of the two mathematical models would result in four input lines to the direction-selective stage. Consequently, T5 cells would be subject to preferred direction enhancement (HRC) and null direction suppression (BLD). My silencing data [MS1] can not rule out such an architecture. All single Tm cell blocks reduced visual motion responses in tangential cells

and the six possible binary combinations further increased the effects. Hence, such a modified elementary motion detector incorporates the necessity of all four input elements in the OFF motion vision pathway. To further test this possibility it is necessary to monitor T5 cell activity while subsequent stimulation of neighboring neuroommatidia. As T4 and T5 cells exhibit a very sharp orientation tuning with nearly no response upon null direction stimulation the presence of inhibition appears to be plausible [MS3]. Therefore, a more detailed analysis of the neurotransmitter systems in Tm cells is necessary. A promising candidate for inhibiting T5 cells is Tm9 as it was reported to be GABAergic in big flies [118].

Nevertheless, it remains an open question how the temporal delay is realized. Are the different temporal kinetics sufficient for the computation of direction selectivity? Here, though the distribution of the synaptic inputs of Tm1, Tm2, and Tm9 on the T5 dendrite was described using electron microscopy it is still unknown where Tm4 contacts are located and whether the four T5 subtypes exhibit different connectivity patterns [91]. Additionally to the spatial offset of the inputs, further or alternative mechanisms causing the temporal delay are probable. T5 cells were shown to express muscarinic and nicotinic cholinergic receptors [91]. The signal via the nicotinic acetylcholine receptor would resemble the instantaneous signal and binding of acetylcholine to the muscarinic cholinergic receptors would activate a secondary messenger system resulting in a temporally delayed de- or hyperpolarization. Moreover, T5 dendrites display a characteristic anatomy. They have a broad base with branches pointing towards a certain direction depending on the T5 subtype and are decreasing in size. Due to the location of the synaptic contacts, inputs from the most distal part of the dendrite would be subject to a delay if T5 cells are not isopotential. However, it is also necessary to take the input resistance into account, which depends on the size of the dendrite at the contact site. Consequently, it is crucial to generate biophysically realistic models that embody all points. Possibly, the sole synaptic integration of all four inputs with their differential temporal dynamics on the T5 dendrite would lead to the generation of direction-selective responses in T5 cells.

## **The Role of Lobula Plate Intrinsic Cells**

The response amplitude reduction in lobula plate tangential cells of single Tm cell blocks correlated with their reported connection strength [91][MS1]. The OFF response reductions were present toward null direction and preferred direction stimulation [MS1]. Noteworthy, a response amplitude reduction in T5 cells is not the only possible explanation for the lobula plate tangential cell signals. Therefore, it is necessary to look at the connectivity motif within the lobula plate. As mentioned in the introduction, excitatory T4 and T5 cells come in four subtypes (a-d). Each subtype has its preferred direction in one cardinal direction and arborize in one of the four layers in the lobula plate. Already suggested in [MS4] T4 and T5 cells do not only contact the lobula plate tangential cells directly, resulting in their preferred direction depolarization, but also give input to so called lobula plate intrinsic cells (LPi). Recently, two classes of LPis, LPi4-3 and LPi3-4,



were described [119]. Their nomenclature describes their anatomy: the first number names the layer of the lobula plate in which their dendrites reside and the second number stands for the layer where they send their axons to. They most probably come in four subtypes as T4/T5 cells (Lpi1-2, Lpi2-1, Lpi3-4, Lpi4-3), but use glutamate as a neurotransmitter [119]. Optogenetic experiments revealed that they provide inhibitory input to the lobula plate tangential cells that house in the layer where the Lpi subtype axons reside. E.g. Lobula plate tangential cells of the vertical system depolarize upon downward and hyperpolarize upon upward stimulation. The preferred direction depolarization is caused by direct excitatory T4d/T5d input. The null direction hyperpolarization is mediated by T4c/T5c cells that activate Lpi3-4 cells [119]. Considering this connectivity motif, any reduction in lobula plate tangential cell signals can also be caused by the loss of direction selectivity in T4/T5 cells. If every T4/T5 subtype responds upon stimulation in every direction, their activity would lead to a simultaneous activation of every Lpi subtype. This would result in an absence of responses in lobula plate tangential cells as their activation gets canceled out by inhibition via Lpis. Consequently, it is crucial to examine the T4/T5 responses directly via calcium imaging when their inputs are inactivated. For blocking Tm9, the response amplitude and the direction selectivity in T5 cells decreases [120]. Nevertheless, responses in calcium imaging experiments exhibit a very high variance. Thus, it would be necessary to use alternative blocking tools (e.g. SwiChR [58]), where control and manipulation conditions can be observed in the same fly. Taken together, it is essential to investigate the changes of T4/T5 signals when blocking their input signals. The resulting changes in response amplitude, direction selectivity, receptive field size or response kinetics could lead to important insights how direction selectivity is computed on their dendrites.

## Vertebrate/Invertebrate Parallels

All sighted animals need to compute the direction of motion, and all of them encounter the same universal stimulus statistics. In consequence, comparing the neuronal implementation across species and phyla might hint at important computational principles and their neuronal substrates. Interestingly, a lot of parallels can be found between the fly visual system and the mouse retina (for review [121]). In both systems photoreceptor signals are split and processed separately in ON and OFF channels [101, 122]. Additionally, the connectivity motif as well as the calcium response dynamics exhibit a lot of similarities. OFF direction-selective starburst amacrine cells (SACs) receive input from multiple non-direction-selective bipolar cells (BC 1, 2, 3a, 3b, and 4) [123]. OFF SACs' preferred direction is outward motion. Every single dendrite computes his own direction-selective response and does not require inhibitory input [124]. Direction selectivity is thought to arise via a spatially offset innervation of the different bipolar cell types. Such a spatial offset of OFF pathway Tm cells on the T5 dendrite is also present [91]. Furthermore, the five bipolar cell types stratify at different depths in the inner plexiform layer. BC1 most superficial, followed by BC2, BC3a, BC3b and BC4. The dendrites of

the four Tm cells in the lobula exhibit a similar stratification arrangement [19]. The axons of Tm9 are located nearest to the lobula border, followed by Tm1, Tm2, and Tm4. In addition to the similarity that they stratify in different depths, the different cell type counterparts also display comparable response properties [125]. BC1 and Tm9 respond in a tonic, Tm1 and BC2/BC3 in a slowly decaying, Tm2/Tm4 and BC4 in a transient fashion. In summary, the apparent structural and anatomical resemblance hypothesizes the parallel evolution of a neural circuit motif generating directionally selective responses.

## LPTC Response/Behavior Relationship

In 1956, observing the turning of a weevil (*Chlorophanus*) on a Y-maze globe led to the development of the Hassenstein-Reichardt correlator [1]. Afterwards, a network of ~60 wide-field integrating neurons in the lobula plate were found to respond in a fashion that can also be predicted by the HRC [126]. Consequently, behavior and tangential cell activity is suitable to detect disturbances in motion detection upon presynaptic manipulations. In [MS1] we found an exponential relationship between the behavioral effects and the motion responses in lobula plate tangential cells when blocking Tm cells. That this correlation was best described by an exponential fit can be explained by the fact that lobula plate tangential cells do not directly innervate the muscles responsible for behavior but that complex post-synaptic cascades further process their responses. Consequently, only strong lobula plate tangential cell response reductions result in substantial behavioral impairment. Nevertheless, it is important to note that we used two different kind of stimuli for the two experimental approaches. Lobula plate tangential cell responses were recorded while stimulating with multiple ON or OFF edges. Behavioral experiments were conducted using the balanced motion stimulus (opposing edges), that is, bright and dark edges move in opposite directions, which leaves the turning behavior of the fly unaffected [98]. Only when the ON and the OFF pathway contribute unequally to the optomotor response, flies will follow the direction of motion of one of the polarities. E.g. when blocking T5, flies follow the direction of ON motion. As we observed no reduction in lobula plate tangential cell responses upon ON stimulation, the comparison of the two experimental approaches is justifiable [MS1]. Looking at the behavioral responses when stimulated with ON and OFF edges separately, however, such distinct phenotypes were not detectable. Even for the genotype (Tm2/Tm9>shi<sup>ts</sup>) with the strongest blocking phenotype in electrophysiology and opposing edge behavior, we only observed a mild reduction in the turning response upon multiple OFF edge stimulation (Figure 9). This can be explained by an integrative, nonlinear transformation between lobula plate tangential cell signals and behavioral output. In behaving flies, calcium accumulates in the terminals of horizontal system lobula plate tangential cells [127]. Consequently, even small responses in lobula plate tangential cells may be transformed in a supra-linear fashion by the postsynaptic network driving walking behavior. The time course of the turning response of Tm2/Tm9 block flies supports this hypothesis. The overall small reduction upon OFF stimulation is small, but the behavior lags behind the response of

control flies, indicating a temporal summation of the signal (Figure 9A).

Further evidence that lobula plate tangential cells drive and are necessary for visuomotor behavior is found in the following studies:

- The *Drosophila* mutant *optomotor-blind*<sup>H31</sup> in which tangential cells are missing or defective exhibit a strong reduction in their optomotor response [10].
- Laser ablating lobula plate tangential precursor cells [11] in larvae or cutting the cells' axons in the adult [12] alters visually driven behavioral responses.
- Extracellular electrical stimulation of the first layer of the lobula plate elicits yaw turning responses [128].
- Optogenetic activation of horizontal system lobula plate tangential cells leads to yaw head movements and flight-turning responses in *Drosophila* [77].

A detailed analysis for the role of all different classes of lobula plate tangential cells including silencing and activation experiments was not performed yet and awaits specific driver lines. Interestingly, lobula plate tangential cell activity is influenced by the behavioral state of the fly. During flight, the membrane voltage of vertical system lobula plate tangential cells is tonically depolarized and visual responses are boosted. This suggests an elevated gain as a result of increased synaptic drive from upstream inputs [83]. When walking, *Drosophila* horizontal system lobula plate tangential cells exhibit stronger calcium transients upon visual motion, a higher response gain and a shift of the temporal frequency tuning toward higher velocities [129]. A similar shift can be observed in electrophysiological recordings of blowfly tangential cells, elicited either by flight or the application of chlordimeform, an octopamine agonist [130]. In simulations this shift can be reproduced by changing the time constants of an elementary motion detector [130], leading to the possibility that the response properties of T4 and T5, or even of their input elements, might already be behaviorally flexible and might change with the locomotor state. Consequently, it is necessary to find the neural substrate underlying the changes of the temporal tuning properties, most probably octopaminergic neurons that send their projections to the optic lobe. The neurons in the expression pattern of the *tdc2-GAL4* line are possible candidates, as immunohistochemistry identified them as octopaminergic [131, 132]. In summary, a strong relationship between lobula plate tangential cell responses and behavioral responses is present, but their responses are influenced by the behavioral state of the fly. Therefore it is important to map the neural network downstream of the lobula plate. However, already ventral cervical nerve motoneurons, which receive direct input from horizontal system lobula plate tangential cells, are additionally influenced by the wind-sensitive Johnston organ [133]. This shows the complexity of this endeavor as it is necessary to unravel how multimodal signals shape behavioral responses.

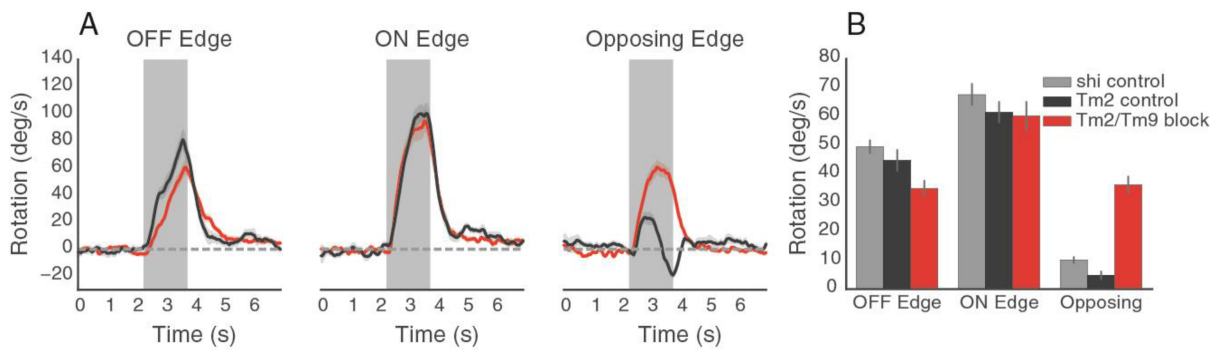


**Figure 9: Turning Behavior to Moving Edges.** (A) Mean traces of the turning behavior of walking flies for stimulation with multiple OFF edges, multiple ON edges and opposing ON and Off edges. Tm2 control: CS>Tm2/+ (black; N=11), and Tm2/Tm9 block: Tm2/Tm9>shi/+ (red; N=17) (B) Turning responses averaged over the duration of stimulation of shi control: CS>shi/+ (grey; N=10), Tm2 control (black; N=11), and Tm2/Tm9 block (red; N=17) flies for stimulation with single OFF edges, ON edges and opposing ON and OFF edges. Errorbars and errorshades indicate +/-SEM.

## Combination of Techniques and Technique Optimization

The data in the publications from the main part were collected using the GAL4/UAS system. We either monitored or changed the activity of certain cell types and characterized their response properties and their role in the neural circuitry. Besides the GAL4/UAS system, there exist two alternative binary transcriptional systems which work in a similar way: The *lexA/lexAop* and the *Q* system [134, 135]. Consequently, one can combine several systems in order to tap the full potential of *Drosophila's* genetic armory. One possibility is the combination of activation/inactivation with simultaneous calcium imaging. This approach makes it possible to analyze interactions of direct synaptic partners in the optic lobe where electrophysiology is not possible due to the small size of the cells presynaptic to the lobula plate tangential cells. Another possibility is be the parallel expression of several channelrhodopsins or calcium sensors whose excitation spectra do not interfere. A new class of red fluorescent calcium indicators called RCaMPs [136] allow monitoring the activity of synaptic partners which have their receptive fields in the same location in space, consequently avoiding the problem of strong calcium signal fluctuations which makes it difficult to combine results from various experiments. The simultaneous usage of several transcriptional systems also enables a sequential activation/inactivation of two cell types presynaptic to a third cell type, whose activity can then be acquired [56].

As mentioned in the introduction using calcium sensors as a proxy for neural activity is accompanied by disadvantages like the nonlinear relationship between fluorescence and calcium changes, slow kinetics, calcium buffering and a clipped dynamic range, making it impossible to detect hyperpolarizations of the membrane potential. To ana-

lyze differences in the response kinetics I compared the actual voltage responses of Tm1 and Tm2 cells with the calcium responses [MS1] upon 2 second flicker stimulation (Figure 10). The resemblance between the data acquired electrophysiologically and via calcium imaging demonstrates that in these cases the calcium signal is a reasonable readout for the temporal dynamics of the membrane voltage. In order to visualize hyperpolarizations during calcium imaging it is possible to artificially depolarize the monitored cell, e.g. via the temperature-sensitive cation channel TrpA1, which makes it possible to detect inhibition through a drop in the calcium signal. Another approach would be the usage of genetically encoded voltage sensors, which were developed over the last years. Comparable to calcium indicators they can be categorized in different families depending on their design principle. The first described genetically encoded voltage sensor (FlaSh) consists of a modified GFP fused into a voltage-dependent  $K^+$  channel, so that voltage changes lead to fluorescence changes [137]. Consequently, FlaSh was the first member of the VSD-based sensor family. As for the calcium sensors they come in either a dual-chromophore FRET based composition (e.g. VSFP-Butterfly [138]) or in a single-chromophore format. Here, the best available sensors are called ArcLight [139] and ASAP1 [140]. ArcLight exhibits the highest response amplitude with  $\sim 35\%$  fluorescence change but slow kinetics ( $> 9\text{ms}$  for both depolarization and repolarization). Though showing weaker response amplitudes ( $\sim 29\%$ ), ASAP1 is capable of detecting action potentials with time constants of  $\sim 2\text{ms}$ . The members of the other family are rhodopsin-based sensors. Microbial-rhodopsins can be repurposed as voltage indicators due to a modification of their light-sensitive membrane proteins. Though showing faster kinetics (up to  $\sim 0.05\text{ms}$  [141]) the rhodopsin-based sensors are dimmer than many VSD-based sensors by  $\sim 2$  orders of magnitude. The best available rhodopsin-based sensors by now are called Archers, exhibiting increased fluorescence compared to the first generations, high voltage sensitivity and fast kinetics [142].

Although synaptic connectivity in the fly optic lobe was characterized in several studies via electron microscopy reconstructions [74, 88, 89, 103, 91], the wiring is not sufficient to resolve the neural implementation of particular computations. This is due to the complex wiring across strata, non-detectable but highly abundant gap-junctions, unknown properties of the synapses and not yet reconstructed brain regions like the lobula. Consequently, so far not all cell types and their connectivity patterns are identified. To circumvent this problem non-cell-directed approaches could find a remedy. One hypothetical experiment is panneural imaging where calcium indicators [143], calcium integrators (e.g. CaMPARI [144]), or voltage indicators are expressed in large areas of the brain, thought to be responsible for the computation or behavior of interest. In *Drosophila* this can be achieved by using the driver line *elav-GAL4*. The locus *elav* is transcribed only within, and ubiquitously throughout, the nervous system [145]. Hence, it is possible to detect activity in certain strata of neuropils and restrict the neural candidates to the cells that are located there. Cell identification can also be done via expression of a photoactivatable fluorescent proteins [146] or photoactivatable calcium indicators [147]. With the latter, subsequent activity monitoring is possible which allows to compare the response properties of the identified cell with the panneural imaging results. Once identified the

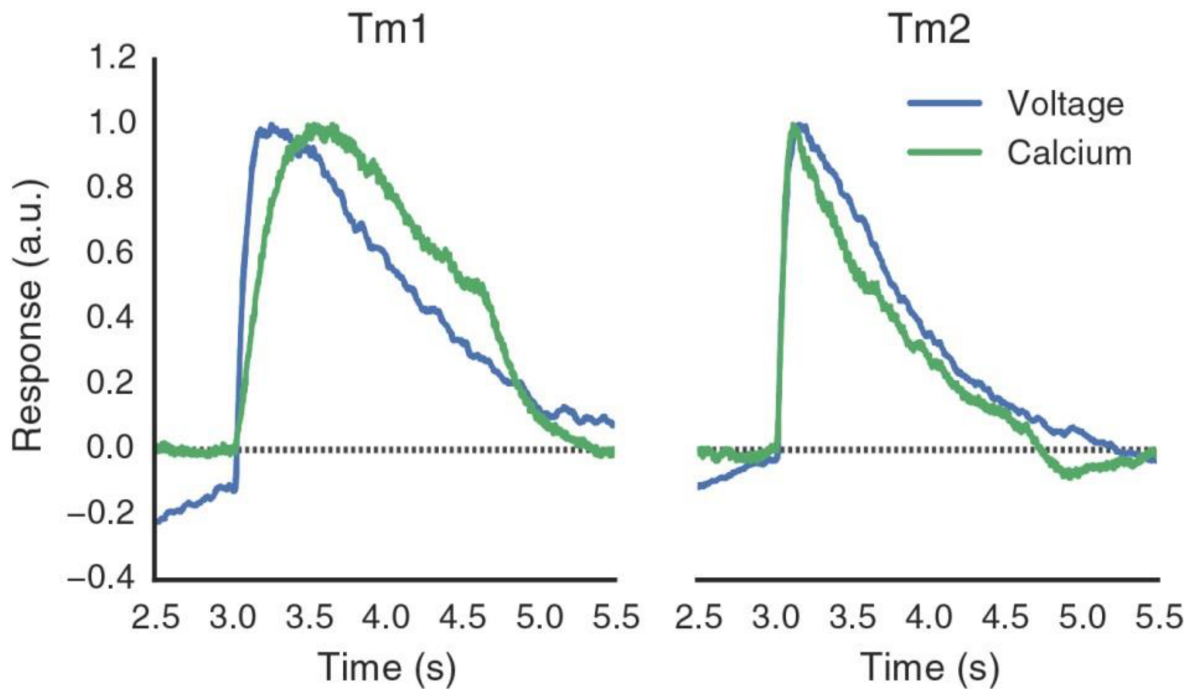


**Figure 10: Comparison of Calcium and Voltage Responses in Tm1 and Tm2.** Voltage traces (blue; kindly provided by Rudy Behnia) and calcium signals (green; [MS1]) of Tm1 and Tm2 cells when stimulated with local brightness decrements for 2s. Traces acquired by both techniques closely resemble each other. For Tm1, the voltage signals are faster than the recorded calcium dynamics and for Tm2, measured calcium signals precede the voltage recordings.

participating nerve cells of the desired assay, cell specific driver lines can be used for further circuit analysis.

## Conclusion and Outlook

In the last years the *Drosophila* motion vision community made a huge step toward unraveling the mechanism of the computation of direction selectivity. The results from the publications of this cumulative thesis contributed substantially in that process. I was able to allocate the generation of OFF direction-selective signals to the dendrites of T5 cells and could characterize their major inputs. My future experiments will focus on this subcircuitry (Tm1/2/4/9 - T5) in order to investigate the remaining components of their intricate interplay.

What is the role of T5's neurotransmitter receptors, its dendrite anatomy and the location of its inputs? Superresolution voltage imaging in the T5 dendrite combined with input and receptor silencing could bear new insights that are necessary to generate biophysically realistic models. The implementation of T5's anatomy, dynamics of presynaptic

## Discussion

---

Tm cells with the distribution and number of synaptic contacts, and the kinetics of T5's receptors in these models will help in answering the question how direction selectivity is computed in the visual system of the fly.

# Bibliography

- [1] Hassenstein, B., and Reichardt, W. 1956. Systemtheoretische Analyse der Zeit-, Reihenfolgen- und Vorzeichenauswertung bei der Bewegungsperzeption des Rüsselkäfers *Chlorophanus*. Z. Naturforsch., 11, 513–524.
- [2] Barlow, H., and Levick, W. 1965. The mechanism of directionally selective units in rabbit's retina. J. Physiol., 178, 477–504.
- [3] Reichardt, W. 1987. Evaluation of optical motion information by movement detectors. J. Comp. Physiol. A., 161, 533–547.
- [4] Borst, A., and Egelhaaf, M. 1989. Principles of visual motion detection. Trends Neurosci., 12, 297–306.
- [5] Götz, K. 1968. Flight control in *Drosophila* by visual perception of motion. Kybernetik, 4, 199–208.
- [6] Schneider, G. 1956. Zur spektralen Empfindlichkeit des Komplexauges von *Calliphora*. Z. vgl. Physiol., 39, 1–20.
- [7] Fermi, V.G., and Reichardt, W. 1963. Optomotorische Reaktionen der Fliege *Musca domestica*. Kybernetik, 2, 15–28.
- [8] Götz, K. 1964. Optomotorische Untersuchung des visuellen Systems einiger Augenmutanten der Fruchtfliege *Drosophila*. Kybernetik, 2, 77–92.
- [9] Eckert, H. 1973. Optomotorische Untersuchungen am visuellen System der Stubenfliege *Musca domestica*. Kybernetik, 14, 1–23.
- [10] Heisenberg, M., Wonneberger, R., and Wolf, R. 1978. Optomotor-blindh31 - a *Drosophila* mutant of the lobula plate giant neurons. J. Comp. Physiol., 124, 287–296.
- [11] Geiger, G., and Nässel, D. 1981. Visual orientation behaviour of flies after selective laser beam ablation of interneurons. Nature, 293, 398–399.
- [12] Hausen, K., and Wehrhahn, C. 1983. Microsurgical lesion of horizontal cells changes optomotor yaw responses in the blowfly *Calliphora erythrocephala*. Proc. R. Soc. Lond., 219, 211–216.



## BIBLIOGRAPHY

---

- [13] Joesch, M., Plett, J., Borst, A., and Reiff, D.F. 2008. Response properties of motion-sensitive visual interneurons in the lobula plate of *Drosophila melanogaster*. *Curr. Biol.*, *18*, 368–374.
- [14] Borst, A., Haag, J., and Reiff, D.F. 2010. Fly motion vision. *Annu. Rev. Neurosci.*, *33*, 49–70.
- [15] Ready, D., Hanson, T., and Benzer, S. 1976. Development of the *Drosophila* retina, a neurocrystalline lattice. *Dev. Biol.*, *53*, 217–240.
- [16] Hofbauer, A., and Campos-Ortega, J.A. 1990. Proliferation pattern and early differentiation of the optic lobes in *Drosophila melanogaster*. *Rouxs Arch. Dev. Biol.*, *198*, 264–274.
- [17] Cajal, S., and Sánchez, D. 1915. Contribución al conocimiento de los centros nerviosos de los insectos. *Trab. Lab. Inv. Biol.*, *13*, 1–168.
- [18] Campos-Ortega, J., and Strausfeld, N. 1972. The columnar organization of the second synaptic region of the visual system of *Musca domestica* L. *Z. Zellforsch. Mikrosk. Anat.*, *124*, 561–585.
- [19] Fischbach, K., and Dittrich, A. 1989. The optic lobe of *Drosophila melanogaster*. i. a golgi analysis of wild-type structure. *Cell Tissue Res.*, *258*, 441–475.
- [20] Land, M. 1997. Visual acuity in insects. *Annu. Rev. Entomol.*, *42*, 147–177.
- [21] Nilsson, D., and Kelber, A. 2007. A functional analysis of compound eye evolution. *Arthropod Struct. Dev.*, *36*, 373–385.
- [22] Zelhof, A., Hardy, R., Becker, A., and Zuker, C. 2006. Transforming the architecture of compound eyes. *Nature*, *443*, 696–699.
- [23] Chou, W., Hall, K., Wilson, D., and Wideman, C. 1996. Identification of a novel *Drosophila* opsin reveals specific patterning of the R7 and R8 photoreceptor cells. *Neuron*, *17*, 1101–1115.
- [24] Hardie, R. 2001. Phototransduction in *Drosophila melanogaster*. *J. Exp. Biol.*, *204*, 3403–3409.
- [25] Hardie, R. 1989. A histamine-activated chloride channel involved in neurotransmission at a photoreceptor synapse. *Nature*, *339*, 704–706.
- [26] Braitenberg, V. 1967. Patterns of projection in the visual system of the fly. I. retina-lamina projections. *Exp. Brain Res.*, *3*, 271–298.
- [27] Kirschfeld, K. 1967. Die Projektion der optischen Umwelt auf das Raster der Rhabdomere im Komplexauge von *Musca*. *Exp. Brain Res.*, *3*, 248–270.

## BIBLIOGRAPHY

---

- [28] Wernet, M.F., Perry, M.W., and Desplan, C. 2015. The evolutionary diversity of insect retinal mosaics: common design principles and emerging molecular logic. *Trends Genet.*, *31*, 316–328.
- [29] Borst, A. 2009. *Drosophila's* view on insect vision. *Curr. Biol.*, *19*, R36–47.
- [30] Strausfeld, N. 1971. The organization of the insect visual system (light microscopy). *Z. Zellforsch.*, *121*, 442–454.
- [31] Rein, K., Zöckler, M., Mader, M.T., Grübel, C., and Heisenberg, M. 2002. The *Drosophila* standard brain. *Curr. Biol.*, *12*, 227–231.
- [32] Morgan, T. 1910. Sex limited inheritance in *Drosophila*. *Science*, *32*, 120–122.
- [33] Muller, H.J. 1928. The production of mutations by x-rays. *Proc. Natl. Acad. Sci. U.S.A.*, *14*, 714.
- [34] Alderson, T. 1965. Chemically induced delayed germinal mutation in *Drosophila*. *Nature*, *207*, 164–167.
- [35] Brand, A., and Perrimon, N. 1993. Targeted gene expression as a means of altering cell fates and generating dominant phenotypes. *Development*, *118*, 401–415.
- [36] Rubin, G., and Spradling, A. 1982. Genetic transformation of *Drosophila* with transposable element vectors. *Science*, *218*, 348–353.
- [37] Pfeiffer, B.D., Jenett, A., Hammonds, A.S., Ngo, T.B.T., Misra, S., Murphy, C., Scully, A., Carlson, J.W., Wan, K.H., Laverty, T.R., Mungall, C., Svirskas, R., Kadonaga, J.T., Doe, C.Q., Eisen, M.B., Celniker, S.E., and Rubin, G.M. 2008. Tools for neuroanatomy and neurogenetics in *Drosophila*. *Proc. Natl. Acad. Sci. U.S.A.*, *105*, 9715–9720.
- [38] Lee, T., and Luo, L. 1999. Mosaic analysis with a repressible cell marker for studies of gene function in neuronal morphogenesis. *Neuron*, *22*, 451–461.
- [39] Luan, H., Peabody, N.C., Vinson, C.R., and White, B.H. 2006. Refined spatial manipulation of neuronal function by combinatorial restriction of transgene expression. *Neuron*, *52*, 425–436.
- [40] Jenett, A., Rubin, G.M., Ngo, T.T.B., Shepherd, D., and Murphy, C. 2012. A GAL4-driver line resource for *Drosophila* neurobiology. *Cell Rep.*, *2*, 991–1001.
- [41] Tsien, R.Y. 1998. The green fluorescent protein. *Annu. Rev. Biochem.*, *67*, 509–544.

## BIBLIOGRAPHY

---

- [42] Löhr, R., Godenschwege, T., and Buchner, E. 2002. Compartmentalization of central neurons in *Drosophila*: a new strategy of mosaic analysis reveals localization of presynaptic sites to specific segments of neurites. *J. Neurosci.*, *22*, 10357–10367.
- [43] Robinson, I., Ranjan, R., and Schwarz, T. 2002. Synaptotagmins I and IV promote transmitter release independently of Ca<sup>2+</sup> binding in the C(2)A domain. *Nature*, *418*, 336–340.
- [44] Nicolai, L., Ramaekers, A., Raemaekers, T., Drozdzecki, A., Mauss, A., Yan, J., Landgraf, M., Annaert, W., and Hassan, B. 2010. Genetically encoded dendritic marker sheds light on neuronal connectivity in *Drosophila*. *Proc. Natl. Acad. Sci. U.S.A.*, *107*, 20553–20558.
- [45] Miyawaki, A., Llopis, J., Heim, R., JM, M., Adams, J., Ikura, M., and Tsien, R. 1997. Fluorescent indicators for Ca<sup>2+</sup> based on green fluorescent proteins and calmodulin. *Nature*, *388*, 882–887.
- [46] Heim, N., and Griesbeck, O. 2004. Genetically encoded indicators of cellular calcium dynamics based on troponin C and green fluorescent protein. *J. Biol. Chem.*, *279*, 14280–14286.
- [47] Mank, M., Reiff, D.F., Heim, N., Friedrich, M.W., Borst, A., and Griesbeck, O. 2006. A FRET-based calcium biosensor with fast signal kinetics and high fluorescence change. *Biophys. J.*, *90*, 1790–1796.
- [48] Baird, G., Zacharias, D., and Tsien, R.Y. 1999. Circular permutation and receptor insertion within green fluorescent proteins. *Proc. Natl. Acad. Sci. U.S.A.*, *96*, 11241–11246.
- [49] Nakai, J., Ohkura, M., and Imoto, K. 2001. A high signal-to-noise Ca<sup>2+</sup> probe composed of a single green fluorescent protein. *Nat. Biotechnol.*, *19*, 137–141.
- [50] Akerboom, J., Chen, T.W., Wardill, T.J., Tian, L., Marvin, J.S., Mutlu, S., Calderón, N.C., Esposti, F., Borghuis, B.G., Sun, X.R., Gordus, A., Orger, M.B., Portugues, R., Engert, F., Macklin, J.J., Filosa, A., Aggarwal, A., Kerr, R.A., Takagi, R., Kracun, S., Shigetomi, E., Khakh, B.S., Baier, H., Lagnado, L., Wang, S.S., Bargmann, C.I., Kimmel, B.E., Jayaraman, V., Svoboda, K., Kim, D.S., Schreiter, E.R., and Looger, L.L. 2012. Optimization of a GCaMP calcium indicator for neural activity imaging. *J. Neurosci.*, *32*, 13819–13840.
- [51] Chen, T.W., Wardill, T.J., Sun, Y., Pulver, S.R., Renninger, S.L., Baohan, A., Schreiter, E.R., Kerr, R.A., Orger, M.B., Jayaraman, V., Looger, L.L., Svoboda, K., and Kim, D.S. 2013. Ultrasensitive fluorescent proteins for imaging neuronal activity. *Nature*, *499*, 295–300.

## BIBLIOGRAPHY

---

- [52] Fenno, L., Yizhar, O., and Deisseroth, K. 2011. The development and application of optogenetics. *Annu. Rev. Neurosci.*, *34*, 389–412.
- [53] Nagel, G., Szellas, T., and Huhn, W. 2003. Channelrhodopsin-2, a directly light-gated cation-selective membrane channel. *Proc. Natl. Acad. Sci. U.S.A.*, *100*, 13940–13945.
- [54] Boyden, E.S., Zhang, F., Bamberg, E., and Nagel, G. 2005. Millisecond-timescale, genetically targeted optical control of neural activity. *Nat. Neurosci.*, *8*, 1263–1268.
- [55] Inagaki, H.K., Jung, Y., Hoopfer, E.D., Wong, A.M., Mishra, N., Lin, J.Y., Tsien, R.Y., and Anderson, D.J. 2013. Optogenetic control of *Drosophila* using a red-shifted channelrhodopsin reveals experience-dependent influences on courtship. *Nat. Methods*, *11*, 325–332.
- [56] Klapoetke, N.C., Murata, Y., Kim, S.S., Pulver, S.R., Birdsey-Benson, A., Cho, Y.K., Morimoto, T.K., Chuong, A.S., Carpenter, E.J., Tian, Z., Wang, J., Xie, Y., Yan, Z., Zhang, Y., Chow, B.Y., Surek, B., Melkonian, M., Jayaraman, V., Constantine-Paton, M., Wong, G.K.S., and Boyden, E.S. 2014. Independent optical excitation of distinct neural populations. *Nat. Methods*, *11*, 338–346.
- [57] Berndt, A., Yizhar, O., Gunaydin, L.A., and Hegemann, P. 2008. Bi-stable neural state switches. *Nat. Neurosci.*, *12*, 229–234.
- [58] Berndt, A., Lee, S.Y., Ramakrishnan, C., and Deisseroth, K. 2014. Structure-guided transformation of channelrhodopsin into a light-activated chloride channel. *Science*, *344*, 420–424.
- [59] Sweeney, S.T., Broadie, K., Keane, J., and Niemann, H. 1995. Targeted expression of tetanus toxin light chain in *Drosophila* specifically eliminates synaptic transmission and causes behavioral defects. *Neuron*, *14*, 341–351.
- [60] Kitamoto, T. 2001. Conditional modification of behavior in *Drosophila* by targeted expression of a temperature-sensitive shibire allele in defined neurons. *J. Neurobiol.*, *47*, 81–92.
- [61] Baines, R.A., Uhler, J.P., Thompson, A., Sweeney, S.T., and Bate, M. 2001. Altered electrical properties in *Drosophila* neurons developing without synaptic transmission. *J. Neurosci.*, *21*, 1523–1531.
- [62] Bergmann, A., Agapite, J., K, M., and Steller, H. 1998. The *Drosophila* gene *hid* is a direct molecular target of Ras-dependent survival signaling. *Cell*, *95*, 331–341.
- [63] Kurada, P., and White, K. 1998. Ras promotes cell survival in *Drosophila* by downregulating *hid* expression. *Cell*, *95*, 319–329.

## BIBLIOGRAPHY

---

- [64] White, K., Tahaoglu, E., and Steller, H. 1996. Cell killing by the *Drosophila* gene *reaper*. *Science*, *271*, 805–807.
- [65] Bausenwein, B., Dittrich, A., and Fischbach, K. 1992. The optic lobe of *Drosophila melanogaster*. *Cell Tissue Res.*, *267*, 17–28.
- [66] Douglass, J., and Strausfeld, N. 1996. Visual motion-detection circuits in flies: parallel direction- and non-direction-sensitive pathways between the medulla and lobula plate. *J. Neurosci.*, *16*, 4551–4562.
- [67] Buchner, E., Buchner, S., and Bülthoff, I. 1984. Deoxyglucose mapping of nervous activity induced in *Drosophila* brain by visual movement. *J. Comp. Physiol.*, *155*, 471–483.
- [68] Hausen, K. 1976. Functional characterization and anatomical identification of motion sensitive neurons in the lobula plate of the blowfly *Calliphora erythrocephala*. *Z. Naturforsch.*, *31*, 629–634.
- [69] Haag, J., and Borst, A. 2001. Recurrent network interactions underlying flow-field selectivity of visual interneurons. *J. Neurosci.*, *21*, 5685–5692.
- [70] Haag, J., and Borst, A. 2004. Neural mechanism underlying complex receptive field properties of motion-sensitive interneurons. *Nat. Neurosci.*, *7*, 628–634.
- [71] Douglass, J., and Strausfeld, N. 1995. Visual motion detection circuits in flies: peripheral motion computation by identified small-field retinotopic neurons. *J. Neurosci.*, *15*, 5596–5611.
- [72] Neher, E., and Sakmann, B. 1976. Noise analysis of drug induced voltage clamp currents in denervated frog muscle fibres. *J. Physiol.*, *258*, 705–729.
- [73] Wilson, R., Turner, G., and Laurent, G. 2004. Transformation of olfactory representations in the *Drosophila* antennal lobe. *Science*, *303*, 366–370.
- [74] Takemura, S.Y., Bharioke, A., Lu, Z., Nern, A., Vitaladevuni, S., Rivlin, P.K., Katz, W.T., Olbris, D.J., Plaza, S.M., Winston, P., Zhao, T., Horne, J.A., Fetter, R.D., Takemura, S., Blazek, K., Chang, L.A., Ogundeyi, O., Saunders, M.A., Shapiro, V., Sigmund, C., Rubin, G.M., Scheffer, L.K., Meinertzhagen, I.A., and Chklovskii, D.B. 2013. A visual motion detection circuit suggested by *Drosophila* connectomics. *Nature*, *500*, 175–181.
- [75] Behnia, R., Clark, D.A., Carter, A.G., Clandinin, T.R., and Desplan, C. 2014. Processing properties of ON and OFF pathways for *Drosophila* motion detection. *Nature*, *512*, 427–430.
- [76] Denk, W., Strickler, J., and Webb, W. 1990. Two-photon laser scanning fluorescence microscopy. *Science*, 73–76.

## BIBLIOGRAPHY

---

- [77] Haikala, V., Joesch, M., Borst, A., and Mauss, A.S. 2013. Optogenetic control of fly optomotor responses. *J. Neurosci.*, *33*, 13927–13934.
- [78] Götz, K. 1987. Course-control, metabolism and wing interference during ultralong tethered flight in *Drosophila melanogaster*. *J. Exp. Biol.*, *128*, 35–46.
- [79] Buchner, E. 1976. Elementary movement detectors in an insect visual system. *Biol. Cybern.*, *24*, 85–101.
- [80] Zhu, Y., Nern, A., Zipursky, S., and Frye, M.A. 2009. Peripheral visual circuits functionally segregate motion and phototaxis behaviors in the fly. *Curr. Biol.*, *19*, 613–619.
- [81] Mronz, M., and Lehmann, F. 2008. The free-flight response of *Drosophila* to motion of the visual environment. *J. Exp. Biol.*, *211*, 2026–2045.
- [82] Seelig, J.D., Chiappe, M., Lott, G.K., Dutta, A., Osborne, J.E., Reiser, M.B., and Jayaraman, V. 2010. Two-photon calcium imaging from head-fixed *Drosophila* during optomotor walking behavior. *Nat. Methods*, *7*, 535–540.
- [83] Maimon, G., Straw, A.D., and Dickinson, M.H. 2010. Active flight increases the gain of visual motion processing in *Drosophila*. *Nat. Neurosci.*, *13*, 393–399.
- [84] Knoll, M., and Ruska, E. 1932. Das Elektronenmikroskop. *Z. Phys.*, *78*, 318–339.
- [85] Erni, R., Rossell, M.D., Kisielowski, C., and Dahmen, U. 2009. Atomic-resolution imaging with a sub-50-pm electron probe. *Phys. Rev. Lett.*, *102*, 096101.
- [86] A, B. 1955. Reconstruction of the nuclear sites of *Salmonella typhimurium* from electron micrographs of serial sections. *J. Gen. Microbiol.*, *13*, 327–329.
- [87] Meinertzhagen, I., and O’Neil, S. 1991. Synaptic organization of columnar elements in the lamina of the wild type in *Drosophila melanogaster*. *J. Comp. Neurol.*, *305*, 232–263.
- [88] Takemura, S.Y., Lu, Z., and Meinertzhagen, I.A. 2008. Synaptic circuits of the *Drosophila* optic lobe: the input terminals to the medulla. *J. Comp. Neurol.*, *509*, 493–513.
- [89] Takemura, S.Y., Karuppudurai, T., Ting, C.Y., Lu, Z., Lee, C.H., and Meinertzhagen, I.A. 2011. Cholinergic circuits integrate neighboring visual signals in a *Drosophila* motion detection pathway. *Curr. Biol.*, *21*, 2077–2084.
- [90] Marta, R., Vitaladevuni, S.N., Mishchenko, Y., Mischenko, Y., Lu, Z., Takemura, S.Y., Scheffer, L., Meinertzhagen, I.A., Chklovskii, D.B., and de Polavieja, G.G. 2011. Wiring economy and volume exclusion determine neuronal placement in the *Drosophila* brain. *Curr. Biol.*, *21*, 2000–2005.

## BIBLIOGRAPHY

---

- [91] Shinomiya, K., Karuppudurai, T., Lin, T.Y., Lu, Z., Lee, C.H., and Meinertzhagen, I.A. 2014. Candidate neural substrates for off-edge motion detection in *Drosophila*. *Curr. Biol.*, *24*, 1062–1070.
- [92] Denk, W., and Horstmann, H. 2004. Serial block-face scanning electron microscopy to reconstruct three-dimensional tissue nanostructure. *PLoS Biol.*, *2*, e329.
- [93] Knott, G., Marchman, H., and Wall, D. 2008. Serial section scanning electron microscopy of adult brain tissue using focused ion beam milling. *J. Neurosci.*, *28*, 2959–2964.
- [94] Gengs, C., Leung, H., Skingsley, D.R., Iovchev, M.I., Yin, Z., Semenov, E.P., Burg, M.G., Hardie, R.C., and Pak, W.L. 2002. The target of *Drosophila* photoreceptor synaptic transmission is a histamine-gated chloride channel encoded by *ort* (*hclA*). *J. Biol. Chem.*, *277*, 42113–42120.
- [95] Laughlin, S., and Hardie, R. 1978. Common strategies for light adaptation in the peripheral visual systems of fly and dragonfly. *J. Comp. Physiol.*, *128*, 319–340.
- [96] Laughlin, S., and Osorio, D. 1989. Mechanisms for neural signal enhancement in the blowfly compound eye. *J. Exp. Biol.*, *144*, 113–146.
- [97] Reiff, D.F., Plett, J., Mank, M., Griesbeck, O., and Borst, A. 2010. Visualizing retinotopic half-wave rectified input to the motion detection circuitry of *Drosophila*. *Nat. Neurosci.*, *13*, 973–978.
- [98] Clark, D.A., Bursztyn, L., Horowitz, M.A., Schnitzer, M.J., and Clandinin, T.R. 2011. Defining the computational structure of the motion detector in *Drosophila*. *Neuron*, *70*, 1165–1177.
- [99] Silies, M., Gohl, D.M., Fisher, Y.E., Freifeld, L., Clark, D.A., and Clandinin, T.R. 2013. Modular use of peripheral input channels tunes motion-detecting circuitry. *Neuron*, *79*, 111–127.
- [100] Rister, J., Pauls, D., Schnell, B., Ting, C.Y., Lee, C.H., Sinakevitch, I., Morante, J., Strausfeld, N.J., Ito, K., and Heisenberg, M. 2007. Dissection of the peripheral motion channel in the visual system of *Drosophila melanogaster*. *Neuron*, *56*, 155–170.
- [101] Joesch, M., Schnell, B., Raghu, S.V., Reiff, D.F., and Borst, A. 2010. ON and OFF pathways in *Drosophila* motion vision. *Nature*, *468*, 300–304.
- [102] Gao, S., Takemura, S.Y., Ting, C.Y., Huang, S., Lu, Z., Luan, H., Rister, J., Thum, A.S., Yang, M., Hong, S.T., Wang, J.W., Odenwald, W.F., White, B.H., Meinertzhagen, I.A., and Lee, C.H. 2008. The neural substrate of spectral preference in *Drosophila*. *Neuron*, *60*, 328–342.

## BIBLIOGRAPHY

---

- [103] Takemura, S.Y., Xu, C., Lu, Z., and Rivlin, P. 2015. Synaptic circuits and their variations within different columns in the visual system of *Drosophila*. *Proc. Natl. Acad. Sci. U.S.A.*, *112*, 13711–13716.
- [104] Tuthill, J.C., Nern, A., Holtz, S.L., Rubin, G.M., and Reiser, M.B. 2013. Contributions of the 12 neuron classes in the fly lamina to motion vision. *Neuron*, *79*, 128–140.
- [105] Tuthill, J., Nern, A., Rubin, G., and Reiser, M. 2014. Wide-field feedback neurons dynamically tune early visual processing. *Neuron*, *82*, 887–895.
- [106] Douglass, J., and Strausfeld, N. 1995. Visual motion detection circuits in flies: peripheral motion computation by identified small-field retinotopic neurons. *J. Neurosci.*, *15*, 5596–5611.
- [107] Schnell, B., Raghu, S.V., Nern, A., and Borst, A. 2012. Columnar cells necessary for motion responses of wide-field visual interneurons in *Drosophila*. *J. Comp. Physiol. A.*, *198*, 389–395.
- [108] Bahl, A., Ammer, G., Schilling, T., and Borst, A. 2013. Object tracking in motion-blind flies. *Nat. Neurosci.*, *16*, 730–738.
- [109] Freifeld, L., Clark, D.A., Schnitzer, M.J., Horowitz, M.A., and Clandinin, T.R. 2013. GABAergic lateral interactions tune the early stages of visual processing in *Drosophila*. *Neuron*, *78*, 1075–1089.
- [110] Ammer, G., Leonhardt, A., Bahl, A., Dickson, B., and Borst, A. 2015. Functional specialization of neural input elements to the *Drosophila* ON motion detector. *Curr. Biol.*, *25*, 2247–2253.
- [111] Joesch, M., Weber, F., Eichner, H., and Borst, A. 2013. Functional specialization of parallel motion detection circuits in the fly. *J. Neurosci.*, *33*, 902–905.
- [112] Eichner, H., Joesch, M., Schnell, B., Reiff, D.F., and Borst, A. 2011. Internal structure of the fly elementary motion detector. *Neuron*, *70*, 1155–1164.
- [113] Gjorgjieva, J., Sompolinsky, H., and Meister, M. 2014. Benefits of pathway splitting in sensory coding. *J. Neurosci.*, *34*, 12127–12144.
- [114] Wardill, T.J., List, O., Li, X., Dongre, S., Marie, M., Ting, C.Y., J, O.C., Tang, S., Lee, C.H., Hardie, R.C., and Juusola, M. 2012. Multiple spectral inputs improve motion discrimination in the *Drosophila* visual system. *Science*, *336*, 925–931.
- [115] Stöckl, A.L., Ribi, W.A., and Warrant, E.J. 2016. Adaptations for nocturnal and diurnal vision in the hawkmoth lamina. *J. Comp. Neurol.*, *524*, 160–175.



## BIBLIOGRAPHY

---

- [116] Franceschini, N., Riehle, A., and Le Nestour, A. 1989. Directionally selective motion detection by insect neurons. In *Facets of Vision*, D.G. Stavenga and R.C. Hardie, eds. (Berlin:Springer), 360–390.
- [117] Hardie, R. 1984. Properties of photoreceptors R7 and R8 in dorsal marginal ommatidia in the compound eyes of *Musca* and *Calliphora*. *J. Comp. Physiol. A*, *154*, 157–165.
- [118] Sinakevitch, I., and Strausfeld, N.J. 2004. Chemical neuroanatomy of the fly's movement detection pathway. *J. Comp. Neurol.*, *468*, 6–23.
- [119] Mauss, A.S., Pankova, K., Arenz, A., Nern, A., Rubin, G.M., and Borst, A. 2015. Neural circuit to integrate opposing motions in the visual field. *Cell*, *162*, 351–362.
- [120] Fisher, Y.E., Leong, J.C., Sporar, K., Ketkar, M.D., Gohl, D.M., Clandinin, T.R., and Silies, M. 2015. A class of visual neurons with wide-field properties is required for local motion detection. *Curr. Biol.*, *25*, 3178–3189.
- [121] Borst, A., and Helmstaedter, M. 2015. Common circuit design in fly and mammalian motion vision. *Nat. Neurosci.*, *18*, 1067–1076.
- [122] Wässle, H. 2004. Parallel processing in the mammalian retina. *Nat. Rev. Neurosci.*, *5*, 747–757.
- [123] Masland, R. 2001. The fundamental plan of the retina. *Nat. Neurosci.*, *4*, 877–886.
- [124] Kim, J.S., Greene, M.J., Zlateski, A., Lee, K., Richardson, M., Turaga, S.C., Purcaro, M., Balkam, M., Robinson, A., Behabadi, B.F., Campos, M., Denk, W., Seung, H., and EyeWriters. 2014. Space-time wiring specificity supports direction selectivity in the retina. *Nature*, *509*, 331–336.
- [125] Baden, T., Berens, P., Bethge, M., and Euler, T. 2013. Spikes in mammalian bipolar cells support temporal layering of the inner retina. *Curr. Biol.*, *23*, 48–52.
- [126] Hausen, K. 1989. The lobula-complex of the fly: structure, function and significance in visual behavior. In *Photoreception and Vision in Invertebrates*, M. Ali, ed. (Plenum), 523–559.
- [127] Schnell, B., Weir, P.T., Roth, E., Fairhall, A.L., and Dickinson, M.H. 2014. Cellular mechanisms for integral feedback in visually guided behavior. *Proc. Natl. Acad. Sci. U.S.A.*, *111*, 5700–5705.
- [128] Blondeau, J. 1981. Electrically evoked course control in the fly *Calliphora erythrocephala*. *J. Exp. Biol.*, *92*, 143–153.

## BIBLIOGRAPHY

---

- [129] Chiappe, M., Seelig, J.D., Reiser, M.B., and Jayaraman, V. 2010. Walking modulates speed sensitivity in *Drosophila* motion vision. *Curr. Biol.*, *20*, 1470–1475.
- [130] Jung, S.N., Borst, A., and Haag, J. 2011. Flight activity alters velocity tuning of fly motion-sensitive neurons. *J. Neurosci.*, *31*, 9231–9237.
- [131] Cole, S.H., Carney, G.E., McClung, C.A., Willard, S.S., and Taylor, B.J. 2005. Two functional but noncomplementing *Drosophila* tyrosine decarboxylase genes. *J. Biol. Chem.*, *280*, 14948–14955.
- [132] Busch, S., Selcho, M., Ito, K., and Tanimoto, H. 2009. A map of octopaminergic neurons in the *Drosophila* brain. *J. Comp. Neurol.*, *513*, 643–667.
- [133] Haag, J., Wertz, A., and Borst, A. 2010. Central gating of fly optomotor response. *Proc. Natl. Acad. Sci. U.S.A.*, *107*, 20104–20109.
- [134] Lai, S.L., and Lee, T. 2006. Genetic mosaic with dual binary transcriptional systems in *Drosophila*. *Nat. Neurosci.*, *9*, 703–709.
- [135] Potter, C.J., Tasic, B., Russler, E.V., Liang, L., and Luo, L. 2010. The Q system: a repressible binary system for transgene expression, lineage tracing, and mosaic analysis. *Cell*, *141*, 536–548.
- [136] Inoue, M., Takeuchi, A., Horigane, S., Ohkura, M., Gengyo-Ando, K., Fujii, H., Kamijo, S., Takemoto-Kimura, S., Kano, M., Nakai, J., Kitamura, K., and Bito, H. 2015. Rational design of a high-affinity, fast, red calcium indicator R-CaMP2. *Nat. Methods*, *12*, 64–70.
- [137] Siegel, M., and Isacoff, E. 1997. A genetically encoded optical probe of membrane voltage. *Neuron*, *19*, 735–741.
- [138] Akemann, W., Mutoh, H., Perron, A., Park, Y.K., Iwamoto, Y., and Knöpfel, T. 2012. Imaging neural circuit dynamics with a voltage-sensitive fluorescent protein. *J. Neurophysiol.*, *108*, 2323–2337.
- [139] Jin, L., Han, Z., Platasa, J., Wooltorton, J.R., Cohen, L.B., and Pieribone, V.A. 2012. Single action potentials and subthreshold electrical events imaged in neurons with a fluorescent protein voltage probe. *Neuron*, *75*, 779–785.
- [140] St-Pierre, F., Marshall, J.D., Yang, Y., and Gong, Y. 2014. High-fidelity optical reporting of neuronal electrical activity with an ultrafast fluorescent voltage sensor. *Nat. Neurosci.*, *17*, 884–889.
- [141] Hochbaum, D., Zhao, Y., Farhi, S., and Klapoetke, N. 2014. All-optical electrophysiology in mammalian neurons using engineered microbial rhodopsins. *Nat. Methods*, *11*, 825–833.

## Bibliography

---

- [142] Flytzanis, N., Bedbrook, C., and Chiu, H. 2014. Archaelhodopsin variants with enhanced voltage-sensitive fluorescence in mammalian and *Caenorhabditis elegans* neurons. *Nat. Commun.*, *5*, 4894.
- [143] Strother, J.A., Nern, A., and Reiser, M.B. 2014. Direct observation of ON and OFF pathways in the *Drosophila* visual system. *Curr. Biol.*, *24*, 976–983.
- [144] Fosque, B.F., Sun, Y., Dana, H., Yang, C., Ohyama, T., Tadross, M.R., Patel, R., Zlatic, M., Kim, D.S., Ahrens, M.B., Jayaraman, V., Looger, L.L., and Schreier, E.R. 2015. Labeling of active neural circuits *in vivo* with designed calcium integrators. *Science*, *347*, 755–760.
- [145] Robinow, S., and White, K. 1988. The locus *elav* of *Drosophila melanogaster* is expressed in neurons at all developmental stages. *Dev. Biol.*, *126*, 294–303.
- [146] Patterson, G.H., and Lippincott-Schwartz, J. 2002. A photoactivatable GFP for selective photolabeling of proteins and cells. *Science*, *297*, 1873–1877.
- [147] Berlin, S., Carroll, E.C., Newman, Z.L., Okada, H.O., Quinn, C.M., Kallman, B., Rockwell, N.C., Martin, S.S., Lagarias, J.C., and Isacoff, E.Y. 2015. Photoactivatable genetically encoded calcium indicators for targeted neuronal imaging. *Nat. Methods*, *12*, 852–858.

# List of Figures

1	The Hassenstein-Reichardt Correlator. . . . .	2
2	The Fly Optic Lobe. . . . .	3
3	<i>Drosophila's</i> Retina. . . . .	4
4	Cell Types of <i>Drosophila's</i> Optic Lobe (modified from [19]). . . . .	5
5	Neurogenetic Toolbox of <i>Drosophila</i> (modified from [29]). . . . .	7
6	State-of-the-art Circuit Neuroscience Techniques. . . . .	11
7	Medulla Connectome Module (modified from [74]). . . . .	13
8	LPTC Response Dynamics and Block Completion. . . . .	140
9	Turning Behavior to Moving Edges. . . . .	147
10	Comparison of Calcium and Voltage Responses in Tm1 and Tm2. . . . .	149

**ÉTIENNE SERBE**  
**serbe@neuro.mpg.de**

**EDUCATION**

---

**Ludwig-Maximilians-Universität München**

Fast-Track PhD-Program "Systemic Neuroscience" in the GSN 2010 - Present

Dissertation Title:

Analysis of the Neural Circuit Underlying the Detection of Visual Motion in *Drosophila melanogaster*

B. Sc., Biology (GPA: **3.7/4.0**; Note: **1.67**) 2007-2010

Thesis: Morphological Analysis of Horizontal Sensitive Lobula Plate Tangential Cells  
of *Drosophila melanogaster* (GPA: **4.0**; Note: **1.0**)

**Allgäu-Gymnasium Kempten**

Allgemeine Hochschulreife 1994-2007

**TEACHING AND MENTORING**

---

**Day of Open Doors at the MPI**

Presentation of the research performed in our department for lay people 2011, 2013

**Mentoring**

For students in their 5th bachelor's semester for future decisions 2010

**Tutoring**

Tutorial in 'Analytical Methods and Mathematical Modelling in Biology' 2008-2009

**CONFERENCE AND SUMMER SCHOOL ATTENDANCES**

---

**MCN-QBI Symposium**

Constructing the Integrated Brain – Neurons, Circuits and Cognition 2015  
(The University of Queensland Brisbane QLD, Australia)

**Methods in Computational Neuroscience**

4 Week Summer School (Woods Hole, USA) 2014

**FENS**

Federation of European Neuroscience Societies (Milan, Italy) 2014

**MFR**

Munich Fly Retreat (Schloss Ringberg, Germany) 2013

**ICIV**

International Conference for Invertebrate Vision (Bäckaskog Slott, Sweden) 2013

**FENS**

Federation of European Neuroscience Societies (Barcelona, Spain) 2012

## Curriculum Vitae

---

### **SFB 870**

Sonderforschungsbereich 870 Retreat (Kloster Seeon, Germany)

2012

## **SKILLS AND TRAINING**

---

### **Scientific writing**

Attendance of the Course "Advanced Scientific Writing"

2013

### **Languages**

German (mother tongue), English (fluent), Spanish (fluent)

### **Software**

Matlab, Origin, Adobe Illustrator, MS Office

## **INTERESTS**

---

### **Sports**

Winter Sports, Football, Slacklining, Hiking

### **Music**

# Affidavit

Hiermit versichere ich an Eides statt, dass ich die vorliegende Dissertation **Analysis of the Neural Circuit Underlying the Detection of Visual Motion in *Drosophila melanogaster*** selbstständig angefertigt habe, mich außer der angegebenen keiner weiteren Hilfsmittel bedient und alle Erkenntnisse, die aus dem Schrifttum ganz oder annähernd übernommen sind, als solche kenntlich gemacht und nach ihrer Herkunft unter Bezeichnung der Fundstelle einzeln nachgewiesen habe.

I hereby confirm that the dissertation **Analysis of the Neural Circuit Underlying the Detection of Visual Motion in *Drosophila melanogaster*** is the result of my own work and that I have only used sources or materials listed and specified in the dissertation.

München, den 30.03.2016

Munich, 30<sup>th</sup> of March

---

Unterschrift  
signature

# List of Publications and Author Contributions

1. Maisak MS<sup>1</sup>, Haag J<sup>1</sup>, Ammer G, **Serbe E**, Meier M, Leonhardt A, Schilling T, Bahl A, Rubin GM, Nern A, Dickson BJ, Reiff DF, Hopp E and Borst A. (2013) A Directional Tuning Map of *Drosophila* Elementary Motion Detectors. **Nature** 500: 212-216.

1.1. M.S.M. and J.H. jointly performed and, together with A.Bo., evaluated all calcium imaging experiments. G.A., **E.S.** and M.M. recorded from tangential cells. A.L., T.S. and A.Ba. performed the behavioral experiments. G.M.R., B.J.D. and A.N. generated the driver lines and characterized their expression pattern. D.F.R. performed preliminary imaging experiments. E.H. helped with programming and developed the PMT shielding for the two-photon microscope. A.Bo. designed the study and wrote the manuscript with the help of all authors.

---

2. Mauss AS, Meier M, **Serbe E** and Borst A. (2014) Optogenetic and Pharmacologic Dissection of Feedforward Inhibition in *Drosophila* Motion Vision. **Journal of Neuroscience** 34(6): 2254-63.

2.1. A.S.M. and A.B. designed research; A.S.M., M.M., and **E.S.** performed research; A.B. contributed unpublished reagents/analytic tools; A.S.M., M.M., **E.S.**, and A.B. analyzed data; A.S.M. and A.B. wrote the paper.

---

3. Meier M<sup>1</sup>, **Serbe E**<sup>1</sup>, Maisak MS, Haag J, Dickson BJ and Borst A. (2014) Neural Circuit Components of the *Drosophila* OFF Motion Vision Pathway. **Current Biology** 24: 385-392.

3.1. M.M., **E.S.** and A.B. designed the study. M.M. and **E.S.** performed electrophysiological recordings. M.M., **E.S.**, M.S.M., and J.H. performed calcium imaging experiments. B.J.D. provided unpublished Gal4-lines. M.M., **E.S.** and A.B. wrote the paper with help of the other authors.



---

List of Publications and Author Contributions

---

4. Bahl A, **Serbe E**, Meier M, Ammer G and Borst A (2015). Neural Mechanisms for *Drosophila* Contrast Vision. **Neuron** 88(6): 1240-52.

4.1. A.Ba. and A.Bo. designed the study. **E.S.** and M.M. performed electrophysiological recordings. G.A. provided the Mi1, Tm3, and Mi1/Tm3-Gal4 lines and did the immunostainings. A.Ba. built the behavioral setup, programmed the visual stimuli, performed the behavioral experiments, and analyzed the data. A.Ba. wrote the paper with help from the other authors.

---

5. **Serbe E**<sup>1</sup>, Meier M<sup>1</sup>, Leonhardt A and Borst A (2016). Comprehensive characterization of the major presynaptic elements to the *Drosophila* OFF motion detector. **Neuron** 89(4): 829-41.

5.1. **E.S.** and M.M. jointly performed and evaluated all calcium imaging and electrophysiology experiments. A.L. performed and evaluated the behavioral experiments. A.L. and A.B. performed computer simulations. A.B., **E.S.**, and M.M. designed the study. **E.S.** and M.M. wrote the manuscript with the help of the other authors.

---

6. Leonhardt A<sup>1</sup>, Ammer G<sup>1</sup>, Meier M, **Serbe E**, Bahl A and Borst A (2016). Asymmetry of *Drosophila* ON and OFF motion detectors enhances real-world velocity estimation. **Nature Neuroscience** doi:10.1038/nn.4262.

6.1. A.L., G.A. and A.Bo. designed the study. A.L. performed behavioral experiments, associated data analysis and all modeling work. G.A., M.M., and **E.S.** performed electrophysiological experiments. G.A. performed calcium imaging. A.L. and G.A. analyzed physiological data. A. Ba. designed the behavioral apparatuses and performed behavioral experiments. A.L. wrote the manuscript with help from all of the authors.

.....  
Etienne Serbe

.....  
Prof. Dr. Alexander Borst  
Supervisor

.....  
Matthias Meier  
Co-first author

---

<sup>1</sup>equal contribution